Functional Models for Non-heme Mononuclear Iron Oxygenases

Mitra, Mainak

2014

Functional Models for Non-heme Mononuclear Iron Oxygenases

Mainak Mitra

LUND
UNIVERSITY

DOCTORAL DISSERTATION
by due permission of the Faculty of Natural Science, Lund University, Sweden.

To be defended at Lecture Hall F, Kemicentrum, Lund.

Friday, November 28, 2014 at 13:00.

Faculty opponent

Dr. George J. P. Britovsek

Imperial College London, London, United Kingdom

Organization

LUND UNIVERSITY

Chemical Physics
Department of Chemistry
P.O. Box 124
SE-221 00, Lund
Sweden

Author(s)

Mainak Mitra

Document name

DOCTORAL DISSERTATION

Date of issue

Sponsoring organization

European Union

Title and subtitle

Functional Models for Non-heme Mononuclear Iron Oxygenases

Abstract

Non-heme mononuclear iron oxygenases catalyze a large number of oxidation reactions in biological systems. The reactions are often proposed to proceed via the intermediacy of high valent Fe(IV) oxo (ferryl) or, Fe(V) oxo (perferryl) intermediates. Therefore, in order to mimic the high valent Fe(IV) oxo chemistry as well as the catalytic processes exhibited by those enzymes, new functional model complexes have been prepared and their reactivities have been studied both experimentally and theoretically.

In order to prepare high valent Fe(IV) oxo complexes, two new pentadenate nitrogen donor-based ligands have been synthesized and their Fe(II) complexes have been synthesized and characterized. The Fe(II) complexes have been converted into the corresponding Fe(IV) oxo complexes using suitable oxidant. The Fe(IV) oxo complexes have been characterized by several spectroscopic techniques and their reactivities in C-H activation and the O-atom transfer reaction have been investigated. Theoretical studies have been carried out to investigate the H-atom transfer reaction. The Fe(II) complexes have also been employed in alkane oxidation catalysis using hydrogen peroxide and peracids.

To make functional models for Rieske oxygenases, three tetradentate nitrogen-donor based ligands have been prepared. The corresponding Fe(II) complexes have been prepared and characterized. The C-H hydroxylation and C=C oxidation reactions have been studied using these complexes as catalyst and hydrogen peroxide as oxidant. Isotope labeling studies and computational studies have been performed to investigate the reaction mechanisms.

A Fe(II) complex of a tetradentate chiral nitrogen-donor based ligand has also been prepared to investigate the asymmetric epoxidation of olefins, using hydrogen peroxide as oxidant.

Key words: Bioinorganic chemistry, iron, oxygenases, mononuclear, high valent, catalysis, transition state, chiral.

Classification system and/or index terms (if any)

Supplementary bibliographical information

Language: English

ISSN and key title

ISBN 978-91-7422-376-7

Recipient's notes

Number of pages 131

Price

Security classification

Signature Mainak Mitra Date 2014-10-28

Functional Models for Non-heme Mononuclear Iron Oxygenases

Mainak Mitra

LUND
UNIVERSITY

Faculty of Natural Science and Deparrtment of Chemistry
ISBN 978-91-7422-376-7

Printed in Sweden by Media-Tryck, Lund University
Lund 2014

Dedicated to my parents

‘*Education is the manifestation of perfection already in man*’ – Swami Vivekananda

List of papers

I. Non-heme Fe(IV)-oxo Complexes of Two New Pentadentate Ligands and Their Reactivities Towards Hydrogen- and Oxygen-Atom Transfer Reactions

Mainak Mitra, Hassan Nimir, Serhiy Demeshko, Matti Haukka, Julio Lloret-Fillol, Franc Meyer, Albert A. Shteinman, Wesley R. Browne, David A. Hrovat, Michael G. Richmond, Miquel Costas,* and Ebbe Nordlander*

To be *submitted*

II. Catalytic C-H oxidations by non-heme mononuclear Fe(II) complexes of pentadentate ligands: Evidence for Fe(IV) oxo intermediate

Mainak Mitra, Hassan Nimir, Albert A. Shteinman, David A. Hrovat, Michael G. Richmond, Miquel Costas,* and Ebbe Nordlander*

Manuscript

III. Evidence that steric factors modulate reactivity of tautomeric iron-oxo species in stereospecific alkane C-H hydroxylation

Mainak Mitra, Julio Lloret-Fillol, Matti Haukka, Miquel Costas,* and Ebbe Nordlander*

Chem. Commun., 2014, **50**, 1408-1410.

IV. An investigation of steric influence on the reactivity of Fe(V) oxo tautomers in stereospecific alkane C-H hydroxylation

Mainak Mitra, Alexander Brinkmeier, Julio Lloret-Fillol, Michael G. Richmond, Miquel Costas,* and Ebbe Nordlander*

Manuscript

V. Highly Enantioselective Epoxidation of Olefins by H_2O_2 Catalyzed by a Non-heme Fe(II) complex of a Chiral Tetradentate Ligand

Mainak Mitra, Mingzhe Sun, Olaf Cusso, Julio Lloret-Fillol, Miquel Costas,* and Ebbe Nordlander*

Manuscript

Publication not included in the thesis

VI. A Bis(μ-phenoxo)-Bridged Dizinc Complex with Hydrolytic Activity

Mainak Mitra, Reena Singh, Monika Pyrkosz, Matti Haukka, Elzbieta Gumienna-Kontecka, and Ebbe Nordlander*

Z. Anorg. Allg. Chem., 2013, **639(8-9)**, 1534-1542.

My contributions to the papers

Paper I. I have performed all syntheses, reactivity studies. I was involved in explaining the mechanistic conclusions. I wrote most part of the manuscript.

Paper II. I have performed the catalytic experiments. I was involved in explaining the mechanistic conclusions. I wrote most part of the manuscript.

Paper III. I have performed all syntheses, catalytic reactivity studies. I was involved in explaining the mechanistic conclusions. I wrote most part of the manuscript.

Paper IV. I have performed most of the syntheses, reactivity studies. I was involved in explaining the mechanistic conclusions. I wrote most part of the manuscript.

Paper V. I was involved in designing the project. I have performed part of the catalysis. I wrote most part of the manuscript.

Abbreviations

TauD	Taurine:α-ketoglutarate dioxygenase
P4H	Prolyl 4-hydrolase
TyrH	Tyrosine hydroxylase
PheH	Phenylalanine hydrolases
Glu	Glutamate
Asp	Aspartate
His	Histidine
N4Py	*N*,*N*-bis(2-pyridylmethyl)-*N*-bis(2-pyridyl)methylamine
HRMS	High resolution mass spectroscopy
BDE	Bond dissociation energy
HAT	Hydrogen atom transfer
OAT	Oxygen atom transfer
KIE	Kinetic isotope effect
NDO	Naphthalene 1,2-dioxygenase
Me	Methyl
TACN	1,4,7-Triazacyclononane
Py	Pyridine
BzIm	Benzimidazole
Im	Imidazole
Pyz	Pyrazole
ee	Enantiomeric excess

Contents

Chapter 1 Introduction

1.1 Bioinorganic chemistry

Bioinorganic chemistry is an important branch of inorganic chemistry and biochemistry. It is referred to as the inorganic chemistry of life. The introduction and gradual advancement of biochemistry during the 20th century led chemists to search for an understanding of the functions of metallobiomolecules on a molecular level, and hence the field of bioinorganic chemistry was born. This field deals with the application of the fundamental principles of chemistry in the biophysical processes of living organisms. It involves the study of all metallic and most non-metallic elements in biological systems.

The scope of bioinorganic chemistry is broad, ranging from chemical physics to clinical medicine.[1] The area of this field has been expanded significantly during the past three decades. This is due to several reasons:[1] (i) improved analytical techniques, (ii) the recognition of roles of essential elements in plant, animal and human nutrition, (iii) rapid preparative methods for metalloproteins, (iv) sophisticated spectroscopic/physical techniques (especially nuclear magnetic resonance (NMR) spectroscopy and protein crystallography) and diffraction techniques, (v) the improved and facile syntheses of small and simple inorganic complexes to mimic the various aspects of biomolecules, (vi) the use of metal complexes for therapeutic agents, and (vii) the growing concern about the environmental hazards caused by some metal ions and elements (e.g. Hg, As etc.).

1.2 Metals in biology

The importance of metals in biology, the environment and medicine has become increasingly evident over the last 30 years. This is why the study of the roles of metals and metal ions in biological systems has become so relevant in the interfaces of inorganic chemistry and biology.

There are 13 metals, namely, Na, K, Mg, Ca (belonging to the main group metals) and V, Cr, Mn, Fe, Co, Ni, Cu, Zn and Mo (belonging to the d-block transition

metals) that are considered to be essential for the biological functions of human and other living systems. Withdrawal or absence of one of these metals from the diet causes functional or structural abnormalities. The abnormalities are related to, or are a consequence of, specific biochemical changes that can be reversed by the presence of the essential metal. The human body requires different amounts of essential metals to survive, function and maintain its physical growth. For example, Ca is present as approximately 1.4 mass % and is the most abundant metal; therefore the recommended daily intake of calcium ranges from 1000 to 1300 mg for adults. Iron is also an important essential metal to the human body, which represents 0.0006 mass % of the body (i.e. 4-5 g of iron). Out of this, 2.5 g iron is bound to hemoglobin, an oxygen transport metalloprotein present in red blood cells (RBC), while most of the remaining part is contained in the ferritin iron storage protein present in all cells. The daily required intake for adults is 8 mg for men and 18 mg for women. Iron deficiency leads to many complications in the body, e.g. anaemia (a condition of decrease in the amount of hemoglobin in blood).

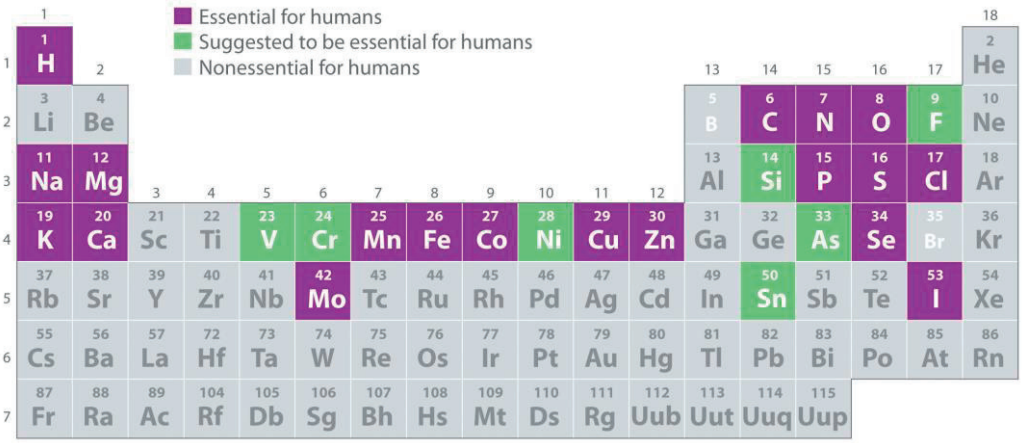

Figure 1. A periodic table of elements that are essential for human life (adapted from ref [2]).

1.3 Metalloenzymes

The overwhelming majority of metalloenzymes are proteins that contain metals that are tightly bound and always isolated with the protein. It has been estimated that one half of all known proteins contain metals, while approximately one third of the proteins are dependent on metals for their biological functions.[3]

Table 1. Lists of some essential metals and enzymes containing those metals in their active sites.

Metal	Examples of metalloenzymes
Iron	Catalase, Hydrogenase
Copper	Cytochrome c oxidase, Laccase
Zinc	Carboxypeptidase, Aminopeptidase
Nickel	Urease, Hydrogenase
Magnesium	Glucose 6-phosphatase, Hexokinase
Cobalt	Methionyl aminopeptidase, Nitrile hydratase
Manganese	Arginase
Molybdenum	Nitrate reductase, Sulfite oxidase

1.4 Active sites in metalloenzymes

The active site of a metalloenzyme is a three-dimensional pocket or groove where the substrate molecule binds and undergoes a chemical transformation. Generally, an enzyme has only one active site. This active site fits specifically with one particular substrate molecule. There are two proposed models describing how the active site of an enzyme fits with its specific substrate: (I) the lock and key model and (II) the induced fit model. According to the lock and key model[4] (proposed by Emil Fischer), the active site is perfectly fit for a specific substrate and after binding the substrate no further modification occurs. According to the induced fit model[5] (proposed by Daniel Koshland), the active site of the enzyme is flexible and it changes until the substrate binding is accomplished. Hence, the substrate is thought to induce changes in the shape of the active site.

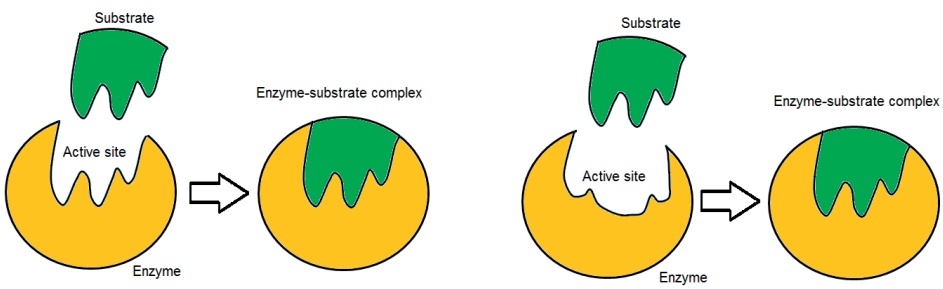

Figure 2. Enzyme-substrate binding according to the lock and key model (top left) and the induced fit model (top right, images taken from Wikipedia commons).

The proteins consist of chains of amino acid residues that contain N (e.g. histidine, arginine), O (e.g. aspartate, glutamate, serine) and S (cysteine and methionine) donor

atoms that can coordinate to the metal ions. A protein-bound metal site consists of one or more metal ions that are coordinated to protein side chains and exogenous terminal and bridging ligands.[3] This defines the first coordination sphere of each metal ion. Such metal sites can be classified into five categories on the basis of their functions:[3]

(i) Structural: The metal sites hold the protein structure together and thus induces tertiary and/or quaternary structures of the protein. An example is the zinc finger proteins, where the protein motifs are folded via coordination to one or more zinc ions.

(ii) Storage: These metal sites are related to the uptake, binding and release of soluble metals. An example is the iron-oxo cluster core in ferritin, a globular protein responsible for the storage of iron inside the body.

(iii) Electron transfer: These metal sites function as relay stations in biological electron transfer, with the metals undergoing one-electron oxidations/reductions. Examples include the iron-sulfur sites in iron-sulfur proteins (e.g. ferredoxins).

(iv) Dioxygen-binding and transport: These metal sites effect the (reversible) binding of dioxygen from air. For example, hemoglobin and myoglobin are iron-containing oxygen- binding proteins. The oxygen binding process is often associated with simultaneous electron transfer.

(v) Catalytic: These metal sites are used for the binding of a substrate and the formation of a product via chemical transformation of the substrate, which often includes redox chemistry. This is the most diverse category in terms of function. The present thesis will highlight some examples of the catalytic metal sites in biology.

1.5 Iron in metalloenzymes

Iron is the fourth most common element (after oxygen, silicon and aluminium) in the Earth's crust, where it constitutes up to 5% of the total elements present. Biologically, iron plays vital roles in oxygen transport and storage as well as in electron transport.[6] With only a few possible exceptions in the bacterial world, there would be no life without iron.[6] There is a large number of metalloenzymes that contain iron in their active sites. Myoglobin and hemoglobin were among the first proteins to be structurally characterized and both of them contain iron-protoporphyrin IX (heme b) as an essential prosthetic center.

1.6 Tools and methods for studying metalloenzymes

It is very important to study the structures of metalloenzymes and their various functions. Therefore, scientists have over decades developed many techniques and equipment for such studies. These techniques and equipment have become more and more sophisticated and sensitive with the gradual advancement of technologies and facilities so that nowadays, there are many tools and methods that are available to study a metalloenzyme. Using small synthetic metal-ligand complexes, chemists have been able to model the active sites of various metalloenzymes and understand details of their functions.

Firstly, once isolated, a metalloenzyme is subjected to testing using different analytical methods, most of which are based on the use of spectroscopy. Table 2 lists different spectroscopy techniques and the information they can provide. Besides spectroscopy, X-ray crystallography (X-ray diffraction), neutron diffraction and electron diffraction are also very useful techniques to determine the structure of the protein/metalloenzyme accurately. Applying these tools, the identity of the metal (or, metals) present in the metalloenzyme is determined and the binding sites of the protein to the metal center as well as the primary structure are identified. Kinetic studies are used to elucidate the function of the metalloenzymes. On the basis of these results, plausible mechanistic hypotheses are derived, which may be further verified by means of modelling the active site of the metalloenzyme using metal-ligand complexes.

There are indirect methods that involve computational studies and they are widely used. The active sites of many enzymes have been modelled and detailed theoretical investigations have been made on the basis these models. These studies provide valuable information about possible transition state configurations, structures of various reactive intermediates and plausible catalytic cycles. Sometimes, a proposed mechanistic cycle can be verified by such studies.

Table 2. Spectroscopic techniques and their applications to biological metal sites

Spectroscopic method	Information obtained
Vibrational (Raman and Infra Red)	Nature of bonds of ligands around metal centers
Electronic absorbance (UV/Visible)	Nature of ligand field and charge transfer transitions (ligand to metal/metal to ligand)
Nuclear Magnetic Resonance (NMR)	Structure and electronic properties of diamagnetic and paramagnetic systems
Electron Spin Resonance or, Electron Paramagnetic Resonance (ESR/EPR)	Detection and identification of free radicals and paramagnetic centers
Mössbauer	Oxidation state and spin state of, normally, ^{57}Fe, sensitive to chemical environment around the metal
Magnetic Circular Dichronism (MCD)	Detection of electronic structures of both ground and excited states
Time-resolved spectroscopy	Deals on the study of the dynamic processes in chemical compounds or, materials.
X-ray photoelectron spectroscopy (XPS)	Measures chemical compositions, empirical formula, chemical and electronic state of the elements within the materials

1.7 Biomimetic chemistry: Modelling the active site of a metalloenzyme

It is often difficult to isolate and purify the real metalloenzyme, a fact that complicates studies of its structural and functional aspects of a metalloenzyme. In some cases, an isolated protein cannot be fully characterized by virtue of its complex structure and lack of crystallization. To overcome such difficulties, researchers have developed a strategy to synthesize metal complexes that can mimic the active site of a metalloenzyme of interest ('biomimetic' modelling). Such model complexes may make it possible to gain many insights into the intrinsic properties of a particular metal site in a metalloenzyme. However, due to the absence of the protein environment surrounding these model metal complexes, they cannot truly reflect the impact of the enzyme active site. Nevertheless, they may be used to understand/investigate the basic roles of the metals present in the active site as well as to develop a view on mechanistic pathways. Also, model complexes are relatively easy to modify by means of varying the surrounding ligand environment, and can

thus provide useful information about a particular donor atom/site. Some model complexes have also shown good catalytic properties that are similar to those of the enzymes and may therefore, in principle, be employed in industrial settings.

Model complexes can mimic the active site of an enzyme structurally, functionally, or they can serve both purposes. It is also possible to verify the influence of structural and functional changes by appropriate modifications. First, model metal complexes are synthesized and isolated, followed by identification by various spectroscopic techniques. Structural comparison is made between the model complex and the active site of enzyme (structural model). Then, the model complexes are explored as catalysts of the particular reaction that the enzyme catalyses (functional model). Often, a structural model complex does not show reactivity that is similar to, or as good as, that of the enzyme (i.e. it is not a functional model) and *vice versa*.

In recent years, a third aspect of synthetic modelling of metalloenzymes has become increasingly popular. This approach is often referred to as "bio-inspired modelling", where the complexes that are prepared and studied are intended to serve as catalysts that reproduce enzymatic reactions, but bear little or no resemblance to the relevant metalloenzyme sites, neither in terms of metal(s) used nor coordination geometries or ligand environments. Such a "bio-inspired" approach is explored in many areas, e.g. artificial photosynthesis, where metal complexes that can function as light harvesters, and catalysts of, for example, water oxidation and proton reduction, are developed.

1.8 Scope of this thesis

The present thesis focuses on the functional mimicry of active sites of mononuclear non-heme iron oxygenase enzymes (*cf.* chapters 2 and 3 for more discussions about iron oxynenases). The studies include synthesis and spectroscopic characterization of mononuclear non-heme iron complexes of N-based polydentate ligands and catalytic oxidation reactions of some model organic substrates. High valent Fe oxo intermediates have also been generated and characterized. The reactivities of these intermediates have been explored in hydrogen atom transfer and oxygen atom transfer processes. Computational modelling studies have been performed to elucidate the structures and orientations of high valent Fe oxo intermediates and to propose plausible reaction mechanisms.

Paper I deals with the synthesis and characterization of two non-heme Fe(IV) oxo complexes of pentadentate ligands and detailed investigations on their reactivities towards hydrogen- and oxygen-atom transfer reactions. Paper II deals with the oxidation catalysis of alkanes and alkenes and studies of reaction mechanism mediated by the Fe(II) complexes of the above pentadentate ligands.

Papers III and IV deal with stereospecific C-H hydroxylation reactions by three Fe(II) complexes of tetradentate ligands and detailed investigations on the mechanisms of hydroxylation by isotope labelling and theoretical studies.

Paper V deals with the asymmetric epoxidation of olefins with hydrogen peroxide as oxidant catalysed by a Fe(II) complex of a tetradentate N4 chiral ligand.

1.9 References

1. K. H. Reddy, *Bioinorganic Chemistry*, New Age International publishers, 2003.
2. B. Averill, P. Eldredge, *GeneralChemistry: Principles, Patterns and Applications*, 2011.
3. R. H. Holm, P. Kennepohl, E. I. Solomon, *Chem. Rev.*, 1996, 96, 2239-2314.
4. E. Fischer, *Einfluss der Configuration auf die Wirkung der Enzyme. Ber. Dtsch. Chem. Ges.*, 1894, 27: 2985–2993
5. D. E. Koshland, *Proc. Natl. Acad. Sci.*, 1958, 44, 98-104.
6. N. N. Greenwood and A. Earnshaw, *Chemistry of the Elements*, Oxford, 1997.

Chapter 2.

High valent Fe(IV) oxo complexes: Reactivities towards H- and O-atom transfer processes

2.1 Introduction.

2.1.1 Fe(IV) oxo intermediates in non-heme mononuclear iron enzymes.

Non-heme mononuclear iron enzymes carry out essential metabolic transformations via activation of molecular oxygen inside living organisms.[1-2] They catalyze oxidation of organic substrates, and the oxidation reactions include hydroxylation, halogenation, desaturation, epoxidation and *cis*-dihydroxylation.[3-7] An example is proline 3-hydrolase which catalyzes the conversion of L-proline into *cis*-3-hydroxy-L-proline in the presence of 2-oxoglutarate and molecular oxygen; 2-oxoglutarate functions as a "sacrificial" substrate (*vide infra*).[7-8] It is often postulated that the key oxidizing intermediate involved in the above-mentioned oxidation reactions is a high valent Fe(IV) oxo (ferryl-oxo or, simply ferryl) species.[6,9-11] The presence of a reactive Fe(IV) oxo intermediate has been established in the catalytic cycles of *E. coli* taurine:α-ketoglutarate dioxygenase (TauD),[12] prolyl 4-hydrolase (P4H),[13] the halogenase CytC3,[14] tyrosine hydroxylase (TyrH),[15] pterin-dependent phenylalanine hydrolases (PheH),[16] and the aliphatic halogenase SyrB2.[17] In all cases, the Fe(IV) center is in a high spin (hs) d^4 configuration. In many of these enzymes, the iron center is bound to a 2-His-1-carboxylate facial triad motif. Figure 1 depicts three proposed Fe(IV) oxo intermediate structures found in the non-heme mononuclear iron-enzyme active sites.

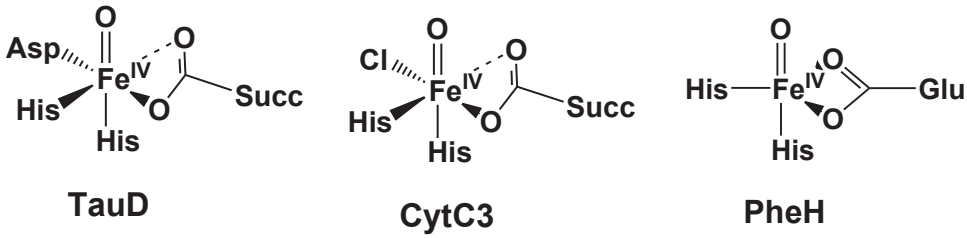

Figure 1. The proposed active site structures of taurine:α-ketoglutarate dioxygenase (TauD), the halogenase CytC3 (CytC3) and pterin-dependent phenylalanine hydroxylase (PheH), containing high valent Fe(IV) oxo centers (succ = succinate, glu = glutamate).

A powerful approach to study the mechanism and to establish a catalytic cycle by which an enzyme oxidizes substrate is to attempt the detection or trapping of reaction intermediates followed by detailed characterization of these intermediates using kinetics and spectroscopic techniques.[1] The first direct detection of an intermediate in a reaction with dioxygen catalyzed by a mononuclear non-heme iron enzyme was reported for HPPD ((4-Hydroxyphenyl)pyruvate dioxygenase).[18] Shortly after this, an Fe(IV) oxo intermediate was detected in the catalytic cycle of TauD by various spectroscopic techniques.[12b,19] On the basis of these novel findings, a general reaction mechanism has been proposed for this class of iron enzymes.[1,6] Molecular oxygen initially coordinates to the Fe(II) center of the active site to form an Fe(III) superoxo species, Fe(III)-$O_2^{\cdot -}$. The superoxo species can itself act as an oxidant, as proposed for Fe-bleomycin.[20] In a second scenario, the O-O bond is homolytically cleaved to generate the reactive Fe^{IV}(=O) intermediate (or even Fe^{V}(=O) intermediate in Rieske oxygenases). The Fe^{IV}(=O) intermediate then reacts with the substrate in a hydrogen atom transfer (HAT) reaction to form a substrate radical and a Fe(III)-OH species. The subsequent step is the so called "oxygen rebound", which has been proposed and identified for heme enzymes;[21] it involves the recombination of the substrate radical with a hydroxyl radical formed by homolytic cleavage of the metal oxygen bond, yielding the oxidized product (Scheme 1). In the whole process, one oxygen atom derived from atmospheric oxygen is inserted into the C-H bonds of the substrate.

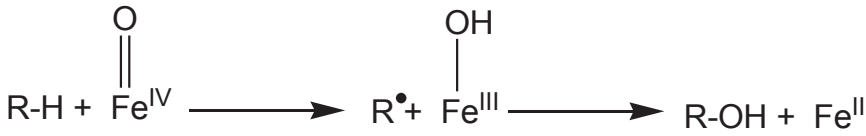

Scheme 1. The oxygen rebound mechanism proposed for non-heme mononuclear iron enzymes, involving a Fe(IV) oxo intermediate.

So called α-keto acid-dependent enzymes (e.g. prolyl 4-hydroxylases, lysyl hydroxylases, TauD, asparagine hydroxylase etc.) are found in microorganisms, plants, and animals and play key roles in vital transformations of environmental, pharmaceutical and biological importance.[6] Figure 2 describes the common proposed mechanism for the α-keto acid-dependent iron oxygenases.[11,22-24] In the resting state of the enzyme, the Fe(II) center is bound to a 2-His-1-carboxylate triad motif and three water molecules. Steady-state kinetics studies on some enzymes emphasise an ordered mechanism in which binding of an α-keto carboxylate (e.g. α-ketoglutarate) to the Fe(II) center occurs prior to dioxygen or substrate binding. The α-keto carboxylate functions as a sacrificial substrate, accepting one of the two oxygens from the dioxygen molecule, while the second oxygen is incorporated into the enzymatic substrate.

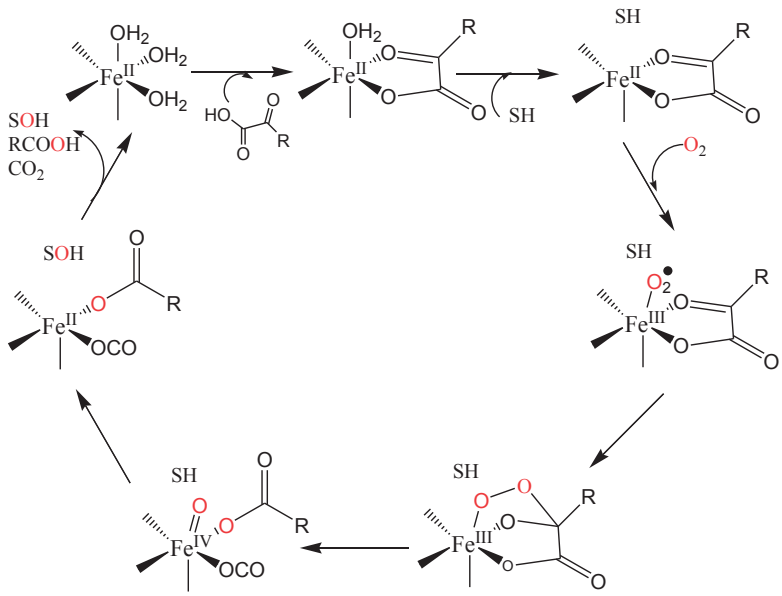

Figure 2. The proposed catalytic cycle of α-keto acid-dependent enzymes, SH = arbitrary substrate.

Trapping and characterization of high valent Fe(IV) oxo intermediates in non-heme iron enzymes have inspired synthetic chemists to design and construct suitable ligand systems for the synthesis of Fe(IV) oxo complexes and to study the reactivities of such complexes in small molecule transformation reactions that enable us to gain a solid understanding of and to interpret the molecular mechanisms of the real enzymes. This will be further discussed below.

2.1.2 Synthetic non-heme mononuclear Fe(IV) oxo complexes

Inspired by Nature, several non-heme mononuclear Fe(IV) oxo complexes have been synthesized and well characterized during the last two decades.[25-28] Except a few complexes,[29-34] most of them are found to contain low spin Fe(IV) centers. The Fe(IV) oxo complexes thus reported have different reactivity rates in hydrogen atom transfer (HAT) and oxygen atom transfer (OAT) reactions. The discrepancy in the observed reactivities of the various Fe(IV) oxo complexes is due to several factors including (I) the nature of the ligand, (II) denticity of the ligand (tetradentate vs pentadentate), and (III) the spin state (high spin vs low spin) of the Fe(IV) center. The ligand field strength plays an important role in tuning the reactivity of the Fe(IV) oxo complex; the field strength is associated with the electronic properties of the donor atoms/moieties of the ligand.

Significant contributions have been made by using Fe(IV) oxo complexes containing a labile coordination site occupied by a solvent molecule that is either *cis* or *trans* with respect to the oxo ligand.[35-38] This permits exchange with other ligands. For example, Que, Shaik, Nam and coworkers[37] have investigated the reactivities of mononuclear Fe(IV) oxo complexes, $[Fe^{IV}(O)(TMC)(X)]^{n+}$ (where TMC is 1,4,8,11-tetramethyl-1,4,8,11-tetraazacyclododecane and X is $NCCH_3$, CF_3SOO^-, N_3^-) and $[Fe^{IV}(O)(TMCS)]^+$ (where TMCS is 1-mercaptoethyl-4,8,11-trimethyl-1,4,8,11-tetraazacyclododecane) and have shown that the more electron donating the axial ligand is, the more reactive the Fe(IV) oxo complex becomes with respect to HAT reactions and the less reactive with respect to oxygen atom transfer to PPh_3.

The spin state of the Fe(IV) center is also an important aspect. It has been predicted that a high spin Fe(IV) oxo complex is more reactive than the corresponding low spin complex.[39] However, the most reactive Fe(IV) oxo complex so far, $[Fe^{IV}(O)(Me_3NTB)]^{2+}$ (where Me_3NTB = tris((*N*-methyl-benzimidazol-2-yl)methyl)amine)), reported by Nam and co-workers, contains a low spin (S = 1) Fe(IV) center in the ground state.[40] Density functional calculations revealed that the reactive state is likely to be S = 2, which has a low energy barrier for the C-H abstraction reaction with respect to the triplet (S = 1) ground state; this is the essential concept of the so-called "two state reactivity" (TSR) model – there is a crossover to a high spin reactive state upon formation of the transition state from the ground state.[40] The geometry of the ligand sometimes dictates the spin state of the Fe(IV) center. The ligand field energy diagram for an octahedral Fe(IV) oxo complex

reveals that the energy gap between the d_{xy} and $d_{x^2-y^2}$ orbitals determines the spin state on the iron.[41] For most Fe(IV) oxo complexes having $S = 1$, this energy gap is larger than the spin pairing energy. If the ligand strength is weakened, then the energy gap becomes smaller than the spin pairing energy leading to $S = 2$ Fe(IV) oxo species as demonstrated in the case of $[Fe^{IV}(O)(H_2O)_5]^{2+}$.[29,42] Attaining $S = 2$ spin states can be approached by adoption of trigonal bipyramidal geometry (TBP) around the Fe(IV)-center, which leads to degeneracy of the d_{xy} and $d_{x^2-y^2}$ orbitals. This requires a tetradentate ligand system with sufficient steric constraints. Examples of such cases are $[Fe^{IV}(O)(TMG_3tren)]^{2+}$ (TMG_3tren = tris(tetramethylguanidino)tren)[30] and $[Fe^{IV}(O)(H_3buea)]^-$ (H_3buea = tris(*tert*-butylureaylethylene)aminato).[32] Despite their high spin character, they do not possess superior reactivities when compared to the low spin Fe(IV) oxo complexes. This fact is explained by the steric inhibition by the bulky ligand, making it difficult for the substrate to approach the Fe(IV) oxo center. Recently, Que, Munck and co-workers reported an Fe(IV) oxo complex, $[Fe^{IV}(O)(Mecyclam\text{-}CH_2C(O)NMe_2)]^+$ with very high thermal stability (half life 5 d at room temperature).[27] This complex, owing to its high stability, is a sluggish catalyst of HAT reactions. Addition of strong base to this complex resulted in the formation of a new oxo iron(IV) complex that is far less stable and can be converted back to the stable complex by treatment with acid. This represents the first example of a conjugate acid-base pair in Fe(IV) oxo chemistry. Goldberg and coworkers have reported a series of Fe(IV) oxo complexes that can mediate ring hydroxylation/halogenations of the ligand coordinating to the Fe-oxo unit.[43] All these studies testify to the diverse nature of synthetic non-heme high valent Fe oxo complexes. This chapter will summarize my investigations within this challenging area of research.

2.2 Motivation behind the work and design of ligands

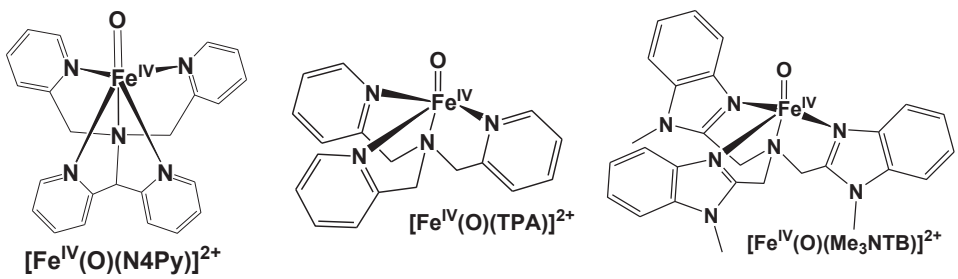

Figure 3. The Fe(IV) oxo complexes, $[Fe^{IV}(O)(N4Py)]^{2+}$ (left), $[Fe^{IV}(O)(TPA)]^{2+}$ (middle) and $[Fe^{IV}(O)(Me_3NTB)]^{2+}$ (right).

The Fe(IV) oxo complex of the pyridine-based pentadentate N4Py ligand, i.e. $[Fe^{IV}(O)(N4Py)]^{2+}$ (Figure 3), constitutes a unique example of the combination of good thermal stability with considerable reactivity.[44] This complex has a half life ($t_{1/2}$) of 60 h at room temperature, allowing it to be crystallographically characterized. At the same time, it possesses sufficient reactivity to oxidize C-H bonds as strong as those in cyclohexane (C-H bond dissociation energy 99.3 kcal/mol) at room temperature. While, the Fe(IV) oxo complex of the pyridine-based tetradentate TPA ligand, $[Fe^{IV}(O)(TPA)]^{2+}$ (Figure 3), is less stable (stable at -40 ˚C for several days) compared to $[Fe^{IV}(O)(N4Py)]^{2+}$ and has moderate reactivities.[45] In contrast, the complex $[Fe^{IV}(O)(Me_3NTB)]^{2+}$ (Figure 3) is the most reactive Fe(IV) oxo complex in HAT and OAT reactions that has thus far been published, but it decomposes very rapidly even at low temperature ($t_{1/2}$ is 2 min at -40 ˚C).[40] These observations indicate that while the pyridine-containing pentadentate ligand (N4Py) stabilizes the high valent Fe(IV) oxo moiety, the (*N*-methyl)benzimidazolyl moiety (as in Me_3NTB) destabilizes it, but enhances the reactivity. Considering these observations, we decided to investigate how the introduction of (*N*-methyl)benzimidazolyl moieties into the pentadentate N4Py ligand framework may affect the properties of the Fe(IV) oxo species.

Thus, two new pentadentate N5-donor ligands, L^1 and L^2 (Figure 4) were synthesized. These ligands are based on the N4Py ligand framework, with one (L^1) or two (L^2) ((2-pyridyl)methyl side arm(s) of N4Py being replaced by (*N*-methylbenzimidazolyl)methyl arm(s). Introduction of the (*N*-methyl)benzimidazolyl moieties permits an assessment of potential electronic and/or steric effects of substituents on the reactivities of high valent Fe(IV) oxo complexes as well as the reactivities of analogous Fe(II) complexes in oxidation catalysis. In general, (*N*-methyl)benzimidazolyl moieties possess greater steric bulk than pyridyl moieties, and (*N*-methyl)benzimidazole is better σ-donor than pyridine[46] but also a better π-acceptor. In Nature, the active sites of iron enzymes contain one or more coordinating imidazole rings from histidine residues of the protein chain. Imidazole is more basic but its electronic properties are similar to benzimidazole. Therefore, it was envisioned that (*N*-methyl)benzimidazole-containing ligands may provide useful information on the impact of basic donor groups on the C-H activation and other organic transformation reactions mediated by high valent Fe-oxo centers.

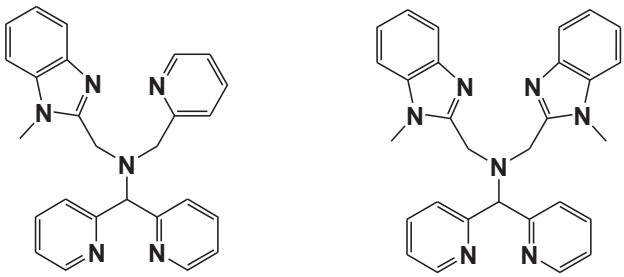

Figure 4. Structures of ligands L^1 (left) and L^2 (right) used for this study.

The ligands were synthesized and were characterized by mass spectra and NMR spectra (*cf.* paper I for detailed synthetic procedures).

2.3 Fe(II) complexes: Synthesis and characterization

The Fe(II) complexes of the two new ligands, namely $[Fe^{II}(L^1)(CH_3CN)](ClO_4)_2$ (**1**·$(ClO_4)_2$) and $[Fe^{II}(L^2)(CH_3CN)](ClO_4)_2$ (**2**·$(ClO_4)_2$; Figure 5) were synthesized (*cf.* paper I for detailed syntheses). Both complexes were obtained as air-stable solids.

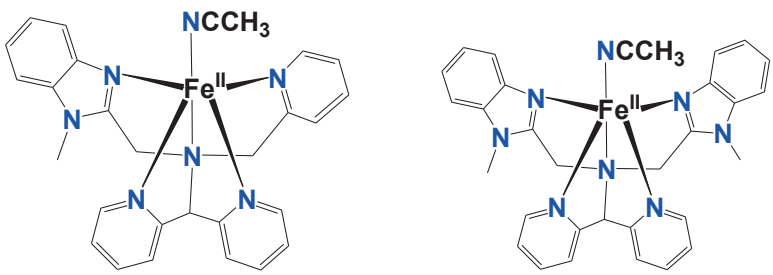

Figure 5. Schematic depiction of the cations of complexes **1**·$(ClO_4)_2$ (left) and **2**·$(ClO_4)_2$ (right).

The complexes were characterized by ESI-MS, elemental analysis, ^{1}H-NMR spectroscopy, IR spectroscopy and UV/Visible spectroscopy (*cf.* paper I). The ^{1}H-NMR spectra of the complexes establish the ls configuration of the Fe(II)-center. The UV/Vis spectra of the complexes have shown two distinct metal to ligand charge transfer (MLCT) transitions originating from the electron donation of t_{2g} orbitals of Fe(II) to the π^* orbitals of the ligand.

The zero field Mössbauer spectra recorded for naturally abundant solid samples of complexes **1**·$(ClO_4)_2$ and **2**·$(ClO_4)_2$ at 80 K further confirm the ls state of the Fe(II)-centers (*cf.* paper I for details).

2.4 Crystal and molecular structures

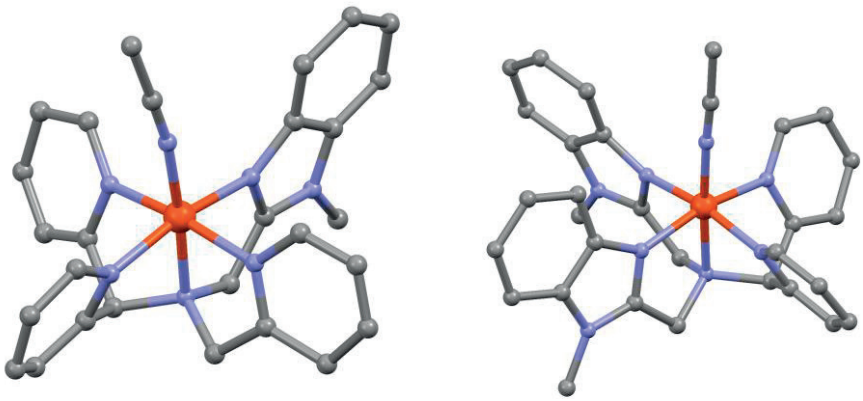

Figure 6. The crystal structures of the cations of **1**·$(ClO_4)_2$ (left) and **2**·$(ClO_4)_2$ (right) (Mercury plot); hydrogen atoms have been omitted for clarity.

The crystal structures of complexes **1**·$(ClO_4)_2$ and **2**·$(ClO_4)_2$ (Figure 6) reveal Fe-N bond distances that are consistent with the presence of low spin Fe(II) centers in both complexes.[47-50] A structural comparison of **1**·$(ClO_4)_2$ and **2**·$(ClO_4)_2$ and the parent complex $[Fe^{II}(N4Py)(CH_3CN)](ClO_4)_2$ is discussed in paper I.

2.5 Synthesis and characterization of Fe(IV) oxo complexes

The Fe(IV) oxo complexes $[Fe^{IV}(O)(L^1)]^{2+}$ (**3**) and $[Fe^{IV}(O)(L^2)]^{2+}$ (**4**) were conveniently synthesized by reaction of the Fe(II) complexes/precursors (**1**·$(ClO_4)_2$ and **2**·$(ClO_4)_2$, respectively) with excess solid PhIO in CH_3CN (Scheme 2).

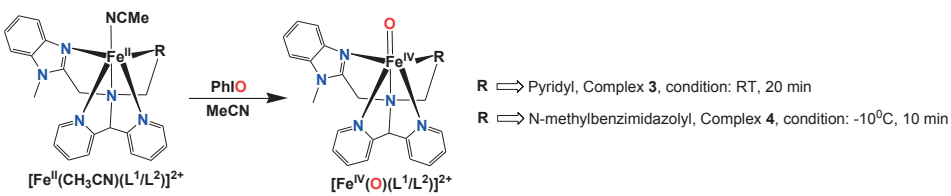

Scheme 2. Generation of the Fe(IV)-oxo complexes **3** and **4** from their precursor Fe(II)-complexes, **1** and **2**, respectively.

Both **3** and **4** exhibit a characteristic absorption in the near IR region with a maximum at λ_{max} = 708 nm ($\varepsilon \approx 400$ M^{-1} cm^{-1}) and 725 nm ($\varepsilon \approx 380$ M^{-1} cm^{-1}),

respectively. This absorption is associated with a ligand field transition rather than a charge transfer transition.[44,45] The parent complex $[Fe^{IV}(O)(N4Py)]^{2+}$, containing four equatorial pyridyl groups, has a corresponding λ_{max} = 695 nm and this value increases gradually as pyridyl groups are replaced by (*N*-methyl)benzimidazolyl groups and may therefore be directly related to and correlated with the donor strength of the pentadentate ligand. Furthermore, Mössbauer spectroscopy was used to confirm the oxidation and spin states of complexes **3** and **4** (Figure 7). The isomer shift values for the two complexes are very similar to those obtained for $[Fe^{IV}(O)(N4Py)]^{2+}$ [44] and $[Fe^{IV}(O)(Bn\text{-}tpen)]^{2+}$,[44] indicating that both **3** and **4** are low spin (*S* = 1) non-heme Fe(IV) oxo complexes.

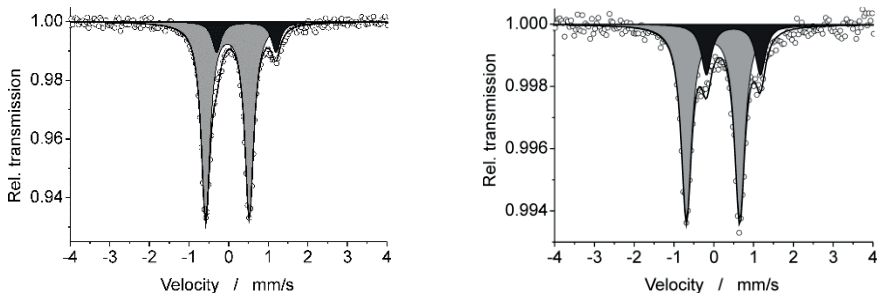

Figure 7. (Left) The zero-field Mössbauer spectrum of ^{57}Fe enriched **3** (light gray) in acetonitrile solution (5 mM) measured at 80 K. The minor black subspectrum corresponds to ca. 14% unidentified Fe(III) impurity. (Right) The zero-field Mössbauer spectrum of ^{57}Fe enriched **4** (light gray) in acetonitrile solution (2 mM) measured at 80 K. The minor black subspectrum corresponds to ca. 20% unidentified Fe(III) impurity. Complex **3**, isomer shift (δ) = -0.03 mm s^{-1} and quadrupole splitting value (ΔE_Q) = 1.1 mm s^{-1}; Complex **4,** δ = -0.02 mm s^{-1} and ΔE_Q = 1.34 mm s^{-1}.

2.6 Stabilities and half-lives of the Fe(IV) oxo complexes 3 and 4

Complexes **3** and **4** are relative stable at room temperature. Complex **3** has a half-life ($t_{1/2}$) of 40 h at ambient temperature and is more stable than complex **4**, for which $t_{1/2}$ is 2.5 h at room temperature. These data may be compared to $t_{1/2}$ of 60 h at room temperature for the parent complex $[Fe^{IV}(O)(N4Py)]^{2+}$, which contains four equatorial pyridyl groups. The relative stabilities for the three complexes are directly related to the successive replacement of pyridylmethyl arms in the N4Py ligand with (*N*-methylbenzimidazolyl)methyl arms, $[Fe^{IV}(O)(N4Py)]^{2+}$ (most stable) > complex **3** > complex **4** (least stable). It may be concluded that the relative stabilities of the

Fe(IV) oxo complexes are also influenced by the relative donor strength of the pentadentate ligands.

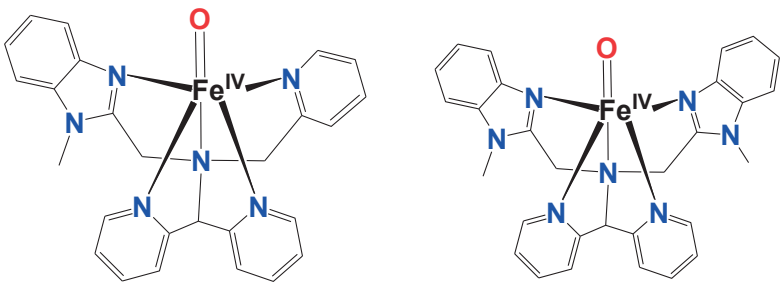

[Fe^{IV}(O)(L^1)]$^{2+}$ (**3**) [Fe^{IV}(O)(L^2)]$^{2+}$ (**4**)

Figure 8. Fe(IV) oxo complexes **3** (left) and **4** (right).

2.7 Reactivities of Fe(IV) oxo complexes

2.7.1 C-H bond activation: Hydrogen-atom transfer (HAT) reactions

The reactivities of complexes **3** and **4** were investigated towards hydrogen atom transfer (HAT) reactions using different alkanes with C-H bond dissociation energies (BDE's) ranging from 81 to 99.3 kcal/mol. It was found that both complexes are capable of oxidizing C-H bonds of the substrate to give moderate to good yields of oxidized products (*cf.* paper I). The reactions were run under pseudo-first-order conditions using excess substrate, and the observed rate constant (k_{obs}) was found to be linearly dependent on the concentration of the substrate. From this analysis, the second order rate constant (k_2) was determined. The products were analysed using gas chromatography. The reactivities of the two Fe(IV)=O complexes are summarized below.

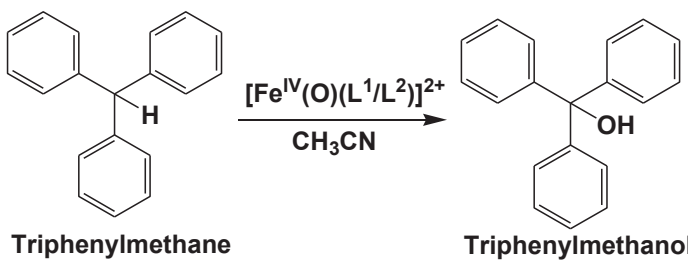

Scheme 3. Hydroxylation of triphenylmethane into triphenylmethanol by complex **3** or **4**.

Complexes **3** and **4** oxidized triphenylmethane, with a C-H BDE of 81 kcal/mol, to triphenyl methanol with 89-90% yields (Scheme 3). When cyclohexane (which has a relatively high C-H BDE of 99.3 kcal/mol) was employed as substrate, **3** and **4** oxidized the substrate to give both cyclohexanol and cyclohexanone in moderate yields (18% and 26%, respectively). The second order rate constants and details of the product analyses for complexes **3** and **4** are listed in paper I and the supplementary material. A plot of log k_2' (k_2' is obtained by dividing k_2 with the number of equivalent C-H bonds of the alkane substrate of interest) versus the C-H BDE for complexes **3** and **4** showed a linear dependency (Figure 9), which is characteristic of the HAT reaction.[44] The second order rate constant (k_2) values obtained for the two complexes indicated that complex **4** is more reactive than complex **3** towards alkane substrates (C-H activation), in accordance with its lower stability.

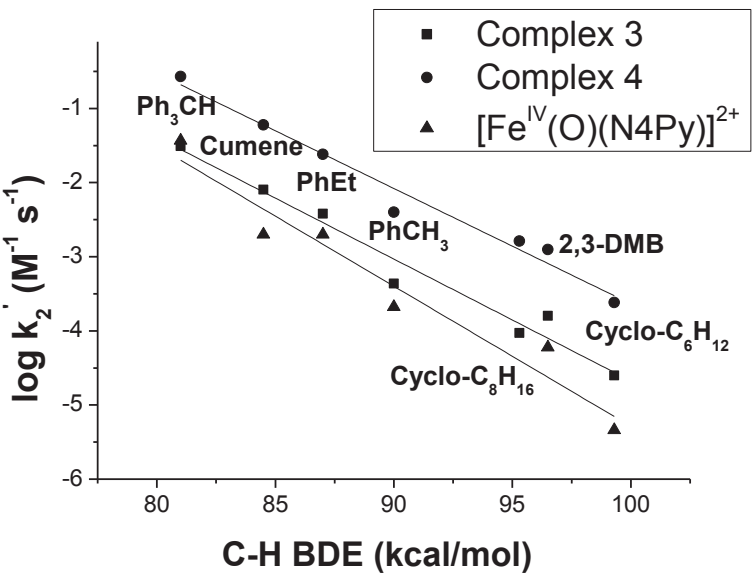

Figure 9. Comparison of log k_2' v/s bond dissociation energy (BDE) of different alkanes between complexes **3**, **4** and $[Fe^{IV}(O)(N4Py)]^{2+}$.

The log k_2' versus C-H BDE plot indicates that the reactivity rates towards HAT reactions are increased from $[Fe^{IV}(O)(N4Py)]^{2+}$ to complex **3** to complex **4** by approximately one order of magnitude, i.e. successive replacement of the pyridylmethyl arms of N4Py with (*N*-methylbenzimidazolyl)methyl arms leads to an increase in the reactivity rate of the corresponding Fe(IV) oxo complex. The introduction of *N*-methylbenzimidazole donor moieties did not appear to lead to any significant steric inhibition of substrate access to the Fe-oxo center, as evidenced by similar k_2 values for the reactions of **4** in separate reactions with sterically bulky

9,10-dihydroanthracene and the smaller 1,4-cyclohexadiene. Therefore, the reactivity trends exhibited by complexes **3** and **4** could be attributed to the electronic influence of the ligand system (*cf.* paper I for detailed discussion).

2.7.2 Oxygen-atom transfer (OAT) reactions

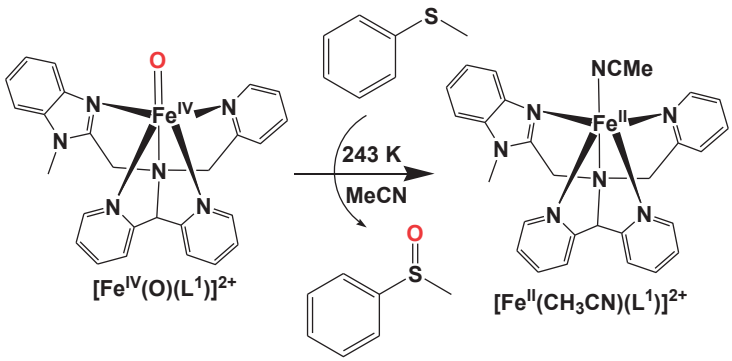

Scheme 4. Oxygen atom transfer (OAT) to thioanisole by complex **3** (or, **4**) at 243 K.

The oxo transfer reactivities of **3** and **4** were investigated using thioanisole ($PhSCH_3$) as a substrate (Scheme 4). Both complexes oxidized thioanisole to its sulfoxide at 243 K, in very good yields. Complex **4** reacted faster and gave slightly higher yield than **3** (88 vs 84%) During the course of the reaction, both complexes were converted into their corresponding Fe(II) precursors as identified by UV/Vis spectrophotometry (*cf.* paper I for details). In presence of excess substrate (5-20 equivalents w.r.t. complex **3** or **4**) the reaction showed pseudo-first order behaviour and the observed rate constant (k_{obs}) was linearly dependent on substrate concentration. From this linear plot, a second order rate constant (k_2) with a value of 3.3×10^{-2} M^{-1} s^{-1} was obtained for complex **3** and 3.1×10^{-1} M^{-1} s^{-1} for complex **4**. Comparing the reactivities between complexes **3**, **4** and $[Fe^{IV}(O)(N4Py)]^{2+}$ in thioanisole oxidation, it can be concluded that the reactivity is increased ten-fold in the order $[Fe^{IV}(O)(N4Py)]^{2+}$ < **3** < **4**. Clearly, the (*N*-methyl)benzimidazole substituent plays a positive role in enhancing the OAT reactivity in a systematic manner.

2.8 Computational studies on the HAT reactivity by the Fe(IV) oxo complexes

The excellent reactivities of the Fe(IV) oxo complexes **3** and **4** in HAT processes can be explained on the basis of the two-state reactivity model as proposed by Shaik.[39a,b,d,g,h,n,40] This involves the transition of reaction surfaces between a triplet

(S = 1) state and a quintet (S = 2) state (*cf.* Section 2.1.2). The lowest energy path for methane activation by complex **3** is shown in Figure 10 (*cf.* Paper I for more details). The ground spin state of complex **3** is a triplet (S = 1) (^{3}**A**). The methane activation via the triplet Fe-oxo (^{3}**A**) state leads a release of 7.5 kcal/mol energy (*cf.* Paper I for more details). On the other hand, the methane activation via a quintet Fe-oxo (^{5}**A**) state leads to a release of 25.8 kcal/mol energy (*cf.* Paper I for more details). Thus, a reaction that proceeds via spin crossover from the ^{3}**A** ground state to the ^{5}**A** state will have significantly lower activation energy than the pure triplet pathway, in keeping with the two-state reactivity model, and the computational study indicates that both complexes **3** and **4** react with substrates via this pathway, as has previously been computed for alkane oxidation by $[Fe^{IV}(O)(N4Py)]^{2+}$.[39b]

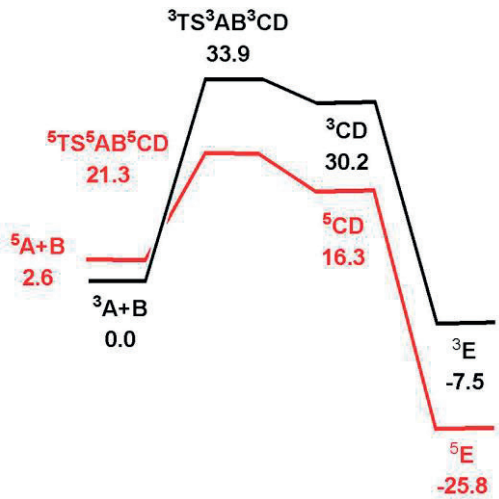

Figure 10. B3LYP potential energy surface for reaction of ^{3}**A**/^{5}**A** and methane (**B**) to give methanol-substituted complexes ^{3}**E** and ^{5}**E**. Energy values are in ΔG in kcal/mol relative to ^{3}**A**+**B**.

2.9 Catalytic oxidation reactions on alkanes with Fe(II) complexes

The catalytic activities of the two Fe(II) complexes, **1**·$(ClO_4)_2$ and **2**·$(ClO_4)_2$, were also investigated in the oxidation of different alkanes, using hydrogen peroxide (H_2O_2), peracetic acid (PAA) or *meta*-chloroperoxybenzoic acid (mCPBA) as oxidant.

Complex **1**·$(ClO_4)_2$ or **2**·$(ClO_4)_2$ oxidizes cyclohexane to produce cyclohexanol and cyclohexanone in the presence of H_2O_2. The complexes gave similar turnover numbers for the formation of the two products, and the overall yields were also similar (39% for **1**·$(ClO_4)_2$ and 32% for **2**·$(ClO_4)_2$, based on oxidant). The alcohol/ketone (A/K) ratio was found to be low (1.2) in both cases, implicating the possible involvement of freely diffusing carbon centered radicals that are trapped by

molecular oxygen, followed by a Russell termination step. Furthermore, the kinetic isotope effect (KIE) was determined for the formation of cyclohexanol in competition experiments between cyclohexane and its d_{12} isotopomer. The KIE values obtained for **1**·$(ClO_4)_2$ and **2**·$(ClO_4)_2$ were 1.45 and 1.7 respectively, and are consistent with the involvement of a hydroxyl radical in the rate-determining step of hydrogen atom abstraction from a C-H bond.

The oxidation of adamantane by **1**·$(ClO_4)_2$/**2**·$(ClO_4)_2$ was examined to probe the nature of the H-abstracting species, on the basis of the tertiary to secondary (C3/C2) C-H bond selectivity. The C3/C2 parameters in this reaction were small (the normalized C3/C2 ratio obtained was 3.6 for **1**·$(ClO_4)_2$ and 4.5 for **2**·$(ClO_4)_2$), and thus consistent with the implication of a highly reactive and poorly selective species. Finally, complex **1**·$(ClO_4)_2$/**2**·$(ClO_4)_2$ together with H_2O_2 oxidized *cis*-1,2-dimethylcylohexane (*cis*-DMCH) to both *cis*- and *trans*-1,2-dimethylcyclohexanol. The reaction took place without retention of *cis*-configuration, again implicating a radical reaction rather than a metal-based reaction. Overall, the reactivity patterns that arise from the oxidation of these mechanistic probes are consistent with Fenton-type activation of H_2O_2 to generate hydroxyl radicals that then attack the substrate, generating freely diffusing carbon-centered radicals.

Analogous reactions were carried out using peracids. When PAA was used as an oxidant, both the conversion and turnover numbers diminished (*cf.* paper II) but mCPBA gave a catalytic efficiency analogous to H_2O_2. An overall yield of 30% was obtained for complex **1**·$(ClO_4)_2$ with a TON of 23 for A and 6.9 for K, and complex **2**·$(ClO_4)_2$ produced an overall yield 32.5% with a TON of 22.3 for A, 10.2 for K 10.2 (*cf*. paper II). The A/K ratios were slightly increased in favour of the alcohol product (for complex **1**·$(ClO_4)_2$, A/K ~ 3; for complex **2**·$(ClO_4)_2$, A/K ~ 2). Furthermore, the KIE values estimated in the competitive oxidation of cyclohexane and its perdeuterated analogue were found to be higher than with H_2O_2 for both complexes (4.2 for complex **1**·$(ClO_4)_2$ and 4.5 for complex **2**·$(ClO_4)_2$). On the basis of the improved A/K ratio and the comparatively higher KIE values, a significant participation of hydroxyl radicals in the peracid-based oxidations may be excluded.

Further, selectivity probes indicated that oxidation with peracids involve species more selective than those involved with H_2O_2. For example, in the oxidation of adamantane by **1**· $(ClO_4)_2$/peracid, the C3/C2 parameters were found to be higher (the normalized C3/C2 ratio obtained for **1** was 15.8 with PAA and 11.4 with mCPBA, as opposed to 3.5 for H_2O_2). For complex **2**, the normalized C3/C2 parameters were 15.0 (with PAA) and 12.3 (with mCPBA). More interestingly, the C3/C2 selectivity/ratio in the oxidation of *cis*-DMCH by **1** was around 1 with H_2O_2, but this selectivity was found be approximately 12 with PAA/mCPBA. Finally, the oxidation of *cis*-DMCH was found to occur without stereoretention, pointing towards the existence of long-lived carbon-centered radicals.

Overall, the reactivity patters exhibited by the Fe(II) complexes in H_2O_2 or peracid media are comparable to those observed for $[Fe^{II}(N4Py)(CH_3CN)](ClO_4)_2$[51,52] suggesting that all these complexes follow the same mechanistic patterns under the conditions described above (*cf*. paper II for detailed discussion).

2.11 Summary and Conclusion

Two new pentadentate N5-donor ligands have been synthesized, and their corresponding Fe(II) complexes have been prepared and fully characterized. High valent Fe(IV) oxo complexes have been synthesized by reaction of the Fe(II) complexes with the two electron oxidant PhIO in CH_3CN. The Fe(IV) oxo complexes have been characterized by UV/Vis spectroscopy, high resolution mass spectrometry and Mössbauer spectroscopy. The Mössbauer spectra of the Fe(IV) oxo complexes have established that they contain low spin ($S = 1$) Fe(IV) ions, and this assignment is further supported by DFT calculations indicating an $S = 1$ ground state. The reactivities of the Fe(IV) oxo complexes have been investigated in hydrogen atom transfer (HAT) and oxygen atom transfer (OAT) processes. The HAT reactivity of the Fe(IV) oxo complexes has been modelled by DFT calculations which indicate a two-state reactivity model involving a spin crossover from the triplet ($S = 1$) ground state to a quintet ($S = 2$) transition state. Catalytic oxidation of alkane substrates by the Fe(II) complexes in H_2O_2 and peracid media have also been investigated. Measurement of kinetic isotope effects and the use of specific substrates as mechanistic probes indicate the involvement of hydroxyl radicals in the H_2O_2-based catalytic system, while in the peracid-based catalytic systems any significant participation of hydroxyl radicals can be excluded.

2.12 References

(1) C. Krebs, D. Galonic Fujimori, C. T. Walsh, J. M. Bollinger Jr., *Acc. Chem. Res.*, 2007, 40, 484-492.
(2) E. G. Kovaleva, J. D. Lipscomb, *Nat. Chem. Biol.*, 2008, 4, 186-193.
(3) E. L. Hegg, L. Que Jr., *Eur. J. Biochem.*, 1997, 250, 625-629.
(4) L. Que Jr., *Nat. Struct. Biol.*, 2000, 7, 182-184.
(5) K. D. Koehntop, J. P. Emerson, L. Que Jr., *J. Biol. Inorg. Chem.*, 2005, 10, 87-93.
(6) M. Costas, M. P. Mehn, M. P. Jensen, L. Que Jr., *Chem. Rev.*, 2004, 104, 939-986.
(7) P. C. A. Bruijnincx, G. van Koten, R. J. M. Klein Gebbink, *Chem. Soc. Rev.*, 2008, 37, 2716-2744.
(8) I. J. Clifton, L.-C. Hsueh, J. E. Baldwin, K. Harlos, C. J. Schofield, *Eur. J. Biochem.*, 2001, 268, 6625-6636.
(9) M. Sono, M. P. Roach, E. D. Coulter, J.H. Dawson, *Chem. Rev.*, 1996, 96, 2841-2887.
(10) B. J. Wallar, J. D. Lipscomb, *Chem. Rev.*, 1996, 96, 2625-2658.
(11) E. I. Solomon, T. C. Brunold, M. I. Davis, J. N. Kemsley, S. K. Lee, N. Lehnert, F. Neese, A. J. Skulan, Y. S. Yang, J. Zhou, *Chem. Rev.*, 2000, 100, 235-349.
(12) (a) J. M. Bollinger Jr., J. C. Price, L. M. Hoffart, E. W. Barr, C. Krebs, *Eur. J. Inorg. Chem.*, 2005, 4245-4254; (b) J. C. Price, E. W. Barr, B. Tirupati, J. M. Bollinger Jr., C. Krebs, *Biochemistry*, 2003, 42, 7497-7508.

(13) L. M. Hoffart, E. W. Barr, R. B. Guyer, J. M. Bollinger Jr., C. Krebs, *Proc. Natl. Acad. Sci. USA*, 2006, 103, 14738-14743.
(14) D. P. Galonic, E. W. Barr, C. T. walsh, J. M. Bollinger Jr., C. Krebs, *Nat. Chem. Biol.*, 2007, 3, 113-116.
(15) B. E. Eser, E. W. Barr, P. A. Frantom, L. Saleh, J. M. Bollinger Jr., C. Krebs, P. F. Fitzpatrick, *J. Am. Chem. Soc.*, 2007, 129, 11334-11335.
(16) A. J. Panay, M. Lee, C. Krebs, J. M. Bollinger Jr., P. F. Fitzpatrick, *Biochemistry*, 2011, 50, 1928-1933.
(17) M. L. Mathews, C. M. Krest, E. W. Barr, F. H. Vaillancourt, C. T. Walsh, M. T. Green, C. Krebs, J. M. Bollinger Jr., *Biochemistry*, 2009, 48, 4331-4343.
(18) K. Johnson-Winters, V. M. Purpero, M. Kavana, T. Nelson, G. R. Moran, *Biochemistry*, 2003, 42, 2072-2080.
(19) (a) C. Krebs, J. C. Price, J. Baldwin, L. Saleh, M. T. Green, J. M. Bollinger Jr., *Inorg. Chem.*, 2005, 44, 742-757; (b) J. C. Price, E. W. Barr, T. E. Glass, C. Krebs, J. M. Bollinger Jr., *J. Am. Chem. Soc.*, 2003, 125, 13008-13009; (c) J. M. Bollinger Jr., C. Krebs, *J. Inorg. Biochem.*, 2006, 100, 586-605.
(20) (a) J. Stubbe, J. W. Kozarich, *Chem. Rev.*, 1987, 87, 1107-1136; (b) S. M. Hecht, *Acc. Chem. Res.*, 1986, 19, 383-391; (c) J. W. Sam, X.-J. Tang, J. Peisach, *J. Am. Chem. Soc.*, 1994, 116, 5250-5256; (d) T. E. Westre, K. E. Loeb, J. M. Zaleski, B. Hedman, K. O. Hodgson, E. I. Solomon, *ibid*, 1995, 117, 1309-1313; (e) R. M. Burger, T. A. Kent, S. B. Horwitz, E. Munck, J. Peisach, *J. Biol. Chem.*, 1983, 258, 1559-1564.
(21) J. T. Groves, *J. Chem. Ed.*, 1985, 62, 928-931.
(22) L. Que Jr., R. Y. N. Ho, *Chem. Rev.*, 1996, 96, 2607-2624.
(23) H. M. Hanauske-Abel, A. M. Popowicz, *Curr. Med. Chem.*, 2003, 10, 1005-1019.
(24) H. M. Hanauske-Abel, V. J. Gunzler, *Theor. Biol.*, 1982, 94, 421-455.
(25) A. R. McDonald, L. Que Jr., *Coord. Chem. Rev.*, 2013, 257, 414-428.
(26) D. Wang, K. Ray, M. J. Collins, E. R. Farquhar, J. R. Frisch, L. Gomez, T. A. Jackson, M. Kerscher, A. Waleska, P. Comba, M. Costas, L. Que Jr., *Chem. Sci.*, 2013, 4, 282-291.
(27) J. England, J. O. Bigelow, K. M. V. Heuvelen, E. R. Farquhar, M. Martinho, K. K. Meier, J. R. Frisch, E. Munck, L. Que, Jr., *Chem. Sci.*, 2014, 5, 1204-1215.
(28) A. Company, G. Sabenya, M. Gonzalez-Bejar, L. Gomez, M. Clemancey, G. Blondin, A. J. Jasniewski, M. Puri, W. R. Browne, J. M. Latour, L. Que Jr., M. Costas, J. Perez-Prieto, J. Lloret-Fillol, *J. Am. Chem. Soc.*, 2014, 136, 4624-4633.
(29) O. Pestovsky, S. Stoian, E. L. Bominaar, X. Shan, E. Munck, L. Que Jr., A. Bakac, *Angew. Chem. Int. Ed.*, 2005, 44, 6871-6874.
(30) J. England, M. Martinho, E. R. Farquhar, J. R. Frisch, E. L. Bominaar, E. Munck, L. Que Jr., *Angew. Chem. Int. Ed.*, 2009, 48, 3622-3626.
(31) J. England, Y. Guo, E. R. Farquhar, V. G. Young Jr., E. Munck, L. Que Jr., *J. Am. Chem. Soc.*, 2010, 132, 8635-8644.
(32) D. C. Lacy, R. Gupta, K. L. Stone, J. Greaves, J. W. Ziller, M. P. Hendrich, A. S. Borovik, *J. Am. Chem. Soc.*, 2010, 132, 12188-12190.
(33) J. P. Bigi, W. H. Harman, B. Lassalle-Kaiser, D. M. Robles, T. A. Stich, J. Yano, R. D. Britt, C. J. Chang, *J. Am. Chem. Soc.*, 2012, 134, 1536-1542.
(34) J. England, Y. Guo, H. K. M. Van, M. A. Cranswick, G. T. Rohde, E. L. Bominaar, E. Munck, L. Que Jr., *J. Am. Chem. Soc.*, 2011, 133, 11880-11883.
(35) J.-U. Rohde, L. Que Jr., *Angew. Chem. Int. Ed.*, 2005, 44, 2255-2258.
(36) J.-U. Rohde, A. Stubna, E. L. Bominaar, E. Munck, W. Nam, L. Que Jr., *Inorg. Chem.*, 2006, 45, 64356445.
(37) C. V. Sastri, J. Lee, K. Oh, Y. J. Lee, J. Lee, T. A. Jackson, K. Ray. H. Hirao, W. Shin, J. A. Halfen, J. Kim, L. Que Jr., S. Shaik, W. Nam, *Proc. Natl. Acad. Sci. USA*, 2007, 104, 19181-19186.
(38) Y. Zhou, X. Shan, R. Mas-Balleste, M. R. Bukowski, A. Stubna, M. Chakrabarti, L. Slominski, J. A. Halfen, E. Munck, L. Que Jr., *Angew. Chem. Int. Ed.*, 2008, 47, 1896-1899.
(39) (a) H. Hirao, L. Que Jr., W. Nam, S. Shaik, *Chem. Eur.J.*, 2008, 14, 1740-1756; (b) H. Hirao, D. Kumar, L. Que Jr., S. Shaik, *J. Am. Chem. Soc.*, 2006, 128, 8590-8606; (c) K. B. Cho, S. Shaik, W.

Nam, *Chem. Commun.*, 2010, 46, 4511-4513; (d) D. Kumar, H. Hirao, L. Que Jr., S. Shaik, *J. Am. Chem. Soc.*, 2005, 127, 8026-8027; (e) H. Hirao, D. Kumar, W. Thiel, S. Shaik, *J. Am. Chem. Soc.*, 2005, 127, 13007-13018; (f) L. Bernasconi, M. J. Louwerse, E. J. Baerends, *Eur. J. Inorg. Chem.*, 2006, 3023-3033; (g) D. Janardanan, Y. Wang, P. Schyman, L. Que Jr., S. Shaik, *Angew. Chem. Int. Ed.*, 2010, 49, 3342-3345; (h) H. Chen, W. Lai, S. Shaik, *J. Phys. Chem. Lett.*, 2010, 1, 1533-1540; (i) C. Geng, S. Ye, F. Neese, *Angew. Chem. Int. Ed.*, 2010, 49, 5717-5720; (j) S. Ye, F. Neese, *Curr. Opin. Chem. Biol.*, 2009, 13, 89-9; (k) E. Godfrey, C. S. Porro, S. P. de Visser, *J. Phys. Chem. A*, 2008, 112, 2464-2468; (l) S. P. de Visser, K. Oh, A. R. Han, W. Nam, *Inorg. Chem.*, 2007, 46, 4632-4641; (m) S. P. de Visser, R. Latifi, L. Tahsini, W. Nam, *Chem. Asian J.*, 2011, 6, 493-504; (n) S. Shaik, H. Chen, D. Janardanan, *Nat. Chem.*, 2011, 3, 19-27.
(40) M. S. Seo, N. H. Kim, K. B. Chao, J. E. So, S. K. Park, M. Clemancey, R, Garcia-Serres, J. M. Latour, S. Shaik, W. Nam, *Chem. Sci.*, 2011, 2, 1039-1045.
(41) A. Decker, J.-U. Rohde, E. J. Klinker, S. D. Wong, L. Que Jr., E. I. Solomon, *J. Am. Chem. Soc.*, 2007, 129, 15983-15996.
(42) O. Pestovsky, A. Bakac, *J. Am. Chem. Soc.*, 2004, 126, 13757-13764.
(43) (a) A. C. McQuilken, Y. Jiang, M. A. Siegler, D. P. Goldberg, *J. Am. Chem. Soc.*, 2012, 134, 8758-8761; (b) S. Sahu, L. R. Widger, M. G. Quense, S. P. de Visser, H. Matsumura, P. Moenne-Loccoz, M. A. Siegler, D. P. Goldberg, *J. Am. Chem. Soc.*, 2013, 135, 10590-10593; (c) L. R. Widger, C. G. Davies, T. Yang, M. A. Siegler, O. Troeppner, G. N. L. Jameson, I. Ivanovic-Burmazovic, D. P. Goldberg, *J. Am. Chem. Soc.*, 2014, 136, 2699-2702; (d) S. Sahu, M. G. Quense, C. G. Davies, M. Durr, I. Ivanovic-Burmazovic, M. A. Siegler, S. P. de Visser, G. N. L. Jameson, D. P. Goldberg, *J. Am. Chem. Soc.*, 2014, 136, 13542-13545.
(44) J. Kaizer, E. J. Klinker, N. Y. Oh, J. U. Rohde, W. J. Song, A. Stubna, J. Kim, E. Munck, W. Nam, L. Que Jr., *J. Am. Chem. Soc.*, 2004, 126, 472-473.
(45) M. H. Lim, J.-U. Rohde, A. Stubna, M. R. Bukowski, M. Costas, R. Y. N. Ho, E. Munck, W. Nam, L. Que Jr., *Proc. Natl. Acad. Sci.*, 2003, 100, 3665-36670
(46) (a) (a) Goodgame, M.; Cotton, F. A. *J. Am. Chem. Soc.*, 1992, 84, 1543-1548; (b) Johnson, C. R.; Shepherd, R. E. *Inorg. Chem.*, 1983, 22, 3506-3513; (c) D. M. L. Goodgame, M. Goodgame, M. J. Weeks, *J. Chem. Soc.*, 1964, 5194-5199.
(47) G. Roelfes, M. Lubben, K. Chen, R. Y. N. Ho, A. Meetsma, S. Genseberger, R. M. Hermant, R. Hage, S. K. Mandal, V. G. Young Jr., Y. Zang, H. Kooijman, A. L. Spek, L. Que Jr., B. L. Feringa, *Inorg. Chem.*, 1999, 38, 1929-1936.
(48) A. K. Patra, M. M. Olmsted, P. K. Mascharak, *Inorg. Chem.*, 2002, 41, 5403-5409.

Chapter 3.

Stereospecific and selective C-H hydroxylation and C=C oxidation by H_2O_2 mediated by Fe(II) complexes of tetradentate ligands: steric and electronic influences on the reactivity

3.1 Introduction: Oxidative transformation of a chemical bond

For the purpose of this thesis, an oxidative transformation of a chemical bond can be defined as the addition/insertion of oxygen inside that bond. This chapter will focus on the oxidation of C-H and C=C bonds.

3.1.1 C-H bond oxidation

Carbon-hydrogen bonds are present in almost every organic substance including saturated hydrocarbons (alkanes). The high availability of hydrocarbons in Nature, e.g. in the form of natural gas or crude oil, makes them energy-rich and low-cost chemical feedstocks.[1] The activation/oxidation of C-H bonds to produce new feedstocks, e.g. alcohols, aldehydes, is of tremendous chemical and economic importance, and is therefore a major research subject for synthetic chemists. However, selective functionalization of C-H bonds is one of the most difficult transformations in organic synthesis. This is because C-H bonds are thermodynamically stable and relatively chemically inert, owing to their relative high bond dissociation energy (BDE) values. Industrial processes employ methodologies that require high temperature (endothermic reactions), and thus large energy consumption and high cost (see Scheme 1 for an example). The major drawback of these processes is the lack of chemoselectivity and regioselectivity, which is essential for the synthesis of valuable/desirable products.

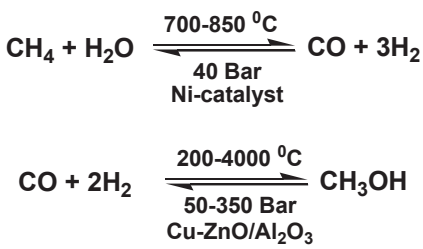

Scheme 1. Schematic depiction of the catalytic reactions involved in industrial production of methanol from methane.[2]

3.1.2 C=C bond oxidation

Alkenes/olefins contain C=C bonds and oxidations of olefins lead to formation of epoxides, *syn*-diols, alcohols, aldehydes, ketones etc. that serve as precursors for useful fine chemicals.[3] Selective oxidation of olefins is also a challenging field of synthetic research, and such oxidations will be discussed in Chapter 4.

3.2 Oxidation reactions in Nature

In Nature, enzymes that carry out the oxidation of substrates using molecular oxygen as oxidant are known as oxygenases. They are classified into two categories: (i) monooxygenases, which transfer one oxygen atom of O_2 into the substrate and convert the other oxygen atom into water and (ii) dioxygenases, which transfer both oxygen atoms of O_2 into the substrate.

Iron is found in the active sites of most of these mono- and dioxygenases. Amongst the various iron oxygenases, cytochrome P450, methane monooxygenases and Rieske oxygenases catalyze an array of extremely challenging oxidative transformations with a high degree of selectivity and catalytic efficiency.[4-5] Discovery and mechanistic investigations of these enzymes is thus a crucial starting point for contemporary catalysis research because they serve as the inspiration for the development of inexpensive, efficient, selective and green 'biomimetic' catalysts.[6-9] The cytochrome P450 enzymes have been extensively studied and their catalytic cycles have been well interpreted/established.[5] The C-H hydroxylation is carried out by an oxo-Fe(IV) porphyrin radical cation by 'rebound mechanism' as proposed by Groves *et al*.[10] Rieske oxygenases are considered to be the non-heme counterparts of cytochrome P450 enzymes and they catalyze a wide range of oxidative transformations that are more diverse than those associated with analogous heme enzymes.[4,11-13]. The next section will discuss this class of non-heme iron dependent enzymes in greater details.

3.3 Rieske oxygenases: Structure and function

Rieske oxygenases are multi-component non-heme iron enzymes found in bacteria.[4] They have two components in their active sites:[4] (I) an oxygenase component where O_2 activation and dihydroxylation of arenes take place and (II) a reductase component that mediates the electron transfer between NAD(P)H and the oxygenase component. In the oxygenase component, the active site contains an Fe(II) center bound to a 2-histidine-1-carboxylate facial motif. Figure 1 describes the active site structure of the oxygenase component of naphthalene 1,2-dioxygenase (NDO) from *Pseudomonas putida*.[14]

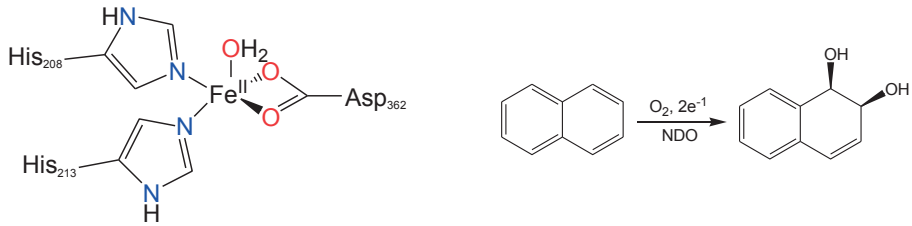

Figure 1. The active site structure (non-heme iron center) of naphthalene 1,2-dioxygenase (NDO), a class of Rieske dioxygenases (left); the *syn*-dihydroxylation of naphthalene catalyzed by NDO (right).

Rieske dioxygenases catalyze the regio- and stereospecific *cis*-dihydroxylation of arenes (Scheme 3), the first step in the biodegradation of pollutants, e.g. aromatic molecules by soil bacteria.[4,15-17] Besides *cis*-dihydroxylation, these enzymes are also known to catalyze benzylic hydroxylation, sulfoxidation, desaturation and O- and N-dealkylation.[15]

Naphthalene 1,2-dioxygenase catalyzes the *syn*-1,2-dihydroxylation of naphthalene (Figure 1). This is the best known enzyme amongst the Rieske oxygenases. The proposed mechanism for the reaction catalyzed by NDO is shown in Figure 2.[9] The catalytic cycle starts with an Fe center in its reduced state (+2) (resting state of the enzyme) that binds the naphthalene substrate, resulting in a loss of water ligand. The Fe(II) center reacts with dioxygen in conjunction with the transfer of one electron from the reductase component (called the Rieske [2Fe-2S] cluster) to form a Fe(III)-hydroperoxo intermediate. This intermediate has been characterized by time-resolved X-ray crystallography.[18] The Fe(III)-OOH intermediate is proposed to react with the substrate by two routes: (i) simultaneous O-O bond cleavage and substrate oxidation generates an Fe(IV) oxo intermediate (analogous to compound II in Cytochrome P450[5,19]) and a hydroxynapthhalene radical species (Figure 2) or, (ii) O-O bond cleavage first forms an Fe(V)(O)(OH) intermediate (analogous to compound I in the catalytic cycle of Cytochrome P450[5,19,20]), which subsequently reacts with naphthalene to form the Fe(III) alkoxyhydroxynaphthalene species (Figure 2).[4,11,21] In the next step, a second electron is transferred from the reductase component to form a Fe(II) alkoxyhydroxynaphthalene species. Finally, protonation of the alkoxide leads to the release of the *syn*-diol product and the regeneration of the resting state of the enzyme.

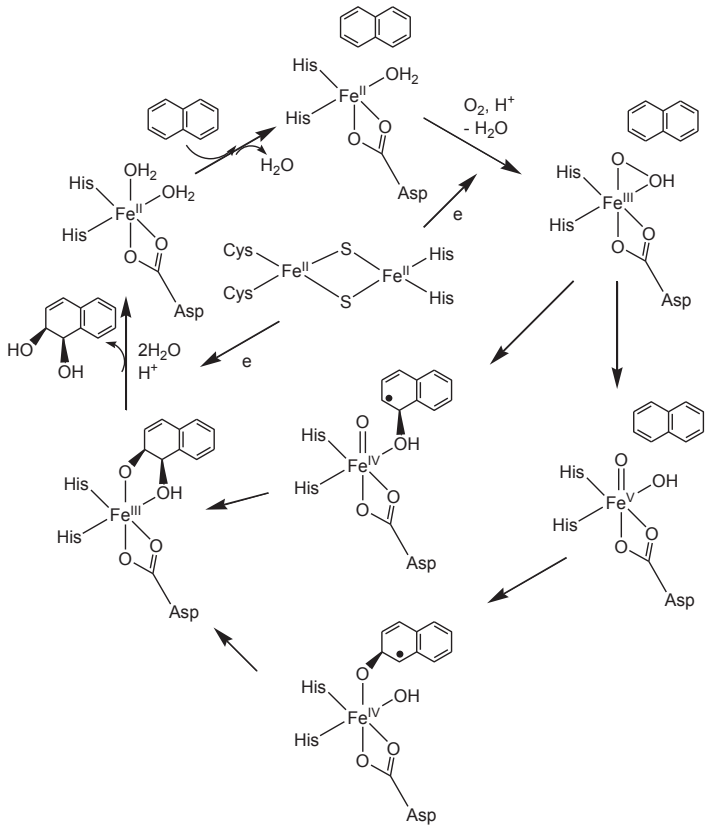

Figure 2. The proposed catalytic cycle for the dihydroxylation of naphthalene by naphthalene 1,2-dioxygenase (NDO).[9]

The fascinating chemistry exhibited by the non-heme iron-dependent oxygenases, in particular the Rieske oxygenases, has inspired synthetic chemists to attempt to achieve good catalytic efficiencies, as well as high degrees of stereospecificity and regio-selectivity with catalysts based on cheap and abundant iron, while using environmentally friendly oxidants such as O_2 or H_2O_2. An additional goal of this bioinspired approach has been to trap/isolate, identify and characterize high valent Fe(V) oxo intermediates analogous to those postulated in the catalytic cycles of Rieske oxygenases.

3.4 Model synthetic non-heme iron complexes: Background and motivation of the present study

There are several non-heme mononuclear iron catalysts that have been reported in the last decade that can perform enzyme-like metal based C-H oxidation without the involvement of free diffusing radicals.[22-26] Amongst these catalyst, the Fe(PyTACN)

family of complexes deserve particular attention owing to their ability to not only catalyze stereo- and regio-selective alkane hydroxylation, but also the epoxidation and *syn*-dihydroxylation reactions of olefins.[26-28] Mechanistic probes employed for these complexes implicate the involvement of an Fe(V)(O)(OH) active oxidant during the catalytic process.[26] The formation of such high valent Fe(V) oxo species has been further verified by variable-temperature mass spectroscopy (VT-MS),[29] EPR spectroscopy,[30] isotope labeling studies and DFT calculations.[27] The involvement of an iron(V)-oxo species as an active oxidant has also been proposed in some other catalytic systems.[31-33] In parallel, there are thus far three Fe(V) oxo complexes that have been fully characterized using spectroscopy.[34]

The Fe(V)(O)(OH) active oxidant (denoted as O in Figure 3) derived from the Fe(PyTACN) family of complexes can exist in two tautomeric forms, O_A and O_B, which are connected through a prototopic oxo-hydroxo tautomerism (involving proton shift from the hydroxide to the terminal oxo ligand).[27,29] Isotope labelling studies have shown that these complexes can incorporate a large percentage range (2-79%) of labelled oxygen from water into hydroxylated products; the level of ^{18}O incorporation provides indirect evidence for the relative reactivities of the two tautomers in C-H hydroxylation reactions.[27] The existence of this kind of tautomerism has also been postulated for [Fe(bpmen)] and [Fe(tpa)] families of the non-heme mononuclear iron complexes.[23a,31a] However, in the latter cases, the percentage of incorporation of labelled water incorporation is always less than 50% and this percentage is inversely related to the strength of the oxidized C-H bond,[31a] leading to a mechanistic scenario involving a competition between substrate attack (substrate with weaker C-H bonds reacts faster) and tautomerism, similar to that described for porphyrin-based systems.[35]

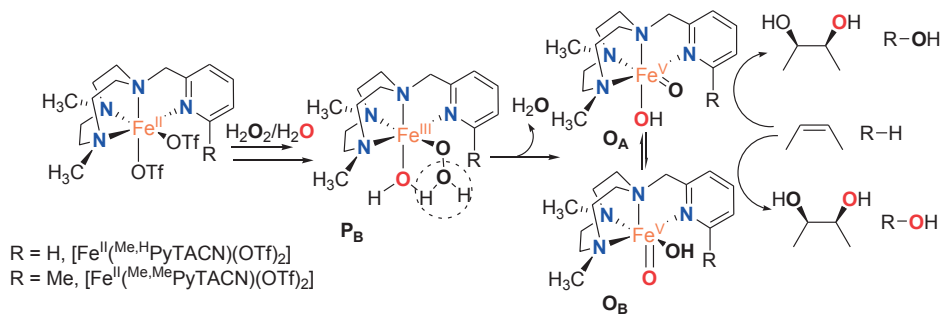

Figure 3. The oxo-hydroxo tautomerism observed in the Fe(PyTACN) family of complexes.

The relative reactivities of O_A and O_B is influenced by the nature of the ligand. Introduction of different electron-donating and -withdrawing groups (e.g. Me_2N, MeO, Me, NO_2, Cl, F etc.) in the α- and γ-positions of the pyridyl ring of PyTACN effects the relative reactivity of O_A and O_B both electronically and sterically.[36] This unique feature found in the Fe(PyTACN) systems served as an inspiration for further

exploration of ligand influence by replacing the pyridylmethyl arm of the PyTACN ligand with other moieties with different steric bulk and electron donating properties. This chapter describes a detailed investigation on the effects of different side arms connected to the TACN ring on the overall catalytic efficiency (in terms of regio- and stereoselectivity) of the new Fe(II) complexes and the discrepancy of the relative reactivities between the iron-oxo tautomers.

3.5 Ligands used in this study

In the present study, three new tetradentate N4 ligands were developed (Figure 4). These are based on the 'PyTACN' ligand framework where the pyridylmethyl arm of 'PyTACN' was replaced with either an (*N*-methyl)benzimidazolylmethyl arm (yielding the ^{Me2,Me}BzImTACN ligand), an (*N*-methyl)imidazolylmethyl arm (the ^{Me2,Me}ImTACN ligand), or a (3,5-dimethyl)pyrazolylethyl arm (the ^{Me2,Me2}PyzTACN ligand). The purpose of these modifications was to address the effects of steric and electronic properties of the side arms on the reactivity patterns of their Fe(II) complexes in the oxidative catalysis of alkanes and alkenes with hydrogen peroxide. The basicity order for the different side arms is as follows: (*N*-methyl)imidazole (pK_a of conjugate acid 7.06) > (*N*-methyl)benzimidazole (pK_a of conjugate acid 5.41) ~ pyridine (pK_a of conjugate acid 5.22) > (3,5-dimethyl)pyrazole (pK_a of conjugate acid 4.12). At the same time, the different heterocyclic N-donor moieties possess different steric bulkiness.

The details of the syntheses of all three ligands are described in papers III and IV.

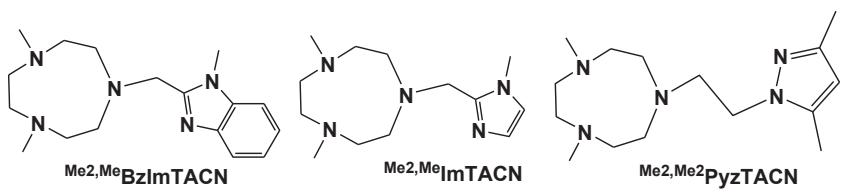

Figure 4. Structures of the tetradentate N4 ligands used in this study.

3.6 Synthesis and characterization of the Fe(II) complexes

The Fe(II) complexes of the three ligands were synthesized by reaction with $[Fe^{II}(CH_3CN)_2(CF_3SO_3)_2]$ (*cf.* paper II and III for detailed synthetic procedures). Figure 5 describes the structures of the three new Fe(II) complexes, $[Fe^{II}(^{Me2,Me}BzImTACN)(CF_3SO_3)_2]$ (**1**^{OTf}), $[Fe^{II}(^{Me2,Me}ImTACN)(CF_3SO_3)_2]$ (**2**^{OTf}) and $[Fe^{II}(^{Me2,Me2}PyzTACN)(CF_3SO_3)_2]$ (**3**^{OTf}). The three complexes were characterized by mass spectroscopy, ^{1}H-NMR spectroscopy, elemental analysis, IR-spectroscopy and UV/Vis spectroscopy (*cf.* papers III and IV for detailed characterizations). The ^{1}H-NMR spectra are paramagnetically shifted; they contain

broad peaks with a spectral window range from -20 to 140 ppm, indicating that the complexes possess high spin Fe(II) ions (*cf.* Supplementary Materials for papers III and IV).

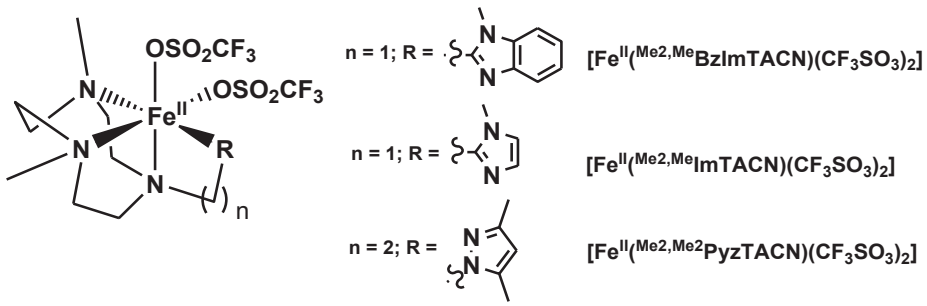

Figure 5. The structures of the Fe(II) complexes investigated in this study.

3.7 Crystal and molecular structures

Complexes $\mathbf{1}^{\mathbf{OTf}}$ and $\mathbf{3}^{\mathbf{OTf}}$ were also characterized by X-ray crystallography. The crystal structures (Figure 6) reveal that in both compounds, the Fe(II) center is in a distorted octahedral coordination environment with four sites occupied by the four nitrogen atoms of the tetradentate ligands, leaving two *cis*-sites available for binding with two triflate anions. The Fe-N and Fe-O bond distances lie in the ranges consistent with the presence of a high spin Fe(II) center, as reported for the Fe(PyTACN) family of complexes and other related Fe(II) complexes.[25a,36] The Fe-N(benzimidazole) bond distance is 2.134(7) Å in complex $\mathbf{1}^{\mathbf{OTf}}$ and the Fe-N(pyrazole) bond distance is 2.209(3) Å in complex $\mathbf{3}^{\mathbf{OTf}}$ (*cf.* papers III and IV for detailed crystallographic data, bond distances and bond angles) while the Fe-N (pyridine) bond distance is 2.165(4) Å in $[Fe^{II}(^{Me,H}PyTACN)(CF_3SO_3)_2]$[26a] and 2.246(2) Å in the more sterically hindered $[Fe^{II}(^{Me,Me}PyTACN)(CF_3SO_3)_2]$.[37]

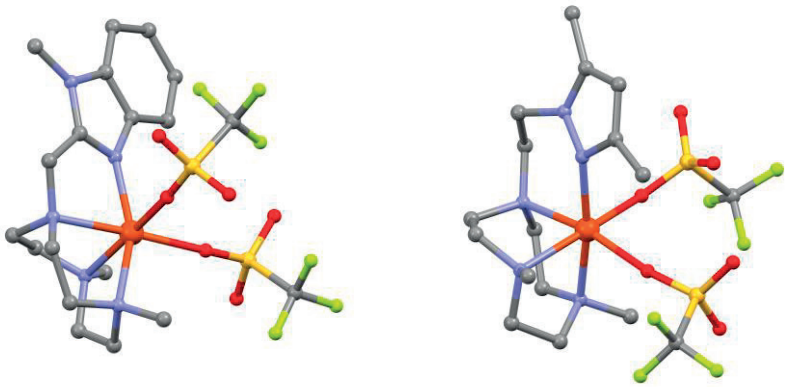

Figure 6. The molecular structures (Mercury plot) of [Fe^{II}(^{Me2,Me}BzImTACN)(CF_3SO_3)$_2$] (left) and [Fe^{II}(^{Me2,Me2}PyzTACN)(CF_3SO_3)$_2$] (right); hydrogen atoms have been omitted for clarity.

3.8 Catalytic oxidation studies

3.8.1 C-H bond oxidation of alkanes

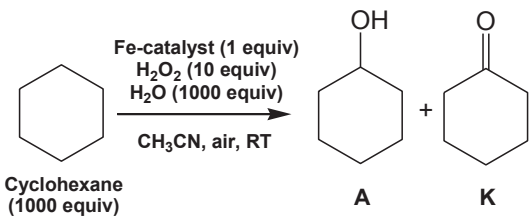

catalyst	TON(A)	TON(K)	A/K
1^{OTf}	8.5	0.8	10.6
2^{OTf}	7.7	0.6	12
3^{OTf}	6.5	0.7	9.4

Scheme 2. The catalytic oxidation of cyclohexane by H_2O_2 effected by the three new Fe(II) catalysts.

The three Fe(II) complexes were investigated in the catalytic oxidation of various alkanes, using H_2O_2 as a co-oxidant. Cyclohexane was employed first as a model substrate. All complexes oxidized cyclohexane efficienctly to form cyclohexanol (A) as the major product with a very small amount of formation of cyclohexanone (K) (Scheme 2) (*cf*. papers III and IV for detailed catalytic results). The A/K ratio was found to be high in all cases (in the range 9-12 for the three complexes, Scheme 2). The time-dependent formation of cyclohexanol from cyclohexane was monitored for complex $\mathbf{1}^{OTf}$; this experiment showed that the initial product was almost exclusively cyclohexanol (the A/K ratio was around 35) and cyclohexanone was formed by the subsequent overoxidation of cyclohexanol (Figure 7). This suggests

that for all three complexes, the active oxidant is metal-based and that any participation of a Russell-type termination mechanism initiated by hydroxyl radicals (leading to an A/K ratio ~ 1) may be ignored.

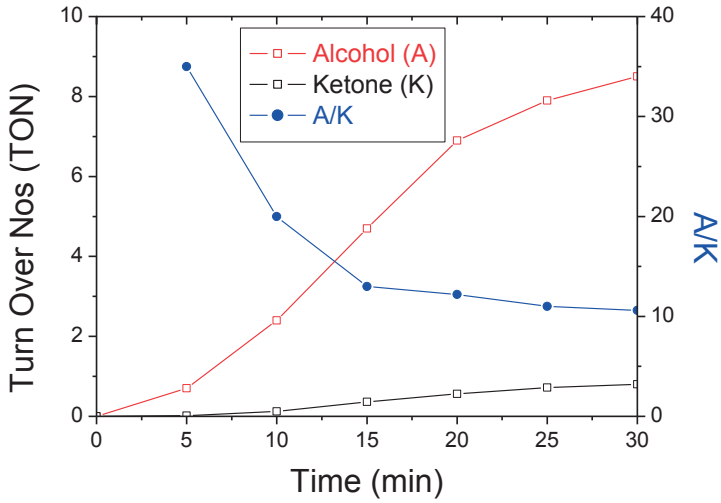

Figure 7. Time course for the oxidation of cyclohexane in presence of H_2O_2 catalyzed by $\mathbf{1}^{\mathbf{OTf}}$.

When the kinetic isotope effect (KIE) was determined in a competitive reaction between cyclohexane and its fully deuterated isotopomer, the values obtained for complexes $\mathbf{1}^{\mathbf{OTf}}$, $\mathbf{2}^{\mathbf{OTf}}$ and $\mathbf{3}^{\mathbf{OTf}}$ were 5.0, 4.6 and 4.0, respectively, supporting the assumption of the involvement of a metal based oxidant in the catalytic oxidation.

Several other mechanistic probes confirmed that the oxidation reactions were metal-based. For example, in the oxidation of adamantane, the normalized C3/C2 selectivity was found to be in the range 12-26 (*cf.* papers III and IV for details) suggesting a preference for tertiary C-H bonds over secondary C-H bonds. The oxidation of *cis*-DMCH was exclusively performed via the *cis*-retention of configuration of the product (*cf.* papers III and IV for details). All these results are consistent with the implication of a selective oxidant (i.e. metal-based oxidant) in the C-H hydroxylation reactions as observed in the Fe(PyTACN) family of complexes.

3.8.2 Oxidation of olefin substrates

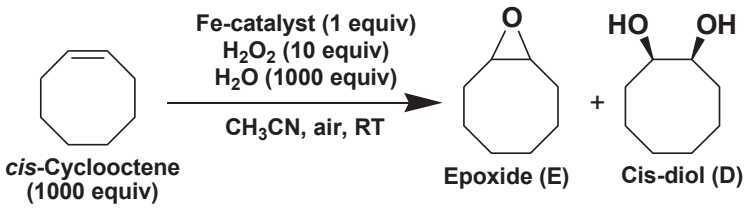

Scheme 3. *syn*-Dihydroxylation/epoxidation of *cis*-cyclooctene with H_2O_2 catalyzed by Fe(II) complexes.

Complexes $\mathbf{1}^{\mathbf{OTf}}$, $\mathbf{2}^{\mathbf{OTf}}$ and $\mathbf{3}^{\mathbf{OTf}}$ also catalyzed the oxidation of *cis*-cyclooctene to produce both *cis*-cycloctene epoxide (E) and *syn*-cycloctane-1,2-diol (D) (Scheme 3) (*cf.* papers III and IV for detailed analysis). The complexes $\mathbf{1}^{\mathbf{OTf}}$ and $\mathbf{2}^{\mathbf{OTf}}$ were found to slightly favour the formation of *syn*-diol over epoxide. Formation of *syn*-cyclooctane-1,2-diol is indicative of the involvement of an Fe(V)(O) oxidant (*vide supra*, Section 3.3) as originally proposed for the Fe(TPA) and Fe(BPMEN) complexes and subsequently observed for the Fe(PyTACN) family of complexes. Isotope labeling studies were able to provide further information re the nature of the active metal-based oxidant, as discussed below.

3.9 Isotope labeling study.

Isotope labeling is a very useful technique to characterize the nature of a metal-based oxidant and also to derive mechanistic conclusions. Therefore, these studies have also been employed in the present research. Complexes $\mathbf{1}^{\mathbf{OTf}}$, $\mathbf{2}^{\mathbf{OTf}}$ and $\mathbf{3}^{\mathbf{OTf}}$ incorporated different amounts (percentages) of ^{18}O into alcohol products in the oxidation of alkanes. In the presence of 10 eq of $H_2{}^{16}O_2$ and 1000 eq of $H_2{}^{18}O$, the levels of water incorporation into alcohol product in the oxidation of cyclohexane were 48, 39 and 3% for complexes $\mathbf{1}^{\mathbf{OTf}}$, $\mathbf{2}^{\mathbf{OTf}}$ and $\mathbf{3}^{\mathbf{OTf}}$, respectively (Scheme 4, *cf.* papers III and IV). Complementary experiments performed with 10 equiv of $H_2{}^{18}O_2$ and 1000 equiv of $H_2{}^{16}O$ showed that peroxide was the source of the remaining oxygen incorporated into the alcohol product.

Interestingly, in the oxidation of substrates containing tertiary C-H bonds (*cis*-DMCH and adamantane), the extent of incorporation of ^{18}O from water into products was dramatically affected by the specific catalyst used. For example, in the oxidation of *cis*-DMCH in the presence of 10 eq of $H_2{}^{16}O_2$ and 1000 eq of $H_2{}^{18}O$, complex $\mathbf{1}^{\mathbf{OTf}}$ incorporated 24% water into product while complex $\mathbf{2}^{\mathbf{OTf}}$ incorporated 31% water into product. However, under similar conditions, complex $\mathbf{3}^{\mathbf{OTf}}$ did not incorporate any significant amount of oxygen originating from water into the alcohol product.

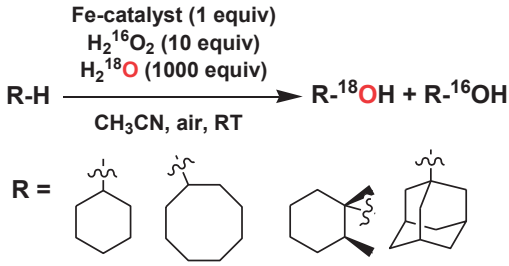

Scheme 4. Incorporation of labeled oxygen from $H_2{}^{18}O$ in C-H hydroxylation catalyzed by Fe(II) complexes.

All complexes incorporate > 90% of ^{18}O into the *syn*-diol product in the oxidation of *cis*-cyclooctene. These results suggest that for all three complexes, an Fe(V)(O)(OH) species containing one oxygen from water and the other oxygen from peroxide is responsible for the observed isotopic pattern. On the other hand, the extent of ^{18}O incorporation in the epoxide is different for each complex (Table 1).

Table 1. ^{18}O incorporation from $H_2{}^{18}O$ in C-H hydroxylation reactions mediated by different Fe(II)-complexes[(1)]

Substrate	Complex **1**^{OTf}	Complex **2**^{OTf}	Complex **3**^{OTf}	Complex **4**^{OTf} [(2)]	Complex **5**^{OTf} [(3)]
Cyclohexane	48	39	3	45	11
Cyclohexane -d_{12}	48	NA	3	40	NA
Cyclooctane	41	43	3	44	NA
Cis-DMCH	26	31	0	79	2
Adamantane	28	39	0	74	3
Cis-cyclooctene epoxide[(4)]	24	36	2	77	5
Syn-cyclooctane-1,2-diol[(4)]	98	92	97	97	78

[(1)] Reaction conditions: catalyst:H_2O_2:$H_2{}^{18}O$:substrate = 1:10:1000:1000, CH_3CN, RT, air; [(2)] [Fe^{II}(^{Me,H}PyTACN)(CF_3SO_3)$_2$]; [(3)] [Fe^{II}(^{Me,Me}PyTACN)(CF_3SO_3)$_2$]; [(4)] *cis*-cyclooctene was employed as the substrate.

3.10 Discussion

The three Fe(II) complexes are capable of catalyzing the hydroxylation of C-H bonds of alkanes with high efficiencies, selectivities and A/K ratios. These results are comparable to the Fe(PyTACN) family of complexes and therefore implicate similar mechanistic interpretations. The stereoretention in the oxidation of *cis*-DMCH, high selectivity in the oxidation of adamantane, and the KIE values strongly indicate that the reactions proceed by metal-based oxidation.

The isotope labeling study explains the origin of the oxygen atom in the alcohol products and the nature of the metal-based oxidant. The isotope labeling experiments performed on the complexes indicate that the oxygen atom(s) in the alcohol product (or, epoxide and *syn*-diol products) originates from the water and the peroxide (*vide supra*). On the basis of these observations, the mechanism that has already been established for the Fe(PyTACN) family of complexes (Scheme 5) can also be applied for the Fe(II) complexes $\mathbf{1}^{\mathbf{OTf}}$, $\mathbf{2}^{\mathbf{OTf}}$ and $\mathbf{3}^{\mathbf{OTf}}$.

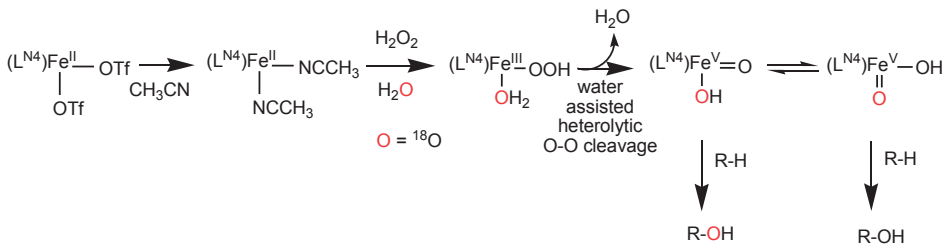

Scheme 5. The mechanism of C-H hydroxylation reaction catalyzed by Fe(II) complexes.

According to the proposed mechanism depicted in Scheme 5, a highly electrophilic $[Fe^{V}(O)(OH)(L^{N4})]^{2+}$ oxidant (O), is formed via water-assisted cleavage of the hydroperoxide intermediate $[Fe^{III}(OOH)(OH_2)(L^{N4})]^{2+}$ (see also Figs 2 and 3 above). Species O can exist in two tautomeric forms: O_A and O_B, which differ in the relative orientation of the side arm connected to TACN ring with respect to the Fe-oxo bond (*cf.* Fig 3 and Scheme 6). For example, in the case of $[Fe^{V}(O)(OH)(^{Me2,Me}BzImTACN)]^{2+}$, the tautomer O_A refers to the orientation of the (*N*-methyl)benzimidazolyl ring parallel to the Fe^{V}=O bond and O_B refers to the orientation of the (*N*-methyl)benzimidazolyl ring perpendicular to the Fe^{V}=O bond (Scheme 6). The relative reactivity of the O_A and O_B tautomers is influenced by the nature of the ligand, in particular the nature of the side arms of the TACN derivatized ligands (e.g. PyTACN, ^{Me2,Me}BzImTACN, ^{Me2,Me}ImTACN, ^{Me2,Me2}PyzTACN etc.), and the differences in the relative reactivities of the tautomers result in the different isotope labelling patterns exhibited by the corresponding Fe-complexes.

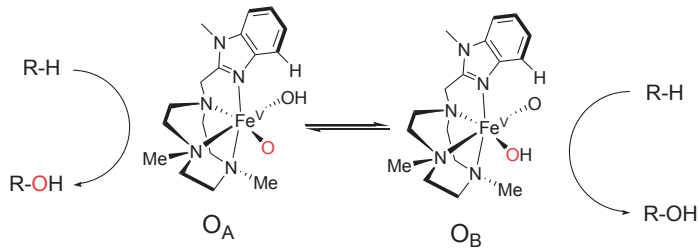

Scheme 6. The proposed structures of the two tautomers O_A and O_B of $[Fe^{V}(O)(OH)(^{Me2,Me}BzImTACN)]^{2+}$.

It appears that the steric bulk of the side arm dictates the relative reactivities of the tautomers. It has been found that for the Fe(PyTACN) family of complexes, there are two distinct categories: for class I catalysts, the tautomers O_A and O_B are equally active, resulting in a large percentage of incorporation of oxygen from water into the cyclohexanol product (39-50%), while for class II catalysts, O_B is more active than O_A, resulting in lower percentages of incorporation of water-derived oxygen into cyclohexanol.[27] For complexes $\mathbf{1}^{\mathbf{OTf}}$ and $\mathbf{2}^{\mathbf{OTf}}$, both O_A and O_B are operative in the oxidation of secondary C-H bonds, giving 39-48% ^{18}O-incorporated product from labelled water. However, when the substrate contains tertiary C-H bonds, O_B reacts faster than O_A in the case of complex $\mathbf{1}^{\mathbf{OTf}}$, resulting in lower ^{18}O incorporation (Table 2). On the other hand, for complex $\mathbf{2}^{\mathbf{OTf}}$, the reactivities of O_A and O_B are more or less comparable. These results suggest that the (*N*-methyl)benzimidazolyl moiety exerts a greater steric influence than the (*N*-methyl)imidazolyl moiety in protecting the approach of (a bulky) substrate towards the Fe-oxo unit of the O_A tautomer. This makes the tautomer O_B intrinsically more reactive than O_A, particularly for substrates containing tertiary C-H bonds. On the other hand, the very low level of incorporation of water-derived oxygen into hydroxylated products by $\mathbf{3}^{\mathbf{OTf}}$, regardless of secondary and tertiary C-H bonds, signifies that O_B performs the hydroxylation reaction exclusively and that the orientation of the methyl group of the substituted pyrazole side arm induces large steric inhibition on the Fe-oxo unit of O_A tautomer.

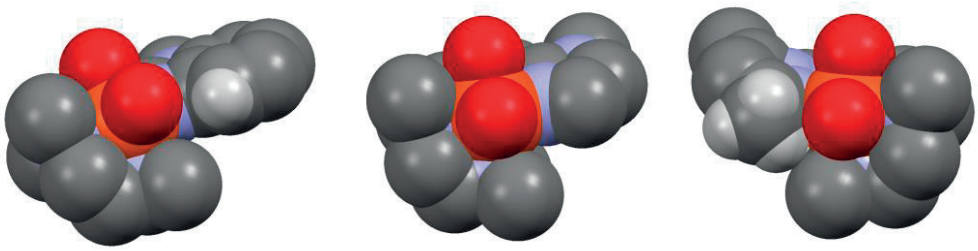

Figure 12. The space filling models (proposed) of the Fe(V)(O)(OH) species of complexes $\mathbf{1}^{\mathbf{OTf}}$ (left), $\mathbf{2}^{\mathbf{OTf}}$ (middle) and $\mathbf{3}^{\mathbf{OTf}}$ (right) obtained by modifying the crystal structures of $\mathbf{1}^{\mathbf{OTf}}$ and $\mathbf{3}^{\mathbf{OTf}}$.

As discussed above, it should be noted that the pyrazole, (*N*-methyl)imidazole and (*N*-methyl)benzimidazole groups have different basicities. Electronic influence on the overall reactivity of the Fe(V)(O)(OH) oxidant can therefore not be excluded, but the possible influence of electronic factors remains to be investigated.

3.11 Summary and conclusion

Three new tetradentate N4 ligands have been prepared. The corresponding Fe(II) complexes have been synthesized and fully characterized. The catalytic C-H hydroxylation of alkanes and olefin oxidation reactions by the three Fe(II) complexes have been investigated using H_2O_2. All complexes exhibit high efficiencies with large A/K ratios, suggesting the reactions to be metal-based oxidation. The large KIE values together with high C3/C2 selectivity in adamantane oxidation and high stereoretention in oxidation of *cis*-DMCH further support the involvement of metal-based oxidants. Isotope labelling experiments performed with these complexes indicate that the active oxidant is an Fe(V)(O)(OH) species which is formed via water assisted heterolytic O-O cleavage of an Fe(III)(HOOH)(OH_2) species. The Fe(V)(O)(OH) species can exist in two tautomeric forms. Isotope labelling studies have shown that the two tautomeric forms have distinct reactivity with a particular substrate and that reactivity is dependent on the nature of the ligand and the substrate. On basis of the isotope labelling studies, the relative reactivities of the two tautomers are attributed to the steric effects exhibited by the different side arm(s) of the tetradentate ligands.

3.12 References

(1) S. Friedle, E. Reisner, S. J. Lippard, *Chem. Soc. Rev.*, 2010, 39, 2768-2779.
(2) J. H. Lunsford, *Catal. Today*, 2000, 63, 165-174.
(3) E. I. Karasevich, V. S. Kulikova, A. E. Shilov, A. A. Shteinman, *Russ. Chem. Rev.*, 1998, 67, 335-355.

(4) M. Costas, M. P. Mehn, M. P. Jensen, L. Que Jr., *Chem. Rev.*, 2004, 104, 939-986.
(5) P. R. Ortiz de Montellano, J. J. De Voss, Eds.; *Cytochrome P450: Structure, Mechanism and Biochemistry*, 3rd ed.; Springer-Verlag: New York, 2008.
(6) N. J. Turner, *Chem. Rev.*, 2011, 111, 4073-4087.
(7) L. Que Jr., W. B. Tolman, *Nature*, 2008, 455, 333-340.
(8) R. E. Parales, S. M. Resnick, *In Applications of Aromatic Hydrocarbons Dioxygenases in Biocatalysis in the Pharmaceutical and Biotechnology Industries*, R. N. Patel, Ed.; CRC Press: Boca Raton, Fl, 2006.
(9) S. M. Barry, G. L. Challis, *ACS Catal.*, 2013, 3, 2362-2370.
(10) J. T. Groves, G. A. McClusky, R. E. White, M. J. Coon, *Biochem. Biophys. Res. Commun.*, 1978, 81, 154-160.
(11) E. G. Kovaleva, J. D. Lipscomb, *Nat. Chem. Biol.*, 2008, 4, 186-193.
(12) M. M. Abu-Omar, A. Loiza, N. Hontzeas, *Chem. Rev.*, 2005, 105, 2227-2252.
(13) P. C. A. Bruijnincx, G. V. Koten, R. J. M. Klein Gebbink, *Chem. Soc. Rev.*, 2008, 37, 2716-2744.
(14) B. Kauppi, K. Lee, E. Carredano, R. E. Parales, D. T. Gibson, H. Eklund, S. Ramaswamy, *Structure*, 1998, 6, 571-586.
(15) D. T. Gibson, S. M. Resnick, K. Lee, J. M. Brand, D. S. Torok, L. P. Wackett, M. J. Schocken, B. E. Haigler, *J. Bacteriol*. 1995, 177, 2615-2621.
(16) D. M. Jerina, J. W. Daly, A. M. Jeffrey, D. T. Gibson, *Arch. Biochem. Biophys.*, 1971, 142, 394-396.
(17) M. D. Wolfe, J. V. Parales, D. T. Gibson, J. D. Lipscomb, *J. Biol. Chem.*, 2001, 276, 1945-1953.
(18) A. Karlsson, J. V. Parales, R. E. Parales, D. T. Gibson, H. Eklund, S. Ramaswamy, *Science*, 2003, 299, 1039-1042.
(19) I. G. Denisov, T. M. Makris, S. G. Sligar, I. Schlichting, *Chem. Rev.*, 2005, 105, 2253-2277.
(20) J. Rittle, M. T. Green, *Science*, 2010, 330, 933-937.
(21) T. D. H. Bugg, S. Ramaswamy, *Curr. Opin. Chem. Biol.*, 2008, 12, 134-140.
(22) M. Costas, K. Chen, L. Que Jr., *Coord. Chem. Rev.*, 2000, 200-202, 517-544.
(23) (a) K. Chen, L. Que Jr., *J. Am. Chem. Soc.*, 2001, 123, 6327-6337; (b) C. Kim, K. Chen, J. Kim, L. Que Jr., *J. Am. Chem. Soc.*, 1997, 110, 5964-5965.
(24) (a) M. S. Chen, M. C. White, *Science*, 2007, 318, 783-787; (b) N. A. Vermeulen, M. Sc Chen, M. C. White, *Tetrahedron*, 2009, 65, 3078-3084; (c) M. S. Chen, M. C. White, *Science*, 2010, 327, 566-571; (d) M. A. Bigi, S. A. Reed, M. C. White, *Nat. Chem.*, 2011, 3, 218-222; (e) L. Gomez, I. Garcia-Bosch, A. Company, J. Benet-Buchholz, A. Polo, X. Sala, X. Ribas, M. Costas, *Angew. Chem. Int. Ed.*, 2009, 48, 5720-5723; (f) P. Liu, Y. Liu, E. L.-M. Wong, S. Xiang, C.-M. Che, *Chem. Sci.*, 2011, 2, 2187-2195; (g) Y. Hitomi, K. Arakawa, T. funabiki, M. Kodera, *Angew. Chem. Int. Ed.*, 2012, 51, 3448-3452; (h) M. C. White, *Science*, 2012, 335, 807-809.
(25) (a) J. England, G. J. P. Britovsek, A. J. P. White, *Inorg. Chem.*, 2005, 44, 8125-8134; (b) J. England, G. J. P. Britovsek, N. Rabadia, A. J. P. White, *Inorg. Chem.*, 2007, 46, 3752-3767; (c) J. England, C. R. Davies, M. Banaru, A. J. P. White, G. J. P. Britovsek, *Adv. Synth. Catal.*, 2008, 350, 883-897; (d) J. England, R. Gondhia, L. Bigorra-Lopez, A. R. Petersen, A. J. P. White, G. J. P. Britovsek, *Dalton Trans.*, 2009, 5319-5334.
(26) (a) A. Company, L. Gomez, M. Guell, X. Ribas, J. M. Luis, L. Que Jr., M. Costas, *J. Am. Chem.. Soc.*, 2007, 129, 15766-15767; (b) A. Company, L. Gomez, X. Fontrodona, X. Ribas, M. Costas, *Chem. Eur. J.*, 2008, 14, 5727-5731.
(27) I. Prat, A. Company, V. Postils, X. Rivas, L. Que Jr., J. M. Luis, M. Costas, *Chem. Eur. J.*, 2013, 19, 6724-6738.
(28) I. Prat, D. Font, A. Company, K. Junge, X. Ribas, M. Beller, M. Costas, *Adv. Synth. Catal.*, 2013, 355, 947-956.
(29) I. Prat, J. S. Mathienson, M. Guell, X. Ribas, J. M. Luis, M. Cronin, M. Costas, *Nat. Chem.*, 2011, 3, 788-793.
(30) O. Y. Lyakin, I. Prat, K. P. Bryliakov, M. Costas, E. P. Talsi, *Catal. Commun.*, 2012, 29, 105-108.
(31) (a) K. Chen, L. Que Jr., *Chem. Commun.*, 1999, 1375-1376; (b) M. Costas, L. Que Jr., *Angew. Chem.*, 2002, 114, 2283-2285; (c) K. Chen, M. Costas, J. Kim, A. K. Tipton, L. Que Jr., *J. Am. Chem. Soc.*, 2002, 124, 3026-3035; (d) S. H. Lee, J. H. Han, H. Kwak, S. J. Lee, E. Y. Lee, H. J. Kim, J. H.

Lee, C. Bae, S. N. Lee, Y. Kim, C. Kim, *Chem. Eur. J.*, 2007, 13, 9393-9398; (e) J. Yoon, S. A. Wilson, Y. K. Jang, M. S. Seo, K. Nehru, B. Hedman, K. O. Hodgson, E. Bill, E. I. Solomon, W. Nam, *Angew. Chem. Int. Ed.*, 2009, 121, 1283-1286; (f) P. Das, L. Que Jr., *Inorg. Chem.*, 2010, 49, 9479-9485.
(32) (a) D. Quinonero, K. Morokuma, D. G. Musaev, R. Mas-Balleste, L. Que Jr., *J. Am. Chem. Soc.*, 2005, 127, 6548-6549; (b) A. Bassan, R. A. M. Blomberg, E. M. P. Seigbahn, L. Que Jr., *Chem. Eur. J.*, 2005, 11, 692-705; (c) A. Bassan, R. A. M. Blomberg, E. M. P. Seigbahn, L. Que Jr., *Angew. Chem. Int. Ed.*, 2005, 44, 2939-2941; (d) A. Bassan, R. A. M. Blomberg, E. M. P. Seigbahn, L. Que Jr., *J. Am. Chem. Soc.*, 2002, 124, 11056-11063.
(33) (a) O. Y. Lyakin, R. V. Ottenbacher, K. P. Bryliakov, E. P. Talsi, *ACS Catal.*, 2012, 2, 1196-1202; (b) O. Y. Lyakin, K. P. Bryliakov, E. P. Talsi, *Inorg. Chem.*, 2011, 50, 5526-5538; (c) O. Y. Lyakin, K. P. Bryliakov, G. J. P. Britovsek, E. P. Talsi, *J. Am. Chem. Soc.*, 2009, 131, 10798-10799.
(34) (a) F. T. De Oliveira, A. Chanda, D. Banarjee, X. Shan, S. Mondal, L. Que Jr., E. L. Bominaar, E. Munck, T. J. Collins, *Science*, 2007, 315, 835-838; (b) K. M. Van Heuvelen, A. T. Fiedler, X. Shan, R. F. De Font, K. K. Meier, E. L. Bominaar, E. Munck, L. Que Jr., *Proc. Natl. Acad. Sci. USA*, 2012, 109, 11933-11938; (c) M. Ghosh, K. K. Singh, C. Panda, A. Weitz, M. P. Hendrich, T. J. Collins, B. B. Dhar, S. Sen Gupta, *J. Am. Chem. Soc.*, 2014, 136, 9524-9527.
(35) J. Bernadou, B. Meunier, *Chem. Commun.*, 1998, 2167-2173.
(36) I. Prat, A. Company, T. Corona, T. Parella, X. Ribas, M. Costas, *Inorg. Chem.*, 2013, 52, 9229-9244.
(37) P. Spannring, I. Prat, M. Costas, M. Lutz, P. C. A. Bruijnincx, B. M. Weckhuysen, R. J. M. Klein Gebbink, *Catal. Sci. Technol.*, 2014, 4, 708-716.

Chapter 4.

Asymmetric epoxidation of olefins by hydrogen peroxide, catalyzed by non-heme Fe(II) complexes of chiral tetradentate ligands

4.1 Introduction

Epoxidation reactions involve the formation of three membered cyclic ethers (epoxides) through oxidation of C=C bonds. Epoxides are used as versatile intermediates in organic syntheses owing to their inherent polarity and strained structure, making them susceptible to attack by nucleophiles, electrophiles, acids, bases etc.[1] This chapter deals with asymmetric epoxidation of olefins.

4.2 Asymmetric epoxidation

Asymmetric epoxidation is one of the most synthetically important organic transformation reactions since it can produce optically active (chiral) epoxides with up to two stereogenic centers.[1] Chiral epoxides are used as precursors to many biologically active chiral molecules that are useful in pharmacy and the chemical industry.[1]

The cytochromes P450 constitute a very large and versatile family of thiolate-ligated heme-containing enzymes and are amongst the most well studied metalloenzymes.[1f,2] They catalyze a wide range of oxidation reactions of biological relevance, including olefin epoxidations, using molecular oxygen as terminal oxidant with excellent efficiency.[2] These enzymes have thus inspired chemists to investigate the use of porphyrin-based iron catalysts in asymmetric epoxidation reactions. Groves and coworkers reported the first asymmetric epoxidation catalyzed by a chiral iron porphyrin complex.[3] Thereafter, several other chiral metalloporphyrin-based catalysts have been reported for asymmetric epoxidation.[1f,4-7]

Other transition metal-based catalysts have been extensively employed for epoxidation reactions in the last three decades. In this area, the investigations by Katsuki and Sharpless on the epoxidation of allylic alcohols (Scheme 1)[8] and the development of manganese salen complexes in the epoxidation of unfunctionalized alkenes by Katsuki *et al*[9] and Jacobsen *et al*[10] are particularly notable.

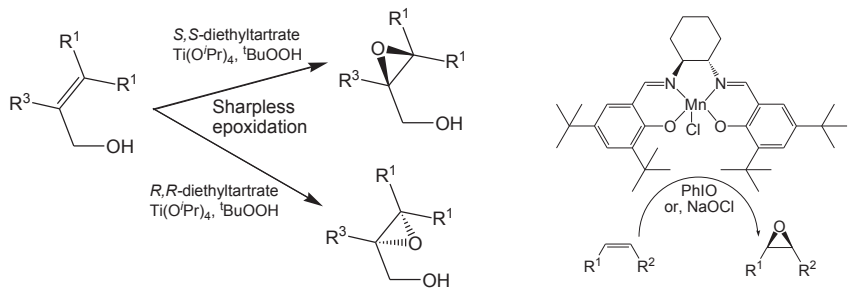

Scheme 1. Sharpless epoxidation of benzylic alcohols (left) and Jacobsen's catalyst for (asymmetric) epoxidation of olefins (right).

4.3 Asymmetric epoxidation of olefins using synthetic non-heme ion complexes: Background and motivation for the present study

Iron-based catalytic systems have often found potential interest because of the inexpensiveness, non-toxicity and ready availability of iron.[11] Although iron porphyrin-based catalysts have been well studied for a long time (*vide supra*), non-heme iron-based catalysts have been much less explored. In 2007, Beller and co-workers reported a new library of ligands for the iron-catalyzed epoxidation of stilbene derivatives with high enantioselectivity, using H_2O_2 as the oxidant.[12] These studies bore promise for future development of non-heme iron-based catalysts for such oxidations. Many other iron complexes have thereafter been prepared in order to improve the efficiency and enantioselectivity in asymmetric epoxidation reactions, and some of these complexes have been found to exhibit very promising catalytic properties.[7,13-15] The use of novel chiral iron-based catalysts together with green oxidants such as dioxygen or H_2O_2 has become a growing research area in the field of asymmetric epoxidation.

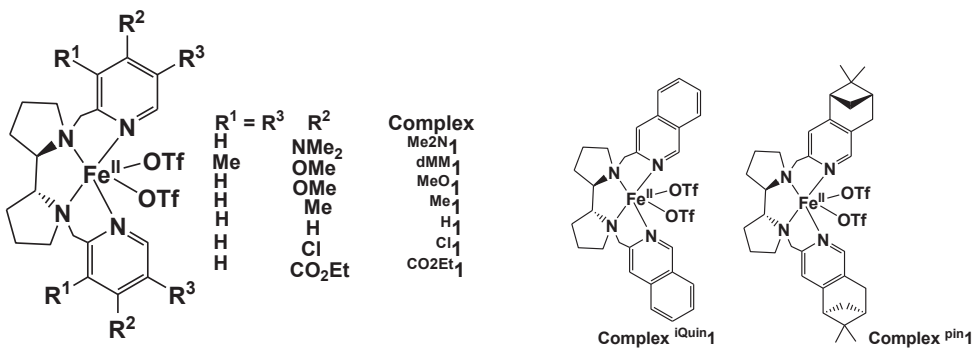

Figure 1. Structures of non-heme Fe(II) complexes bearing chiral ligands that have been utilized for asymmetric epoxidation of olefins.[15]

The development of efficient iron catalysts for asymmetric epoxidation is a challenging task. The factors that determine/affect the efficiency (in terms of substrate conversion or product yield) and enantioselectivity are not understood and therefore need to be thoroughly investigated. It has been previously observed that the presence of a catalytic amount of carboxylic acid can enhance the yield as well as enantioselectivity in iron-based catalytic systems.[13d,15] Costas and coworkers have investigated the electronic properties of the ligands on the catalytic properties of a series of Fe(II) complexes in asymmetric epoxidation reactions (Figure 1).[15] It was found that complex ^{Me2N}**1** (Fig 1) showed excellent catalytic efficiency with high enantioselectivity.[15] Assuming the formation of a high-valent iron-oxo active oxidant, the high activity of ^{Me2N}**1** might be explained by the electron-donating property of the ligand, which may enhance the electrophilicity of the iron-oxo moiety to give high conversion into products.[15] However, proper mechanistic investigations that can explain the high catalytic efficiency of complex ^{Me2N}**1** remain to be undertaken. The present study aimed to examine the possible effects on iron-based asymmetric epoxidation reactions of systematic replacement of the pyridyl moieties of the PDP framework (Figure 1) with (*N*-methyl)benzimidazolyl moieties.

4.4 Ligands used in this present study

The present work has been developed on the basis of two chiral tetradentate ligands L^1 (1-methyl-2-({(*S*)-2-[(*S*)-1-(1-methylbenzimidazol-2-ylmethyl)pyrrolidin-2-yl]pyrrolidin-1-yl} methyl)benzimidazole) and L^2 (1-methyl-2-({(*S*)-2-[(*S*)-1-(pyridin-2-ylmethyl)pyrrolidin-2-yl]pyrrolidin-1-yl}methyl)benzimidazole) (Figure 2). Ligand L^1 has a symmetric structure with two (*N*-methyl)benzimidazolylmethyl moieties being attached to the two nitrogen atoms of the chiral bispyrrolidine backbone. On the other hand, ligand L^2 has an asymmetric structure with one pyridylmethyl moiety and one (*N*-methyl)benzimidazolylmethyl moiety being attached to the two nitrogen atoms of the chiral bispyrrolidine backbone.

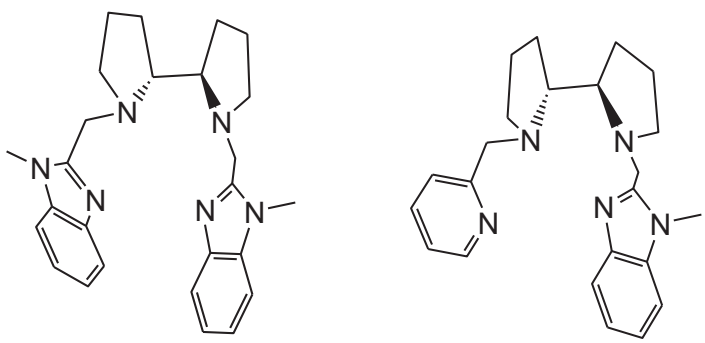

Figure 2. The structures of the chiral tetradentate N4 ligands L^1 (top left) and L^2 (top right) used in this study.

Ligand L^1 was synthesized in one step by reaction of one equiv of (*S*,*S*)-2,2'-bispyrrolidine D-tartrate with 2.3 equiv of 2-(chloromethyl)-1-methylbenzimidazole in the presence of excess base (1M NaOH solution) (Scheme 2). Ligand L^2 was synthesized in two steps (Scheme 2). In the first step, one equiv of (*S*,*S*)-2,2'-bispyrrolidine D-tartrate was reacted with one equiv of 2-(chloromethyl)pyridine hydrochloride in the presence of excess NaOH to form 2-{(*S*)-2-[(*S*)-pyrrolidin-2-yl]pyrrolidin-1-yl)methyl}pyridine (it may be noted that there is only one unique chiral product because of the identical chiralities of the two stereogenic centers of the bispyrrolidine backbone). In the second step, one equiv. of 2-{(*S*)-2-[(*S*)-pyrrolidin-2-yl]pyrrolidin-1-yl)methyl}pyridine was reacted with one equiv of 2-(chloromethyl)-1-methylbenzimidazole in the presence of excess NaOH solution to give the desired ligand L^2.

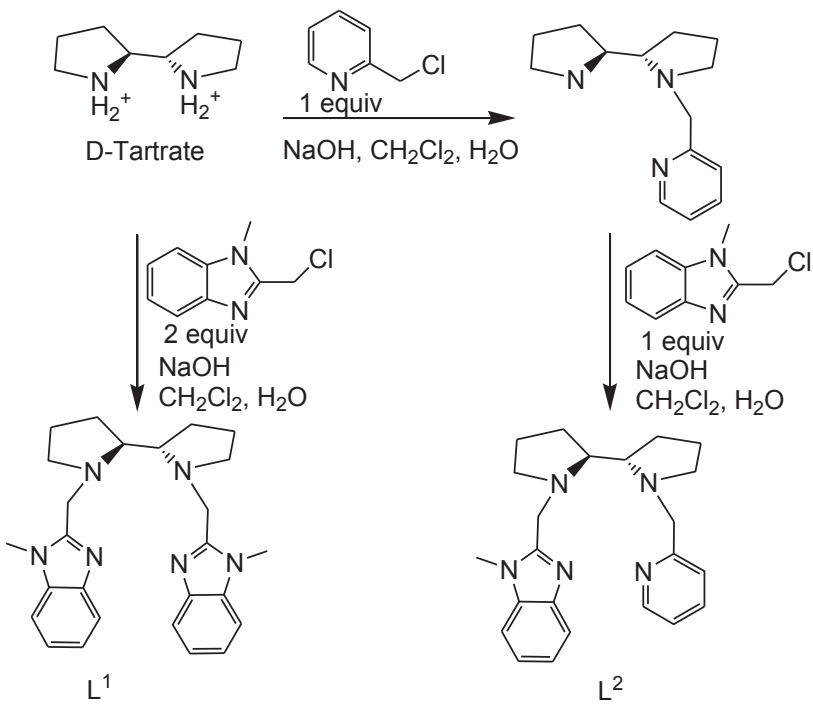

Scheme 2. Schematic presentation of the synthetic routes to ligands L^1 and L^2.

4.5 Synthesis and characterization of the Fe(II) complexes

The Fe(II) complexes of the two chiral ligands L^1 and L^2, namely $[Fe^{II}(L^1)(CF_3SO_3)_2]$ ($\mathbf{1^{OTf}}$) and $[Fe^{II}(L^2)(CF_3SO_3)_2]$ ($\mathbf{2^{OTf}}$) (Figure 3), were synthesized by reaction of L^1 or L^2 with an equimolar amount of

$[Fe^{II}(CH_3CN)_2(CF_3SO_3)_2]$ (*cf.* paper V for experimental conditions). Both complexes were obtained as off-white solids. Complex $\mathbf{1}^{\mathbf{OTf}}$ was characterized by high resolution mass spectroscopy, ^{1}H-NMR spectroscopy and FT-IR spectroscopy (*cf.* paper V). The characterization of complex $\mathbf{2}^{\mathbf{OTf}}$ is underway.

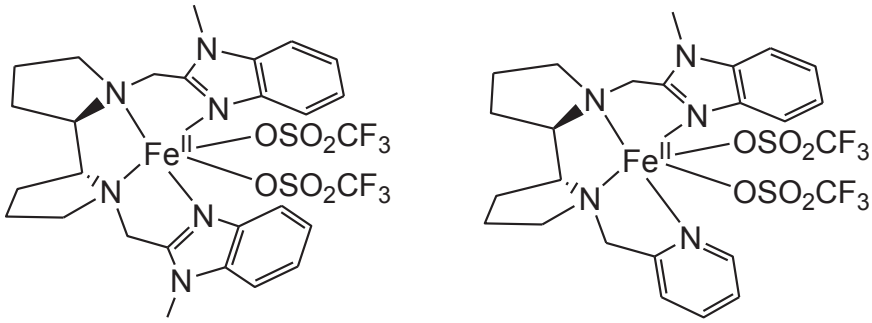

Figure 3. The structures of the Fe(II) complexes, $[Fe^{II}(L^1)(CF_3SO_3)_2]$ (top left) and $[Fe^{II}(L^1)(CF_3SO_3)_2]$ (top right).

4.6 Crystal and molecular structure of complex $\mathbf{1}^{\mathbf{OTf}}$.

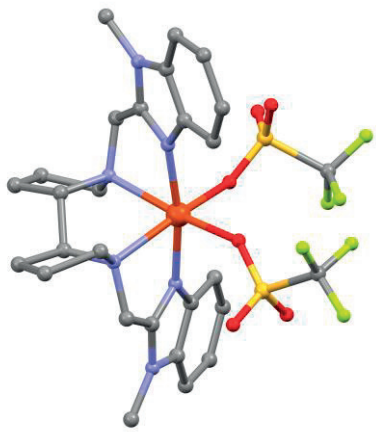

Figure 4. The crystal structure (Mercury plot) of complex $\mathbf{1}^{\mathbf{OTf}}$; H-atoms have been omitted for clarity.

The crystal structure of complex $\mathbf{1}^{\mathbf{OTf}}$ (Figure 4) reveals that the Fe(II) center is in a distorted octahedral coordination environment with four sites being occupied by the nitrogen atoms of the chiral ligand and the two *cis*-sites being occupied by two triflate anions. The Fe-N and Fe-O bond distances are in agreement with the presence of a high spin Fe(II) center. A detailed description of the molecular structure of this complex is found in paper V.

4.7 Catalytic asymmetric epoxidation study.

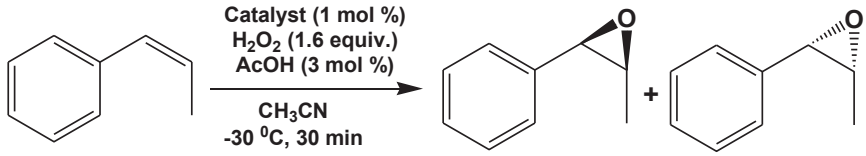

Scheme 3. Catalytic epoxidation of *cis*-β-methylstyrene with H_2O_2 by an Fe catalyst in the presence of acetic acid as an additive.

The complex $\mathbf{1}^{\mathbf{OTf}}$ catalyzed the epoxidation of *cis*-β-methylstyrene to form the two chiral epoxides with a total yield of 60% and an enantiomeric excess (ee) value of 41% (Scheme 3). The catalytic experiment was performed under conditions similar to those reported earlier in order to enable direct comparison between this catalyst and the series of related iron catalysts reported by Costas and coworkers[15] (Figure 1 and Table 1).

Table 1. Comparison of conversion of substrate (*cis*-β-methylstyrene), yield of epoxides and ee's for different Fe catalysts (*cf*. Figure 1).

Entry	Catalyst	AcOH (mol%)	Conversion in % (Yield of epoxides in %)	ee (%)
1	$\mathbf{1}^{\mathbf{OTf}}$	3	84 (60)	41
2	$^{\mathbf{Me2N}}\mathbf{1}$	3	100(87)	62
3	$^{\mathbf{H}}\mathbf{1}$	3	49(26)	19
4	$^{\mathbf{Cl}}\mathbf{1}$	3	32(15)	16
5	$^{\mathbf{CO2Et}}\mathbf{1}$	3	31(13)	21
6	$^{\mathbf{Me}}\mathbf{1}$	3	31(17)	30
7	$^{\mathbf{MeO}}\mathbf{1}$	3	38(26)	38
8	$^{\mathbf{dMM}}\mathbf{1}$	3	82(67)	38
9	$^{\mathbf{pin}}\mathbf{1}$	3	53(41)	30
10	$^{\mathbf{iQuin}}\mathbf{1}$	3	34(15)	19

As seen in Table 1, complex $\mathbf{1}^{\mathbf{OTf}}$ is an efficient catalyst for the epoxidation of *cis*-β-methylstyrene by H_2O_2, and is surpassed only by $^{\mathbf{Me2N}}\mathbf{1}$ under the same reaction conditions.

The catalytic efficiency of this complex was also investigated for the oxidation of the cyclic enone substrate 2-cyclohex-1-one, which is relatively hard to oxidize. The detailed catalytic results are described in paper V. The collective results indicate that $\mathbf{1}^{\mathbf{OTf}}$ is able to epoxidize the alkene substrate with good enantioselectivity (> 80%); however, the yields of the epoxide products are low (< 20%) and the conversion of

substrate is moderate. The low yield and conversion may be due to deactivation of the catalyst being more rapid than substrate conversion, when the substrate is not itself rapidly oxidized.

The mechanism of acetic acid-assisted iron-catalyzed epoxidation of olefins was first proposed by Que and co-workers.[16] It is proposed that an Fe(III)-carboxylate species reacts with H_2O_2 to form an iron(III)-acylperoxo intermediate. Such an intermediate has been trapped very recently by Que and co-workers.[17] In the next step, acid-assisted heterolytic cleavage of the O-O bond of the iron(III)-acylperoxo intermediate results in the formation of the active oxidant, an oxoiron(V) carboxylate species that transfers the oxygen to the olefin substrate. Spectroscopic studies by Talsi and co-workers[18] and computational studies by Rajaraman *et al*.[19] support the formation of an oxoiron(V) carboxylate intermediate. On the other hand, Que, Shaik *et al*.[20] have carried out computational modeling that suggests that the carboxylate has a redox non-innocent nature and therefore can donate an electron to the metal center to form an oxoiron(IV) carboxyl radical intermediate that serves as the oxygen donor to the substrate (a situation similar to the formation of compound I for Cytochrome P450, where the ferryl moiety is coupled with a porphyrin □-cation radical, *cf*. Section 3.2). A similar catalytic cycle for complex $\mathbf{1}^{\mathbf{OTf}}$ can be inferred for the asymmetric epoxidation of olefins (Scheme 4).

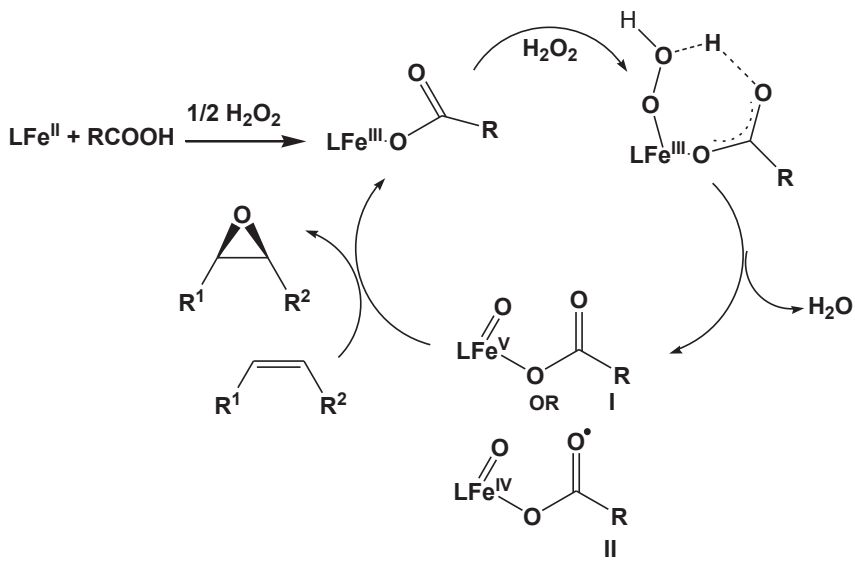

Scheme 4. The proposed catalytic cycle for olefin epoxidation by non-heme iron-complexes.

4.8 Summary and conclusion

Two new chiral tetradentate N4 ligands, L^1 and L^2, have been synthesized and fully characterized. Ligand L^1 is symmetric and L^2 is an asymmetric ligand. The Fe(II) complex of ligand L^1 has been fully synthesized and characterized. The catalytic activity of this Fe complex in asymmetric epoxidation reactions of olefins, using H_2O_2 as the oxidant, has been investigated and the initial results indicate that the complex has the potential to initiate good enantioselective epoxidation, but the yields are relatively poor. Further investigations using various other olefin substrates as well as using other reaction conditions (e.g. catalyst loading, carboxylic acid loading) to optimize the yields are warranted. Furthermore, detailed characterization and investigation of the catalytic activity of the Fe(II) complex of the asymmetric ligand L^2 are in progress.

4.9 References

(1) (a) M. J. Porter, J. Skidmore, *Chem. Comm.*, 2000, 1215-1225; (b) B. S. Lane, K. Burgess, *Chem. Rev.*, 2003 103, 2457-2473; (c) Q. H. Xia, H. Q. Ge, C. P. Ye, Z. M. Liu, K. X. Su, *Chem. Rev.*, 2005, 105, 1603-1662; (d) O. A. Wong, Y. Shi, *Chem. Rev.*, 2008, 108, 3958-3987; (e) D. Diez, M. G. Nunez, A. B. Anton, P. Garcia, R. F. Moro, N. M. Garrido, I. S. Marcos, P. Basabe, J. G. Urones, *Curr. Org. Synth.*, 2008, 5, 186-216; (f) K. Matsumoto, T. Kasturi, In *Catalytic Asymmetric Synthesis*, 3rd ed., Ed.: I. Ojima, Wiley-VCH, New York, 2010, pp. 839-890; (g) G. De Faveri, G. Ilyashenko, M. Watkinson, *Chem. Soc. Rev.*, 2011, 40, 1722-1760.
(2) A. D. N. Vaz, D. F. McGinnity, M. J. Coon, *Proc. Natl. Acad. Sci.*, 1998, 95, 3555-3556.
(3) J. T. Groves, R. S. Myers, *J. Am. Chem. Soc.*, 1983, 105, 5791-5796.
(4) E. Rose, B. Andrioletti, S. Zrig, M. Quelquejeu-Etheve, *Chem. Rev.*, 2005, 34, 573-583.
(5) (a) J. P. Collman, Z. Wang, A. Straumanis, M. Quelquejeu, E. Rose, *J. Am. Chem. Soc.*, 1999, 121, 460-461; (b) C. Perollier, J. Pecaut, R. Ramasseul, J.-C. Marchon, *Inorg. Chem.*,1999, 38, 3758-3759; (c) E. Rose, Q. Z. Ren, B. Andrioletti, *Chem. Eur. J.*, 2004, 10, 224-230; (d) A. Berkessel, M. Frauenkron, *J. Chem. Soc. Perkin Trans. 1*, 1997, 2265-2266; (e) R. Zhang, W.-Y. Yu, T.-S. Lai, C.-M. Che, *Chem. Commun.*, 1999, 409-410; (f) A. Berkessel, P. Kaiser, J. Lex, *Chem. Eur. J.*, 2003, 9, 4746-4756. (6)
(6) (a) J. P. Collman, J. I. Brauman, P. D. Hampton, H. Tanaka, D. S. Bohle, R. T. Hembre, *J. Am. Chem. Soc.*, 1992, 114, 7980-7984; (b) Y. Naruta, N. Ishihara, F. Tani, K. Maruyama, *Bull. Chem. Soc. Jpn.*, 1993, 66, 158- ; (c) J. Sundermeyer, *Angew. Chem. Int. Ed.*, 1993, 32, 1144-1146; (d) J. P. Collman, V. J. Lee, X. Zhang, J. A. Ibers, J. I. Brauman, *J. Am. Chem. Soc.*, 1993, 115, 3834-3835.
(7) H. Srour, P. L. Maux, S. Chevance, G. Simonneaux, *Coord. Chem. Rev.*, 2013, 257, 3030-3050.
(8) T. Katsuki, K. B. Sharpless, *J. Am. Chem. Soc.*, 1980, 102, 5974-5976.
(9) (a) R. Irie, K. Noda, Y. Ito, N. Matsumoto, T. katsuki, *Tetrahedron Lett.*, 1990, 31, 7345-7348; (b) T. Katsuki, *Coord. Chem. Rev.*, 1995, 140, 189-214.
(10) (a) W. Zhang, J. L. Leobach, S. R. Wilson, E. N. Jacobsen, *J. Am. Chem. Soc.*, 1990, 112, 2801-2803; (b) E. N. Jacobsen, W. Zhang, A. R. Muci, J. R. Ecker, L. Deng, *J. Am. Chem. Soc.*, 1991, 113, 7063-7064.
(11) (a) L. Que Jr., W. B. Tolman, *Nature*, 2008, 455, 333-340; (b) E. B. Bauer, *Curr. Org. Chem.*, 2008, 12, 1341-1369; (c) S. Enthaler, K. Junge, M. Beller, *Angew. Chem. Int. Ed.*, 2008, 47, 3317-3321; (c) A. Correa, O. G. Mancheno, C. Bolm, *Chem. Soc. Rev.*, 2008, 8, 1108-1117; (d) L.-X. Liu, *Curr. Org. Chem.*, 2010, 14, 1099-1126; (e) C.-L. Sun Chang-Liang, B.-J. Li, Z.-J. Shi, *Chem. Rev.*, 2011, 111, 1293-1314; (f) M. Darwish, M. Wills, *Catal. Sci. Technol.*, 2012, 2, 243-255; (g) K. Gopalaiah, *Chem. Rev.*, 3013, 113, 3248-3296.

(12) F. G. Gelalcha, B. Bitterlich, G. Anilkumar, M. K. Tse, M. Beller, *Angew. Chem. Int. Ed.*, 2007, 46, 7293-7296.
(13) (a) F. G. Gelalcha, G. Anilkumar, M. K. Tse, A. Bruckner, M. Beller, *Chem. Eur. J.*, 2008,14, 7687-7698; (b) M. Wu, C.-X. Miao, S. Wang, X. Hu, C. Xia, F. E. Kuhn, W. Sun, *Adv. Synth. Catal.*, 2011, 353, 3014-3022; (c) O. Lyakin, R. V. Ottenbacher, K. P. Bryliakov, E. P. Talsi, *ACS Catalysis*, 2012, 2, 1196-1202; (d) K. A. Stingl, K. M. Weib, S. B. Tsogoeva, *Tetrahedron*, 2012, 68, 8493-8501; (e) T. Niwa, M. Nakada, *J. Am. Chem. Soc.*, 2012, 134, 13538-13541; (f) B. Wang, S. Wang, C. Xia, W. Sun, *Chem. Eur. J.*, 2012, 18, 7332-7335; (g) X. Wang, C. Miao, S. Wang, C. Xia, W. Sun, *ChemCatChem*, 2013, 5, 2489-2494; (h) V. A. Yazerski, A. Orue, T. Evers, H. Kleijn, R. J. M. Klein Gebbink, *Catal. Sci. Technol.*, 2013, 3, 2810-2818
(14) Y. Nishikawa, H. Yamamoto, *J. Am. Chem. Soc.*, 2011, 133, 8432-8435.
(15) O. Cusso, I. Garcia-Bosch, X. Ribas, J. Lloret-Fillol, M. Costas, *J. Am. Chem. Soc.*, 2013, 135, 14871-14878.
(16) R. Mas-Balleste, L. Que Jr., *J. Am. Chem. Soc.*, 2007, 129, 15964-15972.
(17) W. N. Oloo, K. K. Meier, Y. Wang, S. Shaik, E. Munck, L. Que Jr., *Nat. Commun.*, 2014,
(18) (a) O. Y. Lyakin, K. P. Bryliakov, E. P. Talsi, *Inorg. Chem.*, 2011, 50, 5526-5538; (b) O. Y. Lyakin, K. P. Bryliakov, G. J. P. Britovsek, E. P. Talsi, *J. Am. Chem. Soc.*, 2009, 131, 10798-10799.
(19) A. Ansari, A. Kaushik, G. Rajaraman, *J. Am. Chem. Soc.*, 2013, 135, 4235-4249.
(20) Y. Wang, D. Janardanan, D. Usharani, K. Han, L. Que Jr., S. Shaik, *ACS Catal.*, 2013, 3, 1334-1341.

Chapter 5.

Concluding remarks

Nature uses specific enzymes to carry out specific reactions that are essential for the sustainability of living organisms. This remarkable feature is an underlying reason for most biomimetic research. The goals of such biomimetic studies are to (i) unravel and/or understand the structure and function of a certain enzyme of interest (ii) replicate the function of the enzyme.

5.1 Summary of the present work

The present work describes some functional models of non-heme mononuclear iron oxygenases. The focus of this work is based on two aspects of the enzymatic systems: (i) catalytic properties and (ii) formation (and isolation) of high valent ferryl (Fe(IV) oxo) species.

Two pentadentate nitrogen donor-based ligands have been developed for the purpose of generation and characterization of non-heme Fe(IV) oxo complexes. First, the Fe(II) complexes of these two ligands have been synthesized and fully characterized. Then, the corresponding Fe(IV) oxo complexes have been prepared and characterized by various spectroscopic techniques. The reactivities of these Fe(IV) oxo complexes have been examined towards hydrogen-atom transfer reactions, using a number of alkane substrates, and oxygen-atom transfer reactions using thioanisole. The rates of the reactivities have been measured and these values suggest that both complexes are efficient catalysts for both C-H activation and O-atom transfer. Computational modelling of the transition states of the H-atom transfer process have been performed and they have provided information on the mechanism(s) of C-H activation by the Fe(IV) oxo complexes.

The catalytic properties of Fe(II) complexes have also been investigated. The catalytic activities of the two Fe(II) complexes that are based on the above-mentioned pentadentate ligands have been found to be moderate, and similar to those of some related pentadentate ligand-based Fe(II) complexes. Theoretical studies have been performed to illustrate the catalytic reaction mechanism. In addition, three new tetradentate N4 ligands have been synthesized and their Fe(II) complexes have been fully characterized. These Fe(II) complexes have been found to perform efficient catalytic oxidation of alkanes and alkenes using hydrogen peroxide as co-oxidant. The mechanistic probes have been studied to elucidate the nature of the active oxidant and for the complexes based on tetradentate ligands, the reactions are proposed to proceed via the involvement of Fe(V) oxo-hydroxo species. Such an

active intermediate has been proposed in the catalytic cycle of Rieske oxygenases. Isotope labeling experiments have been performed to understand the origin of oxygen atom in the hydroxylated products. The steric and electronic properties of the ligands have been investigated to draw a dependency of the origin of the oxygen atom to the relative reactivities of the two taotomers of the Fe(V)(O)(OH) species.

Two chiral ligands and their Fe(II) complexes have been synthesized for the purpose of effecting asymmetric epoxidation reactions using the environmentally friendly oxidant hydrogen peroxide. Experiments performed on one of Fe(II) complexes have shown that it is capable of oxidizing olefins with high enantioselectivity. Further investigations of the two complexes are ongoing.

5.2 Future perspective of the present work

The present work has opened some new directions towards catalysis research and the modulation of the reactivity of synthetic high valent ferryl (or, perferryl) complexes by utilizing properly designed ligands. The study provides further understanding of the impact of electron rich/donating sites surrounding the metal center in non-heme mononuclear iron oxygenases (Chapter 2). As and extension, different and more electron-donating ligand moieites can be introduced to attempt modulation of the reactivity of ferryl species in oxidation reactions in a predictable way. The present work will also be useful to construct such ligands and to understand the basics of high valent Fe(IV) oxo chemistry. Furthermore, these studies also emphasise the role of ligands on the catalytic efficiencies mediated by non-heme Fe(II) complexes.

Developing efficient, low cost catalysts that can be utilized in industry remains a challenging task for the synthetic chemists. The studies summarized in Chapters 2-4 provide some useful understanding on how catalyst properties may be tuned by modification of the side arms of a ligand. The excellent catalytic properties of the Fe(II) complexes suggest that they can also be employed for oxidations of many other organic substrates of interest. The trapping and characterization of Fe(V) oxo species is another future aspect of this present work. The Fe(II) complexes of symmetric and asymmetric chiral ligands warrant thorough investigation as catalysts for asymmetric epoxidation reactions. It is likely that both the yields of epoxide products and the enantioselectivities of the reactions may be improved by optimizing the reaction conditions, including carboxylic acid loading and catalyst loading.

Populärvetenskaplig sammanfattning på svenska

Denna avhandling beskriver funktionella modellkomplex för icke-heminnehållande oxygenas-enzymer där enzymernas aktiva säten innehåller en järnjon. Sådana enzymer katalyserar ett brett spektrum av oxidationsreaktioner med biologisk relevans, vilka utnyttjar molekylärt syre som oxidationsmedel. Dessa reaktioner utförs på ett regio- och stereoselektivt sätt och med hög verkningsgrad. Reaktionerna har föreslagits ske via skapande av högvalenta Fe(IV)-oxo eller Fe(V)-oxo-intermediat, och sådana Fe(IV)-oxo-enheter har påvisats i vissa enzymer. Den intressanta och användbara reaktivitet som dessa enzymer uppvisar har inspirerat forskare att utveckla syntetiska modellkomplex av övergångsmetaller som kan brukas inom katalysforskning och, i ett förlängt perspektiv, industriell katalys. Modellkomplexen har utformats genom att fokusera på antingen de strukturella aspekterna av det aktiva sätet i vissa enzymer, eller på de funktionella aspekterna av enzymerna; vissa modellkomplex kan efterlikna både strukturella och funktionella aspekter hos enzymerna. Reaktivitetsstudier av modellkomplex kan användas för att nå insyn i mekanismerna för såväl den fullständiga enzymatiska reaktionen som vissa delsteg i denna reaktion. Ett fåtal modellkomplex som innehåller högvalenta Fe(IV/V)-oxo-enheter har framställts och deras reaktivitet har undersökts noggrannt.

Molekylärt syre är ett miljövänligt och därför önskvärt oxidationsmedel. Ett närbesläktat alternativt oxidationsmedel som är nästan lika miljövänligt är väteperoxid. Mycken katalysforskning har fokuserats på att använda syntetiska järnkomplex som katalysatorer med syre eller väteperoxid som ”gröna” oxidationsmedel.

Forskningen som beskrivs i denna avhandling syftar till att efterlikna den katalytiska aktiviteten hos icke-heminnehållande järn-oxygenaser och att bidra till karakterisering och reaktivitetsstudier av högvalenta Fe(IV)-oxo-intermediat. Två högvalenta Fe(IV)-oxo-komplex har karakteriserats och deras reaktivitetsmönster indikerar att ligander med goda elektrongivande egenskaper kan öka hastigheten på de reaktioner som utgör delsteg i oxidationen av kolväten. Dessa observationer hjälper oss att förstå varför vissa elektrondonerande sidokedjor till aminosyror (imidazolringen i histidin, carboxylatenheterna i aspartat och glutamat) är vanligt förekommande i de aktiva sätena hos många metallenzymer som fungerar som oxygenaser; dessa aminosyror hjälper till att stabilisera de högvalenta järn-oxo-intermediat som utför själva oxygeneringsprocessen.

Oxidation av alkaner och alkener som katalyseras av Fe(II)-komplex beskrivs i avhandlingen. Dessa komplex visade sig vara i stånd att utföra oxidation av kolväten med hög stereospecificitet, selektivitet och utmärkt effektivitet. Reaktionerna utfördes med hjälp av väteperoxid som oxidationsmedel, och i närvaro av vatten.

Vatten spelar en viktig roll i dessa reaktioner eftersom det underlättar bildandet av ett katalytiskt aktivt (L)Fe(V)(O)(OH)-komplex genom att klyva en syre-syrebindning i ett (L)Fe(III)(OOH)(OH2)-intermediat (L=ligand). De fyrtaligt koordinerande ligander som användes i dessa reaktioner visade sig påverka reaktivitetsmönstren för Fe(V)(O)(OH)-komplexen. Ursprunget till de syreatomer som införlivades i de oxiderade produkterna studerades med hjälp av isotopmärkningsexperiment och datormodellering. Dessa studier bekräftade att reaktionerna troligen fortskrider via bildandet av ett Fe(III)(OOH)(OH2)-intermediat som i sin tur ger upphov till ett Fe(V)(O)(OH)-komplex.

Avhandlingen behandlar också asymmetriska epoxideringsreaktioner som bildar optiskt aktiva epoxider. En epoxid är en cyklisk (triangulär) kol-kol-syre-enhet. Vissa epoxider kan vara optiskt aktiva (den optiska aktiviteten är beroende av identiteten hos de specifika substituenter som är bundna till kolen i den cykliska epoxidenheten). Sådana optiskt aktiva epoxider är mycket användbara startmaterial för framställande av biologiskt och industriellt viktiga molekyler. Relativt lite forskning har fokuserats på användande av järnkomplex som katalysatorer för asymmetriska epoxideringsreaktioner, men detta forskningsområde utvecklas nu snabbt. En optiskt aktiv isomer av en epoxid kan skapas genom användande av en optiskt aktiv katalysator. Avhandlingen innehåller ett exempel på ett Fe(II)-komplex som bär en optiskt aktiv ligand; denna järnförenings förmåga att katalysera syntes av optiskt aktiva epoxider genom reaktioner av alkener med väteperoxid har undersökts.

Acknowledgement

It has been a wonderful 4 years and 3 months of nice and long experience in research and day-to-day life while staying in Sweden. It would have never been possible for me to accomplish my PhD without acknowledging the following people.

First, I would like to thank and express my gratitude to my supervisor *Ebbe Nordlander* for allowing me to work in this interesting research field, for your very friendly and active guidance and for creating a healthy environment inside the lab.

I would like to thank *Albert Shteinman* for your enthusiasm in developing such a nice project, encouraging me in work and discussing the chemistry whenever I needed your help. I also like to thank *Hassan Nimir* for your friendly co-operation with me in some of the syntheses and fruitful discussions.

I would like to thank *Miquel Costas* and *Julio Lloret-Fillol* in Spain for your active guidance in my project and kindness in allowing me to work during my visits in Girona. I would like to thank *Franc Meyer* and *Serhiy Demeshko* in Germany for the assistance in Mössbauer measurement during my visits to Göttingen and discussing my project. I like to thank *Wesley Browne* in the Netherlands for your kindness in allowing me to work in your lab and *Matti Haukka* in Finland for solving crystal structures and *Michael G. Richmond* in U.S.A. for computational works.

I like to thank *Sofi Elmroth*, my co-supervisor, *Ola Wendt* and *Villy Sundström*, the head of the department for your kind assistance and attention whenever I looked for.

I would like to thank all my present lab members (*Ahmed*, *Ahibur*, *Amber*, *Satish*, *Kamal*, *Erik*) and past lab members (*Reena*, *Kamlesh*, *Biswanath*, *Martin*, *Arup*, *Amrendra*, *Lotta*, *Manjula*) for providing wonderful lab atmosphere and helping me whenever I needed. I also like to thank *Alex* and *Bob* for your nice contributions in my project and for the time I spent with you in playing table tennis. I also like to thank my friends here in Sweden and back in India.

I like to thank *Maria Levin* for your kind help in sorting out all administrative works, *Anki* for your help in providing me accommodation and all my colleagues in the Chemical Physics department.

I had a memorable time spent with all of you which I will definitely cherish in rest of my life. I will miss all of you and Lund and Sweden.
Finally, I like to thank my parents and my family members for being my mental strength and support.

Paper I

Non-Heme Fe(IV) Oxo Complexes of Two New Pentadentate Ligands and Their Reactivities Towards Hydrogen- and Oxygen-Atom Transfer Reactions

Mainak Mitra,[†] Hassan Nimir,[‡] Serhiy Demeshko,[§] Matti Haukka,[±] Julio Lloret-Fillol,[#] Franc Meyer,[§] Albert A. Shteinman,[£] Wesley R. Browne,[¶] David A. Hrovat,[€, ¥] Michael G. Richmond,[¥] Miquel Costas,*[,#] and Ebbe Nordlander*[,†]

[†]Chemical Physics, Department of Chemistry, Lund University, Box 124, SE-221 00, Lund, Sweden
[‡] Department of Chemistry and Earth Sciences, College of Arts and Sciences, Qatar University, P.O. Box 2713, Doha, State of Qatar
[§]Institute of Inorganic Chemistry, Georg-August-University Göttingen, Tammanstrasse 4, D-37077 Göttingen, Germany
[±]Department of Chemistry, University of Jyväskylä, P.O.Box-35, FI-40014, Finland
[£] Institute of Problems of Chemical Physics, 142432, Chernogolovka, Moscow district, Russian Federation
[¶]Stratingh Institute for Chemistry, Faculty of Mathematics and Natural Sciences, University of Groningen, Nijenborgh 4, 9747AG Groningen, The Netherlands
[€]Center for Advanced Scientific Computing and Modeling, University of North Texas, Denton, Texas 7603, United States
[¥]Department of Chemistry, University of North Texas, Denton, Texas 76203, United States
[#] QBIS, Department of Chemistry, University de Girona, Campus Montilivi, E-17071 Girona, Spain

Supporting Information

ABSTRACT: Two new pentadentate N5-donor ligands based on the N4Py framework have been synthesized, *viz*. [*N*-(1-methyl-2-benzimidazolyl)methyl-*N*-(2-pyridyl)methyl-*N*-(bis-2-pyridyl methyl)amine] (**L^1**) and [*N*-bis(1-methyl-2-benzimidazolyl) methyl-*N*-(bis-2-pyridylmethyl)amine] (**L^2**), where one or two pyridyl arms of N4Py have been replaced by corresponding (N-methyl)benzimidazolyl-containing arms. The complexes $[Fe^{II}(CH_3CN)(L)]^{2+}$ (L = **L^1**,**L^2**) were synthesized and reaction of these ferrous complexes with iodosyl benzene led to the formation of the ferryl complexes $[Fe^{IV}(O)(L)]^{2+}$ (L = **L^1**, **L^2**), which were characterized by UV/Vis spectroscopy, high resolution mass spectrometry and Mössbauer spectroscopy. The ferryl complexes are relatively stable with half lives at room temperature of 40 h (L = **L^1**) and 2.5 h (L = **L^2**). The redox potentials of the ferrous complexes, visible spectra, and half lives indicate that the ligand field weakens as ligand pyridyl substituents are progressively substituted by (*N*-methyl)benzimidazolyl moieties. The reactivities of the two ferryl complexes in hydrogen atom transfer (HAT) and oxygen atom transfer (OAT) reactions show that both complexes exhibit high reactivities when compared to the analogous N4Py complexes, and that the normalized HAT rates increase by approximately one order of magnitude for each replacement of a pyridyl moiety, i.e. $[Fe^{IV}(O)($ **L^2**$)]^{2+}$ exhibits the highest rates; C-H activation rates can be directly related to bond dissociation energies. Computational modeling of the HAT reactions indicates that the reaction proceeds via the two-state reactivity model, involving a crossover from a low spin ground state to a high spin transition state.

Introduction.

High valent Fe(IV) oxo species have been established as key oxidizing intermediates in the activation of molecular oxygen in many iron-containing enzymes.[1-3] For example, non-heme high spin (*S* = 2) Fe(IV) oxo intermediates have been identified as active oxidizing species in the catalytic cycles of *E. coli* taurine:α-ketoglutarate dioxygenase (TauD),[4] propyl-4-hydroxylase,[5] halogenase CytC3,[6] tyrosine hydroxylase,[7] and the aliphatic halogenase SyrB2[8] by means of various spectroscopic techniques. These reactive intermediates activate C-H bonds in a wide number of substrates, transforming them into hydroxylated, unsaturated, or halogenated products.[4b, 5,6,7,9]

The interesting chemistry that is exhibited by non-heme iron enzymes has inspired extensive efforts to mimic their high-valent intermediates and emulate their reactivities.[2,10] Over the last decade, several non heme Fe(IV) oxo (ferryl) complexes supported by a wide range of pentadentate and tetradentate ligands have been prepared.[2,10,11] These Fe(IV) oxo complexes have been investigated for, *inter alia*, C-H bond activation reactions, C=C bond activation reactions and oxo transfer reactions, and the reactivities of these different non heme Fe(IV) oxo complexes have been found to vary widely. For example, $[Fe^{IV}(O)(TMC)(CH_3CN)]^{2+}$ (TMC = 1,4,8,11-tetramethyl-1,4,8,11-tetraazacyclotetradecane) can only oxidize substrates with C-H bond dissociation energies (BDE's) of <80 kcal/mol;[12] while $[Fe^{IV}(O)(N4Py)]^{2+}$, (N4Py = *N*,*N*-bis(2-pyridylmethyl)-*N*-bis(2-pyridyl)methylamine) and $[Fe^{IV}(O)(Bn\text{-}tpen)]^{2+}$, (Bn-tpen = *N*-benzyl-*N*,*N*',*N*'-tris(2-pyridylmethyl)-1,2-diaminoethane) (Fig.

1) have been shown to oxidize strong C-H bonds, *e.g.* those in cyclohexane (C-H BDE 99.3 kcal/mol) at room temperature.[13]

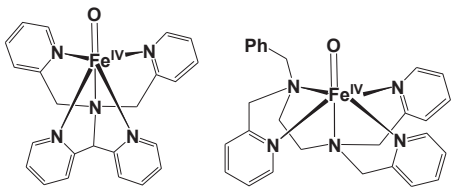

Figure 1. Non heme Fe(IV)-oxo complexes, $[Fe^{IV}(O)(N4Py)]^{2+}$ and $[Fe^{IV}(O)(Bn\text{-}tpen)]^{2+}$.

The spin state on the Fe(IV)-center of the Fe(IV) oxo unit plays a crucial role in terms of reactivity since high spin (S = 2) Fe(IV) oxo complexes have been demonstrated to be more reactive than low spin (S = 1) Fe(IV) oxo complexes.[14] A significant aspect of the observed reactivities and spin states of ferryl complexes is that they can be modulated by the various ligand environments supporting the Fe(IV) oxo unit. A high spin (S = 2) Fe(IV) oxo unit may be achieved by adopting a trigonal bipyramidal (TBP) geometry using tetradentate ligands with sufficient steric constraints, as observed in the case of $[Fe^{IV}(O)(TMG_3tren)]^{2+}$ (TMG_3tren = tris(tetramethylguanidino)tren)[15] and $[Fe^{IV}(O)(H_3buea)]^{-}$ (H_3buea = tris(*tert*-butylureaylethylene)aminato)[16] leading to degeneracy of the second highest occupied molecular orbitals, which have significant d_{xy} and $d_{x^2-y^2}$ character. A detailed investigation was recently made on five low spin Fe(IV)-oxo complexes comprising pentadentate pyridine- and amine- based ligands to examine the correlation of the rates of hydrogen atom transfer and oxygen atom transfer processes with their spectroscopic and electrochemical properties which are controlled by the ligand scaffold.[17] The oxo transfer process to thioanisole by these five Fe-oxo complexes has been correlated to the redox potential of Fe(IV)/Fe(III) couple which was influenced by the ligands bound to the Fe-oxo unit; however, such a direct correlation could not be concluded in the case of hydrogen abstraction processes.

We wish to investigate whether the reactivity of ferryl complexes can be tuned by modification of the steric and electronic properties of ligands, and whether the reactivity of such complexes can be improved while maintaining thermal stability. For this purpose, we chose to modify/derivatize the N4Py ligand framework.[18] Among bio-inspired Fe^{IV}=O complexes, $[Fe^{IV}(O)(N4Py)]^{2+}$ has been shown to exhibit the unique combination of powerful oxidative reactivity towards alkanes, enabling it to cleave strong C-H bonds, while at the same time possessing considerable thermal stability; indeed, the stability has been proven sufficient to permit its structure to be characterized by X-ray crystallography.[19] A number of modifications of the N4Py ligand framework have been made,[20,21] but they do not include the replacement of the pyridyl moieities of this ligand with other nitrogen donor moieties. We were therefore interested in attempting to modify the stability and reactivity of N4Py by tuning the ligand coordination environment, and we chose to introduce (*N*-methyl)benzimidazolyl moieties as these are relatively close analogues of histidine imidazolyls. Although there are a few examples of benzimidazolyl donors exerting profound influence on the reactivities of bio-inspired non-heme iron catalysts in oxidation,[22-24] there is only one previous study involving the coordination of such donor moieties to an isolated/detected/identified Fe^{IV}=O complex.[22] The five-coordinate complex $[Fe^{II}(Me_3NTB)(MeCN)](OTf)_2$ (Me_3NTB = tris((*N*-methyl-benzimidazol-2-yl)methyl)amine), the (*N*-methyl)benizimidazolyl equivalent of the tripodal tris(2-pyridylmethyl)amine (TPA) ligand, reacts with m-CPBA at – 40 °C to form the very reactive (S = 1) $[Fe^{IV}(O)(Me_3NTB)]^{2+}$ complex, which is more reactive than Cyt P450 model compound I ($[Fe^{IV}(O)(TDCPP)^{+}]^{2+}$, TDCPP = *meso*-tetrakis(2,6-dichlorophenyl)porphinato dianion) and the most reactive species among mononuclear non-heme iron(IV) oxo complexes.[23] However, this ferryl species with a trigonal bipyramidal coordination geometry around the iron is unstable and decays fast even at -40 °C ($t_{1/2}$ = 2 min), which has hampered its study.

The two new pentadentate ligands $\mathbf{L^1}$ and $\mathbf{L^2}$ that have been prepared by us are thus based on the N4Py ligand framework, with one ($\mathbf{L^1}$) or two ($\mathbf{L^2}$) of the (2-pyridyl)methyl arms of N4Py being exchanged by one (or two) (*N*-methylbenzimidazolyl)methyl arm(s) (Figure 2). The *N*-methylbenzimidazole moiety contains not only greater steric bulk but also better σ-donor property than the pyridine moiety.[25] It has recently been shown that such a simple change of a ligand donor moiety can affect the catalytic activities of Fe(II) complexes in alkane and alkene oxidation reactions,[24] and it was envisioned that the chemistry of high valent Fe(IV) oxo species, e.g. $[Fe^{IV}(O)(N4Py)]^{2+}$, may also be sensitive to such a change. Here we report two new Fe(II) complexes based on the two ligands, the generation and characterization of their corresponding Fe(IV) oxo complexes and the reactivities of these ferryl species towards hydrogen-atom transfer and oxygen-atom transfer processes.

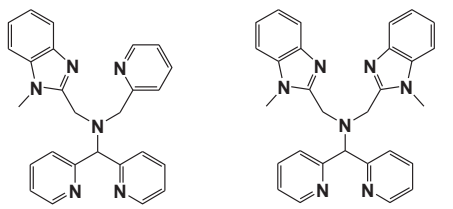

Figure 2. Ligands L^1 (top left) and L^2 (top right).

Results and Discussion

Synthesis and characterization of ligands and complexes

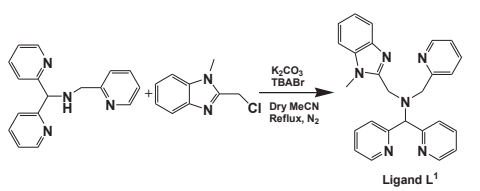

Scheme 1. Synthesis of ligand L^1.

Ligand $\mathbf{L^1}$ was synthesized by reaction of *N*-[di(2-pyridinyl)methyl]-*N*-(2-pyridinylmethyl)methylamine[26] with one equivalent of 2-chloromethyl-1-methylbenzimidazole in refluxing dry acetonitrile, in the presence of K_2CO_3 and tetrabutylammonium bromide (Scheme 1). Ligand $\mathbf{L^2}$ was synthesized by reaction of bis(2-pyridyl)methylamine[27] with 2 equivalents of 2-

chloromethyl-1-methylbenzimidazole in the presence of aqueous NaOH solution (Scheme 2).

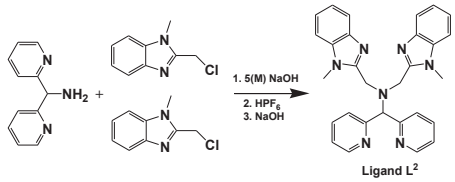

Scheme 2. Synthesis of ligand L^2.

The corresponding Fe(II) complexes, $[Fe^{II}(CH_3CN)(\mathbf{L^1})](ClO_4)_2$ (**1**·$(ClO_4)_2$) and $[Fe^{II}(CH_3CN)(\mathbf{L^2})](ClO_4)_2$ (**2**·$(ClO_4)_2$), were prepared by reaction of one equivalent of $\mathbf{L^1}$/$\mathbf{L^2}$ with one equivalent of hydrated $Fe(ClO_4)_2$ in a minimum amount of dry acetonitrile solvent at room temperature (Scheme 3). Both complexes **1**·$(ClO_4)_2$ and **2**·$(ClO_4)_2$ were isolated and obtained as air-stable solids.

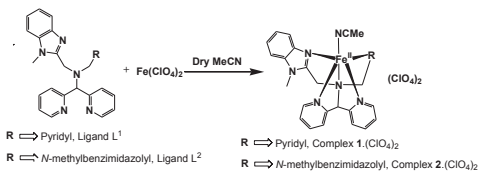

Scheme 3. Synthesis of Fe(II)-complexes, $[Fe^{II}(CH_3CN)(L^1)](ClO_4)_2$ (**1**·$(ClO_4)_2$) and $[Fe^{II}(CH_3CN)(L^2)](ClO_4)_2$ (**2**·$(ClO_4)_2$).

The compact diamagnetic ^{1}H-NMR spectra (Figures S1 and S2, Supplementary Material) and the intense red colour (both in the solid state and in solution) indicate that the complexes contain low spin Fe(II) ions in pseudo-octahedral environments. This is in agreement with what may be expected considering the relatively strong ligand field exerted by the donor moieties of the pentadentate $\mathbf{L^1}$ ligand (*vide infra*) and the coordinated acetonitrile molecule.

The ESI mass spectrum of **1**·$(ClO_4)_2$ in acetonitrile shows peaks at *m/z* = 238 and *m/z* = 258.5 corresponding to the formulations $[Fe^{II}(\mathbf{L^1})]^{2+}$ (calc. 238) and $[Fe^{II}(\mathbf{L^1})(CH_3CN)]^{2+}$ (calc. 258.5), respectively, as well as peaks at *m/z* = 575.1 and *m/z* = 606.1 corresponding to the formulations $[Fe^{II}(\mathbf{L^1})(ClO_4)]^+$ (calc. 575.1) and $[Fe^{II}(\mathbf{L^1})(CH_3CN)(ClO_4)]^+$ (calc. 575.1), respectively (Figure S3, Supplementary Material). Similarly, the ESI-MS of complex **2**·$(ClO_4)_2$ in acetonitrile shows prominent peaks at *m/z* = 264.6 and *m/z* = 628.1 corresponding to the formulations $[Fe^{II}(\mathbf{L^2})]^{2+}$ (calc. 264.6) and $[Fe^{II}(\mathbf{L^2})(ClO_4)]^+$ (calc. 628.1), respectively (Figure S4, Supplementary Material).

The UV-visible spectra of the ligands $\mathbf{L^1}$ and $\mathbf{L^2}$ in acetonitrile solution show high intensity bands in the UV region (wavelength < 300 nm) (Figure S5, Supplementary Material). Upon coordination to the Fe(II) ion, two new charge transfer (CT) bands appear in the visible region. For complex **1**·$(ClO_4)_2$, the CT bands appear at λ_{max} = 387 nm ($\varepsilon \approx 5200$ M^{-1} cm^{-1}) and 466 nm ($\varepsilon \approx 4350$ M^{-1} cm^{-1}), while for complex **2**·$(ClO_4)_2$, the CT bands appear at λ_{max} = 404 nm ($\varepsilon \approx 3230$ M^{-1} cm^{-1}) and 477 nm ($\varepsilon \approx 2125$ M^{-1} cm^{-1}) (Figure 3). These CT bands can be assigned as metal to ligand charge transfer (MLCT) bands arising from electron transfer from low spin Fe(II) t_{2g} orbitals to the π^* orbitals of the ligand.

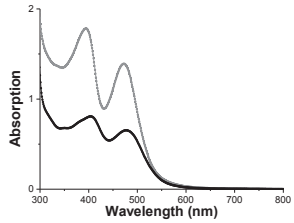

Figure 3. UV/Vis spectra of complexes **1**·$(ClO_4)_2$ (gray) and **2**·$(ClO_4)_2$ (black) (0.25 mM) in acetonitrile.

The natural abundanance ^{57}Fe Mössbauer spectra of the solid samples of complexes **1**·$(ClO_4)_2$ and **2**·$(ClO_4)_2$ measured at 80K confirm the presence of low spin Fe(II) ions in both complexes (Figure 4). The isomeric shift values (δ) and quadrupole splitting values (ΔE_Q) are listed in Table 1. Single-point DFT energy calculations on the S=0, S=1, and S=2 spin states of **1**·$(ClO_4)_2$ and **2**·$(ClO_4)_2$ using the structures obtained from the X-ray diffraction data, confirm the S=0 spin state as the ground-state of each complex.

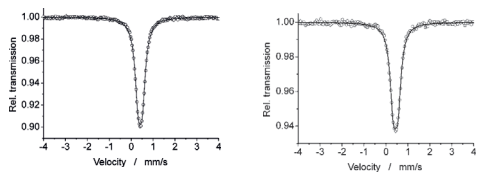

Figure 4. The zero field Mössbauer spectra of complexes **1**·$(ClO_4)_2$ (left) and **2**·$(ClO_4)_2$ (right) collected at Scheme 4.

Table 1. Mössbauer parameters for complexes **1**·$(ClO_4)_2$ and **2**·$(ClO_4)_2$

Complex	isomeric shift value (δ) in mm s^{-1}	quadrupole splitting value (ΔE_Q) in mm s^{-1}
1·$(ClO_4)_2$	0.41	0.19
2·$(ClO_4)_2$	0.44	0.21

Electrochemistry of complexes 1·$(ClO_4)_2$ and 2·$(ClO_4)_2$.

The cyclic voltammograms of complexes **1**·$(ClO_4)_2$ and **2**·$(ClO_4)_2$ were measured in acetonitrile at 298 K using a glassy carbon electrode as the working electrode and SCE as the reference electrode. Complex **1**·$(ClO_4)_2$ showed an irreversible oxidation wave at E_p^a = 0.5 V and two reduction potential waves (E_p^c) at ca. 0.41 and 0.23 V (Figure S, Supplementary Material). On the other hand, complex **2**·$(ClO_4)_2$ showed an electrochemically reversible redox curve at $E_{1/2}$ = 0.395 V for the Fe^{III}/Fe^{II} couple (Figure S, Supplementary Material). In general, strong ligand fields result in higher oxidation potential values for the Fe^{III}/Fe^{II} couple. $[Fe^{II}(CH_3CN)(N4Py)](ClO_4)_2$ has a high redox potential value (1.01 V vs SCE, in acetonitrile).[28] Clearly, successive replacement of the pyridyl moieties in N4PY by (*N*-methyl)benzimidazolyl

moieties led to a lowering of the oxidation potential value of the corresponding Fe(II) complexes and it may thus be concluded that the ligand field strength of the ligand is concomitantly weakened. In this specific case, the weak field indicates relatively poor π-acid properties (relative to the equatorial pyridyl substitutents in N4Py) exerted by the (*N*-methyl)benzimidazolyl moieties in ligands L^1 and L^2.

Crystal and molecular structures of $1\cdot(ClO_4)_2$ and $2\cdot(ClO_4)_2$.

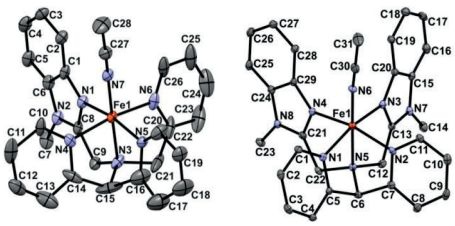

Figure 5. The crystal structures of the cations of $1\cdot(ClO_4)_2$ (left) and $2\cdot(ClO_4)_2$ (right) (ORTEP plot). Thermal ellipsoids are plotted at 30% probability ellipsoids; hydrogen atoms have been omitted for clarity.

Single crystals suitable for X-ray diffraction were grown for both $1\cdot(ClO_4)_2$ and $2\cdot(ClO_4)_2$, and their crystal structures were determined in order to confirm the proposed molecular structures. The structures of the two cationic complexes are shown in Figure 5; relevant crystallographic data are summarized in Table 2 and selected bond distances and bond angles are collated in Table 7 in the experimental section. The crystal structures are similar to that of the "parent" complex $[Fe^{II}(N4Py)(CH_3CN)](ClO_4)_2$[28] and show that the pentadentate ligands $\mathbf{L^1}$ and $\mathbf{L^2}$ coordinate as envisaged, with the sixth coordination site at the iron ion being occupied by a (solvent) acetonitrile molecule. The short Fe-N bond lengths (1.9-2.0 Å) observed for both complexes are in agreement with the presence of low spin Fe(II) centers in $1\cdot(ClO_4)_2$ and $2\cdot(ClO_4)_2$, as observed for $[Fe^{II}(N4Py)(CH_3CN)](ClO_4)_2$[27] and some previously reported related Fe(II) complexes.[21,29,30] A comparison between different Fe-N bond distances in $1\cdot(ClO_4)_2$, $2\cdot(ClO_4)_2$ and $[Fe^{II}(N4Py)(CH_3CN)](ClO_4)_2$ are shown in Table 3. It is not possible to discern clear structural trends, but the following observations may be made: The Fe-N_{Py} (Py = pyridyl) bond distances that are *trans* with respect to each other in $1\cdot(ClO_4)_2$ are non-equivalent (1.948(6) and 1.960(6) Å), while the corresponding distances in the parent complex are virtually equivalent, and the Fe-N_{Py} bond distance that is *trans* to Fe-N_{BzIm} (BzIm = (*N*-methyl)benzimidazolyl) bond is 1.957(6) Å for $1\cdot(ClO_4)_2$. For each replacement of a pyridyl moiety by an (*N*-methyl)benzimidazolyl moiety (going from the parent complex to $1\cdot(ClO_4)_2$ to $2\cdot(ClO_4)_2$), the specific Fe-N bond that is subject to the change is lengthened. Replacement of a pyridyl moiety by a second (*N*-methyl)benzimidazolyl moiety in $2\cdot(ClO_4)_2$ results in a lengthening of both equatorial Fe-N_{Py} bond distances (1.964(3) and 1.983(3) Å) with respect to $1\cdot(ClO_4)_2$. The acetonitrile molecule becomes more tightly bound to the Fe ion in $2\cdot(ClO_4)_2$ (1.901(3) Å) than in $1\cdot(ClO_4)_2$ (1.909(6) Å), and, consequently, the Fe-N_{amine} bond distance, *trans* to the acetonitrile ligand, follows the reverse trend – it is lengthened by approximately 0.048 Å, going from $1\cdot(ClO_4)_2$ to $2\cdot(ClO_4)_2$.

Table 2. Crystallographic data of complexes $1\cdot(ClO_4)_2$ and $2\cdot(ClO_4)_2$

Complex	$1\cdot(ClO_4)_2$	$2\cdot(ClO_4)_2$
Empirical formula	$C_{30}H_{30}Cl_2FeN_8O_8$	$C_{34}H_{34.50}Cl_2FeN_{9.50}O_8$
Formula weight	757.37	830.96
Temperature	150(2) K	100(2) K
Wavelength	0.71073 Å	0.71073 Å
Crystal system	Triclinic	Triclinic
Space group	$P\bar{1}$	$P\bar{1}$
Unit cell dimensions	a = 11.5569(11) Å	a = 11.8930(12) Å
	b = 12.4532(9) Å	b = 12.8968(12) Å
	c = 12.5679(11) Å	c = 13.1477(13) Å
	α = 82.359(5)°	α = 89.788(4)°
	β = 63.653(6)°	β = 67.173(4)°
	γ = 87.358(6)°	γ = 73.470(4)°
Volume	1606.3(2) $Å^3$	1768.8(3) $Å^3$
Z	2	2
Density (calculated)	1.566 Mg/m^3	1.560 Mg/m^3
Absorption coefficient	0.701 mm^{-1}	0.645 mm^{-1}
F(000)	780	858
Crystal size	0.37 x 0.20 x 0.11 mm^3	0.22 x 0.08 x 0.08 mm^3
Theta range for data collection	1.82 to 25.00°.	1.66 to 26.00°.
Index ranges	-13<=h<=12, -14<=k<=14, -14<=l<=13	-14<=h<=14, -15<=k<=15, -16<=l<=15
Reflections collected	10606	23734
Independent reflections	5570 [R(int) = 0.0403]	6845 [R(int) = 0.0604]
Completeness to theta = 25.00°	98.5 %	98.4 %
Absorption correction	Semi-empirical from equivalents	Semi-empirical from equivalents
Max. and min. transmission	0.9288 and 0.7806	0.9520 and 0.8727
Refinement method	Full-matrix least-squares on F^2	Full-matrix least-squares on F^2
Data / restraints / parameters	5570 / 36 / 445	6845 / 0 / 510
Goodness-of-fit on F^2	1.048	1.006
Final R indices [I>2sigma(I)]	R1 = 0.0924, wR2 = 0.2196	R1 = 0.0506, wR2 = 0.0882
R indices (all data)	R1 = 0.1237, wR2 = 0.2369	R1 = 0.1044, wR2 = 0.1042
Largest diff. peak and hole	1.760 and -0.771 e.$Å^{-3}$	0.489 and -0.472 e.$Å^{-3}$

Table 3. Comparison of different Fe-N bond distances between $1\cdot(ClO_4)_2$, $2\cdot(ClO_4)_2$ and $[Fe^{II}(N4Py)(CH_3CN)](ClO_4)_2$

Entry	Complex $1\cdot(ClO_4)_2$	Complex $2\cdot(ClO_4)_2$	$[Fe^{II}(N4Py)(CH_3CN)](ClO_4)_2$
Fe-N_{py} (average)	1.953	1.974	1.972
Fe-N_{BzIm} (average)	1.977	1.981	-------
Fe-N_{MeCN}	1.909	1.901	1.915
Fe-N_{amine}	1.980	2.028	1.961

Generation and characterization of high valent Fe(IV)-oxo complexes.

The two Fe(II) complexes contain a relatively labile coordinated solvent (acetonitrile) molecule and they are easily converted into the corresponding Fe(IV) oxo species upon reaction with the strong O-atom donor agent iodosylbenzene (PhIO). Complex **1**·$(ClO_4)_2$ reacted with excess (10 equivalents) solid PhIO in acetonitrile at room temperature to form a pale green complex, $[Fe^{IV}(O)(\mathbf{L^1})]^{2+}$ (**3**) (Scheme 4).

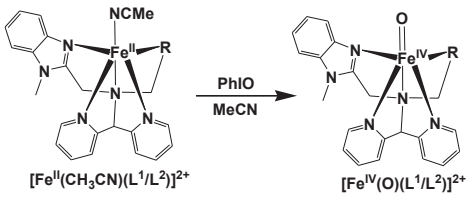

R ⟹ Pyridyl, Complex **3**, condition: RT, 20 min

R ⟹ N-methylbenzimidazolyl, Complex **4**, condition: -10^{0}C, 10 min

Scheme 4. Generation of Fe(IV)-oxo complexes, **3** and **4** from the precursor Fe(II)-complexes, **1** and **2** respectively.

Formation of **3** was monitored using UV/Vis spectrophotometry, which indicated that complex **1** can be converted into complex **3** within 20 min of stirring at room temperature (Figure S8, Supplementary Material). Complex **3** has a characteristic absorbance band in the near IR region, with a maximum at λ_{max} = 708 nm and $\varepsilon \approx 400$ M^{-1} cm^{-1}, a common feature for low spin (S = 1) Fe(IV) oxo species (Figure 6). Similarly, complex **2**·$(ClO_4)_2$ also formed a pale green species, $[Fe^{IV}(O)(\mathbf{L^2})]^{2+}$ (**4**) upon reaction with excess (10 equivalents) PhIO in acetonitrile at low temperature (-10 ºC). Complex **4** has a characteristic absorbance band with a maximum at λ_{max} = 725 nm with $\varepsilon \approx 380$ M^{-1} cm^{-1} (Figure 6). The change of λ_{max} of the near IR spectral Fe^{IV}=O signature for the complexes $[Fe^{IV}(O)(N4Py)]^{2+}$ (four equatorial pyridyl moieties; λ_{max} = 695 nm), **3** (three equatorial pyridyls, one equatorial (*N*-methyl)benzimidazolyl moiety; λ_{max} = 708 nm) and **4** (two equatorial pyridyls, two equatorial (*N*-methyl)benzimidazolyl moieties; λ_{max} = 725 nm) is attributed to the donor strength of the corresponding pentadentate ligand, and indicates that the effective donor strength becomes progressively weaker as (*N*-methyl)benzimidazolyl substituents are introduced in the ligand scaffold.[13,17]

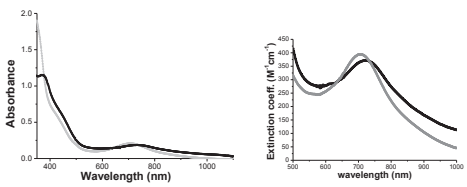

Figure 6. The absorbance spectra of complexes **3** (gray) and **4** (black) [0.5 mM] in acetonitrile (left); the corresponding molar extinction coefficient values (ε) of complexes **3** (gray) and **4** (black) (right).

Complexes **3** and **4** were also characterized by high resolution mass spectrometry (HRMS). The HRMS of an acetonitrile solution containing complex **3** showed major peaks at m/z = 246.0681, corresponding to the formulation $[Fe^{IV}(O)(\mathbf{L^1})]^{2+}$ (m/z calc 246.0675) and at m/z = 591.0847, corresponding to the formulation $[Fe^{IV}(O)(\mathbf{L^1})(ClO_4)]^{1+}$ (m/z calc 591.0841) (Figure S9, Supplementary Material). Similarly, the HRMS of complex **4** (with triflate counter anion, derived from $[Fe^{II}(\mathbf{L^2})(CH_3CN)](CF_3SO_3)_2$, *cf*. Experimental Section for synthesis) in acetonitrile showed major peaks at m/z = 272.5837, corresponding to the formulation $[Fe^{IV}(O)(\mathbf{L^2})]^{2+}$ (m/z calculated 272.5808) and at m/z = 694.1153, corresponding to the formulation $[Fe^{IV}(O)(\mathbf{L^2})(CF_3SO_3)]^{1+}$ (m/z calculated 694.1142) (Figure S12, Supplementary Material).

Mössbauer spectroscopy was also employed to confirm the oxidation state of the iron ions in complexes **3** and **4**. The zero field Mössbauer spectrum of an acetonitrile solution containing 20% of ^{57}Fe enriched sample of **3** showed an isomeric shift value, δ = -0.03 mm s^{-1}, and quadrupole splitting value, ΔE_Q = 1.1 mm s^{-1} (Figure 7), indicating the presence of an Fe(IV) species. Approximately 86% of the Fe sample accounts for the presence of **3**, the remaining absorption corresponds to Fe(III) contaminants. Similarly, the Mössbauer spectrum of **4** measured under the same conditions showed an isomeric shift value, δ = -0.02 mm s^{-1}, and quadrupole splitting value, ΔE_Q = 1.34 mm s^{-1}, indicating the presence of an Fe(IV) species, with ~ 80% of the Fe sample accounting for the presence of **4** (Figure 7). The isomeric shift values for **3** and **4** are very similar to those obtained for $[Fe^{IV}(O)(N4Py)]^{2+}$ (δ = -0.04 mm s^{-1}; ΔE_Q = 0.93 mm s^{-1})[13] and $[Fe^{IV}(O)(Bn\text{-}tpen)]^{2+}$ (δ = 0.01 mm s^{-1}; ΔE_Q = 0.87 mm s^{-1}),[13] indicating that both **3** and **4** are low spin (S = 1) non-heme Fe(IV) oxo complexes. The structure of **3** (as the dication) was investigated by DFT and a triplet Fe(IV) oxo species ^{3}**A** was computed to be the ground-state minimum in keeping with the available experimental data. The corresponding high spin quintet (S=2) state lies 2.6 kcal/mol above the triplet species. Analysis of the unpaired spin density in ^{3}**A** reveals significant unpaired spin population on the iron (1.15) and the oxygen (0.89) centers.

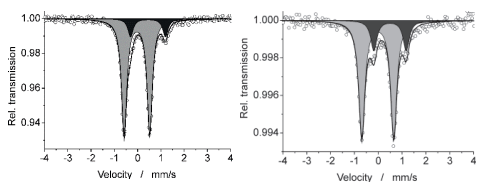

Figure 7. (Left) The zero-field Mössbauer spectrum of ^{57}Fe enriched **3** (light gray) in acetonitrile soln. (5 mM) measured at 80 K. The minor black subspectrum corresponds to ca. 14 % unidentified Fe(III) impurity. (Right) The zero-field Mössbauer spectrum of ^{57}Fe enriched **4** (light gray) in acetonitrile soln. (2 mM) measured at 80 K. The minor black subspectrum corresponds to ca. 20% unidentified Fe(III) impurity.

The half lives ($t_{1/2}$) for complexes **3** and **4** were determined at room temperature. The $t_{1/2}$ for complex **3** is 40 h while for complex **4** it is 2.5 h, demonstrating that complex **4** is thermally much less stable compared to complex **3**. In Table 4, the half lives and the characteristic wavelengths of these two new Fe(IV)-oxo complexes are compared to some previously reported low spin Fe(IV) oxo complexes bearing pentadentate ligands; it may be noted that

the thermal stability of complex **3** is very similar to that of the parent N4Py complex.

Table 4. Comparison of wave lengths and half lives of different low spin (S = 1) Fe(IV) oxo complexes bearing pentadentate ligands.

Complex	λ_{max}, nm (€ in M^{-1} cm^{-1})	$t_{1/2}$ at RT	Reference
$[Fe^{IV}(O)(L^1)]^{2+}$ (**3**)	708 (400)	40 h	*this work*
$[Fe^{IV}(O)(L^2)]^{2+}$ (**4**)	725 (380)	2.5 h	*this work*
$[Fe^{IV}(O)(N4Py)]^{2+}$	696 (400)	60 h	13
$[Fe^{IV}(O)(Bn\text{-}tpen)]^{2+}$	739 (400)	6 h	13
$[Fe^{IV}(O)(TMC\text{-}py)]^{2+}$	834 (260)	7 h	42
$[Fe^{IV}(O)(Me_3cyclam\text{-}CH_2C(O)NMe_2)]^{2+}$	810 (270)	5 d	41
$[Fe^{IV}(O)(BP^1)]^{2+}$	730 (400)	-----	43
$[Fe^{IV}(O)(BP^2)]^{2+}$	730 (380)	-----	43
$[Fe^{IV}(O)(MePy_2TACN)]^{2+}$	736 (310)	-----	44
$[Fe^{IV}(O)(^{Me2}TACNPy2)]^{2+}$	740 (340)	-----	17

Hydrogen atom transfer (HAT) reactions: Reactivities with alkanes.

The Fe(IV) oxo complexes **3** and **4** efficiently oxidize the C-H bonds of various alkanes at room temperature. A series of alkane substrates having different C-H bond dissociation energies (BDE's) (range from 81-99.3 kcal/mol) were investigated and the relative reactivities between complexes **3** and **4** were evaluated.

Reactivity of $[Fe^{IV}(O)(L^1)]^{2+}$ 3. Addition of 20 equivalents of triphenyl methane (C-H BDE = 81 kcal/mol) to **3** resulted in rapid decay of **3** to its Fe(II)-precursor species as identified by UV/Vis spectroscopy (Figure S15, Supplementary Material) and formation of triphenyl methanol with ~ 89% yield. On the other hand, complex **3** reacted with the comparatively less reactive substrate cyclohexane (C-H BDE = 99.3 kcal/mol) at a slower rate to form cyclohexanol and cyclohexanone (total yield ~ 18%); details of product analyses are provided in the Supplementary Material. The decay of the Fe-oxo absorbance band of **3** monitored at 708 nm was monitored under pseudo-first-order conditions, i.e. in presence of excess substrate (50-400 equivalents) for a range of substrates. The second-order rate constants (k_2) for the different substrates were obtained from the slope of plots of the observed pseudo-first-order rate constant, k_{obs}, versus molar concentration, taken at three different substrate concentrations. The k_2 values thus obtained are listed in Table 5. A primary kinetic isotope effect (KIE) value of ~ 14 was obtained by determining the second-order rate constants corresponding to separate reactions of toluene and its d_8 isotopomer with **3** (Figure 8, right), using the same methodology described above.

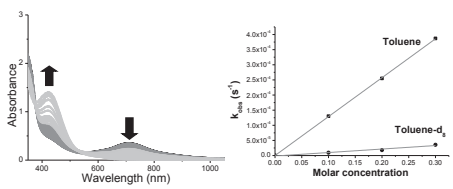

Figure 8. (Left) Kinetic decay of complex **3** (≈ 1mM in acetonitrile) upon addition of 100 equiv. of ethylbenzene. (Right) Determination of the kinetic isotope effect (KIE) for separate reactions with toluene and toluene-d_8 with complex **3** at room temperature.

A plot of logarithmic values of second-order rate constants (log k_2') (k_2' is the second-order rate constant divided by the number of equivalent C-H bonds in the substrate) for absorbance decay versus bond dissociation energies for various hydrocarbons shows a linear correlation (Figure 10). The linear correlation between log k_2' and C-H BDE's of substrates, as well as the observed large KIE value constitute strong evidence of the reactions taking place via hydrogen atom transfer (HAT).

Reactivity of $[Fe^{IV}(O)(L^1)]^{2+}$ 4. Complex **4** also reacted rapidly with different alkane substrates and the decay of the Fe-oxo absorbance was monitored at 725 nm to determine the observed pseudo-first-order rate constants. Complex **4** reacted with triphenyl methane with faster rate producing triphenyl methanol with ~ 90% yield (Figure 9), while its reactivity slowed for substrates with higher C-H BDE. The same kinetic analysis was applied for complex **4** as for **3**; the k_2 values for reactions of **4** with various alkane substrates are listed in Table 5. A linear correlation plot between log k_2' versus C-H BDE's of alkanes was also observed for complex **4** (Figure 10) which also indicates that the reactions proceeded through hydrogen atom transfer in the rate determining step, and a primary KIE value of ~ 11 was obtained for separate reactions of toluene and its d_8 topoisomer with **4**.

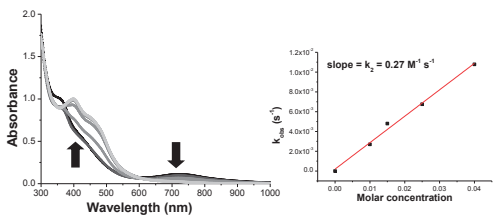

Figure 9. (Left) Kinetic decay of complex **4** (≈ 0.5 mM in acetonitrile) upon addition of 30 equivalents of triphenylmethane. (Right) Determination of second order rate constant for triphenylmethane from k_{obs} versus concentration plot.

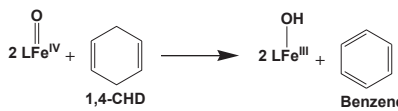

Scheme 5. The reaction of Fe(IV)-oxo complex with 1,4-cyclohexadiene.

The reactivity of complex **4** with substrates like 9,10-dihydroanthracene (9,10-DHA) and 1,4-cyclohexadiene (1,4-CHD) was also investigated in order to examine any possible influence of the bulky methylbenzimidazole group on the access to the Fe(IV) oxo center by the substrate. Both substrates have similar C-H bond dissociation energies (C-H BDE = 77 kcal/mol for 9,10-DHA and 78 kcal/mol for 1,4-CHD), but 9,10-DHA is a sterically bulky substrate relative to 1,4-CHD. The second order rate constants obtained for complex **4** measured at 243 K were 1.4 M^{-1} s^{-1} with 9,10-DHA and 1.2 M^{-1} s^{-1} with 1,4-CHD. Similar values of k_2 for **4** indicated that access to the Fe(IV)-oxo center by the substrates were equally feasible and not influenced by the nearby methylbenzimidazole groups. It should be mentioned that **4** acted as a one electron oxidant in these cases, thereby requiring two equivalents of complex **4** to form benzene (identified by GC) from one equivalent of 1,4-CHD (Scheme 5). While the steric

hindrance in complex **4** has not been probed by an extensive range of substrates, the results above indicate that there is relatively little steric discrimination of substrates by **4** (and implicitly by **3**).

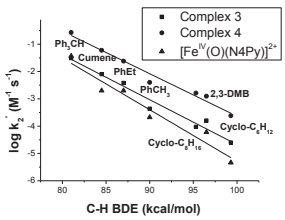

Figure 10. Plot of log k_2' versus C-H bond dissociation energies of different alkane substrates for complex **3** and **4** and $[Fe^{IV}(O)(N4Py)]^{2+}$.

The HAT curve clearly indicates that **4** reacted with faster rates of reactions with different alkane substrates with respect to **3**. The nearly parallel slopes observed for the HAT curves of $[Fe^{IV}(O)(N4Py)]^{2+}$,[13] complex **3** and complex **4** (Figure 10) suggest that simple variation in the side arm of the ligand plays an important role in the reactivity of the Fe(IV) oxo unit in this family of complexes. Considering that there does not seem to be a significant steric discrimination of substrates for complex **4** (*vide supra*), the observed HAT reactivities suggest that the influence of the replacement of a pyridyl side arm by a (*N*-methyl)benzimidazolyl side arm is primarily electronic. Since the reaction of an Fe(IV)-oxo species with a substrate R-H involves the rate determining transfer of a hydrogen atom (one electron coupled with a proton), it may be concluded that the effective basicity of the ferryl unit is increased by the successive introduction of (*N*-methyl)benzimidazolyl side arms in this family of complexes; it may be noted that the addition of one extra (*N*-methyl)benzimidazolyl moiety increases the rate constant by one order of magnitude (Figure 10).

Table 5. C-H bond dissociation energies of different alkane substrates and the second order rate constants (k_2) of **3** and **4** for HAT reactivities

Substrate	BDE (kcal/mol)	k_2 for **3** (M^{-1} s^{-1})	k_2 for **4** (M^{-1} s^{-1})
Triphenylmethane	81	0.031	0.27
Cumene	84.5	0.008	0.06
Ethylbenzene	87	0.0076	0.048
Toluene	90	0.0013	0.012
Cyclooctane	95.3	0.0015	0.026
2,3-Dimethyl butane	96.5	0.00032	0.0025
Cyclohexane	99.3	0.0003	0.0029

O-atom transfer (OAT) reactions: Oxidation of sulfides.

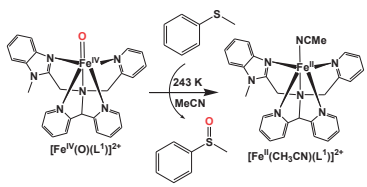

Scheme 6. Oxygen atom transfer (OAT) to thioanisole by complex **3** at 243 K.

The oxo transfer reactivities of **3** and **4** were also investigated, using thioanisole ($PhSCH_3$) as a substrate. Complex **3** reacted with thioanisole at 243 K and transferred the oxygen to form methyl phenyl sulfoxide quantitatively (yield ~ 84%) (Scheme 6). During the course of the reaction, complex **3** was converted into its Fe(II) precursor (complex **1**) as identified by UV/Vis spectrophotometry (Figure 10). The reaction showed pseudo-first order behaviour under condition of excess substrate (5-20 equivalents w.r.t. complex **3** and the observed rate constant (k_{obs}) was linearly dependent on substrate concentration (Figure 11). From this linear plotting, a second order rate constant (k_2) with a value of 3.3×10^{-2} M^{-1} s^{-1} was obtained in the oxidation of thioanisole by complex **3**. Similarly, **4** was reacted with thioanisole under the same conditions, and a faster rate with respect to complex **3** and methyl phenyl sulfoxide was obtained with a yield of ~ 88% . The second order rate constant (k_2) for complex **4** in oxo transfer reaction was found to be 3.1×10^{-1} M^{-1} s^{-1}. Table 8 shows a comparison in the reaction rates of OAT processes between complex **3**, **4** and previously reported Fe(IV)-oxo complexes. In parallel with the observed trend for HAT, the k_2 values suggest that complex **4** is more reactive (by one order of magnitude) than complex **3** in the OAT reaction (i.e. thioanisole oxidation).

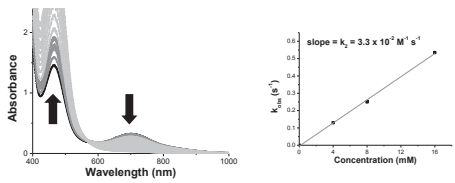

Figure 11. (Left) Conversion of complex **3** into its Fe(II)-precursor in presence of thioanisole (5 equivalents) at 243 K. (Right) Determination of the second order rate constant for the oxygen atom transfer reaction from the k_{obs} vs concentration plot.

Table 6. Comparison of rates of OAT process (thioanisole oxidation) between complex **3**, complex **4** and some other relevant low spin Fe(IV)-oxo complexes.

Complex	k_2 (in M^{-1} s^{-1})	Temp. of measurement	Reference
$[Fe^{IV}(O)(L^1)]^{2+}$ (**3**)	3.3 X 10^{-2}	243 K	*this work*
$[Fe^{IV}(O)(L^2)]^{2+}$ (**4**)	3.1 X 10^{-1}	243 K	*this work*
$[Fe^{IV}(O)(N4Py)]^{2+}$	1.4 X 10^{-2}	263 K	17
$[Fe^{IV}(O)(N4Py)]^{2+}$	2.4 X 10^{-4}	233 K	22
$[Fe^{IV}(O)(Bn\text{-}tpen)]^{2+}$	3.3 X 10^{-1}	263 K	17
$[Fe^{IV}(O)(Bn\text{-}tpen)]^{2+}$	1.4 X 10^{-2}	233 K	22
$[Fe^{IV}(O)(Me_3NTB)]^{2+}$	2.1 X 10^{4}	233 K	22

Discussion. The excellent HAT and OAT reactivities of **3** and **4** may be rationalized using two popular approaches - either Shaik's exchange-enhanced-reactivity (EER) model[22] or the Bell-Evans-Polanyi principle (BEP) of Linear Free Energy Relations (LFER),[31,32] which has been fruitfully developed by J. Mayer for HAT reactions.[33] These approaches are not mutually exclusive but

rather complementary, as the EER approach applies to the kinetics and the BEP to the thermodynamics of the process.

According to the EER, or Two-State Reactivity (TSR) model,[14b] the HAT reactivity of Fe^{IV}=O (S = 1) complexes may be explained by a more reactive quintet (S = 2) transition state that is populated via spin-crossover during movement over the energy surface along the reaction coordinate. This principle shows that an increase of the number of unpaired and spin-identical electrons on the iron center will be favourable to the reactivity of the high spin state in comparison with the low-spin state. Therefore the proximity of the quintet excited state to the triplet (S = 1) ground state in the Fe^{IV}=O complex and correspondingly the easiness of triplet/quintet spin-crossover is significant for its reactivity. Oxygen atom transfer reactions are two-electron processes and hence should not exhibit EER.[34]

In order to elucidate the HAT mechanism(s) for reaction of alkanes with **3** and **4,** and establish the spin states of the active species on the potential energy surface, DFT calculations were carried out on the triplet and quintet states of **3** (^{3}**A** and ^{5}**A**), using methane (**B**) as the substrate. Figure 12 shows the lowest energy pathways that have been computed for methane activation, while Figure 13 shows the pertinent transition-state structures responsible for H-abstraction. The results are in concert with a two-state reactivity model, as popularized by Shaik, involving the triplet (S = 1) and quintet (S = 2) reaction surfaces.[14b,35,36,37]

The side-on approach of methane to the oxo moiety in ^{3}**A** leads to ^{3}**TS**^{3}**AB**^{3}**CD** through a pi-directed manifold. This transition structure lies 33.9 kcal/mol above the triplet oxo ^{3}**A** and affords the corresponding geminate radical pair $[Fe^{III}(OH)(\mathbf{L^1})]^{2+}$ (**C**) and methyl radical **D**. Collapse of ^{3}**CD** completes the formal hydroxylation and gives the MeOH-coordinated complex $[Fe^{II}(MeOH)(\mathbf{L^1})]^{2+}$ (^{3}**F**). The overall process is exergonic by 7.5 kcal/mol.

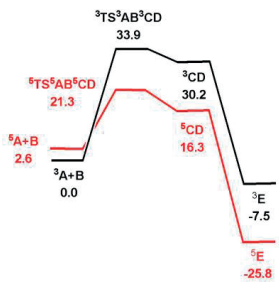

Figure 12. B3LYP potential energy surface for reaction of ^{3}**A**/^{5}**A** and methane (**B**) to give methanol-substituted complexes ^{3}**E** and ^{5}**E**. Energy values are in ΔG in kcal/mol relative to ^{3}**A**+**B**.

Population of the thermodynamically favored quintet surface proceeds through a ^{3}**A** → ^{5}**A** spin crossover. The quintet oxo species (^{5}**A**) undergoes HAT reaction through a linear, sigma-directed transition structure, ^{5}**TS**^{5}**AB**^{5}**CD**, which lies 12.6 kcal/mol lower in energy than the triplet transition structure (^{3}**TS**^{3}**AB**^{3}**CD**). This energetic stabilization more than compensates for the ground-state exchange destabilization experienced by ^{5}**A.** The collapse of the geminate radical pair, ^{5}**CD**, affords the MeOH-coordinated complex $[Fe^{II}(MeOH)(\mathbf{L^1})]^{2+}$ (^{5}**F**) with a net release of 25.8 kcal/mol.[38]

Figure 13. B3LYP-optimized transition-state structures ^{3}**TS**^{3}**AB**^{3}**CD** (left) and ^{5}**TS**^{5}**AB**^{5}**CD** (right).

The BEP/LFER principle establishes the linear correlation of the reaction barrier height ($\Delta\Delta G^{\#}$) with the thermodynamic driving force of reaction determined by the free energy value ($\Delta\Delta G^{o}$). Such Linear Free Energy Relationships have been established for a wide range of heme and non-heme ferryl complexes.[39] According to Mayer,[32] and in correspondence with the LFER principle, the reactivities of Fe^{IV}=O complexes in HAT reactions depend on their redox potentials and on the pK_a of the Fe-OH products according to the Bordwell-Polanyi equation.

$$D_{OH} = 23.06E^{o} + 1.37pK_a + C$$

The ferryl species are electrophilic reagents and, as follows from the Bordwell-Polanyi equation, the rates of HAT reactions should be correlated mainly by the redox potentials of Fe^{IV}=O complexes. Some deviations may be related to contributions by the second term of this equation (pK_a) or the non-adiabaticity of the reaction (EER model). Such an "anti-electrophilic trend" was observed in a study of the axial ligand effect on the HAT reactivity of $[Fe^{IV}(O)(TMC)(X)]^{n+}$,[12] where the least electrophilic complex in the series appears the most reactive. It seems that such a trend is observed only for axial ligands. For equatorial donors an increase of the donor strength of the ligand will lower the redox potential of the Fe^{IV}=O moiety and increase the pK_a of the Fe^{III}-OH product formed upon hydrogen atom transfer. On the other hand, a better electron donor ligand will not only strengthen the FeO-H bond and thus enhance the thermodynamic drive for hydrogen atom transfer, but will also simultaneously weaken the Fe=O bond and thus assist OAT reactivity. This appears to apply to complexes **3** and **4**.

It has been found that ligand donor moieties in *cis*-position to the oxo unit (equatorial donors) exert less influence on the reactivity of Fe^{IV}=O (S = 1) octahedral complexes than those ligated trans (axial)[40] as "*trans*-ligands can interact with both σ- and π-orbitals involved in the Fe=O bond but *cis* ligands cannot".[41] However, in the present case, the effect of replacing equatorial pyridyl donors with (*N*-methyl)benzimidazole units is quite significant. The (number and positions of) equatorial donors in octahedral complexes can modulate the spin state and reactivity of the oxo unit by altering the energies, and thus the occupancies, of the iron d_{xy} and $d_{x^2-y^2}$ orbitals. In **3** and **4,** one or two pyridine moieties in *cis*-position to the oxo ligand have been replaced by (*N*-methyl)benzimidazolyl units, and the electrochemical measurements on the precursors **1** and **2** indicate that this replacement leads to a weaker ligand field. However, the (*N*-methyl)benzimidazolyl units are sufficiently strong-field donors to support a d_{xy}/d_{x2-y2} gap in the Fe^{IV}=O complexes that leads to spin pairing to form the S = 1 ground states for **3** and **4**. A weaker equatorial field should decrease the triplet/quintet gap relative to that of $[Fe^{IV}(O)(N4Py)]^{2+}$. The decrease of field strength may thus, in principle, facilitate the spin crossover required for two-state reactivity (*vide supra*) and can thus explain the increase in

HAT rates that are observed upon substitution of pyridyl moieties by (*N*-methyl)benzimidazolyl moieties in the ligand framework.

As mentioned above, it has previously been found that the activities of Fe^{IV}=O complexes with tetramethylcyclam (TMC) ligands in oxygen-atom transfer reactions correlate directly with the electrophilicity of the Fe^{IV}=O moiety.[12] One may thus expect complexes **3** and **4** to be less electrophilic and more poor OAT reagents than $[Fe^{IV}(O)(N4Py)]^{2+}$; however, our results show that the trend is exactly opposite. Thus, the trends observed in the present study and some others do not follow those found in the TMC study with *trans* (axial) donors. The redox potentials of complexes **1** and **2** (*vide supra*) clearly indicate that the ligand fields exerted by ligands $\mathbf{L^1}$ and $\mathbf{L^2}$ are weaker than that of N4Py, suggesting that the σ-donor properties of the equatorial (*N*-methyl)benzimidazolyl moieties do indeed prevail over their π-acceptor properties (*vide infra*).

Summary and Conclusions.

The octahedral ferryl complexes **3** ($t_{1/2}$ = 40 h, RT) and **4** ($t_{1/2}$ = 2.5 h, RT) with pentadentate N_5-donor ligands (*cf.* Table 5) that have been prepared by us are significantly more stable than the previously studied $[Fe^{IV}(O)(Me_3NTB)]^{2+}$ complex, and have thus permitted detailed spectroscopic and reactivity investigations of ferryl complexes with (*N*-methyl)benzimidazolyl donor moieties. More importantly, **3** and **4** demonstrated excellent hydrogen atom transfer (HAT) and oxygen atom transfer (OAT) activities, surpassing the very active $[Fe^{IV}(O)(N4Py)]^{2+}$ and $[Fe^{IV}(O)(Bn\text{-}tpen)]^{2+}$ complexes by approximately one to two orders of magnitude (Tables 7 and 8, Figures 7-10). For example, in the oxidation of cyclohexane (which has the strongest C-H bonds among the alkanes studied here) the successive replacement of pyridyl moieties of the N4Py ligand by one and two (*N*-methyl)benzimidazolyl moieties led to increases in the corresponding values for the rate constants by one order of magnitude for each nitrogen donor replacement. Despite the increased steric bulk of the (*N*-methyl)benzimidazolyl groups relative to the pyridyl moieties, no influence of this replacement on the access to the Fe(IV)-oxo center by the substrate molecules could be detected.

As expected, the introduction of equatorial (*N*-methyl)benzimidazolyl donors in the N4Py framework reduces the energy difference between the iron d_{xy} and $d_{x^2-y^2}$ orbitals, but the resulting $d_{xy}/d_{x^2-y^2}$ gap is not sufficiently small to make the high spin S = 2 state the ground state of **3** and **4**. While this gap is small, computational modeling of the HAT/hydroxylation of substrates by **3** (*vide supra*) does not support spin crossover, as the preferred spin state for the transition state is the triplet (*S* = 1) state.

Following the principles of the BEP/LFER principle described above, the enhanced reactivities of complexes **3** and **4** relative to that of $[Fe^{IV}(O)(N4Py)]^{2+}$ may be explained by the (*N*-methyl)benzimidazolyl moieties in ligand $\mathbf{L^1}$ and $\mathbf{L^2}$ being stronger σ-donors but weaker π-acceptors relative to the pyridyl substituents of the N4Py ligand, thus enabling increased electron donation in the equatorial plane but an overall weaker ligand field due to the relatively poor π-acceptor properties. The observed reactivities for the new ferryl complexes discussed here may be rationalized by both the BEP/LFER principle and the EER/TSR model.

Experimental Section

Materials:

The reagents and solvents were purchased from Sigma-Aldrich and Fisher chemicals. All solvents were of at least 99.5 % purity and used as received. Reagents were of at least 99 % purity and used without any further purification. *N*-[di(2-pyridinyl)methy]-*N*-(2-pyridinylmethyl)methylamine,[25] bis(2-pyridyl)methylamine,[26] and 2-chloromethyl-1-methylbenzimidazole[45] were prepared according to literature procedures.

Physical methods:

UV/Visible spectra and all kinetic experiments were performed on a 8453 UV/Vis Agilent Technologies equipped with a diode-array detector and a Unisoku which permits monitoring of the temperature of the experiments from -90 ^{0}C to 100 ^{0}C. All UV/Vis spectra were measured ins 1cm quartz cell. NMR spectra were collected on Bruker DPX 400 MHz and Varian Inova 500 MHz spectrometer in $CDCl_3$ and CD_3CN solvents and referenced to the residual signal of the solvent. Elemental analysis was performed using an Elementar Vario EL III instrument. The mass spectrometry (ESI) was performed with a Bruker HCT ultra mass spectrometer. The high resolution mass spectrum (HRMS) was performed using a Bruker FTICR APEX IV instrument. The electrochemical analyses were performed on a model a model CHI760B Electrochemical Workstation (CH Instrument). Tetrabutylammonium hexafluorophosphate $[(t\text{-}Bu_4N)HPF_6]$ was used as a supporting electrolyte and the measurements were carried out using 3 mm diameter Teflon-shrouded glassy carbon working electrode, a Pt wire auxiliary electrode and a SCE reference electrode. Product analyses were performed on a Agilent technologies 7820A with 16 sample automatic liquid sampler and flame ionization detector. The products were identified by their GC retention times. Mössbauer spectra were recorded with a ^{57}Co source in a Rh matrix using an alternating constant acceleration Wissel Mössbauer spectrometer operated in the transmission mode and equipped with a Janis closed-cycle helium cryostat. Isomer shifts are given relative to iron metal at ambient temperature. Simulation of the experimental data was performed with the *Mfit* program (E. Bill, Max-Planck Institute for Chemical Energy Conversion, Mülheim/Ruhr, Germany).

Synthesis of ligand $\mathbf{L^1}$ [*N*-(1-methyl-2-benzimidazolyl)methyl-*N*-(2-pyridyl)methyl-*N*-(bis-2-pyridylmethyl)amine]

A two-necked round bottom flask was charged with *N*-[di(2-pyridinyl)methy]-*N*-(2-pyridinylmethyl)methylamine (1.00 g, 3.6 mmol), 2-chloromethyl-1-methylbenzimidazole (0.651 g, 3.6 mmol), K_2CO_3 (2.5 g, 18 mmol) and tetrabutylammonium bromide (0.23 gm, 0.7 mmol). A total of 50 ml dry CH_3CN was added under a vigorous flow of nitrogen. The mixture was refluxed for 24 h under nitrogen and then the reaction mixture was filtered through a Celite pad. A small amount of CH_2Cl_2 was added to wash the Celite pad. The resulting filtrate was evaporated, the residue was dissolved in a 1 (M) NaOH solution and extracted with CH_2Cl_2. The organic portion was washed with brine solution and dried over Na_2SO_4. Evaporation of the organic solvent gave the crude ligand L^1 as a red oil. This crude product was purified by passing through a silica column using a mixture of CH_2Cl_2:CH_3OH:Et_3N (10:2:1) as eluent. Yield: 1.01 g (67%). ESI-MS: 421.2 $[M+H]^+$; ^{1}H-NMR (400 MHz, $CDCl_3$) δ (ppm) 8.6-8.55 [m, 3H], 7.76 [d, 2H, J = 8 Hz], 7.69-7.6 [m, 3H], 7.5 [m, 3H], 7.2-7.15 [m, 5H], 5.33 [s, 1H], 4.18 [s, 2H], 3.98 [s, 2H], 3.75 [s, 3H]; ^{13}C-NMR (100 MHz, $CDCl_3$) δ (ppm) 159.58 (s), 159.21 (s), 152.0 (s), 149.38 (s), 148.98 (s), 136.52 (s), 136.1 (s),

124.65 (s), 123.72 (s), 122.39 (d), 121.885 (d), 119.580 (s), 72.14 (s), 57.63 (s), 49.36 (s), 30.25 (s).

Synthesis of ligand L^2 [*N*-bis(1-methyl-2-benzimidazolyl)methyl-*N*-(bis-2-pyridylmethyl)amine]

A total of 0.403 g 2-Chloromethyl-1-methylbenzimidazole (2.23 mmol) was dissolved in 2 ml of a 5 (M) NaOH solution. After stirring for about 10 min, bis(2-pyridyl)methylamine (0.206 g, 1.115 mmol) in 2 ml 5 (M) NaOH was added. The stirring was continued for three days at room temperature. After stirring was finished, the sticky solid that was formed was collected and HPF_6 was added dropwise to precipitate a brick-red solid. The resultant solid was dissolved in hot water. After recrystallization from hot water, 5 (M) NaOH was added to basify the reaction mixture (pH > 12). The product was extracted with dichloromethane, dried over Na_2SO_4 and the dichloromethane extract was evaporated to give the desired ligand $\mathbf{L^2}$ as a pale brownish solid. Yield: 0.749 g (71%). ESI-MS: 474.2 $[M+H]^+$; ^{1}H-NMR (500 MHz, $CDCl_3$) δ (ppm) 8.635 [d, 2H, J = 8 Hz], 7.714-7.645 [m, 6H], 7.62 [dt, 2H], 7.19 [m, 4H], 5.402 [s, 1H], 4.285 [s, 4H], 3.619 [s, 6H]; ^{13}C-NMR (125 MHz, $CDCl_3$) δ (ppm) 158.8 (s), 151.9 (s), 149.15 (s), 136.47 (s), 136.05 (s), 124.97 (s), 122.8 (s), 122.39 (d), 119.41 (s), 109.1 (s), 48.31 (s), 29.8 (s).

Synthesis of $[Fe^{II}(CH_3CN)(L^1)](ClO_4)_2$ (1.$(ClO_4)_2$):

A total of 100 mg (0.23 mmol) of ligand $\mathbf{L^1}$ was taken in a vial and dissolved in a minimum amount of CH_3CN. To this solution, 58.6 mg (0.23 mmol) of $Fe(ClO_4)_2$ in CH_3CN was added under stirring at room temperature under air. A red precipitate appeared within 5 min of stirring. After stirring for about 30 min, the reaction mixture was placed into an ethyl acetate bath and stored overnight. The precipitate was collected by filtration, washed with ethyl acetate, dried under vacuum and obtained as a red solid. Yield: 147 mg (82%). ESI-MS (in CH_3CN): *m/z* 238 $[Fe^{II}(L^1)]^{2+}$ (*z* = 2) calc. 238, 258.5 $[Fe^{II}(L^1)(CH_3CN)]^{2+}$ (*z* = 2) calc. 258.5, 575.1 $[Fe^{II}(L^1)(ClO_4)]^+$ (*z* = 1) calc. 575.1, 606.1 $[Fe^{II}(L^1)(CH_3CN)(ClO_4)]^+$ (*z* = 1) calc. 606.1. Anal. calc. (%) C 47.58, H 3.99, N 14.8; Found (%) C 46.97, H 3.98, N 14.93. ^{1}H-NMR (400 MHz, CD_3CN) δ (ppm) 9.39, 9.19, 9.17, 7.97, 7.92, 7.90, 7.88, 7.86, 7.61, 7.59, 7.57, 7.52, 7.5, 7.46, 7.44, 7.42, 7.40, 7.39, 7.37, 7.36, 7.35, 7.25, 7.23, 6.72, 4.77, 4.73, 4.51, 2.11, 1.97, 1.92, 1.77, 1.22, 1.21, 1.19.

Synthesis of $[Fe^{II}(CH_3CN)(L^2)](ClO_4)_2$ (2.$(ClO_4)_2$):

The procedure for the synthesis of complex **2** is identical to that for **1**. A total of 109 mg (0.23 mmol) of ligand $\mathbf{L^2}$ was taken in a vial and dissolved in minimum amount of acetonitrile. To this solution, 58.6 mg (0.23 mmol) of $Fe(ClO_4)_2$ in acetonitrile was added under stirring at room temperature under air. A red precipitate appeared within 5 min of stirring. After stirring for about 30 min, the reaction mixture was placed into an ethyl acetate bath and stored overnight. The precipitate was collected by filtration, washed with ethyl acetate, dried under vacuum and obtained as red solid. Yield: 136 mg (77%). ESI-MS (in CH_3CN): *m/z* 264.6 $[Fe^{II}(L^2)]^{2+}$ (*z* = 2) calc. 264.6, 628.1 $[Fe^{II}(L^2)(ClO_4)]^+$ (*z* = 1) calc. 628.1. Anal. calc. (%) C 49.14, H 4.18, N 16.01; Found (%) C 48.99, H 4.17, N 16.77. ^{1}H-NMR (500 MHz, CD_3CN) δ (ppm) 12.40, 8.44, 5.62, 5.04, 4.47, 3.65, 3.34, 2.19, 1.99, 1.97-1.96, 1.30.

Synthesis of $[Fe^{II}(CH_3CN)(L^2)](CF_3SO_3)_2$ (2.$(CF_3SO_3)_2$):

A total of 71 mg (0.15 mmol) of ligand $\mathbf{L^2}$ was taken in a vial and dissolved in minimum amount of acetonitrile. To this solution, 65.4 mg (0.15 mmol) of $[Fe(CH_3CN)(CF_3SO_3)_2]$ in acetonitrile was added under stirring at room temperature under nitrogen atmosphere. After stirring for about 30 min, the reaction mixture was placed into an ethyl acetate bath and stored overnight. The precipitate was collected by filtration, washed with ethyl acetate, dried under vacuum and obtained as red solid. Yield: 101 mg (78%). ESI-MS (in CH_3CN): *m/z* 264.6 $[Fe^{II}(L^2)]^{2+}$ (*z* = 2) calc. 264.6, 678.1 $[Fe^{II}(L^2)(CF_3SO_3)]^+$ (*z* = 1) calc. 678.1.

Crystal structure determinations.

The crystal of **1**.$(ClO_4)_2$ and **2**.$(ClO_4)_2$ were immersed in cryo-oil, mounted in a Nylon loop, and measured at a temperature of 100 K. The X-ray diffraction data were collected on a Bruker Kappa Apex II and Bruker Kappa Apex II Duo diffractometers using Mo Kα radiation (λ = 0.710 73 Å). The *APEX2*[46] program package was used for cell refinements and data reductions. The structure was solved by charge flipping technique (SUPERFLIP)[47] or direct methods using the *SIR2011*[48] program with the *Olex2*[49] graphical user interface. A semi-empirical numerical absorption correction based on equivalent reflections (*SADABS*)[50] was applied to all data. Structural refinements were carried out using *SHELXL-97*.[51] The crystal of **1.$(ClO_4)_2$** was diffracting only weakly and therefore atoms N2, C16, C17, C18, C19, and C20 were restrained to have the same U_{ij} components within the standard uncertainty of 0.02.In **2.$(ClO_4)_2$** one molecule of the acetonitrile of crystallization was disordered over two sites with equal occupancies. Hydrogen atoms were positioned geometrically and were also constrained to ride on their parent atoms, with C-H = 0.95-0.1.00 Å, and U_{iso} = 1.2-1.5 U_{eq}(parent atom). The crystallographic details are summarized in Table **2**.

Hydrogen atom transfer (HAT) reactions:

Fe(IV) oxo solutions (in the concentration ranges 0.5 mM – 1.0 mM) in CH_3CN were prepared by using excess solid PhIO to optimize yield; after filtration of unreacted PhIO, the solutions represent a reaction system without any methanol or per-acid contaminants. On deaeration of the solutions and a temperature equilibration at 25 ^{0}C in the UV/Vis cuvette, substrates were added to the stirred solutions. The concentrations of substrates used were ranged from 25 mM to 800 mM and were adjusted to achieve convenient times for the reduction of Fe(IV) oxo species. The time course decay of the Fe(IV) oxo was then monitored at 25 ^{0}C by the UV/Vis spectrophotometer. Time courses were subjected to pseudo-first order fit and second order rate constants were evaluated from the concentration dependence data.

To isolate the organic products, the solutions after the end of the reaction was passed through a silica column, using ethyl acetate as the eluent, in order to remove the metal complex. The ethyl acetate solutions were then analyzed by GC using a known strength of biphenyl solution as the quantification standard. All the data obtained from these studies were collected in Table S3.

Oxygen atom transfer (OAT) reactions: The Fe(IV) oxo solutions were prepared as described before. The solutions were placed in cuvette and the temperature of the UV/Vis instrument was monitoed to -30 ºC. Then, appropriate amounts of thioanisole substrate were added to the Fe(IV) oxo solution and the subsequent decay was monitored. Time courses were subjected to pseudo-first order fit and second order rate constants were evaluated from the concentration dependence data.

The products were quantified following the procedure as described before. The chirality of the sulfoxide product was not determined.

Computational Details and Modeling

All DFT calculations were carried out with the Gaussian 09 package of programs.[52] using the B3LYP hybrid functional. This functional is comprised of Becke's three-parameter hybrid exchange functional (B3)[53] and the correlation functional of Lee, Yang, and Parr (LYP).[54] The iron atom was described with the Stuttgart-Dresden effective core potential and SDD basis set,[55] and the 6-31G(d') basis set[56] was employed for all remaining atoms.

All reported geometries were fully optimized, and analytical second derivatives were evaluated at each stationary point to determine whether the geometry was an energy minimum (no negative eigenvalues) or a transition structure (one negative eigenvalue). Unscaled vibrational frequencies were used to make zero-point and thermal corrections to the electronic energies. The resulting potential energies and enthalpies are reported in kcal/mol relative to the specified standard. Standard state corrections were applied to all species to convert concentrations from 1 atm to 1M according to the treatise of Cramer.[57] Internal reaction coordinate (IRC) calculations were performed on **^{3}TS^{3}AB^{3}CD** and **^{5}TS^{5}AB^{5}CD** in order to establish the reactant and product species associated with these transition-state structures. The geometry-optimized structures have been drawn with the *JIMP*2 molecular visualization and manipulation program.[58]

Table 7. Selected bond distances (Å) and bond angles (°) of complexes **1**·$(ClO_4)_2$ and **2**·$(ClO_4)_2$

Complex **1**·$(ClO_4)_2$		Complex **2**·$(ClO_4)_2$	
Fe(1)-N(7)	1.909(6)	Fe(1)-N(6)	1.901(3)
Fe(1)-N(4)	1.948(6)	Fe(1)-N(1)	1.964(3)
Fe(1)-N(5)	1.957(6)	Fe(1)-N(4)	1.979(2)
Fe(1)-N(6)	1.960(6)	Fe(1)-N(3)	1.983(3)
Fe(1)-N(1)	1.977(6)	Fe(1)-N(2)	1.983(3)
Fe(1)-N(3)	1.980(6)	Fe(1)-N(5)	2.028(3)
N(7)-Fe(1)-N(4)	94.2(2)	N(6)-Fe(1)-N(1)	96.21(11)
N(7)-Fe(1)-N(5)	93.3(2)	N(6)-Fe(1)-N(4)	99.96(11)
N(4)-Fe(1)-N(5)	89.2(2)	N(1)-Fe(1)-N(4)	91.27(10)
N(7)-Fe(1)-N(6)	97.5(3)	N(6)-Fe(1)-N(3)	98.00(12)
N(4)-Fe(1)-N(6)	167.7(2)	N(1)-Fe(1)-N(3)	165.72(12)
N(5)-Fe(1)-N(6)	92.2(2)	N(4)-Fe(1)-N(3)	87.72(10)
N(7)-Fe(1)-N(1)	100.1(2)	N(6)-Fe(1)-N(2)	95.90(11)
N(4)-Fe(1)-N(1)	88.9(2)	N(1)-Fe(1)-N(2)	86.84(10)
N(5)-Fe(1)-N(1)	166.6(2)	N(4)-Fe(1)-N(2)	164.14(11)
N(6)-Fe(1)-N(1)	86.9(2)	N(3)-Fe(1)-N(2)	90.25(10)
N(7)-Fe(1)-N(3)	175.7(2)	N(6)-Fe(1)-N(5)	176.64(11)
N(4)-Fe(1)-N(3)	84.2(2)	N(1)-Fe(1)-N(5)	81.65(11)
N(5)-Fe(1)-N(3)	82.5(2)	N(4)-Fe(1)-N(5)	82.72(11)
N(6)-Fe(1)-N(3)	83.9(3)	N(3)-Fe(1)-N(5)	84.08(11)
N(1)-Fe(1)-N(3)	84.1(2)	N(2)-Fe(1)-N(5)	81.43(10)

ASSOCIATED CONTENT

Supporting Information

ESI-MS, ^{1}H-NMR and FT-IR spectra of complexes **1**·$(ClO_4)_2$ and **2**·$(ClO_4)_2$, the UV/Vis spectra of the ligands, the cyclic voltametric diagrams of complexes **1**·$(ClO_4)_2$ and **2**·$(ClO_4)_2$, the kinetic absorbance spectra of formation of complexes **3** and **4**, HRMS of complexes **3** and **4**, detailed product analyses, figures of the optimized ground-state and transition-state structures for the toluene and methane oxidation cycles involving ^{3}**E**, along with tables of atomic coordinates and electronic energies for all optimized structures are available. This material is available free of charge via the Internet at http://pubs.acs.org.

AUTHOR INFORMATION

Corresponding Author

Ebbe Nordlander (Ebbe.Nordlander@chemphys.lu.se)
Miquel Costas (Miquel.Costas@udg.edu)

Author Contributions

The manuscript was written through contributions of all authors. All authors have given approval to the final version of the manuscript

Notes

The authors declare no competing financial interests.

ACKNOWLEDGMENT

This research has been carried out within the framework of the International Research Training Group *Metal Sites in Biomolecules: Structures, Regulation and Mechanisms* (www.biometals.eu) and has also been supported by COST Action CM1003. M.M thanks the European Union for an Erasmus Mundus fellowship. MGR thanks the Robert A. Welch Foundation (grant B-1093) for financial support and acknowledges computational resources through UNT's High Performance Computing Services funded by NSF (CHE-0741936).

REFERENCES

(1) (a) Costas, M.; Mehn, M. P.; Jensen, M. P.; Que, L. Jr. *Chem. Rev.* **2004**, 104, 939-986. (b) Abu-Omar, M. M.; Loaiza, A.; Hontzeas, N. *Chem. Rev.* **2005**, 105, 2227-2252. (c) Shan, X. P.; Que, L. Jr. *J. Inorg. Biochem.* **2006**, 100, 421-433. (d) Kryatov, S. V.; Rybak-Akimova, E. V.; Schindler, S. *Chem. Rev.* **2005**, 105, 2175-2226. (e) Bruijnincx, P. C. A.; van Koten, G.; Klein Gebbink, R. J. M. *Chem. Soc. Rev.* **2008**, 37, 2716-2744. (f) Meunier, B.; de Visser, S. P.; Shaik, S. *Chem. Rev.* **2004**, 104, 3947-3980.
(2) McDonald, A. R.; Que, L. Jr. *Coord. Chem. Rev.* **2013**, 257, 414-428.
(3) (a) Kovaleva, E. G.; Lipscomb, J. D. *Nat. Chem. Biol.* **2008**, 4, 186-193. (b) Groves, J. T. *J. Inorg. Biochem.* **2006**, 100, 434-447.
(4) (a) Bollinger, J. M. Jr.; Price, J. C.; Hoffart, L. M.; Barr, E. W.; Krebs, C. *Eur. J. Inorg. Chem.* **2005**, 4245-4254. (b) Price, J. C.; Barr, E. W.; Tirupati, B.; Bollinger, J. M. Jr.; Krebs, C. *Biochemistry* **2003**, 42, 7497-7508.
(5) Hoffart, L. M.; Barr, E. W.; Guyer, R. B.; Bollinger, J. M. Jr.; Krebs, C. *Proc. Natl. Acad. Sci. USA* **2006**, 103, 14738-14743.
(6) Galonic, D. P.; Barr, E. W.; Walsh, C. T.; Bollinger, J. M. Jr.; Krebs, C. *Nat. Chem. Biol.* **2007**, 3, 113-116.
(7) Eser, B. E.; Barr, E. W.; Frantom, P. A.; Saleh, L.; Bollinger, J. M. Jr.; Krebs, C.; Fitzpatrick, P. F. *J. Am. Chem. Soc.* **2007**, 129, 11334-11335.
(8) Mathews, M. L.; Krest, C. M.; Barr, E. W.; Vaillancourt, F. H.; Walsh, C. T.; Green, M. T.; Krebs, C.; Bollinger, J. M. Jr. *Biochemistry* **2009**, 48, 4331-4343.

(9) (a) Krebs, C.; Fujimori, D. G.; Walsh, C. T.; Bollinger, J. M. Jr. *Acc. Chem. Res.* **2007**, 40, 484-492. (b) Proshlyakov, D. A.; Henshaw, T. F.; Monterosso, G. R.; Ryle, M. J.; Hausinger, R. P. *J. Am. Chem. Soc.* **2004**, 126, 1022-1023.
(10) (a) Nam, W. *Acc. Chem. Res.* **2007**, 40, 522-531. (b) Que, L. Jr. *Acc. Chem. Res.* **2007**, 40, 493-500. (c) Lyakin, Y. O.; Shteinman, A. A. *Kinet. Catal.* **2012**, 53, 694-713.
(11) Hohenberger, J.; Ray, K.; Meyer, K. *Nat. Commun.* **2012**, 3, 720-733.
(12) Sastri, C. V.; Lee, J.; Oh, K.; Lee, Y. J.; Lee, J.; Jackson, T. A.; Ray, K.; Hirao, H.; Shin, W.; Halfen, J. A.; Kim, J.; Que, L. Jr.; Shaik, S.; Nam, W. *Proc. Natl. Acad. Sci. USA* **2007**, 104, 19181-19186.
(13) Kaizer, J.; Klinker, E. J.; Oh, N. Y.; Rohde, J. U.; Song, W. J.; Stubna, A.; Kim, J.; Munck, E.; Nam, W.; Que, L. Jr. *J. Am. Chem. Soc.* **2004**, 126, 472-473.
(14) (a) Hirao, H.; Que, L. Jr.; Nam, W.; Shaik, S. *Chem. Eur.J.* **2008**, 14, 1740-1756. (b) Hirao, H.; Kumar, D.; Que, L. Jr.; Shaik, S. *J. Am. Chem. Soc.* **2006**, 128, 8590-8606. (c) Cho, K. B.; Shaik, S.; Nam, W. *Chem. Commun.* **2010**, 46, 4511-4513. (d) Kumar, D.; Hirao, H.; Que, L. Jr.; Shaik, S. *J. Am. Chem. Soc.* **2005**, 127, 8026-8027. (e) Hirao, H.; Kumar, D.; Thiel, W.; Shaik, S. *J. Am. Chem. Soc.* **2005**, 127, 13007-13018. (f) Bernasconi, L.; Louwerse, M. J.; Baerends, E. J. *Eur. J. Inorg. Chem.* **2006**, 3023-3033. (g) Janardanan, D.; Wang, Y.; Schyman, P.; Que, L. Jr.; Shaik, S. *Angew. Chem. Int. Ed.* **2010**, 49, 3342-3345. (h) Chen, H.; Lai, W.; Shaik, S. *J. Phys. Chem. Lett.* **2010**, 1, 1533-1540. (i) Geng, C.; Ye, S.; Neese, F. *Angew. Chem. Int. Ed.* **2010**, 49, 5717-5720. (j) Ye, S.; Neese, F.; *Curr. Opin. Chem. Biol.* **2009**, 13, 89-9. (k) Godfrey, E.; Porro, C. S.; de Visser, S. P. *J. Phys. Chem. A* **2008**, 112, 2464-2468. (l) de Visser, S. P.; Oh, K.; Han, A. R.; Nam, W. *Inorg. Chem.* **2007**, 46, 4632-4641. (m) de Visser, S. P.; Latifi, R.; Tahsini, L.; Nam, W. *Chem. Asian J.* **2011**, 6, 493-504; (n) Shaik, S.; Chen, H.; Janardanan, D. *Nat. Chem.* **2011**, 3, 19-27.
(15) England, J.; Martinho, M.; Farquhar, E. R.; Frisch, J. R.; Bominaar, E. L.; Munck, E.; Que, L. Jr. *Angew. Chem. Int. Ed.* **2009**, 48, 3622-3626.
(16) Macbeth, C. E.; Golombek, A. P.; Young, V. G. Jr.; Yang, C.; Kuczera, K.; Hendrich, M. P.; Borovik, A. S. *Science* **2000**, 289, 938-941.
(17) Wang, D.; Ray, K.; Collins, M. J.; Farquhar, E. R.; Frisch, J. R.; Gomez, L.; Jackson, T. A.; Kerscher, M.; Waleska, A.; Comba, P.; Costas, M.; Que, L. Jr. *Chem. Sci.* **2013**, 4, 282-291.
(18) Lubben, M.; Meetsma, A.; Wilkinson, E. C.; Feringa, B. L.; Que, L. Jr. *Angew. Chem. Int. Ed.* **1995**, 34, 1512-1514.
(19) Klinker, E. J.; Kaizer, J.; Brennessel, W. W.; Woodrum, N. L.; Cramer, C. J.; Que, L. Jr. *Angew. Chem. Int. Ed.* **2005**, 44, 3690-3694.
(20) (a) McQuilken, A. C.; Jiang, Y.; Siegler, M. A.; Goldberg, D. P. *J. Am. Chem. Soc.* **2012**, 134, 8758-8761. (b) Sahu, S.; Widger, L. R.; Quense, M. G.; de Visser, S. P.; Matsumura, H.; Moenne-Loccoz, P.; Siegler, M. A.; Goldberg, D. P. *J. Am. Chem. Soc.* **2013**, 135, 10590-10593. (c) Widger, L. R.; Davies, C. G.; Yang, T.; Siegler, M. A.; Troeppner, O.; Jameson, G. N. L.; Ivanovic-Burmazovic, I.; Goldberg, D. P. *J. Am. Chem. Soc.* **2014**, 136, 2699-2702.
(21) Draksharapu, A.; Li, Q.; Logtenberg, H.; van den Berg, T. A.; Meetsma, A.; Killen, J. S.; Feringa, B. L.; Hage, R.; Roelfes, G.; Browne, W. R.; *Inorg. Chem.* **2012**, 51, 900-913.
(22) Seo, M. S.; Kim, N. H.; Chao, K. B.; So, J. E.; Park, S. K.; Clemancey, M.; Garcia-Serres, R.; Latour, J. M.; Shaik, S.; Nam, W. *Chem. Sci.* **2011**, 2, 1039-1045.
(23) Wang, B.; Wang, S.; Xia, C.; Sun, W. *Chem. Eur. J.* **2012**, 18, 7332-7335.
(24) Mitra, M.; Lloret-Fillol, J.; Haukka, M.; Costas, M.; Nordlander, E. *Chem. Commun.* **2014**, 50, 1408-140.
(25) (a) Goodgame, M.; Cotton, F. A. *J. Am. Chem. Soc.*, **1992**, 84, 1543-1548. (b) Johnson, C. R.; Shepherd, R. E. *Inorg. Chem.*, **1983**, 22, 3506-3513. (c) Goodgame, D. M. L.; Goodgame, M.; Weeks, M. J.; *J. Chem. Soc.*, 1**964**, 5194-5199.
(26) Roelfes, G.; Branum, M. E.; Wang, L.; Que, L. Jr.; Feringa, B. L. *J. Am. Chem. Soc.* **2000**, 122, 11517-11518.
(27) Niemers, E.; Hiltmann, R. *Synthesis* **1976**, 593-595.
(28) Roelfes, G.; Lubben, M.; Chen, K.; Ho, R. Y. N.; Meetsma, A.; Genseberger, S.; Hermant, R. M.; Hage, R.; Mandal, S. K.; Young, V. G. Jr.; Zang, Y.; Kooijman, H.; Spek, A. L.; Que, L. Jr.; Feringa, B. L. *Inorg. Chem.* **1999**, 38, 1929-1936.
(29) Patra, A. K.; Olmsted, M. M.; Mascharak, P. K. *Inorg. Chem.* **2002**, 41, 5403-5409.
(30) Wong, E.; Jeck, J.; Grau, M.; White, A. J. P.; Britovsek, G. J. P. *Catal. Sci. Technol.* **2013**, 3, 1116-1122.
(31) Bell, R. P. *Proc. R. Soc. Lond. A* **1936**, 154, 414-429.
(32) Evans, M. G.; Polanyi, M. *Trans. Faraday Soc.* **1938**, 34, 11-24.
(33) (a) Meyer, J. M. *Acc. Chem. Res.* **1998**, 31, 441-450. (b) Warren, J. J.; Tronic, T. A.; Meyer, J. M. *Chem. Rev.* **2010**, 110, 6961-7001. (c) Meyer, J. M. *Acc. Chem. Res.* **2011**, 44, 36-46.
(34) Shaik, S., Chen, H., Janardanan, D. *Nat. Chem.* **2011**, 3, 19-27.
(35) D. Janardanan, D. Usharani, H. Chen, S. Shaik, *J. Phys. Chem. Lett.* **2011**, *2*, 2610-2617.
(36) D. Usharani, D. Janardanan, S. Shaik, *J. Am. Chem. Soc.* **2011**, *133*, 176-179.
(37) The DFT-optimized structures for all species on the triplet pi and quintet sigma surfaces have been deposited as SI material.
(38) (a) We have also probed the activation of methane via a quintet pi manifold and find this H-abstraction to lie ca. 7 kcal/mol higher in energy than ^{3}**TS**^{3}**AB**^{3}**CD** in excellent agreement with the recent review by Shaik et al. on related systems. (b) D. Usharani, D. Janardanan, C. Li, S. Shaik, *Acc. Chem. Res.* **2013**, *46*, 471-482.
(39) (a) Shaik, S.; Lai, W.; Chen, H.; Wong, Y. *Acc. Chem. Res.* **2010**, 43, 1154-1165. (b) Ye, S.; Geng, C. Y.; Shaik, S.; Neese, F.; *Phys. Chem. Chem. Phys.* **2013**, 15, 8017-8030.
(40) Zhou, Y.; Shan, X.; Mas-Balleste, R.; Bukowski, M. R.; Stubna, A.; Chakrabarti, M.; Slominski, L.; Halfen, J. A.; Munck, E.; Que, L. Jr. *Angew. Chem. Int. Ed.* **2008**, 47, 1896-1899.
(41) England, J.; Bigelow, J. O.; Heuvelen, K. M.V.; Farquhar, E. R.; Martinho, M.; Meier, K. K.; Frisch, J. R.; Munck, E.; Que, L. Jr. *Chem. Sci.* **2014**, 5, 1204-1215.
(42) Thibon, A.; England, J.; Martinho, M.; Young, V. G.; Frisch, J. R.; Guillot, R.; Girerd, J.-J.; Munck, E.; Que, L. Jr.; Banse, F. *Angew. Chem. Int. Ed.* **2008**, 47, 7064-7067.
(43) Bukowski, M. R.; Comba, P.; Lienke, A.; Limberg, C.; Laorden, C. L. D.; Mas-Balleste, R.; Murz, M.; Que, L. Jr. *Angew. Chem. Int. Ed.* **2006**, 45, 3446-3449.
(44) Company, A.; Sabenya, G.; Gonzalez-Bejar, M.; Gomez, L.; Clemancey, M.; Blondin, G.; Jasniewski, A. J.; Puri, M.; Browne, W. R.; Latour, J. M.; Que, L. Jr.; Costas, M.; Perez-Prieto, J.; Lloret-Fillol, J. *J. Am. Chem. Soc.* **2014**, 136, 4624-4633.
(45) Amrutkar, S. V.; Bhagat, U. D.; Parghamol, P.; Kotgire, S. S.; Ranawat, M. S. *Int. J. Pharm. Pharm. Sci.* **2010**, 2, 84-92.
(46) Bruker AXS, APEX2 - Software Suite for Crystallographic Programs -, Bruker AXS, Inc., Madison, WI, USA, **2009**.
(47) G. M. Sheldrick, *ActaCryst.***2008,** A64, 112-122.
(48) Farrugia, L. J. *J. Appl. Crystallogr.* **1999**, 32, 837-837.
(49) Spek, A. L. *J.Appl.Cryst.* **2003**, *36*, 7-13.
(50) Sheldrick, G. M. *SADABS*, Bruker AXS Scaling and Absorption Correction -, Bruker AXS, Inc., Madison, WI, USA, **2008**.
(51) Sheldrick, G. M. *SHELXTL*, Bruker Analytical X-ray Systems, Bruker AXS, Inc., Madison, WI, USA, **2005**.
(52) Frisch, M. J. *et al*., Gaussian 09, Revision E.01, Gaussian, Inc., Wallingford, CT, USA, **2009**.
(53) Becke, A. D. *J. Chem. Phys.* **1993**, *98*, 5648-5652.
(54) Lee, C.; Yang. W.; Parr, R. G. *Phys. Rev. B* **1988**, 37, 785-789.
(55) (a) Dolg, M.; Wedig, U.; Stoll, H.; Preuss, H. *J. Chem. Phys.* **1987**, *86*, 866. (b) Walch, S. P.; Bauschlicher, C. W. *J. Chem. Phys.* **1983**, *78*, 4597-4605.
(56) (a) Petersson, G. A.; Bennett, A.; Tensfeldt, T. G.; Al-Laham, M. A.; Shirley, W. A.; Mantzaris, J. *J. Chem. Phys.* **1988**, *89*, 2193-2218. (b) Petersson, G. A.; Al-Laham, M. A. *J. Chem. Phys.* **1991**, *94*, 6081-6090.
(57) Cramer, C.J. *Essentials of Computational Chemistry*, 2nd Ed.; Wiley: Chichester, UK, **2004**.
(58) (a) JIMP2, version 0.091, a free program for the visualization and manipulation of molecules: Hall, M. B.; Fenske, R. F. *Inorg. Chem.* **1972**, *11*, 768-775. (b) Manson, J.; Webster, C. E.; Hall, M. B., Texas A&M University, College Station, TX, **2006:** http://www.chem.tamu.edu/jimp2/index.html.

Paper II

Catalytic C-H oxidations by non-heme mononuclear Fe(II) complexes of pentadentate ligands: Evidence for Fe(IV)-oxo intermediate

Mainak Mitra,[a] Hassan Nimir,[b] David A. Hrovat,[c,d] Albert A. Shteinman,[e] Michael G. Richmond,[d] Miquel Costas*[f] and Ebbe Nordlander*[a]

Keywords: Oxidation/Catalysis/Mononuclear/Non-heme/Kinetic isotope effect/Reactive intermediates.

The oxidation reactions of alkanes with hydrogen peroxide and peracids (peracetic acid and m-chloroperoxybenzoic acid) catalysed by two Fe(II) complexes of pentadentate ligands have been investigated. Kinetic isotope effect experiments and the use of other mechanistic probes have also been performed. Catalytic reactions in H_2O_2 medium are consistent with the involvement of hydroxyl radicals in the rate-determining step, and resultant low kinetic isotope effect values. On the other hand, catalytic reactions performed using peracid media indicate the involvement of an oxidant different from the hydroxyl radical. For these reactions, the kinetic isotope effect values are relatively high (within a range of 4.2-5.1) and the C3/C2 selectivity parameters in adamantane oxidation are greater than 11, thereby excluding the presence of hydroxyl radicals in the rate-determining step. A low spin Fe(III)-OOH species has been detected in the H_2O_2-based catalytic system by UV/Vis, mass spectrometry and EPR spectroscopy, while an Fe(IV)-oxo species is postulated to be the active oxidant in peracid-based catalytic systems.

Introduction

The selective functionalization of organic substrate molecules remains a great challenge in catalysis research.[1] For decades, considerable efforts have been made to develop robust and selective homogeneous oxidation catalysts based on transition metals.[2] Nature employs a number of heme and non-heme iron enzymes to carry out analogous vital biological transformations, involving oxidation of substrates that use dioxygen as the ultimate oxidant.[3-5] These metalloenzymes show high regio- and stereoselectivity and operate under mild conditions.[4] Examples of such enzymes include soluble methane monooxygenases[6] and Rieske oxygenases[4,7] (Figure 1).

[a] Chemical Physics, Department of Chemistry, Lund University, Box 124, SE-221 00, Lund, Sweden
E-mail: Ebbe.Nordlander@chemphys.lu.se
[b] Department of Chemistry and Earth Sciences, College of Arts and Sciences, Qatar University, P.O. Box 2713, Doha, State of Qatar
[c] Center for Advanced Scientific Computing and Modeling, University of North Texas, Denton, Texas 7603, United States
[d] Department of Chemistry, University of North Texas, Denton, Texas 76203, United States
[e] Institute of Problems of Chemical Physics, 142432, Chernogolovka, Moscow district, Russian Federation
[f] QBIS, Department of Chemistry, University de Girona, Campus Montilivi, E-17071 Girona, Spain
Email: Miquel.costas@udg.edu

Supporting information for this article is given via a link at the end of the document.

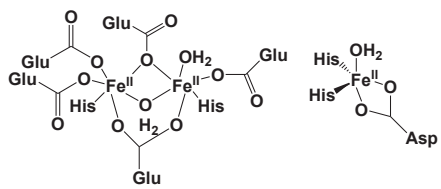

Figure 1. The active site structures of soluble methane monooxygenase (reduced form, left), and a Rieske oxygenase (right).

Inspired by Nature, a wide range of mononuclear non-heme iron complexes have been synthesized and investigated as catalysts for the oxidation of alkanes and alkenes, using hydrogen peroxide, peracids, or dioxygen as an external oxidant.[8-11] Amongst these complexes, mononuclear Fe(II) catalysts bearing tetradentate N4-donor ligands, such as TPA,[12] BPMEN,[13] BQEN,[10b] *S,S*-PDP,[14] ^{Me2}PyTACN,[15] ^{Me2,MeBzIm}TACN[16], deserve special mention (Figure 2). Such Fe(II) complexes exhibit excellent catalytic efficiencies in hydrocarbon oxidation reactions with high stereoretention and C-H bond selectivity. An important structural feature regarding the above-mentioned catalysts is that the Fe(II) ion has two *cis*-coordinated labile sites, which is considered to be a necessary prerequisite for efficient catalytic oxidation.

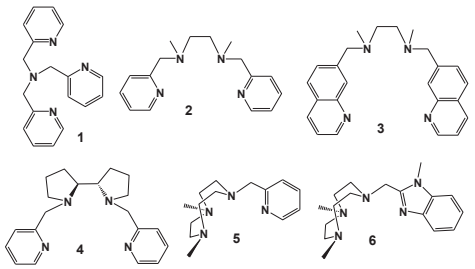

Figure 1. The structures of the ligands, TPA (**1**), BPMEN (**2**), BQEN (**3**), *S*,*S*-PDP (**4**), ^{Me2}PyTACN (**5**) and ^{Me2,MeBzIm}TACN (**6**).

On the other hand, activated bleomycin, a biomolecule and potential antitumor drug that effects the oxidative cleavage of DNA and also the oxidation of hydrocarbons,[17] contains a low spin Fe(III)-hydroperoxo unit surrounded by five nitrogen donors.[18] Therefore, oxygen activation and hydrocarbon oxidation by mononuclear Fe(II) complexes containing pentadentate ligands with one labile coordination site have been studied extensively during the last two decades.[19-27] Reactions with suitable oxidants, e.g. O_2, H_2O_2, PhIO, give rise to Fe(III)-OOH or Fe(IV)=O intermediates that have been characterized by various spectroscopic techniques.[28-30] In contrast to the ferrous complexes of tetradentate ligands that have been discussed above, Fe(II) complexes of pentadentate ligands can form high valent Fe(IV)=O intermediates that possess relatively high thermal stability, permitting thorough investigations of such high-valent intermediates in oxidative transformation reactions. In this context, the pentadentate ligand N4Py and its Fe(II)-complex are noteworthy.[19] Both $[Fe^{III}(OOH)(N4Py)]^{2+}$ [19a,28] and $[Fe^{IV}(O)(N4Py)]^{2+}$ [29] have been synthesized from the Fe(II) precursor complex and characterized. The catalytic activities of the Fe(II) complex of N4Py have been studied[20] and the involvement of $[Fe^{III}(OOH)(N4Py)]^{2+}$ and $[Fe^{IV}(O)(N4Py)]^{2+}$ as possible active oxidants during catalysis has been established both experimentally and theoretically.[20,27,30,31]

We have previously demonstrated that successive replacement of pyridyl substituents of the ligand N4Py by (*N*-methyl)benzimidazolyl moieties results in an increase in the rates of hydrogen atom abstraction reactions and oxo-transfer reaction by the Fe(IV)-oxo complexes $[Fe^{IV}(O)(L^1)]^{2+}$ and $[Fe^{IV}(O)(L^2)]^{2+}$ (L^1 = [*N*-(1-methyl-2-benzimidazolyl)methyl-*N*-(2-pyridyl)methyl-*N*-(bis-2-pyridylmethyl)amine] and L^2 = [*N*-bis(1-methyl-2-benzimidazolyl)methyl-*N*-(bis-2-pyridylmethyl)amine] ; Fig. 2).[32] Here we report oxidation of various hydrocarbons by H_2O_2 or peracids using these Fe(II) complexes as catalyst precursors. Spectrosopic studies of possible reactive intermediates operating during catalysis are also described.

Results and Discussion

The catalytic activities of the two Fe(II) complexes $[Fe^{II}(L^1)(CH_3CN)](ClO_4)_2$ (**1**) and $[Fe^{II}(L^2)(CH_3CN)](ClO_4)_2$ (**2**) (Figure 2) were studied in oxidation of different alkanes, utilizing hydrogen peroxide, peracetic acid (PAA) or *m*-chloroperoxybenzoic acid (mCPBA) as co-oxidants. The oxidation reactions were carried out under standard catalytic conditions (1:100:1000 ratio for catalyst:oxidant:substrate) in acetonitrile at room temperature, and the results were compared to those for $[Fe^{II}(N4Py)(CH_3CN)](ClO_4)_2$. The oxidant was added using a syringe pump and a large excess of substrate was used to minimize over-oxidation of the products.

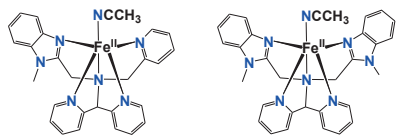

Figure 2. The structures of the Fe(II)-complexes, $[Fe(L^1)(CH_3CN)]^{2+}$ ($\mathbf{1}^{2+}$) (left) and $[Fe(L^2)(CH_3CN)]^{2+}$ ($\mathbf{2}^{2+}$) (right).

Complex **1** together with H_2O_2 oxidizes cyclohexane and a turnover number (TON) of 21.1 for cyclohexanol and 18.0 for cyclohexanone was obtained with an overall yield of 39% (based on oxidant). Under similar conditions, for complex **2**, a TON of 17.4 for cyclohexanol and 14.7 for cyclohexanone was obtained with an overall yield of 32% (Table 1). The alcohol/ketone (A/K) ratio was found to be low (1.2) in both cases, and may be explained by considering the possible involvement of freely diffusing carbon-centered radicals that are trapped by molecular oxygen, followed by a Russell termination step.[9] Addition of 50 mol% (w.r.t. the oxidant, H_2O_2) of acetic acid does not lead to any significant improvement of the overall yield or A/K ratio in cyclohexane oxidation. The kinetic isotope effect (KIE) was determined for the formation of cyclohexanol in competition experiments between cyclohexane and its d_{12} isotopomer. The KIE values obtained for complexes **1** and **2** were 1.45 and 1.7, respectively. These low KIE values are consistent with the involvement of hydroxyl radicals in the rate-determining step of C-H bond cleavage. When cyclooctane was employed as the substrate, both cyclooctanol and

cyclooctanone were formed. Complex **1** together with H_2O_2 (50 eq.) produced cyclooctanol with a TON of 3.7 and cyclooctanone with a TON of 14 and an overall yield of 35.7%, while complex **2** together with H_2O_2 (100 eq.) produced cyclooctanol with a TON of 6.6 and cyclooctanone with a TON of 24.7 and an overall yield of 31.3%.

The oxidation of adamantane by **1**/**2** was examined to probe the nature of the H-abstracting species, on the basis of the tertiary to secondary (C3/C2) C-H bond selectivity. The C3/C2 parameters in this reaction were small (the normalized C3/C2 ratio obtained was 3.6 for **1** and 4.5 for **2**), and thus consistent with the formation of a highly reactive but poorly selective species. Finally, complexes **1**/**2** together with H_2O_2 oxidized *cis*-1,2-dimethylcyclohexane (*cis*-DMCH) to both *cis*- and *trans*-1,2-dimethylcyclohexanol. The reaction took place without retention of *cis*-configuration. Overall, the reactivity patterns that arise from the oxidation of these mechanistic probes are consistent with Fenton type activation of H_2O_2 to generate hydroxyl radicals that then attack the substrate, generating freely diffusing carbon centered radicals.

The behaviour of **1**/H_2O_2 with olefins also supports the mechanistic conclusions derived from the alkane oxidation reactions by H_2O_2. Styrene was converted mainly into benzaldehyde (yield 41%) and only a small amount of styrene epoxide (yield 3%) was obtained. Cyclohexene oxidation afforded the corresponding allylic alcohol and ketone as the major product and a minor amount of cyclohexene epoxide was formed.

Table 1. Catalytic oxidation of cyclohexane carried out by complexes **1** and **2** with H_2O_2[a]

Complex	TON of A[b]	TON of K[c]	Yield (%)[c]	A/K	KIE[d]
1	21.1	18	39	1.2	1.45
2	17.4	14.7	32	1.2	1.7

[a] Reaction conditions: see Experimental section [b] Cyclohexanol [c] Cyclohexanone [d] Kinetic isotope effect was determined for the formation of cyclohexanol from a competitive reaction of a (1:1) mixture of cyclohexane and cyclohexane-d_{12}.

Analogous reactions were carried out using peracids. On using peracetic acid (PAA), both the conversion and turnover numbers diminished. Complex **1** gave an overall conversion of 5% with a TON of 3.8 for cyclohexanol (A) and 1.3 for cyclohexanone (K) (A/K = 3), while complex **2** gave an overall conversion of 9 % with a TON of 5.2 for cyclohexanol and 4.0 for cyclohexanone (A/K = 1.3) (Table 2). On the other hand, mCPBA exhibited a catalytic efficiency analogous to H_2O_2. Complex **1** produced an overall yield of 30%, TON for A = 23, TON for K = 6.9, and complex **2** produced an overall yield 32.5%, TON for A = 22.3, TON for K = 10.2 (Table 2). The A/K ratios were slightly increased in favour of the alcohol product (complex **1**, A/K ~ 3; complex **2**, A/K ~ 2). The KIE values estimated in the competitive oxidation of cyclohexane and its perdeuterated analogue were found to be higher than with H_2O_2 for both complexes (Table 2). On the basis of the improved A/K ratio and comparatively high(er) KIE values, significant participation of hydroxyl radicals in the peracid-based oxidation reactions may be excluded.

Table 2. Catalytic oxidation of cyclohexane carried out by complexes **1** and **2** with PAA and mCPBA[a]

Complex	Oxidant	TON of A[b]	TON of K[c]	Yield (%)	A/K	KIE[d]
1	PAA	3.8	1.3	5.1	3.0	5.0
2	PAA	5.2	4.0	9.2	1.3	5.1
1	mCPBA	23	6.9	30	3.3	4.2
2	mCPBA	22.3	10.2	32.5	2.2	4.5

[a] Reaction conditions: see Experimental section [b] Cyclohexanol [c] Cyclohexanone [d] Kinetic isotope effect was determined for the formation of cyclohexanol from a competitive reaction of a (1:1) mixture of cyclohexane and cyclohexane-d_{12}.

Furthermore, selectivity probes indicated that oxidations with peracids involve species more selective than those involved with H_2O_2 (*vide supra*). For example, in the oxidation of adamantane by **1**/peracid, the C3/C2 parameters were found to be significantly higher (the normalized C3/C2 ratio obtained for **1** was 15.8 with PAA and 11.4 with mCPBA). For complex **2**, the normalized C3/C2 parameters were 15.0 (with PAA) and 12.3 (with mCPBA). More interestingly, the C3/C2 selectivity/ratio in the oxidation of *cis*-DMCH by **1** was around 1 with H_2O_2, but this selectivity was found be approximately 12 with PAA/mCPBA. However, the oxidation of *cis*-DMCH occurs without stereoretention, implicating the presence of long-lived carbon centered radicals.

The catalytic efficiencies of complexes **1** and **2** are comparable to those of $[Fe^{II}(N4Py)(CH_3CN)](ClO_4)_2$ in oxidations utilizing both H_2O_2 and peracids. For example, both complex **1** and complex **2** convert cyclohexane into cyclohexanol and cyclohexanone with overall yields of 39 and 32%, respectively (*vide supra*), while the value for $[Fe^{II}(N4Py)(CH_3CN)](ClO_4)_2$ was 30% (Table 3). The A/K ratio lies in the range 1-2 for all three (pre-)catalysts. The low KIE values suggest significant participation of hydroxyl radicals in

the rate-determining step when H_2O_2 is used as oxidant. When mCPBA was employed as co-oxidant, the yields were found to be similar (30% for complex **1**, 32.5% for complex **2** and 33% for $[Fe^{II}(N4Py)(CH_3CN)](ClO_4)_2$) to those obtained in the analogous H_2O_2 systems, but the A/K ratio slightly improved in the mCPBA system (Table 3). The KIE values for all three complexes were high (in the range 4-5, Table 3) excluding significant participants of hydroxyl radicals.

Table 3. Comparison of catalytic efficiencies between complexes **1**, **2** and $[Fe^{II}(N4Py)(CH_3CN)](ClO_4)_2$ (**3**)[a]

Complex	Oxidant	Total yield (%)[b]	A/K[c]	KIE[d]
1	H_2O_2[e]	39	1.2	1.45
2	H_2O_2[e]	32	1.2	1.7
3[f]	H_2O_2[e]	30.5	1.0	1.5
1	mCPBA[g]	30	3.3	4.2
2	mCPBA[g]	32.5	2.2	4.5
3[h]	mCPBA[g]	33	5.6	4.5

[a] Reaction conditions: 1:100:1000 for cat:oxidant:sub in CH_3CN at RT [b] Total yield of cyclohexanol and cyclohexanone [c] Mol of cyclohexanol/mol of cyclohexanone [d] Kinetic isotope effect was determined for the formation of cyclohexanol from a competitive reaction of a (1:1) mixture of cyclohexane and cyclohexane-d_{12} [e] Under air [f] Ref. [g] Under inert atm. [h] Ref.

Study of reaction intermediates formed during catalysis

UV/Vis spectrophotometry was used to identify possible reactive intermediates involved during the oxidation processes by complex $[Fe^{II}(L^1)(CH_3CN)](CF_3SO_3)_2$ (**1**$^{\mathbf{OTf}}$) (*cf.* Experimental section for synthesis) with H_2O_2 or peracids. Addition of excess H_2O_2 to complex **1**$^{\mathbf{OTf}}$ (0.5 mM) in acetonitrile at room temperature led to the formtion of a transient purple species, having a characteristic absorbance maximum at λ_{max} = 535 nm ($\varepsilon \approx 640\ M^{-1}\,cm^{-1}$) (Figure 3). This species was identified as a $[Fe^{III}(OOH)(L^1)]^{2+}$ complex (**3**) by high resolution mass spectrometry (HRMS) (*cf.* Figures S1-S3, ESI). However, the species decomposed during the mass spectrometric measurement to form the corresponding $[Fe^{IV}(O)(L^1)]^{2+}$ species with prominent mass peak at *m/z* 246.0688 (*cf.* Figures S1-S3, SI). The transient species **3** has a half life of about 3.7 min at room temperature.

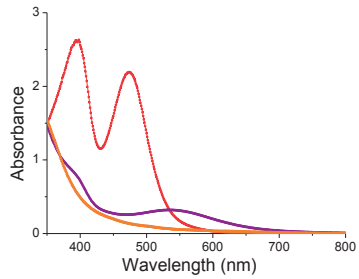

Figure 3. The UV/Vis spectra of **1**$^{\mathbf{OTf}}$ (red line), **3** (purple line) and decay product of **3** (orange line) in acetonitrile measured at room temperature.

An EPR spectroscopy measurement of complex **1**$^{\mathbf{OTf}}$/H_2O_2 in CH_3CN also indicated the formation of **3** as a low spin Fe^{III}-species, exhibiting g-values at 1.98, 2.12, 2.16 (Figure 4). These values are very similar to those obtained for a low spin $[Fe^{III}(OOH)(N4Py)]^{2+}$ species (g-values: 1.98, 2.12, 2.17).[19a]

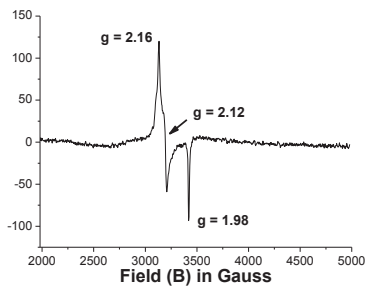

Figure 4. The X-band EPR spectrum (at 80 K) of a frozen solution of **1**$^{\mathbf{OTf}}$ + H_2O_2 in CH_3CN (after mixing at -20 ºC).

Addition of excess H_2O_2 at room temperature to complex **2** in acetonitrile did not lead to purple colouration, rather a brownish yellow colour appeared (Figure 5), which could presumably be an Fe(III)-OH species. However, HRMS collected for a cooled (-20 ºC) acetonitrile solution containing complex **2** with H_2O_2 showed mass peaks at *m/z* 281.0809 and 661.1125 corresponding to the formulations $[Fe^{III}(OOH)(L^2)]^{2+}$ (calc. 281.0822) and $[Fe^{III}(OOH)(L^2)(ClO_4)]^{+}$ (calc. 661.1134) (*cf.* Figure S4-S6, SI). A prominent mass peak at *m/z* 272.5826, corresponding to $[Fe^{IV}(O)(L^2)]^{2+}$ (calc. 272.5808), appeared; this ferryl complex

might be formed by decomposition of the $[Fe^{III}(OOH)(L^2)]^{2+}$ during the measurement.

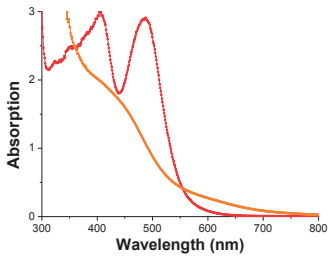

Figure 5. The UV/Vis spectra of **2** (red line) and **2** + H_2O_2 (orange line) in acetonitrile measured at room temperature.

Formation of $[Fe^{III}(OOH)(L^2)]^{2+}$ was further established by EPR spectroscopy. Complex **2** in CH_3CN together with H_2O_2 (at -20 ºC) exhibited EPR signals with g-values 1.98, 2.12, 2.16 (Figure 6), which could be assigned to a low spin $[Fe^{III}(OOH)(L^2)]^{2+}$ species (*vide supra*).

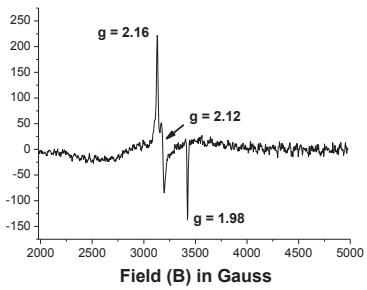

Figure 6. The X-band EPR spectrum (at 80 K) of a frozen solution of **2** + H_2O_2 in CH_3CN (after mixing at -20 ºC).

On the other hand, reaction of $\mathbf{1}^{OTf}$ with mCPBA resulted in formation of a transient $Fe^{IV}(O)$ species, as indicated by UV/Vis spectroscopy and HRMS. The room temperature UV/Vis spectra of $\mathbf{1}^{OTf}$ with excess mCPBA showed formation of a transient species with a broad absorbance maximum in the range 720-725 nm (*cf.* Figure S7, SI). This transient species decayed very rapidly at room temperature to form new species (Figure 7) which possibly could be an Fe(III) species.

The HRMS spectrum of $\mathbf{1}^{OTf}$ together with mCPBA (mixed at -20 ºC) showed formation of $[Fe^{IV}(O)(L^1)]^{2+}$ as well as $[Fe^{IV}(O)(L^1)(CF_3SO_3)]^+$ (*cf.* Figures S8-S10, SI). The isotopic distribution patterns were found to correspond to the formulations of dicationic $[Fe^{IV}(O)(L^1)]^{2+}$ and monocationic $[Fe^{IV}(O)(L^1)(CF_3SO_3)]^+$. Therefore, the transient species observed in the UV/Vis spectra is most likely $[Fe^{IV}(O)(L^1)]^{2+}$, which decays rapidly at room temperature under the reaction conditions.

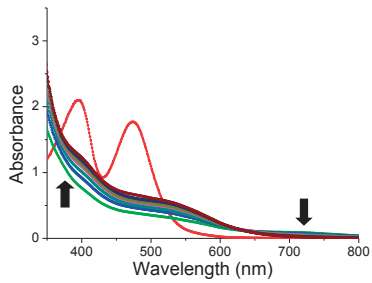

Figure 7. The UV/Vis spectral change taking place upon addition of mCPBA to $\mathbf{1}^{OTf}$ (red line) in CH_3CN at room temperature.

Summary and Conclusions

The complexes $[Fe^{II}(L^1)(CH_3CN)](ClO_4)_2$ (**1**) and $[Fe^{II}(L^2)(CH_3CN)](ClO_4)_2$ (**2**) are competent catalyst precursors for oxidation of alkanes by hydrogen peroxide and peracids (peracetic acid and *m*-chloroperoxybenzoic acid). Kinetic isotope effect measurements and alcohol/ketone ratios indicate that when H_2O_2 is used as an oxidant, a Fenton type mechanism takes place, where the metal complex serves to generate hydroxyl radicals that function as the effective oxidants. Formation of low spin Fe(III)-OOH species from both **1** and **2** have been detected in the H_2O_2-based catalytic system by UV/Vis, mass spectrometry and EPR spectroscopy, and such species may be immediate precursors to hydroxyl radicals, which would be generated by homolytic cleavage of the O-O bond. On the other hand, when the peracids are used as oxidants, relatively high kinetic isotope effects and high C3/C2 selectivity parameters in adamantane oxidation are detected, effectively ruling out a Fenton-type mechanism. For these oxidants, we postulate that the catalytic oxidation mechanism involves $[Fe^{IV}(O)(L)]^{2+}$ (L = L^1, L^2) species that react with the substrates via an oxygen rebound mechanism. These Fe(IV) oxo complexes have previously been isolated and characterized by reaction of **1** or **2** with iodosyl benzene.[32] Overall, the catalytic reactivities of the

Fe(II) complexes follow similar trends (in terms of efficiencies and mechanistic scenarios) to that of $[Fe^{II}(N4Py)(CH_3CN)](ClO_4)_2$ and can be regarded amongst the most efficient non-heme mononuclear iron catalysts.

Experimental Section

Materials and methods.

All solvents were of at least 99.5% purity and used as received. Reagents were of at least 99% purity and used without any further purification. The reagents and solvents were purchased from Sigma-Aldrich and Fisher chemicals.

UV/Visible spectra and all the kinetic experiments were performed on a VWR double-beam UV/Vis spectrophotometer. The reaction mixture in case of kinetic experiments and the complex solution in case of spectra scan were placed in 1cm quartz cell. The mass spectrometry (ESI) was performed with a Bruker HCT ultra. The high resolution mass spectrum (HRMS) was performed using a Bruker FTICR APEX IV instrument. EPR spectra (X-band, 9.46 GHz) were recorded on a Bruker ECS 106 spectrometer at 80 K using liquid nitrogen. Product analyses were performed on an Agilent technologies 7820A gas chromatograph with a 16 sample automatic liquid sampler and flame ionization detector. The products were identified by their GC retention times.

Syntheses.

The Fe(II) complexes, $[Fe^{II}(L^1)(CH_3CN)](ClO_4)_2$ (**1**) and $[Fe^{II}(L^2)(CH_3CN)](ClO_4)_2$ (**2**) were prepared using literature procedure.[32]

Synthesis of $[Fe^{II}(CH_3CN)(L^1)](CF_3SO_3)_2$ (1^{OTf}):

A total of 63 mg (0.15 mmol) of ligand $\mathbf{L^1}$ was taken in a vial and dissolved in minimum amount of acetonitrile To this solution, 65.4 mg (0.15 mmol) of $[Fe(CH_3CN)_2(CF_3SO_3)_2]$ in acetonitrile was added under stirring at room temperature under nitrogen atmosphere. After stirring for about 30 min, the reaction mixture was placed into an ethyl acetate bath and stored overnight. The precipitate was collected by filtration, washed with ethyl acetate, dried under vacuum and obtained as red solid. Yield: 87 mg (71 %). ESI-MS (in CH_3CN): *m/z* 238.1 $[Fe^{II}(L^1)]^{2+}$ (*z* = 2) calc. 238.1, 625.1 $[Fe^{II}(L^1)(CF_3SO_3)]^+$ (*z* = 1) calc. 625.1.

Reaction conditions for catalysis. In a typical reaction, 2ml of 100 mM (200 µmol) H_2O_2 (diluted from 35% H_2O_2 aqueous solution) or 2ml of 100 mM (200 µmol) PAA/mCPBA solution in CH_3CN was delivered by syringe pump in air or under nitrogen to a stirred solution of catalyst, i.e. complex **1** (2 µmol), and the substrate (2000 µmol) inside a vial. The final concentrations of the reagents were ~0.7 mM iron catalyst, ~70 mM oxidant and ~700 mM substrate. After syringe pump addition, a known amount of biphenyl solution was added as an internal standard. The iron complex was removed by passing the reaction mixture through a small silica column followed by elution with ethyl acetate. Finally, the solutions were subjected to GC analysis. The organic products were identified and their yields were determined by comparison with authentic compounds.

To determine the kinetic isotope effect, an equimolar mixture of cyclohexane and cyclohexane-d_{12} was used as a substrate and the reactions were performed under nitrogen atmosphere.

Supporting Information

High resolution mass spectra of the reactive intermediates and the UV/Vis spectrum of $\mathbf{1^{OTf}}$ with mCPBA are available in the Supporting Information file.

Acknowledgments

This research has been carried out within the framework of the International Research Training Group *Metal Sites in Biomolecules: Structures, Regulation and Mechanisms* (www.biometals.eu) and has also been supported by COST Action CM1003. M.M thanks the European Union for an Erasmus Mundus fellowship.

[1] a) T. Newhouse, P. S. Baran, *Angew. Chem. Int. Ed.* **2011**, *50*, 3362-3374; b) L. McMurray, F. O'Hara, M. J. Gaunt, *Chem. Soc. Rev.* **2011**, *40*, 1885-1898; c) M. Bordeaux, A. Galarneau, J. Drone, *Angew. Chem. Int. Ed.* **2012**, *51*, 10712-10723.

[2] (a) *C-H and C-X Bond Functionalization*, (Ed. X. Rivas) Royal Society of Chemistry, Camridge, **2013**; (b) *Biomimetic Oxidations Catalyzed by Transition Metal Complexes*, (Ed. B. Meunier), Imperial College Press, london, **2000**.

[3] A. E. Shilov, G. B. Shul'pin, *Chem. Rev.* **1997**, *97*, 2879-2932.

[4] M. Costas, M. P. Mehn, M. P. Jensen, L. Que, Jr., *Chem. Rev.* **2004**, *104*, 939-986.

[5] S. V. Kryatov, E. V. Rybak-Akimova, S. Schindler, *Chem. Rev.* **2005**, *105*, 2175-2226.

[6] M. Merkx, D. A. Kopp, M. H. Sazinsky, J. L. Blazyk, J. Muller, S. J. Lippard, *Angew. Chem. Int. Ed.* **2001**, *40*, 2782-2807.

[7] M. M. Abu-Omar, A. Loaiza, N. Hontzeas, *Chem. Rev.* **2005**, *105*, 2227-2252.

[8] L. Que Jr., W. B. Tolman, *Nature* **2008**, *455*, 333-340.

[9] M. Costas, K. Chen, L. Que Jr., *Coord. Chem. Rev.* **2000**, *200-202*, 517-544.

[10] a) G. J. P. Britovsek, J. England, A. P. J. White, *Inorg. Chem.* **2005**, *44*, 8125-8134; b) J. England, G.J. P. Britovsek, N. Rabadia, A. P. J. White, *Inorg. Chem.* **2007**, *46*, 3752-3767; c) J. England, R. Gondhia, L. Bigorra-Lopez, A. R. Petersen, A. P. J. White, G. J. P. Britovsek, *Dalton Trans.* **2009**, 5319-5334.

[11] K. P. Bryliakov, E. P. Talsi, *Coord. Chem. Rev.* **2014**, *276*, 73-96.

[12] a) C. Kim, K. Chen, J. Kim, L. Que Jr., *J. Am. Chem. Soc.* **1997**, *119*, 5964-5965; b) J. Kim, R. G. Harrison, C. Kim, L. Que Jr., *J. Am. Chem. Soc.* **1996**, *118*, 4373-4379.

[13] a) K. Chen, L. Que Jr., *Chem. Commun.* **1999**, 1375-1376; b) K. Chen, L. Que Jr., *J. Am. Chem. Soc.* **2001**, *123*, 6327-6337.

[14] M. S. Chen, M. C. White, *Science* **2007**, *318*, 783-787.

[15] a) A. Company, L. Gomez, M. Guell, X. Rivas, J. M. Luis, L. Que Jr., M. Costas, *J. Am. Chem. Soc* **2007**, *129*, 15766-15767; b) A. Company, L. Gomez, X. Fontrodona, X. Rivas, M. Costas, *Chem. Eur. J.* **2008**, *14*, 5727-5731.

[16] M. Mitra, J. Lloret-Fillo, M. Haukka, M. Costas, E. Nordlander, *Chem. Commun.* **2014**, *50*, 1410-1412.

[17] a) J. Stubbe, J. W. Kozarich, *Chem. Rev.* **1987**, *87*, 1107-1136; b) S. M. Hecht, *Acc. chem. Res.* **1986**, *19*,383-391.

[18] a) J. W. Sam, X.-J. Tang, J. Perisach, *J. Am. Chem. Soc.* **1994**, *116*, 5250-5256; b) T. E. Westre, K. E. Loeb, J. M. Zaleski, B. Hedman, K. O. Hodgson, E. I. Solomon, *ibid.* **1995**, *117*, 1309-1313; c) R. M. Burger, T. A. Kent, S. B. Howitz, E. Munck, J. Perisach, *J. Biol. Chem.* **1983**, *258*, 1559-1564.

[19] a) M. Lubben, A. Meetsma, E. C. Wilkinson, B. L. Feringa, L. Que Jr., *Angew. Chem. Int. Ed.* **1995**, *34*, 1512-1514; b) G. Roelfes, M. Lubben, S. W. Leppard, E. P. Schudde, R. M. Hermant, R. Hage, E. C. Wilkinson, L. Que Jr., B. L. Feringa, *J. Mol. Catal. A* **1997**, *117*, 223-227.

[20] G. Roelfes, M. Lubben, R. Hage, L. Que Jr., B. L. Feringa, *Chem. Eur. J.* **2000**, *6*, 2152-2159.

[21] V. Balland, D. Mathieu, N. Pons-Y-Moll, J. F. Bartoli, F. Banase, P. Battiioni, J.-J. Girerd, D. Mansuy, *J. Mol. Catal. A: Chem.* **2004**, *215*, 81-87.

[22] I. Bernal, I. M. Jensen, K. B. Jensen, C. J. McKenzie, H. Toftlund, J.-P. Tuchagues, *J. Chem. Soc., Dalton Trans.* **1995**, 3667-3675

[23] G. Roelfes, V. Vrajmasu, K. Chen, R. Y. N. Ho, J. U. Rohde, C. Zondervan, R. M. la Crois, E. P. Schudde, M. Lutz, A.L. Spek, R. hage, B. L. Feringa, E. Munck, L. Que Jr., *Inorg. Chem.* **2003**, *42*, 2639-2653.

[24] A. K. Patra, M. M. Olmstead, P. K. Mascharak, *Inorg. Chem.* **2002**, *41*, 5403-5409.

[25] A. Grohmann, *Adv. Inorg. Chem.* **2004**, *56*, 179-202.

[26] M. You, M. S. Seo, K. M. Kim, W. Nam, J. Kim, *Bull. Korean Chem. Soc.* **2006**, *27*, 1140-1145.

[27] T. A. van den Berg, J. W. de Boer, W. R. Browne, G. Roelfes, B. L. Feringa, *Chem. Commun.* **2004**, 2550-2551.

[28] G. Roelfes, M. Lubben, K. Chen, R. Y. N. Ho, A. Meetsma, S. Genseberger, R. M. Hermant, R. hage, S. K. Mandal, V. G. Young Jr., Y. Zang, H. Kooijman, A. L. Spek, L. Que Jr., B. L. Feringa, *Inorg. Chem.* **1999**, *38*, 1929-1936.

[29] a) J. Kaizer, E. J. Klinker, N. Y. Oh, J. U. Rohde, W. J. Song, A. Stubna, J. Kim, E. Munck, W. Nam, L. Que Jr., *J. Am. Chem. Soc.* **2004**, *126*, 475-473; b) E. J. Klinker, J. Kaizer, W. W. Brennessel, N. L. Woodrum, C. J. Cramer, L. Que Jr., *Angw. Chem. Int. Ed.* **2005**, *44*, 3690-3694.

[30] N. Lehnert, F. Neese, R. Y. N. Ho, L. Que Jr., E. Solomon, *J. Am. Chem. Soc.* **2002**, *124*, 10810-10822.

[31] D. Kumar, H. Hirao, L. Que Jr., S. Shaik, *J. Am. Chem. Soc.* **2005**, *127*, 8026-8027.

[32] M.Mitra, H. Nimir, S. Demeshko, M. Haukka, J. Lloret-Fillol, M. Meyer, A. Shteinman, W. R. Browne, D. A. Hrovat, M. G. Richmond, M. Costas, E. Nordlander, *Unpublished results*.

Paper III

ChemComm

COMMUNICATION

View Article Online
View Journal | View Issue

Evidence that steric factors modulate reactivity of tautomeric iron–oxo species in stereospecific alkane C–H hydroxylation†

Cite this: *Chem. Commun.*, 2014, 50, 1408

Received 11th October 2013,
Accepted 1st November 2013

DOI: 10.1039/c3cc47830k

www.rsc.org/chemcomm

Mainak Mitra,[a] Julio Lloret-Fillol,[b] Matti Haukka,[c] Miquel Costas*[b] and Ebbe Nordlander*[a]

A new iron complex mediates stereospecific hydroxylation of alkyl C–H bonds with hydrogen peroxide, exhibiting excellent efficiency. Isotope labelling studies provide evidence that the relative reactivity of tautomerically related oxo–iron species responsible for the C–H hydroxylation reaction is dominated by steric factors.

While the selective functionalization of hydrocarbons remains a significant challenge for chemists,[1] several iron-dependent oxygenases are able to mediate the hydroxylation of C–H bonds under mild conditions, using dioxygen as the terminal oxidant.[2] Examples include the cytochrome P450 enzymes,[3] and the family of non-heme iron-dependent Rieske oxygenases.[4] In both cases, C–H hydroxylation occurs with almost complete stereoretention, and is accomplished *via* the intermediacy of an electrophilic high valent iron–oxo species that attacks the C–H bond *via* the so-called oxygen-rebound mechanism (Scheme 1).[5]

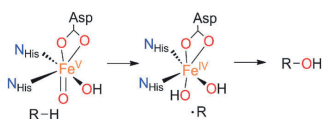

Scheme 1 Schematic mechanism for C–H hydroxylation by a Rieske oxygenase enzyme.

[a] *Chemical Physics, Department of Chemistry, Lund University, P.O. Box 124, Lund, SE-221 00, Sweden. E-mail: Ebbe.Nordlander@chemphys.lu.se; Fax: +46-46-22-24119; Tel: +46-46-22-28118*

[b] *QBIS Group, Department of Chemistry and Institut de Quimica Computacional i Catalisi (IQCC), Universitat de Girona, Campus Montilivi, 17071 Girona, Catalonia, Spain. E-mail: miquel.costas@udg.edu; Fax: +34-972-41-81-50; Tel: +34-972-41-98-42*

[c] *University of Jyväskylä, Department of Chemistry, P.O. Box 35, FI-40014 University of Jyväskylä, Finland*

† Electronic supplementary information (ESI) available: Ligand synthesis, complex synthesis, proton NMR spectra, ESI-MS and IR spectra of the complex, crystallographic data for complexes $\mathbf{1}^{\mathbf{OTf}}$ and $\mathbf{1}^{\mathbf{H_2O}}$, catalysis experiments and results and details of isotope labelling experiments. CCDC 960138 and 960139. For ESI and crystallographic data in CIF or other electronic format see DOI: 10.1039/c3cc47830k

A fundamental difference between heme and non-heme sites is that active sites in the latter contain lower coordination numbers, and a number of them form reactive intermediates containing a *cis*-Fe(O)(X) unit (X = HO(H), Cl, Br). This leads to a versatile reactivity that opens new mechanistic scenarios. Arene *cis*-dihydroxylation and aliphatic chlorination constitute unique examples of the reactivity exhibited by *cis*-Fe(O)(X) units (X = OH, Cl and Br).[4,5b,6]

The reactivity of non-heme oxygenases has inspired the design of synthetic model complexes as selective C–H oxidation catalysts.[7] Mechanistic studies have shown that in selected cases reactions are metal based, involving high-valent oxo–iron species, and are fundamentally distinct from radical pathway Fenton processes.[8] The Fe(PyTACN) family of complexes (Scheme 2) belongs to the group of catalysts that mediate C–H hydroxylation with retention of configuration.[8d] We and others have proposed a mechanistic scenario resembling the "peroxide shunt"[3] of cytochrome P450 and model systems. A highly electrophilic $[Fe^{V}(O)(OH)(L^{N4})]^{2+}$ oxidant (**O**), formed *via* water-assisted cleavage of a hydroperoxide $[Fe^{III}(OOH)(OH_2)(L^{N4})]^{2+}$ ($\mathbf{P_B}$) (Scheme 2), is ultimately responsible for C–H oxidation reactions.[8a,d,9–11] Intermediate **O** can exist as two tautomerically related species, $\mathbf{O_A}$ and $\mathbf{O_B}$, that differ in the relative positions of the oxo and hydroxide ligands, and are connected through prototopic oxo–hydroxo tautomerism. We have also previously studied C–H oxidation reactions using a set of catalysts where electronic properties of the PyTACN ligand were systematically tuned, and found that the relative reactivity of $\mathbf{O_A}$ and $\mathbf{O_B}$ in C–H oxidations remains basically the same, irrespective of the catalyst.[8d]

In this work we turn our attention towards investigation of steric effects. Towards this end, C–H oxidation reactions catalyzed

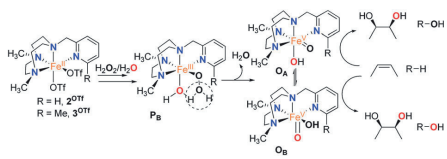

Scheme 2 Mechanism for substrate oxidation by Fe(PyTACN) complexes.

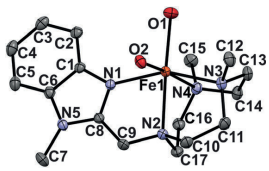

Fig. 1 Molecular structure of $[Fe^{II}(H_2O)_2(^{Me_2,BzIm}TACN)]^{2+}$ ($\mathbf{1^{H_2O}}$) with 30% probability ellipsoids; H-atoms have been omitted for clarity.

using the new iron complex $[Fe^{II}(CF_3SO_3)_2(^{Me_2,BzIm}TACN)]$ (Fig. 1), $\mathbf{1^{OTf}}$, were studied. The new tetradentate ligand ^{Me_2,BzIm}TACN has been developed by replacing the pyridyl arm of the PyTACN scaffold by an *N*-methyl benzimidazolyl substituent. The sp^2 character and the rigidity of the latter substituent should provide a well-defined steric demand, intermediate between the α-H and the α-Me groups of a pyridine (Scheme 2, catalysts $\mathbf{2^{OTf}}$ and $\mathbf{3^{OTf}}$). On the other hand, the relative donor capacities of pyridine and benzimidazole can be estimated to be very similar by comparing the pK_a values of their conjugate acids (5.22 for pyridine, 5.41 for benzimidazole and 5.57 for α-Me pyridine), and therefore differences in reactivity among this set of complexes can be traced to steric factors.

The complexes $[Fe^{II}(CF_3SO_3)_2(^{Me_2,BzIm}TACN)]$, $\mathbf{1^{OTf}}$, and $[Fe^{II}(H_2O)_2(^{Me_2,BzIm}TACN)](CF_3SO_3)_2$, $\mathbf{1^{H_2O}}$, were prepared and characterized following standard procedures (see ESI† for details). The X-ray structures of $\mathbf{1^{OTf}}$ and $\mathbf{1^{H_2O}}$ are very similar to those of $\mathbf{2^{OTf}}$ and $\mathbf{3^{OTf}}$ and have an iron center in a distorted octahedral environment surrounded by the four N atoms of the ligand, with the TACN ring capping one face of the octahedron, and two oxygen atoms of triflate anions ($\mathbf{1^{OTf}}$) or water molecules ($\mathbf{1^{H_2O}}$) *cis* to each other (*cf.* Fig. 1 and ESI†).[8d] Average Fe–N_{TACN} and Fe–O_{H_2O} distances are 2.23 Å and 2.13 Å respectively, characteristic of a high spin ferrous center.[12]

Complex $\mathbf{1^{OTf}}$ was found to be an outstanding catalyst in C–H oxidation reactions with H_2O_2. Catalytic oxidation of cyclohexane was chosen for appropriate comparison with literature precedents.[8,13] Syringe pump addition of 10 equivalents (w.r.t. the complex) of H_2O_2 together with 1000 equivalents of H_2O‡ to a CH_3CN solution containing **1** and a substrate (1000 equivalents) over 30 min in air at room temperature resulted in the formation of cyclohexanol (A) with a turnover number (TON) of 8.5 and a small amount of cyclohexanone (K) with a TON of 0.8, giving an alcohol/ketone (A/K) ratio of 10.6. The efficiency w.r.t. consumption of the oxidant was around 99–100%, and remains unusually high (54%) when 100 equiv. of H_2O_2 are employed. Interestingly, when followed over time, the A/K product ratio in oxidation of cyclohexane showed that the initial value of A/K was around 35, which gradually decreased to 10.6 (*cf.* Fig. S5, ESI†). This provides strong evidence that cyclohexanol is the almost exclusive primary product of the alkane oxidation reaction, and cyclohexanone is a result of further oxidation of the alcohol, thereby eliminating the significant implication of a Russell-type termination mechanism initiated by hydroxyl radicals and producing equal amounts of alcohol and ketone.

Several mechanistic probes further substantiate that the reactions are metal-based. The intermolecular kinetic isotope effect was determined for the formation of cyclohexanol from a mixture (1 : 3) of cyclohexane and its deuterated isotopomer cyclohexane-d_{12}, and was found to be 5. Also, complex $\mathbf{1^{OTf}}$ oxidizes adamantane with a large C3/C2 normalized selectivity (14) towards the tertiary C–H bond. The oxidation of *cis*-1,2-dimethylcyclohexane (DMCH) leads to the corresponding tertiary alcohol product with 97% retention of configuration. These data are consistent with the implication of selective oxidants whose relative reactivities against C–H bonds are modulated by their bond strengths and steric properties.[7a] The reactivity of $\mathbf{1^{OTf}}$ against these mechanistic probes is thus in good accordance with that described for iron catalysts that mediate stereospecific C–H hydroxylation, including those of the [Fe(PyTACN)] family.[8d] Since these catalysts operate *via* a $[Fe^{V}(O)(OH)(L^{N4})]^{2+}$ (**O**) oxidant,[8a,d,10,11] the same was tentatively inferred for $\mathbf{1^{OTf}}$. Strong experimental evidence in favor of this scenario arises from olefin *cis*-dihydroxylation reactions. The water assisted cleavage of the O–O bond (Scheme 2) determines the oxygen atom inventory in the HO–Fe^{V}═O oxidant (**O**). One of the oxygen atoms originates from the water molecule, while the second oxygen atom is derived from the peroxide. *cis*-Dihydroxylation reactions incorporate both oxygen atoms of **O** into the product and consequently *syn*-diols must contain one oxygen atom that originates from water and one oxygen from the peroxide.[11] Indeed, $\mathbf{1^{OTf}}$ catalyzes the oxidation of cyclooctene ($\mathbf{1^{OTf}}$: H_2O_2 : $H_2{}^{18}O$: cyclooctene, 1 : 10 : 1000 : 1000) affording *cis*-cyclooctene epoxide (TON = 2) and *syn*-cyclooctane-1,2-diol (TON = 7). The *syn*-diol is 98% $^{16}O^{18}O$ labeled, providing strong support in favor of **O** as the oxidant.

Having obtained positive evidence that $\mathbf{1^{OTf}}$ operates through the same mechanism as that of $\mathbf{2^{OTf}}$ and $\mathbf{3^{OTf}}$, we proceeded to investigate the relative reactivity of the $\mathbf{O_A}$/$\mathbf{O_B}$ tautomers in C–H hydroxylation reactions. Since the origin of the oxygen atoms is determined in the peroxide precursor ($\mathbf{P_B}$), the relative reactivity of $\mathbf{O_A}$ and $\mathbf{O_B}$ in C–H hydroxylation can be probed using isotopically labeled water and hydrogen peroxide (Scheme 2). The oxidation of cyclohexane by $\mathbf{1^{OTf}}$ in the presence of 10 equivalents of $H_2{}^{18}O_2$ and 1000 equivalents of H_2O afforded 45% ^{18}O-labeled cyclohexanol. Complementary experiments with 10 equivalents of H_2O_2 and 1000 equivalents of $H_2{}^{18}O$ afforded 48% ^{18}O-labeled cyclohexanol (Table 1).

Similar levels of ^{18}O-label incorporation from $H_2{}^{18}O$ were observed in the case of cyclooctane (41%) and cyclohexane-d_{12} (48%). These levels of water incorporation are unusually high, only bypassed in the literature by $\mathbf{2^{OTf}}$,[8d] and constitute strong evidence that $\mathbf{O_A}$ and $\mathbf{O_B}$ are roughly equally reactive against secondary C–H bonds. Most interestingly, when the substrates contain tertiary C–H bonds (*e.g.* DMCH and adamantane), the percentages of ^{18}O incorporation from $H_2{}^{18}O$ were found to be in the range 25–29%, indicating a preferential oxidation *via* $\mathbf{O_A}$.

Interpretation of these values can be done by considering those obtained using $\mathbf{2^{OTf}}$ and $\mathbf{3^{OTf}}$ in analogous reactions. Table 1 shows that hydroxylation of tertiary C–H bonds mediated by $\mathbf{2^{OTf}}$ is predominantly performed by $\mathbf{O_B}$ as shown by the large extent of oxygen atoms originating from water in the alcohol

Table 1 Comparison of percentage of ^{18}O incorporation into alcohol products by different Fe-catalysts using 1000 equivalents of $H_2{}^{18}O$

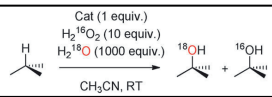

Substrate	1^{Otf}	2^{Otf}	3^{Otf}	Fe(TPA)[b]
Cyclohexane	48	45	11	29
Cyclohexane-d_{12}	48	40	—	35
Cyclooctane	41	44	—	23
cis-DMCH	26	79	2	6
Adamantane	28	74	3	6
cis-Cyclooctene epoxide[a]	24	77	5	9
syn-Cyclooctane-1,2-diol[a]	98	97	78	86

[a] Cyclooctene was employed as a substrate. [b] $[Fe(TPA)(CH_3CN)_2]^{2+}$, Ref. 8a.

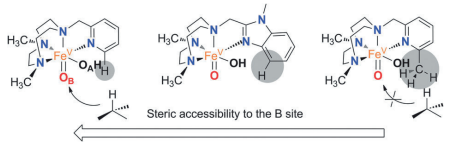

Fig. 2 Comparative analysis of the steric bulk in proximity to site B.

product (up to 79%, *cf.* Table 1). Instead, hydroxylation of secondary C–H bonds occurs with incorporation of ~40% of oxygen atoms from water, suggesting comparable reactivity of both tautomers. In sharp contrast, hydroxylation catalyzed by $\mathbf{3^{Otf}}$ exhibits a relatively small extent (~10%) of water incorporation in hydroxylation of secondary C–H bonds, and negligible (<3%) incorporation in the hydroxylation of tertiary C–H sites, indicating that hydroxylation is almost exclusively performed by $\mathbf{O_A}$.

Therefore, the relative reactivity of the two tautomeric forms of the $[Fe^{V}(O)(OH)(L^{N4})]^{2+}$ (**O**) intermediate is finely tuned among the series of catalysts ($\mathbf{1^{Otf}}$–$\mathbf{3^{Otf}}$), a fact that contrasts with the small effects exerted when the electronic properties of the pyridine in a series of catalysts is altered.[8d] Trends observed for $\mathbf{1^{Otf}}$–$\mathbf{3^{Otf}}$ may thus be rationalized on the basis of steric effects. The benzylimidazole ring introduces steric bulk in the proximity of position B at the iron center that is intermediate between that set by pyridine and 6-Me-pyridine arms (Fig. 2). Accordingly, when secondary C–H bonds are hydroxylated, $\mathbf{1^{Otf}}$ behaves as $\mathbf{2^{Otf}}$, *i.e.* tautomers $\mathbf{O_A}$ and $\mathbf{O_B}$ are equally implicated in the C–H oxidation reaction. On the other hand, oxidation of sterically more demanding tertiary C–H bonds yields levels of water incorporation that suggest predominant participation of $\mathbf{O_A}$ as in the case of $\mathbf{3^{Otf}}$, although unlike in the latter case, implication of $\mathbf{O_B}$ remains significant (~25%) because steric hindrance at position B induced by the C–C-sp^2 benzylimidazole moiety is smaller than the one caused by a C-sp^3 methyl substituent.

In conclusion, the present work adds to the growing evidence that the coordination environment at non-heme sites opens reactivity scenarios unattainable by hemes. Here we have shown that systematic tuning of the steric properties of the two sites in the *cis*-Fe(O)(X) unit translates into systematic differences in relative reactivity of the two iron–oxo tautomers. We postulate that analogous steric conditions may influence the relative reactivities of putative tautomers in non-heme iron oxygenases.

This work has been supported by the European Union (the Erasmus Mundus program), the International Research Training Group *Metal Sites in Biomolecules: Structures, Regulation and Mechanisms* (www.biometals.eu), and COST Action CM1003. M.C. acknowledges ERC-29910, MINECO of Spain for CTQ2012-37420-C02-01/BQU and CSD2010-00065, catalan DIUE (2009SGR637) and an ICREA academia award. J.Ll. thanks MICINN for a RyC contract. We thank Prof. Albert A. Shteinman for fruitful discussions and Dr Santanu Mandal for ^{13}C-NMR measurements.

Notes and references

‡ Analogous product yields and A/K selectivity values were obtained when H_2O (1000 equiv.) was not specifically added.

1 (*a*) T. Newhouse and P. S. Baran, *Angew. Chem., Int. Ed.*, 2011, **50**, 3362–3374; (*b*) L. McMurray, F. O'Hara and M. J. Gaunt, *Chem. Soc. Rev.*, 2011, **40**, 1885–1898; (*c*) M. Bordeaux, A. Galarneau and J. Drone, *Angew. Chem., Int. Ed.*, 2012, **51**, 10712–10723.
2 (*a*) C. E. Tinberg and S. J. Lippard, *Acc. Chem. Res.*, 2011, **44**, 280–288; (*b*) M. Costas, M. P. Mehn, M. P. Jensen and L. Que Jr., *Chem. Rev.*, 2004, **104**, 939–986; (*c*) M. M. Abu-Omar, A. Loaiza and N. Hontzeas, *Chem. Rev.*, 2005, **105**, 2227–2252; (*d*) E. G. Kovaleva and J. D. Lipscomb, *Nat. Chem. Biol.*, 2008, **4**, 186–193.
3 (*a*) J. T. Groves, *Cytochrome P-450. Structure, Mechanism, and Biochemistry*, ed. P. R. Ortiz de Montellano, Plenum Press, New York, 2005, pp. 1–43; (*b*) P. R. Ortiz de Montellano, *Chem. Rev.*, 2010, **110**, 932–948.
4 (*a*) D. T. Gibson and R. E. Parales, *Curr. Opin. Biotechnol.*, 2000, **11**, 236–243; (*b*) A. Karlsson, J. V. Parales, R. E. Parales, D. T. Gibson, H. Eklund and S. Ramaswamy, *Science*, 2003, **299**, 1039–1042.
5 (*a*) J. T. Groves, G. A. McClusky, R. E. White and M. J. Coon, *Biochem. Biophys. Res. Commun.*, 1978, **81**, 154–160; (*b*) S. Chakrabarty, R. N. Austin, D. Deng, J. T. Groves and J. D. Lipscomb, *J. Am. Chem. Soc.*, 2007, **129**, 3514–3515.
6 D. P. Galonić, E. W. Barr, C. T. Walsh, J. M. Bollinger and C. Krebs, *Nat. Chem. Biol.*, 2007, **3**, 113–116.
7 (*a*) L. Que and W. B. Tolman, *Nature*, 2008, **455**, 333–340; (*b*) M. C. White, *Science*, 2012, **335**, 807–809; (*c*) E. B. Bauer, *Curr. Org. Chem.*, 2008, **12**, 1341–1369.
8 (*a*) K. Chen and L. Que Jr., *J. Am. Chem. Soc.*, 2001, **123**, 6327–6337; (*b*) J. Yoon, S. A. Wilson, Y. K. Jang, M. S. Seo, K. Nehru, B. Hedman, K. O. Hodgson, E. Bill, E. I. Solomon and W. Nam, *Angew. Chem., Int. Ed.*, 2009, **48**, 1257–1260; (*c*) S. H. Lee, J. H. Han, H. Kwak, S. J. Lee, E. Y. Lee, H. J. Kim, J. H. Lee, C. Bae, S. N. Lee, Y. Kim and C. Kim, *Chem.–Eur. J.*, 2007, **13**, 9393–9398; (*d*) I. Prat, A. Company, V. Postils, X. Ribas, L. Que, J. M. Luis and M. Costas, *Chem.–Eur. J.*, 2013, **19**, 6724–6738; (*e*) Y. Hitomi, K. Arakawa, T. Funabiki and M. Kodera, *Angew. Chem., Int. Ed.*, 2012, **51**, 3448–3452.
9 DFT calculations indicate that the isomeric peroxide $\mathbf{P_A}$ is not implicated in chemistry. See ref. 8*d*.
10 (*a*) D. Quinonero, K. Morokuma, D. G. Musaev, R. Mas-Balleste and L. Que Jr., *J. Am. Chem. Soc.*, 2005, **127**, 6548–6549; (*b*) A. Bassan, M. R. A. Blomberg, P. E. M. Siegbahn and L. Que Jr., *J. Am. Chem. Soc.*, 2002, **124**, 11056–11063.
11 (*a*) I. Prat, J. S. Mathieson, M. Guell, X. Rivas, J. M. Luis, L. Cronin and M. Costas, *Nat. Chem.*, 2011, **3**, 788–793; (*b*) W. N. Oloo, A. J. Fielding and L. Que Jr., *J. Am. Chem. Soc.*, 2013, **135**, 6438–6441.
12 (*a*) D. Blakesley, S. C. Payne and K. S. Hagen, *Inorg. Chem.*, 2000, **39**, 197–198; (*b*) Y. Zang, J. Kim, Y. Dong, E. C. Wilkinson, E. H. Appelman and L. Que Jr., *J. Am. Chem. Soc.*, 1997, **119**, 4197–4205.
13 (*a*) J. England, C. R. Davies, M. Banaru, A. J. P. White and G. J. P. Britovsek, *Adv. Synth. Catal.*, 2008, **350**, 883–897; (*b*) G. J. P. Britovsek, J. England and A. J. P. White, *Inorg. Chem.*, 2005, **44**, 8125–8134; (*c*) P. Comba, M. Maurer and P. Vadivelu, *Inorg. Chem.*, 2009, **48**, 10389–10396; (*d*) Y. Mekmouche, S. Ménage, C. Toia-Duboc, M. Fontecave, J.-B. Galey, C. Lebrun and J. Pecaut, *Angew. Chem., Int. Ed.*, 2001, **40**, 949–952; (*e*) Y. He, J. D. Gorden and C. R. Goldsmith, *Inorg. Chem.*, 2011, **50**, 12651–12660.

Paper IV

An investigation of steric influence on the reactivity of Fe(V) oxo tautomers in stereospecific alkane C-H hydroxylation

Mainak Mitra,[a] Alexander Brinkmeier,[a] Julio Lloret Fillol,[b] Michael G. Richmond,[c] Miquel Costas,*[,b] Ebbe Nordlander*[,a]

[a] Chemical Physics, Department of Chemistry, Lund University, Box 124, SE-221 00, Lund, Sweden
[b] QBIS, Department of Chemistry, University de Girona, Campus Montilivi, E-17071 Girona, Spain
[c] Department of Chemistry, University of North Texas, Denton, Texas 76203, United States

Abstract

Two new tetradentate N4 ligands, ^{Me2,Me2}PyzTACN (1-(2-(3,5-Dimethyl-1*H*-pyrazol-1-yl)ethyl)-4,7-dimethyl-1,4,7-triazacyclononane) and ^{Me2,Me}ImTACN (1-((1-Methyl-1*H*-imidazol-1-yl)methyl)-4,7-dimethyl-1,4,7-triazacyclononane) have been synthesized and their Fe(II) complexes have been prepared and characterized. The Fe(II) complexes have been found to be capable of hydroxylating C-H bonds of alkanes with excellent efficiencies, using hydrogen peroxide as oxidant. The high kinetic isotope effect values for C-H bond activation, large normalized C3/C2 bond selectivity in adamantane oxidation and high degrees of stereoretention in the oxidation of *cis*-1,2-dimethylcyclohexane are indicative of metal-based oxidation processes. The complexes are also able to oxidize cyclooctene to form its corresponding epoxide and *syn*-diol. For [Fe^{II}(^{Me2,Me2}PyzTACN)(CF_3SO_3)$_2$] the epoxide is the main product, while for the analogous [Fe^{II}(^{Me2,Me2}PyzTACN)(CF_3SO_3)$_2$] complex, the *syn*-diol predominates. The active oxidant is proposed to be an (L)Fe^{V}(O)(OH) species (L = ^{Me2,Me2}PyzTACN, ^{Me2,Me}ImTACN) which may exist in two tautomeric forms related by a proton shift between the oxo and hydroxo ligands. Isotope labeling experiments are in agreement with the oxygen atom in the hydroxylated products originating from both water and hydrogen peroxide, and labeling experiments involving oxygen atom transfer to sterically bulky substrates provide indirect information on the steric influence exerted by the two ligands. These studies indicate that the ^{Me2,Me2}PyzTACN, exerts a greater steric influence than the ^{Me2,Me}ImTACN ligand.

Introduction

Over the last two decades, a number of transition metal-based complexes have been developed as catalysts for selective oxidations of C-H and C=C bonds in unsaturated and saturated alkanes and alkenes.[1] Iron is often a metal of choice for such catalytic transformations because it is inexpensive, non-toxic and highly abundant.[2] In the course of this research, emphasis has also been made on the use of green oxidants, such as dioxygen or hydrogen peroxide, and improvement of selectivities and efficiencies in the oxidation reactions.[1] In Nature, oxygenases carry out a wide range of oxidations of organic substrates, and many of them contain iron in their active sites.[3,4,5] These iron oxygenases are usually highly selective towards specific C-H bonds, in the presence of several other C-H bonds in the substrate, and utilize atmospheric oxygen as the ultimate oxidant. An example is the Rieske oxygenase family of non-heme iron enzymes, which contain an Fe(II) center bound to two histidine residues and one aspartate in the active site.[5,6a] This enzyme family catalyzes the *cis*-dihydroxylation of arenes via activation of dioxygen (Scheme 1) as the first step in

biodegradation of pollutants.[5] The proposed active species consists of a formally high valent Fe(V) center bound to an oxo and a hydroxo group that are *cis* to each other (Scheme 1).[6] The mechanism of C-H hydroxylation is proposed to consist of two concerted steps that are directly related to the "oxygen rebound" mechanism, which has been identified for the cytochrome P450 family of heme oxygenases; this mechanism involves (*i*) abstraction of a hydrogen atom from a substrate C-H bond by the oxo group to form a transient substrate-based alkyl radical and an Fe(IV)$(OH)_2$ moiety, and (*ii*) interaction of the alkyl radical with one of the hydroxyl groups of the Fe(IV)$(OH)_2$ moiety to form the product (Scheme 1).[6b] With the reactivities of non-heme iron oxygenases such as Rieske oxygenases serving as an inspiration, several mononuclear non-heme iron catalysts have been developed to address the challenging oxidations of poorly reactive C-H and C=C bonds.[7-10]

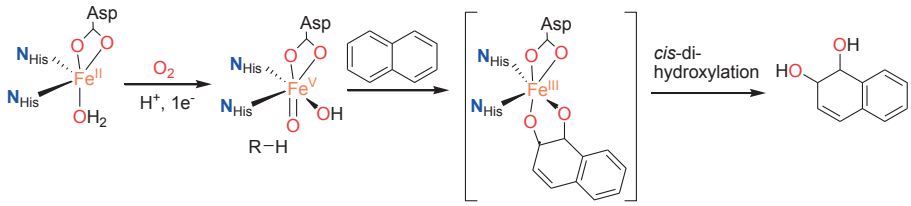

Scheme 1. Proposed reaction mechanism for *cis*-dihydroxylation by Rieske dioxygenases.

The Fe(PyTACN) family of complexes has been shown to mediate C-H hydroxylation via stereoretention of configuration and with excellent efficiencies.[11,12] Isotope labeling studies and other mechanistic studies strongly indicate that the oxidations occur via the involvement of high valent Fe(V)-oxo intermediates.[11-13] The reactive intermediate in C-H hydroxylation reactions has been identified as a highly electrophilic $[Fe^{V}(O)(OH)(L^{N4+})]^{2+}$ oxidant (L^{N4} corresponds to tetradentate TACN-based ligands) which is formed via water-assisted O-O cleavage of the hydroperoxo precursor $[Fe^{III}(OOH)(OH_2)(L^{N4})]^{2+}$.[13] The $[Fe^{V}(O)(OH)(L^{N4})]^{2+}$ oxidant can exist in two tautomeric forms, corresponding to structures O_A and O_B in Scheme 2, because of the unsymmetric nature of the tetradentate TACN-derivatives that serve as ligands.[12] the two tautomers differ in the relative positions of the *cis*-coordinated oxo and hydroxo groups, and are connected through a prototopic oxo-hydroxo tautomerism (the barrier to this proton transfer is relatively high (*vide infra*). Investigations have been made on the influence on C-H hydroxylation reactions exerted by manipulation of the electronic as well as steric properties via introduction of different groups (e.g. Me, F, NO_2, NMe_2) in α and γ positions of the pyridine ring of the PyTACN ligand.[12,14] These studies indicated that electronic properties of the groups in γ position on the pyridine ring have no direct effect on the relative reactivities between the two tautomers O_A and O_B, while the steric properties of the groups in the α position of the pyridine ring do influence the relative reactivity between the tautomers.[12,14] The discrimination between the relative reactivities of O_A and O_B was found to be more pronounced in cases of substrates containing tertiary C-H bonds.[12] Replacement of the pyridyl arm of the PyTACN ligand with a corresponding (*N*-methyl)benzimidazolyl arm led to the formation of the complex $[Fe^{II}(^{Me2,Me}BzImTACN)(CF_3SO_3)_2]$.[15] Reactivity (catalytic oxidation) studies on this complex were entirely in keeping with the proposed formation of an active Fe(V)(O)(OH) oxidant, and it was found that the (*N*-methyl)benzimidazolyl moiety exerted a steric influence in discriminating the relative reactivities of O_A and O_B that lies in between that of pyridyl and α-

Me-pyridyl moieties, in full agreement with the crystal structures of the Fe(II) complexes of the three ligands. Importantly, [Fe^{II}(^{Me2,Me}BzImTACN)(CF_3SO_3)$_2$] was found to maintain high efficiencies and selectivities in the hydroxylation of alkanes and olefins.[15]

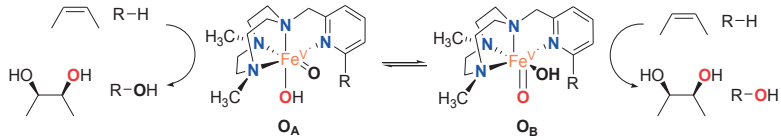

Scheme 2. Oxidation of alkane and olefin by the two tautomers O_A and O_B observed in reactions catalyzed by Fe(PyTACN) family of complexes.

In this work, we describe the syntheses of two new tetradentate N4 ligands, ^{Me2,Me2}PyzTACN and ^{Me2,Me}ImTACN (Fig. 1). These ligands are based on the PyTACN ligand scaffold, where the pyridyl side arm is replaced by (*N*-methyl)imidazolyl and 3,5-dimethylpyrazolyl arms, respectively. The ligand ^{Me2,Me2}PyzTACN contains an ethylene spacer connecting one of the amines of the trisazacyclononane (TACN) ring and the N(2) atom of the 3,5-dimethylpyrazole, whereas the corresponding spacer is a methylene in ^{Me2,Me}ImTACN, in direct correspondence to the ligand frameworks of BzImTACN and PyTACN. The (*N*-methyl)imidazolyl moiety (pK_a of conjugate acid: 7.06) is more basic than (*N*-methyl)benzimidazolyl (pK_a of conjugate acid: 5.41) and pyridine (pK_a of conjugate acid: 5.22), while 3,5-dimethylpyrazole is less basic (pK_a of conjugate acid: 4.12). Collectively, the different ligands discussed above are thus expected to span a range of steric and electronic demands, while yielding structurally similar Fe(II) complexes which in turn may give rise to analogous Fe(V)(O)(OH) complexes that will exist in tautomeric forms. Thus, the ligands are expected to exert not only electronic but also steric influence on the relative reactivities of the Fe(V)(O)(OH) O_A and O_B tautomers operating in the C-H hydroxylation reactions. Here, we describe the syntheses and characterization of two new Fe(II) complexes of the ^{Me2,Me2}PyzTACN and ^{Me2,Me}ImTACN ligands, and an investigation of the catalytic hydroxylation reactions effected by these two iron complexes. Isotope labeling studies and computational methods have also been performed to elucidate the C-H hydroxylation reaction mechanism(s) and to assess the steric and electronic influence of the ligands on the reactivities of the iron catalysts.

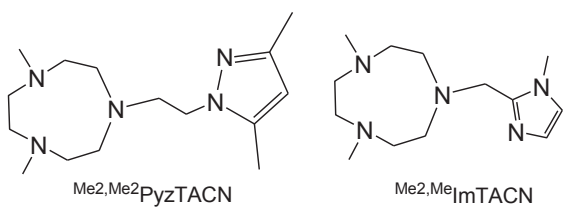

Figure 1. Structures of the tetradenate ligands ^{Me2,Me2}PyzTACN and ^{Me2,Me}ImTACN.

Results and Discussion

The two new tetradentate N4 ligands ^{Me2,Me2}PyzTACN and ^{Me2,Me}ImTACN were synthesized by reaction of TACN·3HBr [1,4-dimethyl-1,4,7-triazacyclononane·trihydrobromide] with the corresponding chloromethylene/chloroethylene precursor complex of the five membered

heterocyclic ring (pyrazole and imidazole). In the case of the pyrazole ligand, 1.2 equiv of TACN·3HBr was reacted with 1-(2-chloroethyl)-3,5-dimethyl-1*H*-pyrazole (one equiv) in refluxing dry MeCN for 5 d, in the presence of K_2CO_3 and NaI (Scheme 3, *cf*. Experimental Section for detailed synthesis). The ligand was purified by dissolving in hexane - the impurities remained undissolved. After filtration, the filtrate was evaporated to obtain the pure ligand. For the synthesis of ^{Me2,Me}ImTACN, the TACN·3HBr salt was initially converted into the corresponding free base using NaOH and then extracted with CH_2Cl_2 to obtain free TACN. This TACN free base (one equiv) was reacted for 20 h with 2-chloromethyl-1-methylimidazole·HCl (one equiv) in refluxing dry MeCN under N_2 atmosphere, in the presence of K_2CO_3 to give the desired ligand ^{Me2,Me}ImTACN (Scheme 3, *cf*. Experimental section for detailed synthesis). The ligand was obtained in pure form by extraction with hexane.

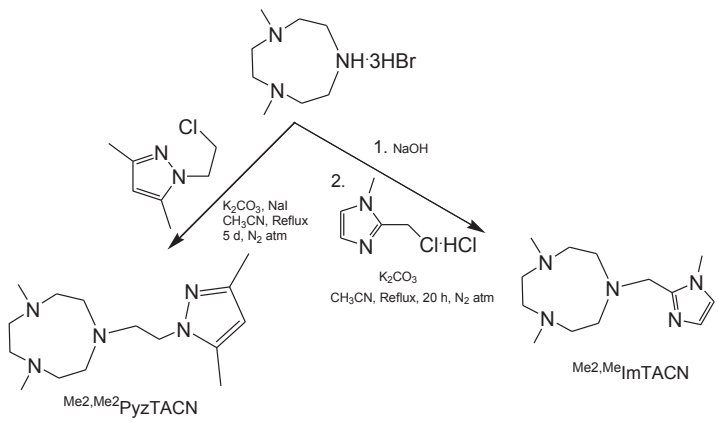

Scheme 3. Schematic synthetic routes to the ligands ^{Me2,Me2}PyzTACN and ^{Me2,Me}ImTACN.

The Fe(II) complexes of the two ligands were synthesized inside a dry atmosphere box. Reaction of one equivalent of $[Fe^{II}(CH_3CN)_2(CF_3SO_3)_2]$ with one equivalent of ^{Me2,Me2}PyzTACN in dry THF resulted in precipitation of the corresponding complex $[Fe^{II}(^{Me2,Me2}PyzTACN)(CF_3SO_3)_2]$ (**1**^{OTf}), which was collected by filtration, washed with a small amount of THF and dried under vacuum (*cf.* Experimental section for a detailed description of the synthesis). The corresponding reaction with the ^{Me2,Me}ImTACN ligand in dry THF led to the formation of a complex that mostly remained in solution. The reaction solution was evaporated under vacuum and a small amount of a CH_2Cl_2:CH_3CN (4:1) mixture was added to the resultant residue. Diffusion of diethyl ether into the resultant solution resulted in precipitation of the complex $[Fe^{II}(^{Me2,Me}ImTACN)(CF_3SO_3)_2]$ (**2**^{OTf}).

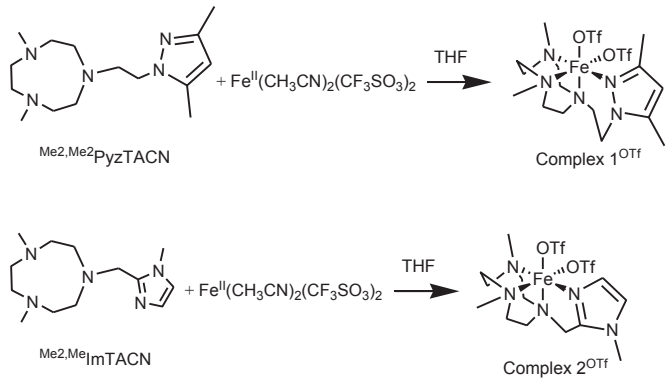

Scheme 3. Synthesis of Fe(II) complexes $\mathbf{1}^{\mathbf{OTf}}$ (top) and $\mathbf{2}^{\mathbf{OTf}}$ (bottom).

The complexes $\mathbf{1}^{\mathbf{OTf}}$ and $\mathbf{2}^{\mathbf{OTf}}$ were characterized by mass spectrometry and ^{1}H NMR spectroscopy. The high resolution mass spectrum (HRMS) of $\mathbf{1}^{\mathbf{OTf}}$ in CH_3CN showed prominent mass peaks at *m/z* = 167.5903 and 484.1303, corresponding to the formulations $[Fe^{II}(^{Me2,Me2}PyzTACN)]^{2+}$ (calc. 167.5881) and $[Fe^{II}(^{Me2,Me2}PyzTACN)(CF_3SO_3)]^{+}$ (calc. 484.1287), respectively (Figures S1-S3, Supplementary Material). The HRMS of complex $\mathbf{2}^{\mathbf{OTf}}$ in CH_3CN showed prominent mass peaks at *m/z* = 153.5751 and 456.0970, corresponding to the formulations $[Fe^{II}(^{Me2,Me}ImTACN)]^{2+}$ (calc. 153.5724) and $[Fe^{II}(^{Me2,Me}ImTACN)(CF_3SO_3)]^{+}$ (calc. 456.0974), respectively (Figures S4-S6). The ^{1}H NMR spectra of the two complexes were measured in CD_3CN solvent (*cf.* Figures S7-S8). Both complexes gave broad paramagnetically shifted spectra in spectral windows ranging from -10 to 120 ppm, indicative of the presence of high spin ferrous ions.

Crystal and molecular structure of $[Fe^{II}(^{Me2,Me2}PyzTACN)(CF_3SO_3)_2]$ ($\mathbf{1}^{\mathbf{OTf}}$)

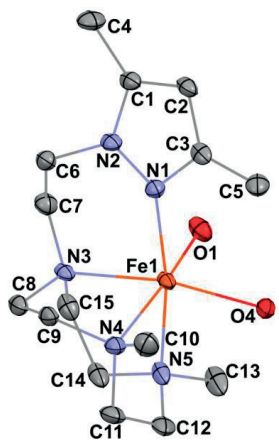

Figure 2. The X-Ray crystal structure (ORTEP plot) of complex $\mathbf{1}^{\mathbf{OTf}}$ with 50% probability ellipsoids; the hydrogens and the triflate anions, except the oxygen directly bound to the metal, have been omitted for clarity.

In order to confirm its identity, the solid-state structure of $\mathbf{1}^{\mathbf{OTf}}$ was established by X-Ray crystallography. The details of the structure determination are collected in Table 1 and the selected bond distances and bond angles are listed in Table 2. The X-Ray structure (Figure 1) shows that the Fe(II) center is in a slightly distorted octahedral coordination geometry. The ligand ^{Me2,Me2}PyzTACN is tetradentate with the three nitrogens of the triazacyclononane ring bound facially to the metal center and the pyrazole ring providing a fourth coordinated nitrogen. The two triflate anions are coordinated in *cis* positions on the Fe(II) ion. The Fe-N bond distances lie in the range 2.2-2.25 Å, which are typical distances observed for high spin Fe(II) complexes.[16] The Fe-O_{OTf} bond distances are 2.088(3) and 2.199(3) Å. In order to ensure that coordination of the pyrazole nitrogen would be geometrically possible, the ^{Me2,Me2}PyzTACN ligand was designed to contain an ethylene spacer between the TACN ring and the pyrazole moiety, distinguishing this ligand from the related ligands discussed here, all of which contain methylene spacers in the corresponding positions. The Fe-N (pyrazole) bond distance is 2.209(3) Å while the Fe-N (pyridine) bond distance is 2.165(4) Å in $[Fe^{II}(^{Me,H}PyTACN)(CF_3SO_3)_2]$ ($\mathbf{3}^{\mathbf{OTf}}$)[11a] and 2.246(2) Å in $[Fe^{II}(^{Me,Me}PyTACN)(CF_3SO_3)_2]$ ($\mathbf{4}^{\mathbf{OTf}}$),[17] and the Fe-N (benzimidazole) bond distance is 2.134(7) Å in $[Fe^{II}(^{Me2,Me}BzImTACN)(CF_3SO_3)_2]$ ($\mathbf{5}^{\mathbf{OTf}}$).[15] The differences in Fe-N bond distance may be attributed to the relative basicities of the heterocyclic N-donor moieties. The (*N*-methyl)benzimidazole and pyridine moieties are better Lewis bases than the pyrazole. The $_{OTf}$O-Fe-O_{OTf} angle is much larger in $\mathbf{1}^{\mathbf{OTf}}$ (93.6(1)º) than that of $\mathbf{3}^{\mathbf{OTf}}$ (91.64(14)º),[11a] $\mathbf{4}^{\mathbf{OTf}}$ (94.9(7)º)[17] and $\mathbf{5}^{\mathbf{OTf}}$ (89.1(3)º),[15] which could be due to the presence of the longer bridging ethylene spacer and the resulting greater steric demand between the methyl group of the pyrazole side arm and the triflate anions. It should be noted that one of the methyl groups of the pyrazole moiety is parallel to the oxygen of the triflate anion and perpendicular to the oxygen of the second triflate anion (*cf.* Fig. 2).

Table 1. Crystal data for $\mathbf{1}^{\mathbf{OTf}}$

Empirical formula	$C_{17}H_{29}F_6FeN_5O_6S_2.C_4H_{10}O$ $\mathbf{1}^{\mathbf{OTf}}$
Formula weight	707.54
Temperature	100(2) K
Wavelength	0.71073 Å
Crystal system	Monoclinic
Space group	$P2_1/n$
Unit cell dimensions	a = 8.9370(17) Å
	b = 16.024(3) Å
	c = 19.794(4) Å
	α = 90˚
	β = 92.782(3)˚
	γ = 90˚

Volume	2831.29 $Å^3$
Z	4
Density (calculated)	1.660 Mg/m^3
Absorption coefficient	0.771 mm^{-1}
F(000)	1472
Crystal size	0.30 x 0.15 x 0.15 mm^3
Theta range for data collection	1.636 to 28.083 °
Index ranges	-11<=h<=7, -20<=k<=18, -25<=l<=24
Reflections collected	16414
Independent reflections	6388
Completeness	99.8% (theta = 25.242)
Absorption correction	Empirical
Max. and min. transmission	1.0 and 0.707660
Refinement method	Full-matrix least-squares on F^2
Data / restraints / parameters	6388/0/338
Goodness-of-fit on F^2	1.096
Final R indices [I>2sigma(I)]	R1 = 0.0576, wR2 = 0.1346
R indices (all data)	R1 = 0.0976, wR2 = 0.1493
Largest diff. peak and hole	0.571 and -0.768 $e.Å^{-3}$

Table 2. Selected bond distances (Å) and bond angles (º) in $\mathbf{1^{OTf}}$

Fe(1)-N(1)	2.209(3)
Fe(1)-O(1)	2.088(3)
Fe(1)-N(3)	2.227(4)
Fe(1)-O(4)	2.199(3)
Fe(1)-N(4)	2.208(4)
Fe(1)-N(5)	2.249(3)
N(1)-Fe(1)-O(1)	91.4(1)
N(1)-Fe(1)-N(3)	91.3(1)
N(1)-Fe(1)-O(4)	99.2(1)
N(1)-Fe(1)-N(4)	97.1(1)
N(1)-Fe(1)-N(5)	171.0(1)
O(1)-Fe(1)-N(3)	89.1(1)
O(1)-Fe(1)-O(4)	93.6(1)
O(1)-Fe(1)-N(4)	166.7(1)
O(1)-Fe(1)-N(5)	90.4(1)

N(3)-Fe(1)-O(4)	169.1(1)
N(3)-Fe(1)-N(4)	80.6(1)
N(3)-Fe(1)-N(5)	80.0(1)
O(4)-Fe(1)-N(4)	95.0(1)
O(4)-Fe(1)-N(5)	89.5(1)
N(4)-Fe(1)-N(5)	79.7(1)

Catalytic C-H bond oxidation studies

The catalytic properties of $\mathbf{1}^{\mathbf{OTf}}$ and $\mathbf{2}^{\mathbf{OTf}}$ were tested in the hydroxylation of several alkanes employing H_2O_2 as the oxidant. In a typical catalytic experiment, 10 equiv of H_2O_2 (from a stock solution of 70 mM H_2O_2 in CH_3CN) was delivered by a syringe pump to a CH_3CN solution containing the Fe(II) complex (1 mM), alkane substrate (1 M) and H_2O (1 M) over a period of 30 min. The catalysis experiments were performed under air at room temperature. Under these conditions, both complexes oxidized cyclohexane into cyclohexanol ($\mathbf{1}^{\mathbf{OTf}}$: TON 6.5; $\mathbf{2}^{\mathbf{OTf}}$: TON 7.7) as the main product with high alcohol/ketone (A/K) ratios ($\mathbf{1}^{\mathbf{OTf}}$: A/K 9.4; $\mathbf{2}^{\mathbf{OTf}}$: 12) and high conversions of the oxidant (H_2O_2) into products ($\mathbf{1}^{\mathbf{OTf}}$: 72 %; $\mathbf{2}^{\mathbf{OTf}}$: 83.4 %). Such high conversion and high A/K ratios are comparable to those obtained with related iron complexes under analogous experimental conditions.[7a,10d,11,15,16d,18] The catalytic efficiencies of these two complexes with different alkane substrates are summarized in Table 3.

Table 3. Catalytic C-H bond oxidation of various alkanes by Fe-complexes using H_2O_2

Catalyst	Substrate	TN (A)	TN (K)	A/K	Yield (%)
$\mathbf{1}^{\mathbf{OTf}}$	Cyclohexane	6.5	0.7	9.4	72
$\mathbf{2}^{\mathbf{OTf}}$	Cyclohexane	7.7	0.64	12	83.4
$\mathbf{1}^{\mathbf{OTf}}$	Cyclohexane-d_{12}	4	0.5	8	45
$\mathbf{2}^{\mathbf{OTf}}$	Cyclohexane-d_{12}	5	0.5	10	55
$\mathbf{1}^{\mathbf{OTf}}$	Cyclooctane	6	0.6	10	66
$\mathbf{2}^{\mathbf{OTf}}$	Cyclooctane	6.2	0.6	9.8	69
$\mathbf{1}^{\mathbf{OTf}}$	n-hexane	3	0.8	3.8	38
$\mathbf{2}^{\mathbf{OTf}}$	n-hexane	3.6	0.64	5.6	43
$\mathbf{1}^{\mathbf{OTf}}$	2,3-dimethylbutane	2.6	-----	-----	26
$\mathbf{2}^{\mathbf{OTf}}$	2,3-dimethylbutane	3.5	-----	-----	35.2

The remarkably high A/K ratios observed for these complexes suggests the involvement of a metal-based oxidant, as proposed previously.[19] Several other mechanistic substrate probes were used to verify the involvement of a metal-based active oxidant. The kinetic isotope effect (KIE) values obtained in the oxidation of a mixture of cyclohexane and its deuterated topoisomer (1:3 molar ratio) were 4.0 for $\mathbf{1}^{\mathbf{OTf}}$ and 4.6 for $\mathbf{2}^{\mathbf{OTf}}$. Both of the complexes showed a preference for selective oxidation of tertiary C-H bonds over secondary C-H bonds in the oxidation of adamantane (normalized 3º/2º ratios were 12 for $\mathbf{1}^{\mathbf{OTf}}$ and 26 for complex $\mathbf{2}^{\mathbf{OTf}}$). Finally, in the oxidation of *cis*-1,2-dimethylcyclohexane (*cis*-DMCH), the complexes showed a high degree of stereoretention, excluding any significant involvement of long-lived carbon-centered radicals or cations in the C-H oxidation reactions.

Isotope labeling studies

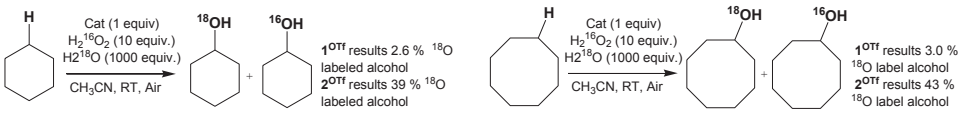

Scheme 4. ^{18}O label incorporation by complexes $\mathbf{1}^{\mathbf{OTf}}$ and $\mathbf{2}^{\mathbf{OTf}}$ in the oxidation of cyclohexane (left) and cyclooctane (right).

Isotope labeling experiments were performed using $H_2{}^{18}O_2$ and $H_2{}^{18}O$ in order to gain insight into the hydroxylation mechanism as well as the origin of the oxygen atom incorporation into the (alcohol) products. In the oxidation of cyclohexane, $\mathbf{1}^{\mathbf{OTf}}$ (1 equiv) was found to introduce only 2.6% labelled oxygen into the alcohol product in the presence of 10 equiv H_2O_2 and 1000 equiv of $H_2{}^{18}O$ (Scheme 4). The complementary experiment performed with reverse labelling, *i.e.* 10 equiv $H_2{}^{18}O_2$ and 1000 equiv H_2O resulted in an ^{18}O-label incorporation of 86% into the alcohol. It may thus be concluded that peroxide is the main source of oxygen in the alcohol product and only 11% of oxygen atoms are incorporated from air/water (mass balance) for this specific hydroxylation reaction. In the oxidation of other alkane substrates containing secondary C-H bonds, complex $\mathbf{1}^{\mathbf{OTf}}$ with 10 equiv H_2O_2 and 1000 equiv of $H_2{}^{18}O$ gave rise to similar low percentages of incorporated labeled oxygen (from water) into the alcohol (3% for cyclohexane-d_{12} and cyclooctane).

On the other hand, $\mathbf{2}^{\mathbf{OTf}}$ gave rise to considerably greater incorporation of oxygen from water into the products. In the presence of 10 equiv H_2O_2 and 1000 equiv of $H_2{}^{18}O$, complex $\mathbf{2}^{\mathbf{OTf}}$ (1 eq.) gave 39 and 43% labeled alcohols in the oxidation of cyclohexane and cyclooctane, respectively (Scheme 4). The complementary experiment with 10 equiv $H_2{}^{18}O_2$ and 1000 equiv H_2O resulted in the formation of 55% labeled cyclohexanol in oxidation of cyclohexane. Thus, for this complex, both peroxide and H_2O are the sources of oxygen in the alcohol products.

In the oxidation of tertiary C-H bonds (*cis*-DMCH and adamantane), $\mathbf{1}^{\mathbf{OTf}}$ did not incorporate any oxygen from water into the products (~ 0% ^{18}O incorporation) (*cf.* Table 4). On the other hand, the equivalent experiments with $\mathbf{2}^{\mathbf{OTf}}$ led to the incorporation of 39% and 31% oxygen incorporations from water into product(s) in the oxidation of adamantane and *cis*-DMCH, respectively (*cf.* Table 4).

cis-Dihydroxylation vs epoxidation in the oxidation of alkenes

Complexes $\mathbf{1}^{\mathbf{OTf}}$ and $\mathbf{2}^{\mathbf{OTf}}$ catalyzed the oxidation of alkenes in the presence of H_2O_2 and H_2O to give both epoxide and *cis*-dihydroxylated products. Under catalytic conditions (1:10:1000 for catalyst:oxidant:substrate), $\mathbf{1}^{\mathbf{OTf}}$ oxidized *cis*-cyclooctene to give *cis*-cyclooctene epoxide (TON 8.2) as a major product with the concomitant formation of a minor amount of *syn*-cyclooctane-1,2-diol (TON 0.5), i.e. an epoxide:diol (E/D) ratio of 16.5. Addition of H_2O (1000 equiv) slightly increased the formation of *syn*-diol (TON 1.1), but has almost no influence in the yield of epoxide (TON 8.2). When 100 equiv of H_2O_2 was employed, the yield of both epoxide (TON 53) and *cis*-diol (TON 4.8) was increased. In oxidation of 1-

octene, complex $\mathbf{1}^{\mathbf{OTf}}$ in the presence of 100 equiv H_2O_2 yielded 1-octene epoxide (TON 16.5) as the major product together with a minor amount of *syn*-dihydroxylated product (TON 2.5). Complex $\mathbf{2}^{\mathbf{OTf}}$, on the other hand, preferred formation of *syn*-diol over epoxide in the oxidation of *cis*-cyclooctene; in this reaction, complex $\mathbf{2}^{\mathbf{OTf}}$ (1 equiv) together with H_2O_2 (10 equiv) produced *syn*-cyclooctane-1,2-diol with a TON of 5.9 and *cis*-cyclooctene epoxide with a TON of 3.9 (E/D = 0.6) and an overall conversion of 96% (w.r.t the oxidant). In the oxidation of the terminal alkene 1-octene, complex $\mathbf{2}^{\mathbf{OTf}}$ (1 equiv) together with H_2O_2 (10 equiv) produced *cis*-diol with a TON of 4.4 and epoxide with a TON of 1.5 (E/D = 3) and a conversion of approximately 36%.

In order to investigate the identity of the active oxidant, isotope labeling studies were made for both complexes, employing *cis*-cyclooctene as substrate. Such studies on the Fe(PyTACN) family of complexes and the related complex $\mathbf{5}^{\mathbf{OTf}}$ have established that the oxygen atom in the *cis*-dihydroxylated product is originating from the oxygen coordinated to the iron metal center in *cis*-binding mode. In the presence of 10 equiv H_2O_2 and 1000 equiv $H_2{}^{18}O$, $\mathbf{1}^{\mathbf{OTf}}$ (1 equiv) introduced 92% ^{18}O into the product *syn*-cyclooctane-1,2-diol during the oxidation of *cis*-cyclooctene, while complex $\mathbf{2}^{\mathbf{OTf}}$ gave 97% label incorporation under the same conditions. These results are in full agreement with previous isotope labelling results which indicate that a high valent $Fe^{V}(O)(OH)$ species is formed via water assisted O-O cleavage of $Fe^{III}(OOH)(OH_2)$[13] and acts as the active oxidant in the hydroxylation reactions. In accordance with this assumption and the expected reactivity pattern, the labelling studies confirm that one of the two oxygen atoms in the *syn*-diol product originates from water and the other from hydrogen peroxide.

Table 4. ^{18}O incorporation from $H_2{}^{18}O$ in C-H hydroxylation reactions mediated by different Fe(II)-complexes[1]

Substrate	Complex $\mathbf{1}^{\mathbf{OTf}}$	Complex $\mathbf{2}^{\mathbf{OTf}}$	Complex $\mathbf{3}^{\mathbf{OTf}}$	Complex $\mathbf{4}^{\mathbf{OTf}}$	Complex $\mathbf{5}^{\mathbf{OTf}}$
Cyclohexane	3	39	45	11	48
Cyclohexane-d_{12}	3	NA	40	NA	48
Cyclooctane	3	43	44	NA	41
Cis-DMCH	0	31	79	2	26
Adamantane	0	39	74	3	28
Cis-cyclooctene[2] epoxide	2	36	77	5	24
Syn-cyclooctane-1,2-diol[2]	97	92	97	78	98

[1] Reaction conditions: catalyst:H_2O_2:$H_2{}^{18}O$:substrate = 1:10:1000:1000, CH_3CN, RT, air; [2] *cis*-cyclooctene was employed as the substrate.

When the incorporation of water into the other oxidation product, *cis*-cyclooctene epoxide, was analyzed, complex $\mathbf{1}^{\mathbf{OTf}}$ behaved drastically different from complex $\mathbf{2}^{\mathbf{OTf}}$. The incorporation of ^{18}O using labeled water was 36% for complex $\mathbf{2}^{\mathbf{OTf}}$, while that for complex $\mathbf{1}^{\mathbf{OTf}}$ was only ~ 2%. For the related complexes $\mathbf{5}^{\mathbf{OTf}}$ and $\mathbf{3}^{\mathbf{OTf}}$, the amount of ^{18}O-labeled epoxide formed were 24 and 77%, respectively. On basis of these labelling studies, we may assign $\mathbf{3}^{\mathbf{OTf}}$ as belonging to what has been designated the class I category complexes,[12] where the oxygen in the epoxide originates mainly from water, and complex $\mathbf{1}^{\mathbf{OTf}}$ belongs to the

class II complexes where the oxygen comes exclusively from peroxide. The complexes $\mathbf{2}^{\mathbf{OTf}}$ and $\mathbf{5}^{\mathbf{OTf}}$ may be placed in intermediate positions between these two categories.

Computational Modelling

In order to gain an understanding of the relative energies of the postulated $Fe^{V}(O)(OH)$ tautomers, computational modelling of the two tautomers generated from $[Fe^{II}(^{Me2,Me}BzImTACN)(CF_3SO_3)_2]$ ($\mathbf{5}^{\mathbf{OTf}}$). The ground-state stability ordering of the two ^{Me2,Me}BzIm compounds was computationally investigated by Density Functional Theory (DFT), and here the tautomeric species that contains an oxo moiety coplanar with the benzimidazole ligand is labeled as **A** (*note*: corresponding to O_B). Species **B** represents the isomer whose oxo moiety is perpendicular to the heterocyclic ligand (*note*: corresponding to O_A). The DFT analyses confirm the quartet state ($S = 3/2$) as the thermodynamically favoured spin state for both isomers, with ^{4}**A** found to lie 2.4 kcal/mol lower in energy than ^{4}**B**. Figure 3 shows the geometry-optimized structure for the two tautomers. The corresponding doublet spin states of ^{2}**A** and ^{2}**B** ($S = 1/2$) lie 11.5 and 9.1 kcal/mol higher in energy than their respective quartet counterparts. Having established the ground-state stability ordering and spin-state preference for the two isomeric oxo-hydroxyl compounds, the lability of proton transfer between these tautomers was next explored. Proton transfer between the different oxygen centers in ^{4}**A** and ^{4}**B** occurs through transition structure ^{4}**TS**^{4}**A**^{4}**B**, as depicted in Figure 3, and basically involves the synchronous transfer of the hydrogen between the two oxygen centers. The free-energy barrier is high and in excess of 30 kcal/mol, and these data are in keeping with the reported configurational stability of the related pyridyl-derivatives prepared by Company and Costas.[12] The absence of facile proton transfer between the two oxygen centers in ^{4}**A** and ^{4}**B** suggests that the oxo-based C-H abstractions observed in these studies must originate from structurally different oxidants that do not allow equilibration of the oxo moiety on the time scale of the chemical reactions, a feature supported by the isotopic labeling studies.

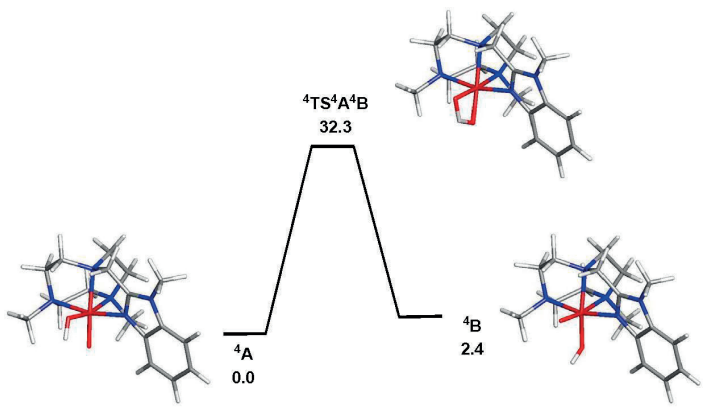

Figure 3. B3LYP-optimized structures and potential energy surface for the isomerization of ^{4}**A** to ^{4}**B**. Energy values are in ΔG in kcal/mol relative to ^{4}**A**.

In order to elucidate the mechanism of the hydrogen-atom transfer (HAT) of alkanes by ^{4}**A** and ^{4}**B**, DFT calculations were carried out using methane (**C**) as the substrate. This particular substrate was chosen in order to simplify the calculations and reduce the computational time. Figure 4 shows the geometry-optimized transition-state structures involved in the H-abstraction and the resulting MeOH-substituted compounds, while Figure 5 shows the potential energy surface for these reactions. H-abstraction is site selective and is mediated by the oxo moiety in ^{4}**A** and ^{4}**B**, leading to the respective transition-state structures ^{4}**TS**^{4}**AC**^{6}**D** and ^{4}**TS**^{4}**BC**^{6}**E**, each of which exhibits a similar activation barrier on the order of 25 kcal/mol. The expected geminate radical pairs that follow each H-abstraction could not be found by IRC calculations, presumably a manifestation of the flat nature of the reaction surface en route to the alcohol product. Collapse of the geminate radical pair in each reaction via a rebound process, coupled with a spin crossover to the thermodynamically favored high-spin sextet species (S = 5/2), completes the hydroxylation sequence and affords the MeOH-substituted products ^{6}**D** and ^{6}**E**. Both hydroxylation routes are exergonic in nature, and the MeOH-substituted product having the alcohol ligand disposed perpendicular to the heterocyclic ligand is 3.1 kcal/mol more stable due to reduced interactions between the coordinated alcohol and ligand scaffold.

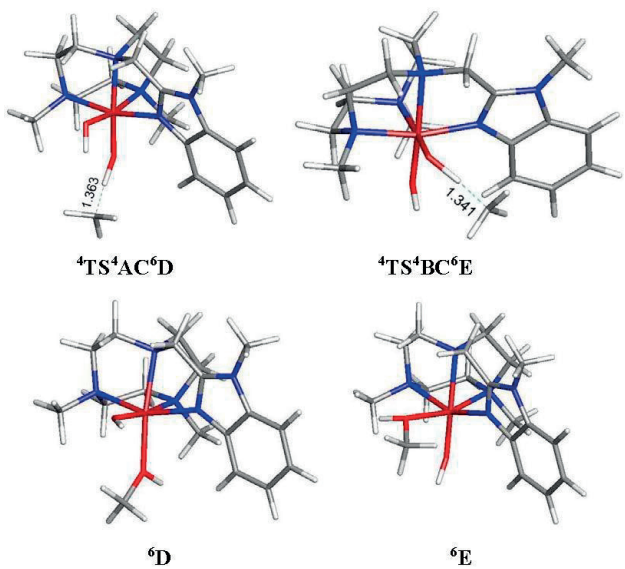

Figure 4. B3LYP-optimized transition structures ^{4}**TS**^{4}**AC**^{6}**D** and ^{4}**TS**^{4}**BC**^{6}**E** and the MeOH-substituted products ^{6}**D** and ^{6}**E** from the methane (**C**) hydroxylation reaction using ^{4}**A** and ^{4}**B**.

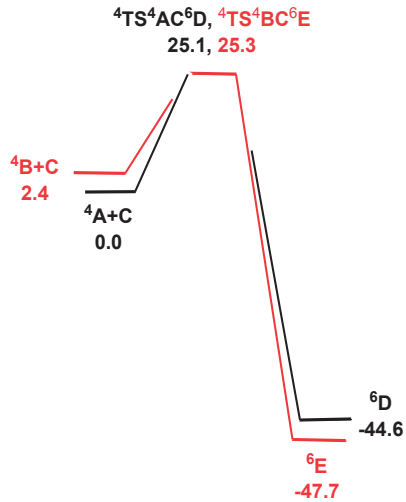

Figure 5. Potential energy surface for the reaction of ^{4}**A** and ^{4}**B** with methane (**C**). Energy values are in ΔG in kcal/mol relative to ^{4}**A** and **C**.

Summary and Conclusions

We have previously demonstrated the steric influence exerted by ligands on the reactivities of iron(V) oxo-hydroxo tautomers operating in C-H hydroxylation reactions.[15] This study further addresses and strengthens the fact that the ligand exerts a profound influence on the oxygen atom transfer reactivity, with the steric bulk of the donor moiety of the pendant arm attached to the TACN ligand deciding the relative ease of approach of a substrate with a sterically hindered tertiary C-H bond to the oxo ligand of the O_B tautomer (as opposed to the O_A tautomer, where the oxo ligand is more accessible) of the proposed active Fe(V)(O)(OH) oxidant. As there is evidence that this specific oxo ligand originates from water,[12,13] the relative incorporation of oxygen from $H_2{}^{18}O$ into a (sterically bulky) alkane substrate (especially those containing tertiary C-H bonds) may be used as a guide to the steric influence of the ligand on substrate access to the O_B oxo ligand – low incorporation of labelled oxygen into the oxidation product indicates steric hindrance by the ligand. The levels of incorporation of ^{18}O from water into the substrates (cyclohexane, cyclooctane, adamantane, *cis*-DMCH, *cis*-cyclooctene) are listed in Table 3. For complex $\mathbf{1}^{\mathbf{OTf}}$, the very low percentage of ^{18}O incorporation (< 3%) from $H_2{}^{18}O$ in the products suggests that the tautomer O_A predominates over O_B (irrespective of substrates containing secondary or tertiary C-H bonds) in the C-H hydroxylation reaction. On the other hand, the levels of ^{18}O incorporation (within the range 30-45%) from $H_2{}^{18}O$ into products for complex $\mathbf{2}^{\mathbf{OTf}}$ indicate that both O_A and O_B are equally reactive towards substrates with little preference of O_A over O_B for substrates containing tertiary C-H bonds.

While the high percentage (above 90%) ^{18}O incorporation in the *syn*-diol product in oxidation of *cis*-cyclooctene by complexes $\mathbf{1}^{\mathbf{OTf}}$ and $\mathbf{2}^{\mathbf{OTf}}$ (*cf.* Table 4) demonstrates the involvement of Fe(V)(O)(OH) oxidant as observed for Fe(PyTACN) complexes, the different range of ^{18}O

incorporation into the epoxide product also discriminate the relative reactivity between O_A and O_B. The amounts of labeled epoxide were 2% and 36% for complexes $\mathbf{1}^{\mathbf{OTf}}$ and $\mathbf{2}^{\mathbf{OTf}}$ respectively, clearly implying that epoxidation reaction catalyzed by complex $\mathbf{1}^{\mathbf{OTf}}$ is performed exclusively by O_A and in complex $\mathbf{2}^{\mathbf{OTf}}$, O_A and O_B are roughly equally active.

On the basis of these measurements, the order of steric interference of the ligand with the O_B oxo ligand (i.e. tautomer O_B) is $\mathbf{1}^{\mathbf{OTf}} > \mathbf{4}^{\mathbf{OTf}} > \mathbf{5}^{\mathbf{OTf}} > \mathbf{2}^{\mathbf{OTf}} > \mathbf{3}^{\mathbf{OTf}}$. The crystal structures of the Fe(II) catalysts, which are direct precursors to the active perferryl ($Fe^{V}(O)$) oxidants, provide a structural basis for the steric influence of the ligands. In Figure 6, space filling plots of the crystal structures of the above-mentioned complexes are plotted and correlated to the steric influence exerted by the ligands.

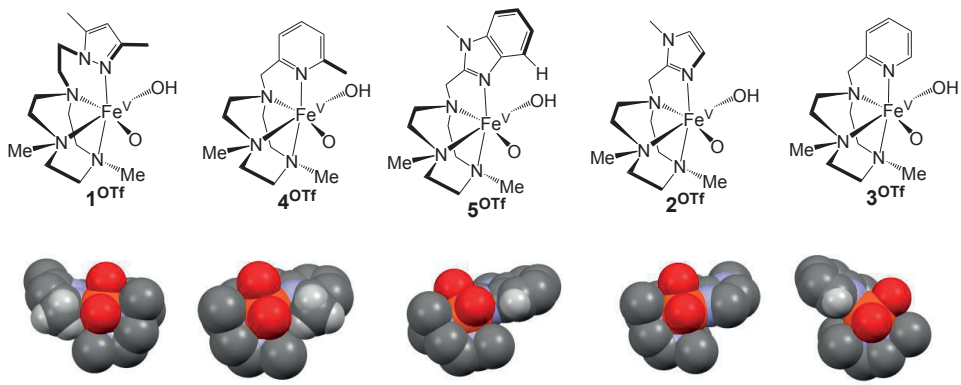

Figure 6. The schematic depictions (top) and the space filling models (bottom) of the Fe(V)(O)(OH) species of complexes $\mathbf{1}^{\mathbf{OTf}}$, $\mathbf{4}^{\mathbf{OTf}}$, $\mathbf{5}^{\mathbf{OTf}}$, $\mathbf{2}^{\mathbf{OTf}}$, and $\mathbf{3}^{\mathbf{OTf}}$ obtained by modifying the crystal structures of $\mathbf{1}^{\mathbf{OTf}}$ $\mathbf{4}^{\mathbf{OTf}}$, $\mathbf{5}^{\mathbf{OTf}}$, and $\mathbf{3}^{\mathbf{OTf}}$.

As shown above, the computational modelling of the HAT reactions effected by the postulated tautomeric $Fe^{V}(O)(OH)$ oxidants derived from $\mathbf{5}^{\mathbf{OTf}}$ do support that the ligand does influence the HAT reactivity in the manner discussed above. It should be noted that different basicities or, donor properties possessed by the side arms ((*N*-methyl)imidazole, (*N*-methyl)benzimidaole and 3,5-dimethylpyrazole) of the tetradentate ligands might have some influence on the reactivity of Fe(V)(O)(OH) oxidant in general, and the relative reactivities of the two tautomers in particular. However, this is not as apparent or conclusive as the steric properties of the side arms from the present investigation. Thus, the possible effects of electronic properties of the ligands on the reactivities need to be clarified and further studies are undertaken towards this direction.

Experimental section

Reagents and Materials

Reagents and solvents were of at least 99% purity and used as received without any further purification. $H_2{}^{18}O_2$ (90% ^{18}O-enriched, 2% solution in $H_2{}^{18}O$) and $H_2{}^{18}O$ (95% ^{18}O-enriched) were purchased from ICON isotopes. All reagents and solvents were purchased from Sigma Aldrich or Fisher Scientific. Dichloromethane and

acetonitrile were dried by distillation from CaH_2; diethyl ether was dried by distillation from Na/benzophenone. The starting materials 1-(2-chloroethyl)-3,5-dimethyl-1*H*-pyrazole,[20] 1-(2-chloromethyl)-2-methylimidazole hydrochloride[21] and 4,7-dimethyl-1,4,7-triazacyclononane trihydrobromide (TACN·3HBr)[22] were synthesized according to a literature procedures.

Instrumentation

Infrared spectra were collected on a Nicolet Avatar 360 FTIR spectrometer. UV-Visible spectroscopy was performed in a 1 cm quartz cell using an Agilent Technology 8453 UV-Vis spectrophotometer equipped with a diode-array detector. NMR spectra were recorded on a Bruker DPX 400 MHz and Varian Inova 500 MHz spectrometers in $CDCl_3$ or CD_3CN solvent using standard conditions, and were referenced to the residual proton signal of the solvent. Elemental analysis was performed on a 4.1 Vario EL 3 elemental analyzer from Elementar. The ESI-MS experiments were performed with a Bruker Esquire 6000 LC/MS chromatograph, using acetonitrile as a mobile phase. The product analyses after catalysis experiments were carried out on an Agilent Technology7820A gas chromatograph equipped with a 16-sample automatic liquid sampler, flame ionization detector and EzChrom Elite Compact software. GC-MS analyses were performed on an Agilent Technology 7890A GC system equipped with a 5975C inert XL EI/CI MSD with Triple-Axis Detector. The products were identified by comparison of their GC retention times and, in the case of GC/MS, with those of authentic compounds.

Synthesis

Synthesis of ^{Me2,Me2}PyzTACN [1-(2-(3,5-Dimethyl-1*H*-pyrazol-1-yl)ethyl)-4,7-dimethyl-1,4,7-triazacyclononane]

A mixture of 1-(2-chloroethyl)-3,5-dimethyl-1*H*-pyrazole (243 mg, 1.53 mmol, 1.0 equiv), 1,4-dimethyl-1,4,7-triazacyclononane (289 mg, 1.84 mmol, 1.2 equiv), K_2CO_3 (1.27 g, 9.18 mmol, 6.0 equiv), NaI (229 mg, 1.53 mmol, 1.0 equiv) and Na_2SO_4 (435 mg, 3.06 mmol, 2.0 equiv) in CH_3CN were stirred for 5 days at 90 ºC under N_2 atmosphere. After cooling down to room temperature, the resultant mixture was filtered through a celite pad, after which the celite pad was washed with CH_2Cl_2. The filtrate was washed with 1 M NaOH (2 × 50 ml) and saturated brine solution (50 ml). The organic phrase was dried over Na_2SO_4 and the solvent was removed under reduced pressure. Then 50 ml hexane was added to the resulting residue and stirred overnight at room temperature. The solution was filtered through a celite pad. Removal of the solvent under reduced pressure gave the desired ligand as a yellow oil. Yield: 201 mg (47%). ESI-MS: *m/z* 280 $[M+H]^+$; 302 $[M+Na]^+$. ^{1}H-NMR (500 MHz, $CDCl_3$) δ (ppm): 5.74 (s, 1H), 4.01 (t, 2H), 2.91 (t, 2H), 2.76-2.74 (m, 4H), 2.65 (s, 4H), 2.64-2.62 (m, 4H), 2.34 (s, 6H), 2.22 (s, 3H), 2.19 (s, 3H); ^{13}C-NMR (125 MHz, $CDCl_3$) δ (ppm): 147.2, 138.6, 104.8, 58.2, 57.5, 56.9, 56.2, 47.0, 46.7, 13.4, 11.7.

Synthesis of ^{Me2,Me}ImTACN [1-((1-Methyl-1*H*-imidazol-1-yl)methyl)-4,7-dimethyl-1,4,7-triazacyclononane]

A mixture of 1-(2-chloromethyl)-2-methylimidazole hydrochloride (166 mg, 1.0 mmol, 1.0 equiv), 1,4-dimethyl-1,4,7-triazacyclononane (157.2 mg, 1.0 mmol, 1.0 equiv) and K_2CO_3 (268 mg, 2.0 mmol, 2.0 equiv) in extra dry CH_3CN were refluxed for about 20 h under N_2 atmosphere. The resulting yellow solution was then filtered through a celite pad and the celite pad was washed with $CHCl_3$. The filtrate was evaporated under reduced pressure and the resulting residue was stirred overnight with hexane (30 ml) and a small amount of CH_2Cl_2 (5 ml) at room temperature. The solution was filtered through a celite pad and removal of the solvent gave the ligand as yellow oil. Yield: 138 mg (55%). ESI-MS: *m/z* 252.1 $[M+H]^+$. ^{1}H-NMR (500 MHz, $CDCl_3$) δ (ppm): 6.87 (s, 1H), 6.8 (s, 1H), 3.71 (s, 3H), 3.66 (s, 2H), 2.75-2.73 (m, 4H), 2.67 (s, 4H), 2.59-2.57 (m, 4H), 2.29 (s, 6H); ^{13}C-NMR (125 MHz, $CDCl_3$) δ (ppm): 146.1, 127.0, 121.3, 57.0, 56.7, 55.7, 55.0, 46.5, 33.0.

Synthesis of $[Fe^{II}(^{Me2,Me2}PyzTACN)(CF_3SO_3)_2]$ (1^{OTf})

A solution of ^{Me2,Me2}PyzTACN (190 mg, 0.68 mmol, 1.0 equiv) in THF (1.0 ml) was added to a solution of $[Fe^{II}(CH_3CN)_2(CF_3SO_3)_2]$ (296 mg, 0.68 mmol, 1.0 equiv) in THF (2.0 ml) and stirred overnight at room temperature inside a glove box. A white solid was precipitated which was filtered off and washed with THF (2 × 2 ml). After this, it was dissolved in CH_2Cl_2/CH_3CN (3.0 ml/three drops) and filtered through celite. Removal of

the solvent under reduced pressure gave the desired complex as a white solid. Yield: 199 mg (41%). X-ray quality crystals were grown by slow diffusion of ether into a solution of the metal complex in CH_2Cl_2 with few drops of CH_3CN. HRMS (*m/z*) 167.5903 $[Fe^{II}(^{Me2,Me2}PyzTACN)]^{2+}$ (calc. 167.5881) (*z* = 2); 484.1303 $[Fe^{II}(^{Me2,Me2}PyzTACN)(CF_3SO_3)]^{+}$ (calc. 484.1287) (*z* = 1); Elemental analysis $C_{17}H_{29}F_6N_5O_6S_2Fe$ (MW = 633.406 g/mol) Calc. (%) C 32.24, H 4.61, N 11.06; Found (%) C 33.09, H 4.92, N 10.83; ^{1}H-NMR (400 MHz, CD_3CN) 130.4, 98.4, 66.5, 52.5, 34.6, 34.0, 13.5, -3.41; UV/Vis λ (nm) 194 (ε = 8327 $M^{-1}cm^{-1}$), 220 (ε = 6922 $M^{-1}cm^{-1}$); FTIR (KBr) ν (cm^{-1}) 2963-2863, 1672, 1558, 1501, 1474, 1430, 1371, 1355, 1324, 1293, 1233, 1163, 1133, 1090, 1070, 1061, 1030, 910, 804, 788, 776, 759, 751, 638, 576, 516.

Synthesis of $[Fe^{II}(^{Me2,Me}ImTACN)(CF_3SO_3)_2]$ (2^{OTf})

A solution of ^{Me2,Me}ImTACN (125.6 mg, 0.5 mmol, 1.0 equiv) in THF (1.0 ml) was added to a solution of $[Fe^{II}(CH_3CN)_2(CF_3SO_3)_2]$ (217.6 mg, 0.5 mmol, 1.0 equiv) in THF (1.5 ml) and stirred overnight at room temperature inside a glove box. The colour of the solution changed to pale yellow. The reaction solution was evaporated under vacuum and the residue was dissolved in CH_2Cl_2/CH_3CN (4:1 mixture) and filtered through celite. Diffusion of ether into the resultant solution resulted the complex as light yellowish white solid. Yield: 137 mg (45%). HRMS (*m/z*) 153.5751 $[Fe^{II}(^{Me2,Me}ImTACN)]^{2+}$ (calc. 153.5724) (*z* = 2); 456.0970 $[Fe^{II}(^{Me2,Me}ImTACN)(CF_3SO_3)]^{+}$ (calc. 456.0974) (*z* = 1); Elemental analysis $C_{15}H_{25}F_6N_5O_6S_2Fe$ (MW = 605.353 g/mol) Calc. (%) C 29.76, H 4.16, N 11.57; Found (%) C 30.55, H 4.28, N 11.08; ^{1}H-NMR (500 MHz, CD_3CN) 99.43, 82.93, 69.52, 64.56, 55.36, 50.00, 33.54, 21.24, 6.72, 4.06, 3.65, 3.59, 3.05-3.02, 2.88-2.82, 2.77-2.74, 2.66, 2.59, 2.51-2.48, 2.21, 1.94, 1.81, 1.56, 1.32, 1.24, 1.21, 0.05; UV/Vis λ (nm) 365 (ε = 3100 $M^{-1}cm^{-1}$), 512 (ε = 60 $M^{-1}cm^{-1}$); FTIR (KBr) ν (cm^{-1}) 2921, 1634, 1458, 1259, 1176, 1032, 756, 642, 580, 519.

Crystal structure determination for complex 1^{OTf}

Colourless crystals of $\mathbf{1^{OTf}}$ were grown from slow diffusion of ethyl ether in a CH2Cl2 solution of the compound, and used for low temperature (100(2) K) X-ray structure determination. The measurement was carried out on a *BRUKER SMART APEX CCD* diffractometer using graphite-monochromated Mo *Kα* radiation (*λ* = 0.71073 Å) from an x-Ray Tube. The measurements were made in the range 1.636 to 28.083° for θ. Hemi-sphere data collection was carried out with ω and φ scans. A total of 16414 reflections were collected of which 6388 [R(int) = 0.0502] were unique. Programs used: data collection, Smart[23]; data reduction, Saint+[24]; absorption correction, SADABS[25]. Structure solution and refinement was done using SHELXTL[26].

The structure was solved by direct methods and refined by full-matrix least-squares methods on F^2. The non-hydrogen atoms were refined anisotropically. The H-atoms were placed in geometrically optimized positions and forced to ride on the atom to which they are attached. A considerable amount of electron density attributable to a disordered Ethyl Ether solvent molecule per asymmetric unit was removed with the SQUEEZE option of PLATON[27]. Those solvent molecules are, however, included in the reported chemical formula and derived values (e.g. formula weight, F(000), etc.).

Reaction Conditions for Catalysis Experiments

In a typical reaction, 360 μL of H_2O_2 (25 μmol), taken from a 70 mM H_2O_2 stock solution in CH_3CN together with 45 μL of water (2500 μmol), was delivered by syringe pump over 30 min at room temperature under air to a vigorously stirred CH_3CN solution (2.14 ml) containing the Fe-catalyst (2.5 μmol) and the alkane substrate (2500 μmol). The final concentrations were 1 mM for catalyst, 10 mM for the oxidant, 1000 mM for H_2O and 1000 mM for substrate (1:10:1000:1000 for cat:ox:H_2O:sub). For adamantane, due to the low solubility, only 50 μmol of the substrate was used and so the final concentration was 20 mM. At the conclusion of the syringe pump addition, 500 μL of a biphenyl solution of a known concentration (~25 mM) was added to the reaction mixture as an internal standard. The reaction mixture was then passed through a small silica column (to remove the iron complex), followed by elusion with 2 ml ethyl acetate. Finally, the solution was subjected to GC analysis. The organic products were identified and their yields were calculated by using authentic compounds as quantitative standards.

For the measurement of kinetic isotope effects (KIE), a substrate mixture of cyclohexane:cyclohexane-d_{12} in a ratio of 1:3 was used to improve the accuracy of the obtained KIE value.

Isotope labeling studies

Catalytic reaction conditions using $H_2{}^{18}O$: In a typical reaction, 290 μL of H_2O_2 (20 μmol), taken from a 70 mM H_2O_2 stock solution in CH_3CN, was delivered by syringe pump over 30 min at room temperature under air to a vigorously stirred CH_3CN solution (1.71 ml) containing the Fe-catalyst (2.0 μmol), substrate (2000 μmol) and $H_2{}^{18}O$ (2000 μmol). The final concentrations were 1 mM for catalyst, 10 mM of the oxidant, 1000 mM for $H_2{}^{18}O$ and 1000 mM for substrate (1:10:1000:1000 for cat:H_2O_2:$H_2{}^{18}O$:sub). For adamantane, due to the low solubility, only 50 μmol of the substrate was used and so the final concentration was 20 mM.

Catalytic reaction conditions using $H_2{}^{18}O_2$: In a typical reaction, 34 μL of $H_2{}^{18}O_2$ (20 μmol) taken from a 2% (wt/wt) $H_2{}^{18}O_2$ solution in $H_2{}^{18}O$ was delivered by syringe pump over 30 min at room temperature under air to a vigorously stirred CH_3CN solution (2 ml) containing the Fe-catalyst (2.0 μmol), substrate (2000 μmol) and 45 μL of H_2O. The final concentrations were 1 mM for catalyst, 10 mM for the oxidant, 1000 mM for H_2O and 1000 mM for substrate (1:10:1000:1000 for cat:$H_2O_2{}^{18}$:H_2O:sub).

In the oxidation of adamantane and *cis*-1,2-dimethylcyclohexane, the solution (after syringe pump addition) was passed through a small silica column to remove the Fe-catalyst, followed by elution with 2 ml ethyl acetate. For other substrates, the reaction solution was treated with 1 ml acetic anhydride and 0.1 ml of 1-methylimidazole to esterify the alcohol products for GC-MS analyses (tertiary alcohols are not esterified under these conditions). Samples were concentrated by removing part of the solvent under vacuum and subjected to GC-MS analyses.

Computational Details and Modeling

All DFT calculations were carried out with the Gaussian 09 package of programs.[28] using the B3LYP hybrid functional. This functional is comprised of Becke's three-parameter hybrid exchange functional (B3)[29] and the correlation functional of Lee, Yang, and Parr (LYP).[30] The iron atom was described with the Stuttgart-Dresden effective core potential and SDD basis set,[31] and the 6-31G(d') basis set[32] was employed for all remaining atoms.

All reported geometries were fully optimized, and analytical second derivatives were evaluated at each stationary point to determine whether the geometry was an energy minimum (no negative eigenvalues) or a transition structure (one negative eigenvalue). Unscaled vibrational frequencies were used to make zero-point and thermal corrections to the electronic energies. The resulting potential energies and enthalpies are reported in kcal/mol relative to the specified standard. Standard state corrections were applied to all species to convert concentrations from 1 atm to 1M according to the treatise of Cramer.[33] The geometry-optimized structures have been drawn with the *JIMP*2 molecular visualization and manipulation program.[34]

Supporting information

ESI-MS, ^{1}H-NMR, UV/Vis and FT-IR spectra of complexes $\mathbf{1}^{\mathbf{OTf}}$ and $\mathbf{2}^{\mathbf{OTf}}$ are available.

Acknowledgements

This research has been carried out within the frameworks of the International Research Training Group *Metal sites in biomolecules: structures, regulation and mech*anisms (www.biometals.eu) and COST Action CM1003. M.M. thanks the European Commission for an Erasmus Mundus fellowship.

References

(1) (a) B. Meunier, *Biomimetic Oxidations Catalyzed by Transition Metal Complexes* Imperial College London Press: London, **2000**; (b) H. Arakawa, M. Aresta, J. N. Armor, M. A. Barteau, E. J. Beckman, A. T. Bell, J. E. Bercaw, C. Creutz, E. Dinjus, D. A. Dixon, K. Domen, D. L. DuBois, J. Eckert, E. Fujita, D. H. Gibson, W. A.

Goddard, D. W. Goodman, J. Keller, G. J. Kubas, H. H. Kung, J. E. Lyons, L. E. Manzer, T. J. Marks, K. Morokuma, K. M. Nicholas, R. Periana, L. Que Jr., J. Rostrup-Nielson, W. M. H. Sachtler, L. D. Schmidt, A. Sen, G. A. Somorjai, P. C. Stair, B. R. Stults, W. Tumas, *Chem. Rev.* **2001**, 101, 953-996; (c) J.-E. Bäckvall, *Modern Oxidation Methods*; Wiley-VCH; Weinheim, Germany, **2004**; (d) G. B. Shul'pin, *Mini-Rev. Org. Chem.* **2009**, 6, 95-104.
(2) (a) C.-L. Sun, B.-J. Li, Z.-J. Shi, *Chem. Rev.* **2011**, 111, 1293-1314; (b) A. Correa, O. G. Mancheno, C. Bolm, *Chem. Soc. Rev.* **2008**, 37, 1108-1117; (c) S. Enthaler, K. Junge, M. Beller, *Angew. Chem. Int. Ed.* **2008**, 47, 3317-3321; (d) L.-X. Liu, *Curr. Org. Chem.* **2010**, 14, 1099-1126; (e) *Iron Catalysis in Organic Chemistry* (B. Plietker), Willey-VCH, Weinheim, **2008**.
(3) (a) P. R. Ortiz de Montellano, *Chem. Rev.*, 2010, 110, 932-948; (b) P. R. Ortiz de Montellano, J. J. De Voss, *Nat. Prod. Rep.*, 2002, 19, 477-493.
(4) (a) E. Y. Tshuva, S. J. Lippard, *Chem. Rev.*, 2004, 104, 987-1012; (b) P. C. A. Bruijnincx, G. van Koten, R. Gebbink, *Chem. Soc. Rev.*, 2008, 37, 2716-2744; (c) E. G. Kovaleva, J. D. Lipscomb, *Nat. Chem. Biol.*, 2008, 4, 186-193; (d) M. H. Sazinsky, S. J. Lippard, *Acc. Chem. Res.*, 2006, 39, 558-566.
(5) M. Costas, M. P. Mehn, M. P. Jensen, L. Que Jr., *Chem. Rev.*, 2004, 104, 939-986.
(6) (a) S. M. Barry, G. L. Challis, *ACS Catal.*, 2013, 3, 2362-2370, (b) M. D. Wolfe, J. V. Parales, D. T. Gibson, J. D. Lipscomb, *J. Biol. Chem.*, 2001, 276, 1945-1953; (c) S. Chakrabarty, R. N. Austin, D. Deng, J. T. Groves, J. D. Lipscomb, *J. Am. Chem. Soc.*, 2007, 129, 3514-3515.
(7) (a) L. Que Jr., W. B. Tolman, *Nature*, 2008, 455, 333-340; (b) E. P. Talsi, K. P. Bryliakov, *Coord. Chem. Rev.*, 2012, 256, 1418-1434; (c) H. Lu, P. Zhang, *Chem. Soc. Rev.*, 2011, 40, 1899-1909; (d) C. M. Che, J. S. Huang, *Chem. Commun.*, 2009, 3996-4015; (e) M. Costas, *Coord. Chem. Rev.*, 2011, 255, 2912-2932; (f) K. P. Bryliakov, E. P. Talsi, *Coord. Chem. Rev.*, 2014, 276, 73-96.
(8) (a) A. Thibson, V. Jollet, C. Ribal,K. Senechal-David, L. Billion, A. B. Sorokin, F. Banse, *Chem. Eur. J.*, 2012, 18,2715-2724; (b) K. Moller,G. Wienhofer, K. Schroder, B. Join, K. Junge, M. Beller, *Chem. Eur. J.*, 2010, 16, 10300-10303.
(9) (a) M. C. White, A. G. Doyle, E. N. Jacobsen, *J. Am. Chem. Soc.*, 2001, 123, 7194-7195; (b) Y. Mekmouche, S. Menage, C. Toia-Duboc, M. Fontecave, J. B. Galey, C. Lebrun, J. Pecaut, *Angew. Chem. Int. Ed.*, 2001, 40, 949-952; (c) J. Y. Ryu, J. Kim, M. Costas, K. Chen, W. Nam, L. Que Jr., *Chem. Commun.*, 2002, 1288-1289; (d) M. Fujita. M. Costas, L. Que Jr., *J. Am. Chem. Soc.*, 2003, 125, 9912-9913; (e) G. Dubois, A. Murphy, T. D. P. Stack, *Org. Lett.*, 2003, 5, 2469-2472; (f) M. Klopstra, G. Roelfes, R. Hage, R. M. Kellogg, B. L. Feringa, *Eur. J. Inorg. Chem.*, 2004, 846-856; (g) M. R. Bukowski, P. Comba, A. Lienke, C. Limberg, C. L. de Laorden, R. Mas-Balleste, M. Merz, L. Que Jr., *Angew. Chem. Int. Ed.*, 2006, 45, 3446-3449; (h) S. Taktak, W. H. Ye, A. M. Herrera, E. V. Rybak-Akimova, *Inorg. Chem.*, 2007, 46, 2929-2942; (i) C. Marchi-Delpierre, A. Jorge-Robin, A. Thibson, S. Menage, *Chem. Commun*, 2007, 1166-1168; (j) R. Mas-Balleste, L. Que Jr., *J. Am. Chem. Soc.*, 2007, 129, 15964-; (k) P. Comba, G. Rajaraman, *Inorg. Chem.*, 2008, 47, 78-93; (l) P. Liu, E. L. M. Wong, A. W. H. Yuen, C. M. Che, *Org. Lett.*, 2008, 10, 3275-3278; (m) P. C. A. Bruijnincx, I. L. C. Buurmans, S. Gosiewska, M. A. H. Moelands, M. Lutz, A. L. Spek, G. van Koten, R. J. M. Klein Gebbink, *Chem. Eur. J.*, 2008, 14, 1228-1237; (n) M. Wu, C. X. Miao, S. F. Wang, X. X. Hu, C. G. Xia, F. E. Kuhn, W. Sun, *Adv. Synth. Catal.*, 2011, 353, 3014-; (o) Y. Feng, J. England, L. Que Jr., *ACS Catal.*, 2011, 1, 1035-1042; (p) F. Oddon, E. Girgenti, C. Lebrun, C. Marchi-Delpierre, J. Pecaut, S. Menage, *Eur. J. Inorg. Chem.*, 2012, 85-96; (q) E. A. Mikhalyova, O. V. Makhlynets, T. D. Palluccio, A. S. Filatov, E. V. Rybak.Akimova, *Chem. Commun.*, 2012, 48, 687-689; (r) R. Wang, S. F. wang, C. G. Xia, W. Sun, *Chem. Eur. J.*, 2012, 18, 7332-7335.
(10) (a) G. Roelfes, M. Lubben, R. Hage, L. Que Jr., B. L. Feringa, *Chem. Eur. J.*, 2000, 6, 2152-2159; (b) T. A. van den Berg, J. de Boer, W. R. Browne, G. Roelfes, B. L. Feringa, *Chem. Commun.*, 2004, 2550-2551; (c) V. B. Romakh, B. Thierrien, G. Suss-Fink, G. B. Shul'pin, *Inorg. Chem.*, 2007, 46, 3166-3175; (d) P. Comba, M. Maurer, P. Vadivelu, *Inorg. Chem.*, 2009, 48, 10389-10396; (e) R. Mayilmurugan, H. Stoeckli-Evans, E. Suresh, M. Palaniandavar, *Dalton Trans.*, 2009, 5101-5114; (f) L. Gomez, I. Garcia-Bosch, A. Company, J. Benet-Buchholz, A. Polo, X. Sala, X. Ribas, M. Costas, *Angew. Chem. Int. Ed.*, 2009, 48, 5720-5723; (g) M. S. Chen, M. C. White, *Science,* 2010, 327, 566-571; (h) P. C. A. Bruijnincx, I. L. C. Buurmans, Y. X. Huang, G. Juhasz, M. Viciano-Chumillas, M. Quesada, J. Reedijk, M. Lutz, A. L. Spek, E. Munck, E. L. Bominaar, R. J. M. Klein Gebbink, *Inorg. Chem.*, 2011, 50, 9243-9255; (i) P. Liu, Y. G. Liu, E. L. M. Wong, S. Xiang, C. M. Che, *Chem. Sci.*, 2011, 2, 2187-2195; (j) M. A. Bigi, S. A. Reed, M. C. White, *Nat. Chem.*, 2011, 3, 216-222; (k) Y. He, J. D. Gorden, C. R. Goldsmith, *Inorg. Chem.*, 2011, 50, 12651-12660; (l) M. C. White, *Science,* 2012, 335, 807-809; (m) K. E. Djernes, O. Moshe, M. Mettry, D. D. Richards, R. J. Hooley, *Org. Lett.*, 2012, 14, 788-791; (n) Y. Hitomi, K. Arakawa, T. Funabiki, M. Kodera, *Angew. Chem. Int. Ed.*, 2012, 51, 3448-3452; (o) K. E. Djernes, M. Padilla, M. Mettry, M. C. Young, R. J. Hooley, *Chem. Commun.*, 2012, 48, 11576-11578.
(11) (a) A. Company, L. Gomez, M. Guell, X. Ribas, J. M. Luis, L. Que Jr., M. Costas, *J. Am. Chem. Soc.*, 2007, 129, 15766-15767; (b) A. Company, L. Gomez, X. Fontrodona, X. Ribas, M. Costas, *Chem. Eur. J.*, 2008, 14, 5727-5731.

(12) I. Prat, A. Company, V. Postils, X. Rivas, L. Que Jr., J. M. Luis, M. Costas, *Chem. Eur. J.*, 2013, 19, 6724-6738.
(13) I. Prat, J. S. Mathienson, M. Guell, X. Ribas, J. M. Luis, M. Cronin, M. Costas, *Nat. Chem.*, 2011, 3, 788-793.
(14) I. Prat, A. Company, T. Corona, T. Parella, X. Ribas, M. Costas, *Inorg. Chem.*, 2013, 52, 9229-9244.
(15) M. Mitra, J. Lloret-Fillol, M. Haukka, M. Costas, E, Nordlander, *Chem. Commun.*, 2014, 50, 1408-1410.
(16) (a) A. Diebold, K. S. Hagen, *Inorg. Chem.*, 1998, 37, 215-223; (b) D. W. Blakesley, S. C. Payne, K. S. Hagen, *Inorg. Chem.*, 2000, 39, 1979-1989; (c) K. Chen, L. Que Jr., *J. Am. Chem. Soc.*, 2001, 123, 6327-6337; (d) G. J. P. Britovsek, J. England, A. P. J. White, *Inorg. Chem.*, 2005, 44, 8125-8134; (e) A. J. Simaan, S. Dopner, F. Banse, S. Bourcier, G. Bouchoux, A. Boussac, P. Hildebrandt, J. J. Girerd, *Eur. J. Inorg. Chem.*, 2000, 1627-1633.
(17) P. Spannring, I. Prat, M. Costas, M. Lutz, P. C. A. Bruijnincx, B. M. Weckhuysen, R. J. M. Klein Gebbink, *Catal. Sci. Technol.*, 2014, 4, 708-716.
(18) (a) J. England, G. J. P. Britovsek, N. Rabadia, A. J. P. White, *Inorg. Chem.*, 2007, 46, 3752-3767; (b) J. England, C. R. Davies, M. Banaru, A. J. P. White, G. J. P. Britovsek, *Adv. Synth. Catal.*, 2008, 350, 883-897; (c) J. England, R. Gondhia, L. Bigorra-Lopez, A. R. Petersen, A. J. P. White, G. J. P. Britovsek, *Dalton Trans.*, 2009, 5319-5334.
(19) M. Costas, K. Chen, L. Que Jr., *Coord. Chem. Rev.*, 2000, 200-202, 517-544.
(20) G. Esquius, J. Pons, R. Yanez, J. Ros, R. Mathieu, B. Donnadieu, N. Lugan, *Eur. J. Inorg. Chem.*, 2002, 2999-3006.
(21) (a) C. Robinson, J. Zhang, D. Garrod, T. Perrior, G. Newton, K. Jenkins, R. Beevers, M. Major, M. Stewart, *Pyruvamide Compounds as Inhibitors of Dust Mite Group 1 Peptiside Allergen and their Use*, US 2012/0322722 Al. 21.01.2011.; (b) E. Alcade, M. Alemany, M. Gisbert, *Tetrahedron*, 1996, 52, 15171-15188.
(22) C. Flassbeck, K. Wieghart, *Z. Anorg. All. Chem.*, 1992, 608, 60-68.
(23) Bruker Advanced X-ray Solutions. SMART: Version 5.631, 1997-2002.
(24) Bruker Advanced X-ray Solutions. SAINT +, Version 6.36A, 2001.
(25) G. M. Sheldrick, *Empirical Absorption Correction Program*, Universität Göttingen, 1996
Bruker Advanced X-ray Solutions. SADABS Version 2.10, 2001.
(26) G. M. Sheldrick, *Program for Crystal Structure Refinement*, Universität Göttingen, 1997
Bruker Advanced X-ray Solutions. SHELXTL Version 6.14, 2000-2003. SHELXL-2013 (Sheldrick, 2013)
(27) A. L. Spek, (2005). PLATON, A Multipurpose Crystallographic Tool, Utrecht University, Utrecht, The Netherlands.
(28) M. J. Frisch, *et al*., Gaussian 09, Revision E.01, Gaussian, Inc., Wallingford, CT, USA, 2009.
(29) A. D. Becke, *J. Chem. Phys.*, 1993, *98*, 5648-5652.
(30) C. Lee, W. Yang, R. G. Parr, *Phys. Rev. B*, 1988, 37, 785-789.
(31) (a) M. Dolg, U. Wedig, H. Stoll, H. Preuss, *J. Chem. Phys.*, 1987, *86*, 866-872; (b) S. P. Walch, C. W. Bauschlicher, *J. Chem. Phys.*, 1983, *78*, 4597-4605.
(32) (a) G. A. Petersson, A. Bennett, T. G. Tensfeldt, M. A. Al-Laham, W. A. Shirley, J. Mantzaris, *J. Chem. Phys.*, 1988, *89*, 2193-2218; (b) G. A. Petersson, M. A. Al-Laham, *J. Chem. Phys.*, 1991, *94*, 6081-6090.
(33) C. J. Cramer, *Essentials of Computational Chemistry*, 2nd Ed.; Wiley: Chichester, UK, 2004.
(34) (a) JIMP2, version 0.091, a free program for the visualization and manipulation of molecules: M. B. Hall, R. F. Fenske, *Inorg. Chem.*, 1972, *11*, 768-775. (b) J. Manson, C. E. Webster, M. B. Hall, Texas A&M University, College Station, TX, **2006:** http://www.chem.tamu.edu/jimp2/index.html

Paper V

Highly Enantioselective Epoxidation of Olefins by H_2O_2 Catalyzed by a Non-heme Fe(II) complex of a Chiral Tetradentate Ligand

Mainak Mitra,[a] Mingzhe Sun,[a] Olaf Cusso,[b] Julio Lloret-Fillol,[b] Miquel Costas,*[b] Ebbe Nordlander*[a]

[a] Chemical Physics, Department of Chemistry, Lund University, Box 124, SE-221 00 Lund, Sweden. Fax: +46 46 22 24119; Tel: +46 46 22 28118; E-mail: Ebbe.Nordlander@chemphys.lu.se
[b]QBIS, Universitat de Girona, Girona, Spain, E-17071. Fax: +34 972 41 81 50; Tel: +34 972 41 98 42; E-mail: Miquel.Costas@udg.edu

Supporting Information

ABSTRACT: The new chiral tetradentate N4-donor ligand 1-methyl-2-({(*S*)-2-[(*S*)-1-(1-methylbenzimidazol-2-yl methyl)pyrrolidin-2-yl]pyrrolidin-1-yl}methyl) benzimidazole (*S*,*S*-^{PDBz}L), based on a chiral dipyrrolidene backbone, has been synthesized and its corresponding Fe(II) complex has been prepared and fully characterized. The X-ray structure of the complex reveals that the Fe(II) ion is in a distorted octahedral coordination environment with two *cis*-oriented coordination sites occupied by (labile) triflate anions. The ability of the iron complex to catalyze asymmetric epoxidation reactions of olefins with H_2O_2 was investigated, using 2-cyclohexen-1-one, 2-cyclopenten-1-one and *cis*-β-methylstyrene as substrate. Different carboxylic acids were used as additives to enhance yields and enantioselectivities. The catalysis results indicate that the Fe(II) complex is capable of effecting comparatively high enantioselectivities (> 80%) in the epoxidation reactions albeit with low product yields.

Introduction:

Optically active (chiral) epoxides are widely used in organic synthesis and industry as intermediates and building blocks for synthesis of drugs and agrochemicals.[1] Amongst various methods developed over years to synthesize chiral epoxides,[1] the catalytic asymmetric epoxidation of olefins has proven to be a very useful techniques that is employed both in fine chemical and industrial syntheses. Since the pioneering work by Sharpless and coworkers in the 1980s,[2] there have been numerous efforts to develop efficient catalytic systems,[1a,b,c,3-4] including chiral metal complexes[5-6] and organocatalysts,[7-8] for such transformations. Development of environmentally benign and cheap catalysts and oxidants with wide ranges of applications remain great challenges to synthetic chemists.[9] With the growing demand for green and sustainable chemistry, use of iron-based catalysts employing H_2O_2 as an oxidant has been an attractive research area because of the low cost, low toxicity and high abundance of iron in nature.[10] Collman *et al.*[11] reported the first enantioselective epoxidation of styrene derivatives catalyzed by iron-porphyrin complexes with iodosobenzene as an oxidant in 1999. Beller and co-workers[12] have reported a methodology for the asymmetric epoxidation of stilbene derivatives using an *in situ* iron-based catalyst, giving up to 97% ee. Several non-heme iron-catalyzed asymmetric epoxidation reactions are reported with various olefin substrates giving moderate to good yield and enantioselectivity.[13-15]

The factors that indirectly control the yield and enantioselectvity in iron-catalysed asymmetric epoxidation need to be thoroughly investigated. The presence of catalytic amounts of a carboxylic acid has been found to enhance both the yield and enantioselectivity in epoxide formation.[13d,15] A mechanistic scenario that has been proposed by Que and co-workers[16] for the iron-catalysed epoxidation of alkenes with H_2O_2/acetic acid involves the formation of a carboxylate-Fe(V) species as the active oxidant via acetic acid-assisted heterolytic O-O bond cleavage of the hydroperoxide ligand in an Fe(III)(OOH)($HOOCH_3$) precursor (Scheme 1). A recent computational study suggests that the carboxylic acid, owing to its non-innocent redox nature, can be oxidized by one electron and reduce the Fe ion to form a Fe(IV)-carboxyl radical intermediate,[17] similar to the Cytochrome P450 compound I. Electronic factors imposed by the ligand on the iron ion play an important role in the activation of H_2O_2 and O-atom transfer, as observed in the epoxidation of different olefin substrates catalyzed by a series of [Fe^{II}(PDP)(CF_3SO_3)$_2$] complexes (PDP = 2-({(*S*)-2-[(*S*)-1-(pyridyl-2-ylmethyl)pyrrolidin-2-yl] pyrrolidin-1-yl}methyl)pyridine), where the pyridine rings are substituted with electron withdrawing or donating moieties (Me_2N, MeO, Me, H, Cl, CO_2Et) at the *meta* and *para*-positions, Figure 1), giving up to 99% yield and 99% enantioselectivity.[15] Electron-rich ligands decrease the electrophilicity of the Fe-oxo entity, favouring the transition state to be shifted towards a more product-like complex, while electron-deficient ligands increase the electrophilicity of the Fe-oxo unit, making it more indiscriminate and less stereoselective.[18]

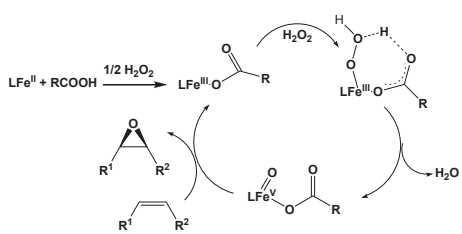

Scheme 1. Proposed mechanism for olefin epoxidation catalyzed by a non-heme Fe(II) complex.

In the present work, we have developed a new tetradentate ligand, *S,S*-^{PDBz}L (1-methyl-2-({(*S*)-2-[(*S*)-1-(1-methylbenzimidazol-2-ylmethyl)pyrrolidin-2-yl]pyrrolidin-1-yl}methyl)benzimidazole) (Figure 1), where we have introduced two (*N*-methyl)benzimidazolylmethyl arms attached to the two nitrogen atoms of the chiral 2,2'-bispyrrolidine backbone. We have previously observed that an (*N*-methyl)benzimidazolyl-containing ligand can enhance the catalytic reactivity of an Fe(II) complex in stereospecific C-H hydroxylation reactions,[19] and were therefore interested in investigating the influence of a chiral ligand containing (*N*-methyl)benzimidazolyl donor moieties on Fe(II)-catalyzed asymmetric epoxidation. Herein we report the synthesis and characterization of a non-heme Fe(II)-complex based on the ligand *S,S*-^{PDBz}L and results obtained on alkene epoxidation catalyzed by this complex.

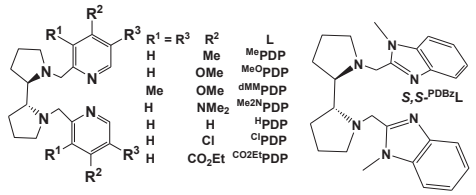

Figure 1. Structures of tetradentate ligands $^{(R1=R2,R3)}$PDP and *S,S*-^{PDBz}L.

Results and discussions.

Synthesis and characterization of ligand and metal complex.

The chiral ligand *S,S*-^{PDBz}L was synthesized by reaction of one eq. of (*S,S*)-2,2'-bispyrrolidine tartrate with two eq. of 2-(chloromethyl)-1-methylbenzimidazole[20] in the presence of base (NaOH) (Scheme 2; *cf.* Experimental Section for a detailed description of the synthesis). The ^{1}H NMR spectrum established the formation of the ligand which has characteristic peaks at 2.32 ppm for the hydrogens at the tertiary carbons of the bispyrrolidine unit and two doublets at 4.23 and 3.63 ppm for the hydrogens of the bridging methylene groups. The ESI mass spectrum also confirmed the formation of the ligand.

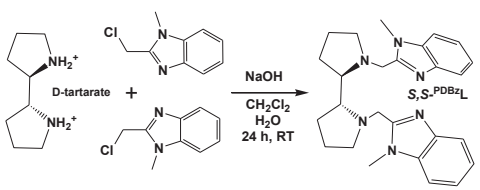

Scheme 2. Synthesis of the ligand *S,S*-^{PDBz}L.

Reaction of equimolar amounts of *S,S*-^{PDBz}L and $[Fe^{II}(CH_3CN)_2(CF_3SO_3)_2]$ in THF under inert atmosphere gave the metal complex $[Fe^{II}(S,S\text{-}^{PDBz}L)(CF_3SO_3)_2]$ (**1**^{OTf}) as a light yellow solid (Scheme 3, *cf.* Experimental Section). The analogous acetonitrile derivative $[Fe^{II}(S,S\text{-}^{PDBz}L)(CH_3CN)_2](SbF_6)_2$ (**1**^{SbF6}) was prepared in two steps: initial reaction of one eq. *S,S*-^{PDBz}L with one equivalent of $FeCl_2$ in MeCN to afford $[Fe^{II}(S,S\text{-}^{PDBz}L)Cl_2]$, followed by reaction two eq. $AgSbF_6$ with one eq. of $[Fe^{II}(S,S\text{-}^{PDBz}L)Cl_2]$ in CH_3CN to form the desired complex, **1**^{SbF6}, as a red microcrystalline solid.

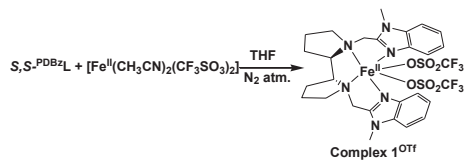

Scheme 3. Synthesis of the metal complex $[Fe^{II}(S,S\text{-}^{PDBz}L)(CF_3SO_3)_2]$ (**1**^{OTf}).

Complexes **1**^{OTf} and **1**^{SbF6} were characterized by high resolution mass spectroscopy (HRMS). The HRMS of **1**^{OTf} in CH_3CN showed a prominent mass peak at *m/z* 242.1042 corresponding to the formulation $[Fe^{II}(S,S\text{-}^{PDBz}L)]^{2+}$ (i.e. *z* = 2, calc. 242.1014) and at *m/z* 633.1517 corresponding to the formulation of $[Fe^{II}(S,S\text{-}^{PDBz}L)(CF_3SO_3)]^+$ (calc. 633.1558) (Figures S1-S3, Supplementary Material). The HRMS of complex **1**^{SbF6} in MeCN also showed prominent mass peaks at *m/z* 242.1022 and 719.0956 corresponding to the formulations of $[Fe^{II}(S,S\text{-}^{PDBz}L)]^{2+}$ (calc. 242.1014) and $[Fe^{II}(S,S\text{-}^{PDBz}L)(SbF_6)]^+$ (calc. 719.0980), respectively (Figures S4-S5, Supplementary Material).

The ^{1}H-NMR spectra of **1**^{OTf} and **1**^{SbF6} were measured in CD_3CN. The spectral window exhibited by both complexes range from -20 to 140 ppm, which is indicative of a high spin Fe(II) complex (Figures S6-S7, Supplementary Material).

Amongst the different absorption peaks in the IR spectrum of **1**^{OTf} (Figure S8, Supplementary Material) the peak at 725 cm^{-1} corresponds to the aromatic =C-H out-of-plane bending vibration and 513 cm^{-1} corresponds to the Fe-O stretching frequency. The IR spectrum of complex **1**^{SbF6} (Fig. S9, Supplementary Material) reveals peaks at 2275 cm^{-1}, corresponds to the C≡N stretches of the coordinated acetonitriale molecules, and the aromatic =C-H out-of-plane bending vibration appears at 748 cm^{-1}.

The UV/Vis spectrum of **1**^{OTf} in MeCN showed an absorption maximum at λ_{max} = 198 nm ($\varepsilon = 1.76 \times 10^5$ M^{-1} cm^{-1}) while **1**^{SbF6} in CH_3CN showed an absorption maximum at λ_{max} = 197 nm ($\varepsilon = 1.47 \times 10^5$ M^{-1} cm^{-1}). These bands are assigned to identical high energy intra-ligand charge transfer transitions.

Crystal and molecular structure of complex $\mathbf{1}^{\mathbf{OTf}}$.

The solid state structure of complex $\mathbf{1}^{\mathbf{OTf}}$ was confirmed by X-ray crystallography. The details of the structure determination are listed in Table 2 and selected bond distances and bond angles are listed in Table 3. The molecular structure (Fig. 2) shows that the iron ion adopts a distorted octahedral coordination geometry. Four coordination sites are occupied by the nitrogen atoms of the tetradentate *S,S*-^{PDBz}L ligand while the remaining two *cis*-sites are occupied by the oxygen atoms of the triflate anions. The two (*N*-methyl)benzimidazole rings remain above and below the plane containing the iron, the two nitrogens of the *S,S*-bispyrrolidine backbone and the two oxygen atoms of the triflate anions, and are almost perpendicular with respect to each other. The Fe-N bond distances range from 2.15 to 2.25 Å and the Fe-O bond distances range from 2.12 to 2.17 Å, which are in agreement with a high spin Fe(II) ion.[21]The bulky (*N*-methy)benzimidazolyl moieties introduce steric strain making the O-Fe-O angle smaller (96.7(2)º) relative to the corresponding angle in [Fe^{II}(^{MeO}PDP)(CF_3SO_3)$_2$] (108.47(5)º).[15]

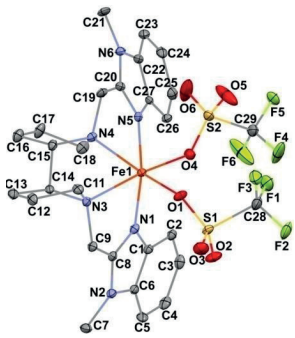

Figure 2. An ORTEP plot of the molecular structure of $\mathbf{1}^{\mathbf{OTf}}$, showing the atom numbering scheme. The thermal ellipsoids are drawn with 30% probability and the hydrogen atoms are omitted for clarity.

Catalytic asymmetric epoxidation.

Relatively simple cyclic enones have been generally less explored as substrates for asymmetric epoxidation than α,β-unsaturated aromatic ketones. In this study, focus has therefore been made on using the challenging substrate 2-cyclohexe-1-one for asymmetric epoxidation. The yields of the two chiral epoxide products have been determined by gas chromatography, using a chiral column. In a typical catalytic experiment, H_2O_2 was delivered using a syringe pump to a stirred solution of CH_3CN containing the Fe catalyst, $\mathbf{1}^{\mathbf{OTf}}$, and the substrate (Scheme 4) (*cf.* Experimental Section for detailed catalytic conditions). The catalytic reactions were carried out in air and at low temperature (-30 ºC). As mentioned above, previous studies have shown that the presence of a carboxylic acid enhances the efficiency of the catalyst, and the choice of carboxylic acid plays an important role in tuning the efficiency and selectivity of the asymmetric epoxidation reactions. In a recent study reported by Costas and coworkers,[15] it was found that the presence of racemic 2-ethylhexanoic acid (2-eha) resulted in high enantiomeric excess (ee) and relative good yields in iron-catalyzed asymmetric epoxidation reactions. Therefore, the study of epoxidation of 2-cyclohexe-1-one was performed using 2-eha.

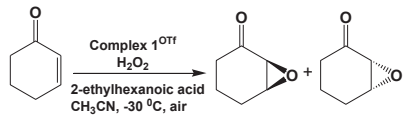

Scheme 4. Schematic depiction of the epoxidation reaction of 2-cyclohexe-1-one by $\mathbf{1}^{\mathbf{OTf}}$ using H_2O_2, with 2-ethylhexanoic acid as an additive.

The complex $\mathbf{1}^{\mathbf{OTf}}$ (4 mol%) oxidized 2-cyclohexe-1-one to form the two epoxides with low yield (16%) in the presence of H_2O_2 (2 equiv w.r.t. substrate) and 2-eha (3 equiv w.r.t. substrate; Scheme 4), although the conversion of the substrate into oxidized products was 43% (based on oxidant). Furthermore, the ee value obtained was 89%. An increase of the carboxylic acid loading did not lead to any significant change in the epoxide yield or the ee value (with 5 equiv acids the yield of epoxides was 10% and ee was 86% and with 10 equiv acids the yield of epoxides was 13% and ee was 87%; entries 1-3, Table 1). The effect of different amount of catalyst loading on the substrate conversion, yield of epoxides and ee value was examined. In all cases, the amounts of H_2O_2 (2 equiv w.r.t. substrate) and carboxylic acid (10 equiv w.r.t. substrate) were kept fixed. Changing the catalyst loading from 4 mol% to 2 mol% resulted in a decrease in conversion of substrate into oxidized products (30%) and the yield of epoxides (10%), while maintaining high ee value (87%; entry 4, Table 1). Increasing the catalyst loading from 4 mol% to 8 mol% (or 10 mol%) increased the conversion of substrate into products (66 and 67% for 8 and 10 mol% catalyst loading, respectively), but the epoxide yield was more or, less similar (entry 5, Table 1). Finally, the amount of H_2O_2 was varied while the amounts of catalyst (4 mol%) and carboxylic acid (10 equiv w.r.t. substrate) were kept fixed. Addition of 1.3 equiv of H_2O_2 resulted in a conversion of 55% with a yield of epoxides of 11% and ee value of 84%, while addition of 3 equiv of H_2O_2 resulted in conversion of 68% but poor yield of epoxides (7%) and lowering of the ee value (74%; entries 6-8, Table 1).

As expected, complex $\mathbf{1}^{\mathbf{SbF6}}$ exhibited the same behaviour as $\mathbf{1}^{\mathbf{OTf}}$ (entries 3 and 9, Table 1). On changing the carboxylic acid, both the yields and enantioselectivities were diminished (2% yield and 60% ee for trimethylacetic acid and 1% yield and 58% ee for *S*-ibuprofen; entries 9-11, Table 1).

Table 1. Catalytic epoxidation of 2-cyclohexen-1-one by complex $\mathbf{1}^{\mathbf{OTr}}$[1]

Entry	Catalyst (mol%)	CA[2] (equiv)	Equiv of H_2O_2	Conversion of substrate (%)	Yield of epoxides (%)	ee[3] (%)
1	$\mathbf{1}^{\mathbf{OTf}}$ (4)	2-eha (3)	2	43	16	89
2	$\mathbf{1}^{\mathbf{OTf}}$ (4)	2-eha (5)	2	52	10	86
3	$\mathbf{1}^{\mathbf{OTf}}$ (4)	2-eha (10)	2	64	13	87
4	$\mathbf{1}^{\mathbf{OTf}}$ (2)	2-eha (10)	2	30	10	87
5	$\mathbf{1}^{\mathbf{OTf}}$ (8)	2-eha (10)	2	66	11	84
6	$\mathbf{1}^{\mathbf{OTf}}$ (4)	2-eha (10)	1.3	55	11	87
7	$\mathbf{1}^{\mathbf{OTf}}$ (4)	2-eha (10)	1.6	59	12	87
8	$\mathbf{1}^{\mathbf{OTf}}$ (4)	2-eha (10)	3	68	7	74
9	$\mathbf{1}^{\mathbf{SbF6}}$ (4)	2-eha (10)	2	64	13	86
10	$\mathbf{1}^{\mathbf{SbF6}}$ (4)	$(CH_3)_3CO_2H$ (10)	2	72	2	60
11	$\mathbf{1}^{\mathbf{SbF6}}$ (4)	*S*-Ibuprofen (10)	2	2	1	58

[1]Reaction conditions: experimental section; [2]carboxylic acids; [3]enantiomeric excess.

Complex $\mathbf{1}^{\mathbf{OTf}}$ was further investigated in the oxidation of 2-cyclopenten-1-one where it provided low conversion of the substrate (52%) with very low yield of epoxide (4%) and moderate enantioselectivity (ee 76%).

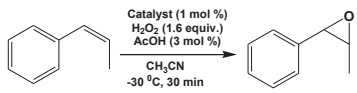

Scheme 5. Epoxidation of *cis*-β-methylstyrene with H_2O_2 in presence of acetic acid catalyzed by Fe(II) complexes.

Cis-β-methylstyrene was also employed as a substrate and the conditions for catalysis were used as reported earlier,[15] in order to enable direct comparison of $\mathbf{1}^{\mathbf{OTf}}$ with related Fe(II) complexes. Under catalytic conditions (*cf.* Experimental Section for details), complex $\mathbf{1}^{\mathbf{OTf}}$ oxidized *cis*-β-methylstyrene to form epoxides with 60% yield and an ee of 41% (Scheme 5). Under the same conditions, the catalyst $[Fe^{II}(^{H}PDP)(CF_3SO_3)_2]$ ($^{\mathbf{H}}\mathbf{1}$) (^{H}PDP = 2-({(*S*)-2-[(*S*)-1-(pyridyl-2-ylmethyl)pyrrolidin-2-yl]pyrrolidin-1-yl}methyl)pyridine) and $[Fe^{II}(^{Me2N}PDP)(CF_3SO_3)_2]$ ($^{\mathbf{Me2N}}\mathbf{1}$) (^{Me2N}PDP is the modified PDP ligand where the *para*-positions of the two pyridyl rings are occupied by Me_2N groups, *cf.* Figure 1) provided an epoxide yield of 26% with ee of 19% and 87% with ee of 62%, respectively.[15]

Conclusion

The new tetradentate N4 ligand *S,S*-^{PDBz}L, with an *S,S*-bispyrrolidine chiral backbone, has been synthesized. The corresponding Fe(II) complexes, $[Fe^{II}(S,S\text{-}^{PDBz}L)(CF_3SO_3)_2]$ ($\mathbf{1}^{\mathbf{OTf}}$) and $[Fe^{II}(S,S\text{-}^{PDBz}L)(CH_3CN)_2](SbF_6)_2$ ($\mathbf{1}^{\mathbf{SbF6}}$) were synthesized and fully characterized. The complex $\mathbf{1}^{\mathbf{OTf}}$ exhibited highly enantioselective epoxidations (ee > 80%) in the oxidation of cyclic olefin 2-cyclohexen-1-one, albeit with low yields of the chiral epoxides (10-15%). It has previously been shown that while the complex $[Fe^{II}(^{Me2N}PDP)(CF_3SO_3)_2]$ provided poor yield (12%) and moderate enantioselectivity (ee 76%) in the epoxidation of 2-cyclohexen-1-one, the complex $[Fe^{II}(^{MeO}PDP)(CF_3SO_3)_2]$ (Figure 1) showed excellent yield (99%) and high enantioselectivity (ee 84%) under similar conditions. This difference was attributed to the rapid deactivation of the former catalyst during the course of oxidation of the substrate, when the substrate oxidizes slowly under the reaction conditions. The similar reactivities of $\mathbf{1}^{\mathbf{OTf}}$ and $[Fe^{II}(^{Me2N}PDP)(CF_3SO_3)_2]$ towards the substrate 2-cyclohexen-1-one might therefore be due to similar fast deactivation of the Fe-catalyst. With *cis*-β-methylstyrene, $\mathbf{1}^{\mathbf{OTf}}$ provided moderate yield (60%) and lower enantioselectivity (ee 41%). The relative orientation of the bulky (*N*-methyl)benzimidazole groups may also provide excessive steric constraints on the approach of the incoming substrate to interact with the active metal-oxo species, causing poor yield of the epoxides and unwanted side products. Further studies of the catalytic properties of $\mathbf{1}^{\mathbf{OTf}}$ and $\mathbf{1}^{\mathbf{SbF6}}$ are needed to optimize reaction conditions and explore a wider range of substrates.

Experimental Section

Reagents and Materials:

Reagents and solvents were of at least 99% purity and used as received without any further purification. All reagents and solvents were purchased from Sigma Aldrich or Fisher Scientific. Dichloromethane and acetonitrile were dried by distillation from CaH_2; diethyl ether was dried by distillation from Na/benzophenone. The starting material 2-(chloromethyl)-1-methylbenzimidazole was synthesized according to a literature procedure.[19]

Instrumentation:

Infrared spectra were collected on a Nicolet Avatar 360 FTIR spectrometer. UV-Visible spectroscopy was performed in a 1 cm quartz cell using an Agilent Technology 8453 UV-Vis spectrophotometer equipped with a diode-array detector. NMR spectra were recorded on a Bruker DPX 400 MHz spectrometer in $CDCl_3$ or CD_3CN solvent using standard conditions and were referenced to the residual proton signal of the solvent. Elemental analysis was performed on a 4.1 Vario EL 3 elemental analyzer from Elementar. The ESI-MS experiments were performed with a Bruker Esquire 6000 LC/MS chromatograph, using acetonitrile as a mobile phase. The product analyses after catalysis experiments were carried out on an Agilent Technology 7820A gas chromatograph equipped with a 16-sample automatic liquid sampler, flame ionization detector and EzChrom Elite Compact software.

Synthesis:

Synthesis of 1-methyl-2-({(*S*)-2-[(*S*)-1-(1-methylbenzimidazol-2-ylmethyl)pyrrolidin-2-yl]pyrrolidin-1-yl}methyl)benzimidazole (*S*, *S*-^{PDBz}L)

A 100 ml round bottom flask was charged with (*S*,*S*)-2,2'-bispyrrolidine tartrate (0.4 g, 1.38 mmol, 1 equiv) in CH_2Cl_2 (15 ml). To this stirring solution, 2-(chloromethyl)-1-methylbenzimidazole (0.573 g, 3.174 mmol, 2.3 equiv)

was added. Then, 5.0 ml of a 1 M NaOH solution was added. After 72 h of stirring at room temperature, the reaction mixture was diluted with 30 ml 1 M NaOH solution. The aqueous layer was extracted with 3 x 15 ml CH_2Cl_2 and the organic part was collected, dried over Na_2SO_4 and concentrated under vacuum to obtain the crude product. The crude ligand was then passed through a column packed with silica gel and eluted with 5% CH_3OH: 2% NaOH: 82% CH_2Cl_2: 11% petroleum ether. The collected fractions were combined, washed with 1 M NaOH solution, dried over Na_2SO_4 and the solvent was evaporated to obtain the ligand as a pale orange solid. Yield: 0.366 g (63.2%). HRMS: 429.2760 $[M+H]^+$, calc. 429.2761. ^{1}H-NMR (400 MHz, $CDCl_3$) δ (ppm): 7.72 (m, 2H), 7.33-7.21 (m, 6H), 4.23 (d, 2H), 3.80 (s, 6H), 3.66 (d, 2H), 2.80 (dt, 4H), 2.32 (m, 2H), 1.79 (m, 4H), 1.68 (m, 4H). ^{13}C-NMR (100 MHz, $CDCl_3$) δ (ppm): 152.4, 142.2, 136.1, 122.4, 121.8, 119.6, 109.0, 65.2, 55.6, 52.5, 29.9, 26.2, 24.0.

Synthesis of $[Fe^{II}(S,S\text{-}^{PDBz}L)(CF_3SO_3)_2]$ (1^{OTf}):
This reaction was performed inside a dry atmosphere box. $[Fe^{II}(CH_3CN)_2(CF_3SO_3)_2]$ (166.8 mg, 0.38 mmol) was dissolved in 1 ml THF and added drop-wise to a stirring solution of $S,S\text{-}^{PDBz}L$ (163.2 mg, 0.38 mmol) in THF (1 ml). A yellow precipitate appeared upon addition of the Fe salt to the ligand solution. After stirring for about 1 h, the yellow precipitate was filtered off and dried under vacuum. The resultant solid was dissolved in 3 ml CH_2Cl_2 and filtered through a celite pad. The resulting filtrate was removed under vacuum to afford a light yellow microcrystalline product. Yield: 225.8 mg (76%). HRMS: (*m/z*) 242.1042 $[Fe^{II}(S,S\text{-}^{PDBz}L)]^{2+}$ (z = 2), calc. 242.1014; 633.1517 $[Fe^{II}(S,S\text{-}^{PDBz}L)(CF_3SO_3)]^+$ (z = 1), calc. 633.1558; Elemental analysis $C_{28}H_{32}N_6O_6F_6S_2Fe$ (MW = 782.554 g/mol) calc. (%) C 42.97, H 4.12, N 10.74; Found (%) C 43.16, H 4.01, N 10.29; FT-IR (ATR) ν (cm^{-1}) 3011, 2956, 1456, 1304, 1214, 1157, 1034, 752, 634, 513, 429.

Synthesis of $[Fe^{II}(S,S\text{-}^{PDBz}L)(CH_3CN)_2](SbF_6)_2$ (1^{SbF6}):
The ligand $S,S\text{-}^{PDBz}L$ (108.9 mg, 0.254 mmol) was dissolved in 1.5 ml CH_3CN. A total of 32 mg $FeCl_2$ (32.3 mg, 0.254 mmol) was added into the stirring solution. A yellow precipitate appeared within a few seconds of stirring. After 4h of stirring, the solvent of the reaction mixture was removed under vacuum and the resultant solid was washed with CH_3CN and ether, and dried under an N_2 flow to afford $[Fe^{II}(S,S\text{-}^{PDBz}L)Cl_2]$ (88.6 mg, yield 63%). This complex (88.6 mg, 0.16 mmol) was suspended in 5 ml CH_3CN. A total of 110 mg of $AgSbF_6$ (109.7 mg, 0.32 mmol) was added into the stirred suspension, whereupon a white precipitate immediately appeared. The colour of the solution gradually changed from light yellow to orange. After 4 h of stirring, the mixture was filtered though a celite column in the dark. The solvent was removed under vacuum to provide $[Fe^{II}(S,S\text{-}^{PDBz}L)(CH_3CN)_2](SbF_6)_2$ as a red solid. Yield: 157.7 mg (95%). HRMS: (*m/z*) 242.1022 $[Fe^{II}(S,S\text{-}^{PDBz}L)]^{2+}$ (z = 2), calc. 242.1014; 719.0956 $[Fe^{II}(S,S\text{-}^{PDBz}L)(SbF_6)]^+$ (z = 1), calc. 719.0980; Elemental analysis $C_{30}H_{38}N_8F_{12}Sb_2Fe$ (MW = 1038.021 g/mol) calc. (%) C 34.71, H 3.69, N 10.79; Found (%) C 35.97, H 4.33, N 10.44.

Crystal structure determination.

Orange crystals of $\mathbf{1^{OTf}}$ were grown by slow diffusion of diethyl ether into a CH_2Cl_2 solution of the compound. Collection of diffraction data was carried out at (100(2) K) on a BRUKER SMART APEX CCD diffractometer using graphite-monochromated Mo *K*α radiation (λ = 0.71073 Å). The measurements were made in the θ range 2.172 to 27.744°. A full-sphere data collection was carried out with ω and φ scans. A total of 82922 reflections were collected of which 8370 were unique. Programs used: data collection, Smart[22]; data reduction, Saint+[23]; absorption correction, SADABS[24]. Structure solution and refinement was done using SHELXTL[25]

The structure was solved by direct methods and refined by full-matrix least-squares methods on F^2. The non-hydrogen atoms were refined anisotropically. The H-atoms were placed in geometrically optimized positions and forced to ride on the atom to which they are attached. The structure crystallized in the chiral space group $P6_5$.

Table 2. Crystal data for complex $\mathbf{1^{OTf}}$.

Empirical formula	$\mathbf{C_{28}H_{32}F_6FeN_6O_6S_2.CH_2Cl_2}$ ($\mathbf{1^{OTf}}$)
Formula weight	867.49
Temperature	100(2) K
Wavelength	0.71073 Å
Crystal system	Hexagonal
Space group	$P6_5$
Unit cell dimensions	a = 10.8264(3) Å b = 10.8264(3) Å c = 52.532(2) Å α = 90° β = 90° γ = 120°
Volume	5332.4(4) $Å^3$
Z	6
Density (calculated)	1.621 Mg m^{-3}
Absorption coefficient	0.775 mm^{-1}
F(000)	2664
Crystal size	0.3 X 0.3 X 0.25 mm^3
Theta range for data collection	2.172 to 27.744°
Index ranges	-14<=h<=14, -14<=k<=14, -68<=l<=68
Reflections collected	82922
Independent reflections	8370
Completeness	100% (to theta = 25.242)
Absorption correction	Empirical
Max. and min. transmission	1.0 and 0.900775
Refinement method	Full-matrix least-squares on F^2
Data/restraints/parameters	8370/3/471
Goodness-of-fit on F^2	1.053
Final R indices [I>2sigma(I)]	R1 = 0.0592, wR2 = 0.1622
R indices (all data)	R1 = 0.0632, wR2 = 0.1668
Largest diff. peak and hole	2.223 and -1.601 e.$Å^{-3}$

Table 3. Selected bond distances (Å) and bond angles (º) in complex $\mathbf{1}^{\mathbf{OTf}}$.

Fe(1)-N(1)	2.148(4)
Fe(1)-O(1)	2.115(6)
Fe(1)-N(3)	2.249(6)
Fe(1)-N(4)	2.237(6)
Fe(1)-O(4)	2.168(6)
Fe(1)-N(5)	2.149(5)
N(1)-Fe(1)-O(1)	96.8(2)
N(1)-Fe(1)-N(3)	76.5(2)
N(1)-Fe(1)-N(4)	98.1(2)
N(1)-Fe(1)-O(4)	90.0(2)
N(1)-Fe(1)-N(5)	170.8(2)
O(1)-Fe(1)-N(3)	91.1(2)
O(1)-Fe(1)-N(4)	160.6(2)
O(1)-Fe(1)-O(4)	96.7(2)
O(1)-Fe(1)-N(5)	87.5(2)
N(3)-Fe(1)-N(4)	80.3(2)
N(3)-Fe(1)-O(4)	165.1(2)
N(3)-Fe(1)-N(5)	95.4(2)
N(4)-Fe(1)-N(5)	76.1(2)
O(4)-Fe(1)-N(5)	97.6(2)

Reaction conditions for catalysis.

Conditions for epoxidation of 2-cyclohexen-1-one and 2-cyclopenten-1-one.

An acetonitrile solution (750 µL) of the alkene substrate (0.0825 mmol, final concentration 0.11 M) and $\mathbf{1}^{\mathbf{OTf}}$ or $\mathbf{1}^{\mathbf{SbF6}}$ (3.32 µmol, 4 mol%, final concentration 4.4 mM) was prepared in a 10 ml vial equipped with a stir bar, and cooled in an acetonitrile freeze bath (temp -30 ºC). A total of 12 µL of the carboxylic acid in CH_3CN was directly added to the reaction solution. Then 37.7 µL of 1:1 (v:v) H_2O_2 (30% wt/wt in H_2O):CH_3CN was delivered to the reaction solution over a period of 30 min, using a syringe pump. Then the reaction solution was further stirred at 30 ºC for 30 min. At this point, a known amount of biphenyl solution was added as internal standard. The solution was passed through a small alumina column and the column was rinsed with 2 × 1 ml ethyl acetate and the resultant elute was subjected to GC analysis. The racemic products were identified by their GC retention times and the yields were determined from the integration area of the GC spectrum.

Conditions for epoxidation of *cis*-β-methylstyrene.

An acetonitrile solution (750 µL) of *cis*-β-methyl styrene (0.0825 mmol, final concentration 0.11 M) and $\mathbf{1}^{\mathbf{OTf}}$ (final concentration 1.1 mM) was prepared in a 10 ml vial equipped with stir bar and, cooled in an acetonitrile freeze bath (temp -30 ºC). A total of 12.5 µL of the acetic acid (0.2 M solution, 3 mol %) in CH_3CN was directly added to the reaction solution. Then 26.7 µL of 1:1 (v:v) H_2O_2 in water (30% wt/wt):CH_3CN was delivered to the reaction solution over a period of 30 min using a syringe pump. Then the reaction solution was further stirred at 30 ºC for 30 min. At this point, a known amount of biphenyl solution was added as internal standard. The solution was passed through a small alumina column and the column was rinsed with 2 × 1 ml ethyl acetate, and the resultant elute was subjected to GC analysis. The racemic products were identified by their GC retention times and the yields were determined from the integration area of the GC spectrum.

ASSOCIATED CONTENT

Supporting Information
^{1}H-NMR, HRMS, FT-IR spectra for complexes $\mathbf{1}^{\mathbf{OTf}}$ and $\mathbf{1}^{\mathbf{SbF6}}$ are available.

AUTHOR INFORMATION

Corresponding Author
Ebbe Nordlander: Ebbe.Nordlander@chemphys.lu.se
Miquel Costas: Miquel.Costas@udg.edu

ACKNOWLEDGMENT

This research has been carried out within the frameworks of the International Research Training Group *Metal sites in biomolecules: structures, regulation and mech*anisms (www.biometals.eu) and COST Action CM1003. M.M. thanks the European Commission for an Erasmus Mundus fellowship.

REFERENCES

(1) (a) M. J. Porter, J. Skidmore, *Chem. Commun.*, 2000, 1215-1225; (b) B. S. Lane, K. Burgess, *Chem. Rev.*, 2003 103, 2457-2473; (c) Q. H. Xia, H. Q. Ge, C. P. Ye, Z. M. Liu, K. X. Su, *Chem. Rev.*, 2005, 105, 1603-1662; (d) O. A. Wong, Y. Shi, *Chem. Rev.*, 2008, 108, 3958-3987; (e) D. diez, M. G. Nunez, A. B. Anton, P. garcia, R. F. Moro, N. M. Garrido, I. S. Marcos, P. Basabe, J. G. Urones, *Curr. Org. Synth.*, 2008, 5, 186-216; (e) K. Matsumoto, T. Kasturi, In *Catalytic Asymmetric Synthesis*, 3rd ed., Ed.: I. Ojima, Wiley-VCH, New York, 2010, pp. 839-890; (f) G. De Faveri, G. Ilyashenko, M. Watkinson, *Chem. Soc. Rev.*, 2011, 40, 1722-1760.
(2) K. B. Sharpless, *Angew. Chem. Int. Ed.*, 2002, 41, 2024-2032.
(3) (a) H. Wynberg, B. J. Greijdanus, *J. Chem. Soc. Chem. Commun.*, 1978, 427-428 ; (b) S. Julia, J. Guixer, J. Masana, J. Rocas, S. Colonna, R. Annuziata, H. J. Molinari, *J. Chem. Soc. Perkin Trans. 1*, 1982, 1317-1324; (c) D. Enders, J. Zhu, G. Raabe, *Angew. Chem. Int. Ed.*, 1996, 35, 1725-1728; (d) D. Yang, Y.-C. Yip, M.-W. Tang, M.-K. Wong, J.-H. Zheng, K.-K. Cheung, *J. Am. Chem. Soc.*, 1996, 118, 491-492; (e) M. Bougauchi, S. Watanabe, T. Arai, H. Sasai, M. Shibakasi, *J. Org. Chem.*, 1998, 63, 8090-8091; (f) E. J. Corey, F.-Y. Zhang, *Org. Lett.*, 1999,

1, 1287-1290; (g) O. Jacques, S. J. Richards, R. F. W. Jackson, *Chem. Commun.*, 2001, 1712-1713; (h) C. Li, E. A. Pace, M. C. Liang, E. Lobkovsky, T. D. Galimore, J. A. Porco Jr., *J. Am. Chem. Soc.*, 2001, 123, 11308-11309; (i) A. Berkessel, M. Guixa, F. Schimdt, J. M. Neudorfl, J. Lex, *Chem. Eur. J.*, 2007, 13, 4482-4498; (m) A. Erkkila, P. M. Pihko, M.-R. Clarke, *Adv. Synth. Catal.*, 2007, 349, 802-806; (n) G. Peris, C. E. Jakobsche, S. J. Miller, *J. Am. Chem. Soc.*, 2007, 129, 8710-8711; (o) W. Zhang, H. Yamamoto, *J. Am. Chem. Soc.*, 2007, 129, 286-287.

(4) (a) W. Adam, C. R. Saha-Moller, P. A. Ganeshpure, *Chem. Rev.*, 2001, 101, 3499-3548; (b) A. Lattanzi, *Curr. Org. Synth.*, 2008, 5, 117-133.

(5) (a) T. Kasturi, K. B. Sharpless, *J. Am. Chem. Soc.*, 1980, 102, 5974-5976; (b) W. Zhang, J. L. Loebach, S. R. Wilson, E. N. Jacobsen, *J. Am. Chem. Soc.*, 1990, 112, 2801-2803; (c) R. Irie, K. Noda, Y. Ito, N. Matsumoto, T. Kasturi, *Tetrahedron Lett.*, 1990, 31, 7345-7348; (d) K. Matsumoto, Y. Sawada, B. Saito, K. Sakai, T. Kasturi, *Angew. Chem. Int. Ed.*, 2005, 117, 5015-5019; (e) Y. Sawada, K. Matsumoto, S. Kondo, H. Watanabe, T. Ozawa, K. Suzuki, B. Saito, T. Kasturi, *Angew. Chem. Int. Ed.*, 2006, 45, 3478-3480; (f) A. U. Barlan, A. Basak, H. Yamamato, *Angew. Chem. Int. Ed.*, 2006, 45, 5849-5852. ()

(6) E. M. McGarrigle, D. G. Gilheany, *Chem. Soc. Rev.*, 2005, 105, 1563-1602.

(7) (a) Y. Shi, *Acc. Chem. Res.*, 2004, 37, 488-496; (b) D. Yang, *Acc. Chem. Res.*, 2004, 37, 497-505; (c) Y. Zhu, Q. Wang, R. G. Cornwall, Y. Shi, *Chem. Rev.*, 2014, 114, 8199-8256

(8) (a) T. Ooi, D. Ohara, M. Tamura, K. Maruoka, *J. Am. Chem. Soc.*, 2004, 126, 6884-6845; (b) M. Marigo, J. Franzen, T. B. Poulsen, K. A. Jorgensen, *J. Am. Chem. Soc.*, 2005, 127, 6964-6965; (c) X. W. Wang, C. M. Reisinger, B. List, *J. Am. Chem. Soc.*, 2008, 130, 6070-6071; (d) X. J. Lu, Y. Liu, B. F. Sun, B. Cindric, L. Deng, *J. Am. Chem. Soc.*, 2008, 130, 8134-8135; (e) C. M. Reisinger, X. W. Wang, B. List, *Angew. Chem. Int. Ed.*, 2008, 47, 8112-8115.

(9) F. G. Gelalcha, *Adv. Synth. Catal.*, 2014, 356, 261-299.

(10) (a) L. Que Jr., W. B. Tolman, *Nature*, 2008, 455, 333-340; (b) E. B. Bauer, *Curr. Org. Chem.*, 2008, 12, 1341-1369; (c) S. Enthaler, K. Junge, M. Beller, *Angew. Chem. Int. Ed.*, 2008, 47, 3317-3321; (c) A. Correa, O. G. Mancheno, C. Bolm, *Chem. Soc. Rev.*, 2008, 8, 1108-1117; (d) L.-X. Liu, *Curr. Org. Chem.*, 2010, 14, 1099-1126; (e) C.-L. Sun Chang-Liang, B.-J. Li, Z.-J. Shi, *Chem. Rev.*, 2011, 111, 1293-1314; (f) M. Darwish, M. Wills, *Catal. Sci. Technol.*, 2012, 2, 243-255; (g) K. Gopalaiah, *Chem. Rev.*, 3013, 113, 3248-3296.

(11) J. P. Collman, Z. Wang, A. Straumanis, M. Quelquejeu, E. Bose, *J. Am. Chem. Soc.*, 1999, 121, 460-461.

(12) F. G. Gelalcha, B. Bitterlich, G. Anilkumar, M. K. Tse, M. Beller, *Angew. Chem. Int. Ed.*, 2007, 46, 7293-7296.

(13) (a) F. G. Gelalcha, G. Anilkumar, M. K. Tse, A. Bruckner, M. Beller, *Chem. Eur. J.*, 2008,14, 7687-7698; (b) O. Lyakin, R. V. Ottenbacher, K. P. Bryliakov, E. P. Talsi, *ACS Catalysis*, 2012, 2, 1196-1202; (c) T. Niwa, M. Nakada, *J. Am. Chem. Soc.*, 2012, 134, 13538-13541; (d) B. Wang, S. Wang, C. Xia, W. Sun, *Chem. Eur. J.*, 2012, 18, 7332-7335; (e) X. Wang, C. Miao, S. Wang, C. Xia, W. Sun, *ChemCatChem*, 2013, 5, 2489-2494; (f) V. A. Yazerski, A. Orue, T. Evers, H. Kleijn, R. J. M. Klein Gebbink, *Catal. Sci. Technol.*, 2013, 3, 2810-2818

(14) Y. Nishikawa, H. Yamamoto, *J. Am. Chem. Soc.*, 2011, 133, 8432-8435.

(15) O. Cusso, I. Garcia-Bosch, X. Ribas, J. Lloret-Fillol, M. Costas, *J. Am. Chem. Soc.*, 2013, 135, 14871-14878.

(16) R. Mas-Balleste, L. Que Jr., *J. Am. Chem. Soc.*, 2007, 129, 15964-15972.

(17) Y. Wang, D. Janardanan, D. Usharani, K. Han, L. Que Jr., S. Shaik, *ACS Catalysis*, 2013, 3, 1334-1341.

(18) E. N. Jacobsen, W. Zhang, A. R. Muci, J. R. Ecker, L. Deng, *J. Am. Chem. Soc.*, 1991, 113, 7063-7064.

(19) M. Mitra, J. Lloret-Fillol, M. Haukka, M. Costas, E. Nordlander, *Chem. Commun.*, 2014, 50, 1408-1410.

(20) S. V. Amrutkar, U. D. Bhagat, P. Pargharmol, S. S. Kotgire, M. S. Ranawat, *Int. J. Pharm. Pharm. Sci.*, 2010, 2, 84-92.

(21) (a) A. Diebold, K. S. Hagen, *Inorg. Chem.*, 1998, 37, 215-223; (b) D. W. Blakesley, S. C. Payne, K. S. Hagen, *Inorg. Chem.*, 2000, 39, 1979-1989; (c) K. Chen, L. Que Jr., *J. Am. Chem. Soc.*, 2001, 123, 6327-6337; (d) G. J. P. Britovsek, J. England, A. P. J. White, *Inorg. Chem.*, 2005, 44, 8125-8134; (e) A. J. Simaan, S. Dopner, F. Banse, S. Bourcier, G. Bouchoux, A. Boussac, P. Hildebrandt, J. J. Girerd, *Eur. J. Inorg. Chem.*, 2000, 1627-1633; (f) I. Prat, A. Company, T. Corona, T. Parella, X. Ribas, M. Costas, *Inorg. Chem.*, 2013, 52, 9229-9244.

(22) Bruker Advanced X-ray Solutions. SMART: Version 5.631, 1997-2002.

(23) Bruker Advanced X-ray Solutions. SAINT +, Version 6.36A, 2001.

(24) G. M. Sheldrick, *Empirical Absorption Correction Program*, Universität Göttingen, 1996; Bruker Advanced X-ray Solutions. SADABS Version 2.10, 2001.

(25) G. M. Sheldrick, *Program for Crystal Structure Refinement*, Universität Göttingen, 1997; Bruker Advanced X-ray Solutions. SHELXTL Version 6.14, 2000-2003.SHELXL-2013 (Sheldrick, 2013)